Universitat de València

Programa Oficial de Doctorado en Física

An Effective Field Theory study of heavy meson-heavy antimeson molecules based on Heavy Quark Symmetries

Carlos Hidalgo Duque,
supervised by Dr. Juan M. Nieves Pamplona

Valencia - August 15$^{\text{th}}$, 2015

Universitat de València

Programa Oficial de Doctorado en Física

D. Juan Miguel Nieves Pamplona, Investigador Científico del Consejo Superior de Investigaciones Científicas (CSIC),

CERTIFICA: Que la presente Memoria *An Effective Field Theory study of heavy meson-heavy antimeson molecules based on Heavy Quark Symmetries* ha sido realizada bajo mi dirección en el Departamento de Física Teórica de la Universidad de Valencia por D. Carlos Hidalgo Duque como Tesis para obtener el grado de Doctor en Física.

Y para que así conste, en cumplimiento de la legislación vigente, presenta ante el Departamento de Física Teórica, la referida memoria, firmando el presente certificado en Burjassot (Valencia) a 15 de agosto de 2015.

Fdo: Dr. Juan Miguel Nieves Pamplona

Contents

Resumen en castellano

El estudio de las interacciones hadrónicas en el régimen de energías bajas e intermedias ha experimentado grandes avances en los últimos años. La descripción de la dinámica de QCD a bajas energías por medio de teorías efectivas, en las que los grados de libertad son mesones y bariones, ha sido ampliamente explotada para explicar el complejo espectro experimental observado. En particular, la teoría quiral de perturbaciones y sus extensiones unitarias han permitido entender y clasificar multitud de estados excitados, tanto mesónicos como bariónicos, de baja energía.

En esta tesis, hemos extendido estas ideas al sector del quark *charm* y *bottom*, donde el aluvión de nuevos mesones y bariones con *charm* o *charm* oculto encontrados por las colaboraciones BABAR, CLEO, BELLE, BES o LHCb, ha estimulado mucho trabajo teórico. Recientemente, varias de estas colaboraciones han descubierto nuevos estados con masas alrededor de 4000 MeV, que no parecen tener una estructura quark-antiquark $c\bar{c}$. Se les ha denominado partículas X, Y, Z. Algunos de estos estados son las resonancias isoescalares $X(3872), X(3940), X(4160), Y(4260)$ y las isovectoriales $Z(3900), Z(4020)$. Además, otros estados observados con *charm* explícito tampoco tienen una interpretación simple dentro de los modelos quark convencionales, como por ejemplo los mesones $D_s(2317)$, $D_s(2460)$... o los bariones $\Lambda_c(2595)$ y $\Lambda_c(2625)$. En el sector del quark *bottom* también se han encontrado resonancias similares, como los estados mesónicos $Z_b(10610)$ y $Z_b'(10650)$, o las resonancias bariónicas $\Lambda_b(5912)$ y $\Lambda_b(5920)$. Entre estos nuevos estados descubiertos, las resonancias $X(3872)$, $Z_b(10610)$ y $Z_b'(10650)$ han sido de especial relevancia en esta tesis. La resonancia $X(3872)$ se observó por primera vez por la Colaboración Belle en 2003 con números cuánticos $J^{PC} = 1^{++}$. Los estados isovectoriales $Z_b(10610)$ y $Z_b(10650)$, con números cuánticos $J^{PC} = 1^{+-}$, han sido descubiertos más recientemente, también por la Colaboración Belle. Estas resonancias se pueden describir de forma natural como estados moleculares débilmente ligados, formados por la interacción de un par mesón-antimesón pesado.

Para justificar esta descripción, hemos estudiado la interacción entre los mesones $D^{(*)}\bar{D}^{(*)}$ (y sus equivalentes en el sector del quark *bottom*) incorporando restricciones derivadas de la simetría de quarks pesados (HQS). HQS es una simetría interna de spin-sabor que aparece en QCD cuando las masas de los quark es mucho mayor que la escala de confinamiento Λ_{QCD}. HQS predice que todas las interacciones de spin son despreciables para quarks infinitamente masivos. Para masas finitas (como la del quark *charm*), hay correcciones del orden (Λ_{QCD}/m_Q), pero la simetría es todavía bastante precisa. Por ejemplo, aunque los mesones D y D^* no están degenerados, su diferencia de masas es sólo del orden de la masa del pión. Esta simetría es especialmente útil para simplificar el estudio de sistemas complejos que incluyen quarks pesados y ligeros. Por medio de HQS, pueden establecerse relaciones entre las propiedades de diversos estados (como sus masas o sus constantes de desintegración). HQS también engloba una simetría de sabor que relaciona la dinámica de los sectores *charm* y *bottom*.

Usando simetría de sabor $SU(3)$ en el sector ligero, además de HQS, hemos deducido la interacción de contacto (en onda s) entre mesones $D^{(*)}\bar{D}^{(*)}$ más general compatible con la simetría de spin de quarks pesados (HQSS). Hemos estudiado también los efectos del potencial debido al

intercambio de un pión, y comprobado numéricamente que son de orden superior. Asimismo, se han discutido efectos de canales acoplados, que resultan estar aún más suprimidos.

Los estados ligados se generan dinámicamente resolviendo la ecuación de Lippmann - Schwinger (LSE), utilizando las interacciones anteriores como *kernel* de la misma. Dado que nuestra interacción a primer orden es de contacto aparecen divergencias ultravioletas, cuya renormalización es abordada en detalle. De este modo, los estados ligados moleculares del sistema mesón-antimesón dentro de nuestro modelo aparecen como polos de la matriz T.

A primer orden, el modelo efectivo que proponemos depende de cuatro contratérminos indeterminados a priori. Los valores de estos contratérminos no están restringidos por las simetrías y, por tanto, deben ajustarse a datos experimentales (lo mismo que sucede, por ejemplo, en la teoría de perturbaciones quiral). Para ello, hemos identificado algunos estados moleculares generados dinámicamente dentro del modelo con algunas resonancias exóticas. Una vez fijados los contratérminos, predecimos una familia de estados moleculares, cuyos miembros están relacionados con las resonancias usadas como *input* por medio de HQS.

Así, en el Capítulo 3, se describe un lagrangiano efectivo, que incorpora la simetría de sabor $SU(3)$ en el sector ligero y la simetría de spin de quarks pesados, y se utiliza para describir los estados ligados mesón-antimesón en el sector charm. Como se ha mencionado, a primer orden estas simetrías inducen una gran simplificación y la teoría sólo involucra interacciones de contacto entre los campos del mesón y antimesón pesados. En este contexto, discutimos como las desintegraciones de la resonancia $X(3872)$, que violan la simetría de isospin, pueden usarse para fijar la interacción entre los mesones D y $\bar{D}^*$ en el canal isovectorial. Como consecuencia, podemos descartar la existencia de un compañero isovectorial de la resonancia $X(3872)$. A continuación, asumiendo que las resonancias $X(3915)$ e $Y(4140)$ son estados moleculares $D^*\bar{D}^*$ y $D_s^*\bar{D}_s^*$ respectivamente, se determina el espectro completo de estados moleculares con isospin $I = 0, \frac{1}{2}$ e 1, incluyendo sectores con extrañeza explícita y también no explícita ($s\bar{s}$). Una de las predicciones más importantes de este capítulo es la resonancia compañera de la $X(3872)$, con números cuánticos $J^{PC} = 2^{++}$, que llamamos X_2. Esta resonancia, compuesta por un par $D^*\bar{D}^*$ débilmente ligado, presenta la misma dinámica que la resonancia $X(3872)$. Mencionar también que se ha realizado un estudio exhaustivo de las incertidumbres teóricas, debidas a violaciones de simetría $SU(3)$ de sabor y de simetría de spin de quarks pesados, que afectan a nuestras predicciones.

Posteriormente, en el Capítulo 4, hemos estudiado la teoría efectiva presentada en el Capítulo 3 en una caja finita. Este análisis es interesante porque el estudio de teorías efectivas en retículos espacio-temporales está aumentando y, por tanto, es necesario un mejor conocimiento de los efectos de volumen finito. Como volumen finito se ha utilizado el más sencillo posible: una caja de lados iguales, pero el formalismo desarrollado se puede emplear para geometrías más complejas (cajas rectangulares, e.g.). Al trabajar en un volumen finito, las integrales sobre el espacio de momentos deben sustituirse por sumas sobre un conjunto discreto de momentos (similar al fenómeno bien conocido que surge al estudiar el potencial pozo cuadrado infinito en mecánica cuántica). Realizando estos cambios, hemos encontrado los resultados correspondientes al Capítulo 3 para el caso de un volumen finito. Hemos estudiado la dependencia en L (longitud de la caja) de los niveles de energías en los distintos sectores de spin, isospin, extrañeza y conjugación de carga, y estimado el tamaño de las correcciones debidas al tamaño finito. Después, se ha realizado un análisis del problema inverso, con objeto de estudiar la propagación de los errores de los niveles medidos en la caja en la predicción final de la energía de los estados físicos. Con este fin, se generan, con nuestro modelo, unos estados sintéticos (ficticios, simulando el resultado de una medida real) dotándolos de una cierta incertidumbre, alrededor de 10 MeV, respecto al valor central obtenido (el valor especificado tiene su justificación ya que se trata del nivel de precisión que esperamos que las simulaciones de QCD puedan conseguir en unos años). Hemos probado

distintos tipos de algoritmos para determinar las propiedades de los estados generados. Los resultados obtenidos sugieren que el mejor algoritmo involucra la introducción de un potencial auxiliar y el uso de los niveles de energías medidos por encima y debajo del umbral, a diferencia de los que usan sólo un conjunto de datos, generalmente los desfasajes medidos en la caja finita. Asimismo hemos observado que el correcto análisis de estados muy cercanos al umbral no es sencillo y requiere técnicas específicas. Este resultado debería tenerse especialmente en cuenta para el estudio de estados débilmente ligados, como las resonancias $X(3872)$ o X_2, en volúmenes finitos.

En el Capítulo 5 hemos extendido nuestra teoría efectiva al sector *bottom* aprovechando la simetría de sabor implícita en HQS. Esta simetría establece que la dinámica de quarks suficientemente pesados no depende de sabor. Las correcciones esperadas son del orden $\mathcal{O}(\Lambda_{QCD}/m_Q)$. Gracias a esta simetría también podemos utilizar resonancias exóticas del sector bottom para determinar los contratérminos. En este capítulo, tomamos como *input* las resonancias $X(3872)$ y uno de los estados $Z_b(10610)/Z_b'(10650)$, lo cual nos ha permitido determinar tres de los cuatro contratérminos de una forma más robusta que en el Capítulo 4. Así se predicen una serie de estados cuya observación experimental, nuevamente, indicaría la bondad de nuestras hipótesis acerca de la naturaleza molecular de las resonancias utilizadas. A partir de la resonancia $X(3872)$ recuperamos el estado X_2, pero, al extender el análisis al sector *bottom* obtenemos sus equivalentes en dicho sector, los estados X_b y X_{b2}. Por otro lado, hemos encontrado los estados compañeros de las resonancias $Z_b(10610)$ y $Z_b'(10650)$ en el sector *charm*, que en el modelo, aparecen como estados virtuales. En cualquier caso, resulta tentador y además plausible, identificar estos estados con las resonancias isovectoriales $Z_c(3900)$ y $Z_c(4020)$ recientemente descubiertas por la colaboración BESIII. Los efectos debidos al potencial inducido por el intercambio de un pión en el sector bottom han sido evaluados también. En concreto, se ha analizado con detalle el sector isoescalar (ya que, en este sector, el efecto del intercambio del pión es tres veces mayor que en el sector isovectorial), y hemos obtenido diferencias numéricas muy pequeñas entre estas nuevas predicciones y las anteriores, donde los efectos del intercambio de un pión se habían ignorado. Este resultado nos ha permitido seguir despreciando el potencial de intercambio de un pión en los análisis posteriores.

En el Capítulo 6, hemos estudiado la interacción entre bariones doblemente pesados y mesones pesados (D, D^*, $\bar{B}$, $\bar{B}^*$). En este sector, hemos apuntado, gracias a la simetría antiquark-diquark para quarks pesados, la posible existencia de bariones exóticos (pentaquarks). La simetría relaciona la dinámica de un diquark pesado con la dinámica de un antiquark pesado basándose en que dan lugar a la misma carga de color, y a que la configuración de los grados de libertad ligeros apenas depende del subsector pesado. Además, demostramos que en el límite $m_Q \to \infty$, $Q = b, c$, estas interacciones mesón-barión quedan determinadas por los mismos contratérminos que aparecen al estudiar las interacciones $P^{(*)}\bar{P}^{(*)}$, con $P^{(*)} = D^{(*)}, B^{(*)}$. Aunque el estudio es cualitativo, con numerosas incertidumbres teóricas que se intentan estimar de forma razonable, se predicen estados ligados mesón-barión con tres quarks pesados (b y/o c) y $J^P = 5/2^-$ y $3/2^-$ en el sector isoescalar, cuya dinámica estaría controlada por los contratérminos que aparecen en el canal de la $X(3872)$. Con números cuánticos $I(J^P) = 1\,(1/2^-)$ y $1\,(3/2^-)$ encontramos moléculas hadrónicas $\Xi_{bb}^*\bar{B}^*$ que estarían íntimamente relacionadas con los estados exóticos $Z_b(10610)$ y $Z_b(10650)$ (moléculas $B^{(*)}\bar{B}^*$).

En el Capítulo 7 se realiza un análisis paralelo de los estados moleculares mesón-antimesón, en el límite estricto $m_Q \to \infty$, utilizando funciones de Green de dos puntos, que se podrían emplear en cálculos de reglas de suma o simulaciones de LQCD. Para tal fin, se construyen las corrientes interpoladoras adecuadas para estudiar estos estados mesón-antimesón en los distintos sectores de spin y conjugación de carga. En este contexto, se ha discutido de nuevo la mezcla de isospin de la resonancia $X(3872)$.

En los Capítulos 8 y 9 hemos analizado ciertas desintegraciones de algunos de los estados moleculares estudiados en los capítulos anteriores. El Capítulo 8 se ha dedicado a estudiar la desintegración hadrónica $X(3872) \to D^0\bar{D}^0\pi^0$. Este proceso es especialmente interesante porque es sensible a los detalles de la interacción $D\bar{D}$ a largas distancias. Hemos demostrado como una medida experimental precisa de la anchura diferencial de esta desintegración hadrónica podría ser utilizada para determinar la función de ondas del par $D\bar{D}^*$ en el interior de la resonancia. Como la desintegración puede depender de las interacciones de estados finales (FSI) entre los mesones $D\bar{D}$, esta desintegración también se puede utilizar para fijar las constantes de baja energía (contratérminos) que controlan la dinámica $P^{(*)}\bar{P}^{(*)}$.

Finalmente, en el Capítulo 9, hemos analizado las desintegraciones del estado compañero de la $X(3872)$ con números cuánticos $J^{PC} = 2^{++}$, la resonancia X_2, en los sectores *charm* y *bottom*. Se analizan primero las desintegraciones hadrónicas de dicho estado $X_2 \to P\bar{P}$ y $X_2 \to P\bar{P}^*$. Estas desintegraciones representan la mayor contribución a la anchura de la resonancia, y por tanto, el mejor canal para detectar experimentalmente el estado. La anchura de este proceso resulta ser del orden de varios MeVs. Además, se realiza, utilizando una simulación Montecarlo, un estudio exhaustivo de las incertidumbres teóricas de nuestras predicciones. En este capítulo hemos estudiado también las desintegraciones radiativas $X_2 \to P\bar{P}^*\gamma$, cuya anchura es del orden de decenas de keV. Este proceso, al igual que la desintegración hadrónica $X(3872) \to D^0\bar{D}^0\pi^0$ estudiada en el Capítulo 8, es sensible a los detalles de la función de onda del par de mesones $(P^*\bar{P}^*)$ que forman la molécula, en la región de largas distancias, y por tanto, es relevante para determinar la naturaleza del estado molecular X_2. La desintegración radiativa también se ve afectada por las FSI de los mesones $P\bar{P}^*$ salientes, lo que utilizamos, como en el capítulo anterior, para obtener nuevas restricciones en el valor de los contratérminos que aparecen en la teoría efectiva a orden dominante.

La mayor parte de este trabajo ya ha sido publicado [1, 2, 3, 4, 5, 6, 7] y presentado en varias conferencias internacionales.

Abstract

The study of the low and intermediate energy hadronic interactions has experienced great advances in the last few years. The fact that low energy QCD dynamics can be described by means of effective theories, in which the degrees of freedom are mesons and baryons, has been widely exploited to explain the complex experimental observed spectrum.

In this thesis, we have extended these ideas to the quark charm and bottom sectors. The whole new set of meson and baryon states with open charm and hidden charm found by the BABAR, CLEO, BELLE, BES or LHCb collaborations has stimulated a lot of theoretical work. Recently, several of these collaborations have discovered new exotic states with masses around 4000 MeV, which do not seem to have a simple quark-antiquark $c\bar{c}$ structure. They have been called XYZ particles. Some of these states are the isoscalar resonances $X(3872), X(3940), X(4160), Y(4260)$ and the isovector $Z_c(3900), Z_c(4020)$. In addition, other observed states with explicit charm do not have either a simple interpretation within conventional quark models, such as the $D_s(2317)$, $D_s(2460)$ mesons or the $\Lambda_c(2595)$, $\Lambda_c(2625)$ baryons. In the bottom sector, exotic resonances have also been found, such as the mesonic states $Z_b(10610)$ y $Z_b'(10650)$ and the baryon resonances $\Lambda_b(5912)$ and $\Lambda_b(5920)$. Among these discovered states, the $X(3872)$, $Z_b(10610)$ and $Z_b'(10650)$ are of paramount relevance in this thesis. The $X(3872)$ resonance was observed for the first time by the Belle Collaboration in 2003 with quantum numbers $J^{PC} = 1^{++}$. The isovector states $Z_b(10610)$ and $Z_b(10650)$, $J^{PC} = 1^{+-}$, were discovered more recently, also by the Belle Collaboration. These resonances can naturally be described as molecular states, composed by a loosely bound heavy meson-antimeson pair.

To justify this description, we have studied the interaction between $D^{(*)}\bar{D}^{(*)}$ mesons (and similarly in the quark bottom sector), incorporating the restrictions derived from the Heavy Quark Symmetry (HQS). HQS is a spin-flavour underlying symmetry of QCD that appears when the quark masses are much larger than the confinement scale Λ_{QCD}. HQS predicts that spin interactions are negligible in the limit of infinite quark masses. For finite masses, such as that of the charm quark, there are some corrections of the order (Λ_{QCD}/m_Q) but the symmetry is still quite precise. For instance, despite the D and D^* mesons are not degenerate, the mass difference between the two mesons is less than a pion mass. This symmetry is specially useful to simplify the study of composite systems involving both light and heavy quarks. Owing to HQS, simple relationships among properties (such as masses or decay constants) of different spin states can be formulated. HQS also embodies a flavour symmetry that relates the charm and bottom sectors. Assuming an additional $SU(3)$ flavour-symmetry in the light sector, we have deduced the most general contact (s-wave) interaction between $P^{(*)}\bar{P}^{(*)}$ ($P^{(*)} = D^{(*)}$, $B^{(*)}$) mesons compatible with Heavy Quark Spin Symmetry (HQSS). We have also studied One Pion Exchange (OPE) and coupled channel effects on the potential, which turned out to be numerically small and suppressed in the counting.

Bound states are dynamically generated by solving the Lippmann-Schwinger Equation (LSE), using the previous interactions as its kernel. Since the potential at leading order (LO) is a contact

interaction, there are ultraviolet divergences in the theory, whose renormalization has also been discussed in detail. In this manner, meson-antimeson molecules predicted by our model appear as poles in the T-matrix.

At LO, the effective theory depends on four undetermined Low Energy Constants (LECs). The values of these LECs are not restricted by any elementary model or further underlying symmetry and must be fitted to reproduce experimental observations. Hence, we identify some exotic resonances as molecular states to fix the LECs (as occurs in Chiral Perturbation Theory). Once these counter-terms are determined, we have predicted a whole family of molecular HQS partners of the resonances used as inputs.

Thus, in Chapter 3, we describe an effective Lagrangian incorporating light $SU(3)$-flavour and heavy quark spin symmetries and it is used to describe hidden-charm meson-antimeson bound states. As mentioned above, at LO, the effective field theory entails a remarkable simplification and it only involves contact range interactions among the heavy meson and antimeson fields. In this context, we show that the isospin violating decays of the $X(3872)$ can be used to constrain the interaction between the D and the $\bar{D}^*$ mesons in the isovector channel. As a consequence, we can rule out the existence of an isovector partner of the $X(3872)$. Next, and assuming that the $X(3915)$ and $Y(4140)$ are $D^*\bar{D}^*$ and $D_s^*\bar{D}_s^*$ molecular states, we determine the full spectrum of molecular states with isospin $I = 0, \frac{1}{2}$ and 1. The predicted spectrum includes open and hidden-strangeness sectors as well. One of the most relevant predictions in this chapter is the partner of the $X(3872)$, called X_2. This resonance, a loosely bound $D^*\bar{D}^*$ state with quantum numbers $J^{PC} = 2^{++}$, has the same dynamics as the $X(3872)$.

Next, in Chapter 4, we have studied the HQS EFT in a finite box. This analysis is interesting since the study of EFTs in lattice is increasing and further understanding of finite volume effects is mandatory. The procedure followed is the substitution of an infinite volume by a finite volume in the formalism. As the basic volume unit we have used a cube; but other more complex geometries could be used (e.g., rectangular boxes). This replacement imposes that the momentum-space integrals have to be substituted by a sum over a discrete set of three-momenta (as can be seen in the infinite square potential in quantum mechanics). Within this formalism, first the energy levels in the box are evaluated, and from them some synthetic data are generated. These data are then employed to study the inverse problem of getting the energies of the bound states and phase shifts for $D\bar{D}$ or $D^*\bar{D}^*$. Different strategies are investigated and we conclude that a method based on the fit to the data by means of a potential and a conveniently regularized loop function, is the most efficient and allows us to produce accurate results in the infinite volume starting from levels of the box with errors far larger than the uncertainties obtained in the final results. Finally, in this chapter, the regularization method based on Gaussian wave functions is discussed and shown to be rather efficient in the finite box analysis and, as a byproduct, a practical and fast method to calculate the Lüscher function with high precision is presented.

In Chapter 5, we extend the EFT formalism outlined in Chapter 3 to the bottom sector taking advantage of Heavy Flavour Symmetry (HFS). This symmetry basically states that for quarks heavy enough (as the charm and bottom quarks), dynamics are flavour-independent, up to corrections of the order $\mathcal{O}(\Lambda_{QCD}/m_Q)$. Thanks to this symmetry, one could also use possible exotic states discovered in the bottom sector to determine the LECs. In this chapter, we use as an input the $X(3872)$ resonance and one of the $Z_b(10610)/Z_b'(10650)$ states. We are thus able to fix three of the four LECs and obtain a set of states whose experimental determination would be again a test of the molecular assumptions used. From the $X(3872)$ state, we have re-obtained the X_2 state but, we have also found the equivalent states in the bottom sector, the X_b and X_{b2} states. We have also obtained partners of the $Z_b(10610)$ and $Z_b'(10650)$ states in the charm sector, these Z_c/Z_c' states appear in our scheme as virtual states. These states were (likely) experimentally observed and we are convinced that they probably correspond to

the recently reported $Z_c(3900)$ and $Z_c(4025)$ resonances by the BESIII Collaboration. The OPE effects in the bottom sector have been numerically computed as well. We have analyzed in detail the isoscalar sector (the OPE potential in the isoscalar sector is three times larger than in the isovector sector), where small deviations from the previous results have been found. This result allows us to keep neglecting the OPE effects in the following analyses.

In Chapter 6, a similar EFT analysis is used to predict the possible existence of exotic (pentaquark) baryons. This has been accomplished by means of the Heavy Antiquark-Diquark Symmetry (HADS). This symmetry relates the dynamics of a heavy diquark with that of a heavy antiquark (because both systems have the same $\bar{3}$ colour configuration). Thus, the doubly heavy baryons have approximately the same light-quark structure as the heavy antimesons. As a consequence, the existence of a heavy meson-antimeson molecule implies the possibility of a partner composed of a heavy meson and a doubly heavy baryon. In this regard, the $D\bar{D}^*$ molecular nature of the $X(3872)$ hints at the existence of several baryonic partners with isospin $I = 0$ and $J^P = \frac{5}{2}^-$ or $\frac{3}{2}^-$. Moreover, assuming that the $Z_b(10650)$ is a $B^*\bar{B}^*$ bound state, the existence of $\Xi_{bb}^*\bar{B}^*$ hadronic molecules with quantum numbers $I(J^P) = 1(\frac{1}{2}^-)$ and $I(J^P) = 1(\frac{3}{2}^-)$ have been predicted. These states are of special interest since they can be considered to be triply heavy pentaquarks.

In Chapter 7, a parallel analysis of these molecular states has been carried out using a formalism based on two point Green functions, in the strict heavy quark limit. To that end, some suited interpolating currents have been defined for the different spin-parity-charge conjugation sectors. They can be used in sum rule or LQCD studies of these exotic molecular states. The isospin mixing of the $X(3872)$ has been also discussed from this perspective.

In chapters 8 and 9 we analyze certain decays of some of the molecular states studied in the previous chapters. Chapter 8 is devoted to the study of the hadron decay $X(3872) \to D^0\bar{D}^0\pi^0$. This process is of special interest because it is sensitive to the long-distance structure of the $X(3872)$. Indeed, we have argued that a precise experimental determination of this width might shed some light on the inner nature of the resonance. Moreover, it can also serve to further constrain the LECs because the final state interactions (FSI) between the final $D\bar{D}$ states might significantly affect the decay width.

Finally, in Chapter 9, we have studied the decays of the $J^{PC} = 2^{++}$ molecular partner of the $X(3872)$ state (X_2 state) in both the charm and bottom sectors. We first analyze the hadron decays $X_2 \to P\bar{P}$ and $X_2 \to P\bar{P}^*$. These decays represent the largest contribution to the total decay width of the state and turn out to be of the order of few MeV. Next, we have also studied the $X_2 \to P\bar{P}^*\gamma$ radiative decays. The decay width is predicted to be tens of keV and it is discussed how this process, as the $X(3872) \to D^0\bar{D}^0\pi^0$ hadronic decay studied in Chapter 8, is sensitive to the long-distance details of the $D^*\bar{D}^*$ wave function and, therefore, might reveal the nature of the studied resonance. The radiative decay is also affected by the FSI of the outgoing $P\bar{P}^*$ meson pair, what might provide additional constrains on the counter-terms that appear in the EFT at LO.

Most of this work has already been published [1, 2, 3, 4, 5, 6, 7] and presented in several international conferences.

Chapter 1

Motivation

The spectroscopic properties of bound states tell us a great deal about the symmetries and underlying dynamics of their components. For instance, the hydrogen atom has been an extraordinary source of information about several aspects of quantum electrodynamics, from the accidental $SO(4)$ symmetry in the spectrum to radiative corrections, to some aspects of the renormalization techniques that are necessary to explain the Lamb shift. Another enlightening example is provided by the classification of hadrons according to isospin, $SU(3)$ flavour, etc., which reveals properties of the underlying strong dynamics binding the hadrons and has been instrumental in the past for the development of quantum chromodynamics (QCD). Conversely, a deeper understanding of QCD and its symmetries will eventually give new insights into the hadron spectrum. In that sense, anomalies in the experimental spectrum difficult to accommodate within theoretical models provoke deeper theoretical analysis aiming at explaining those anomalies. In this thesis we focus on the study of heavy meson molecules, states not included within the conventional constituent quark models, where only mesons and baryons are naturally accommodated.

The existence of heavy meson molecules was predicted almost 40 years ago by Voloshin and Okun [8, 9]. Heavy meson-heavy antimeson molecules are interesting objects from the theoretical point of view. The main component of these states is the set of hadrons conforming the molecule, where the other degrees of freedom play a minor role in their description. In general this is only true if the separation between the hadrons is large enough to retain their individual character. As far as they are not tightly bound, the meson and antimeson will preserve their individuality and will not probe the specific details of the short-range interaction responsible of their binding. Moreover, each of the constituent heavy hadrons will be unable to *see* the internal structure of the other heavy hadron. This suggests that genuine molecular states show a clear separation of scales between their long and short structure. This separation of scales can be exploited to formulate an effective field theory (EFT) to study these hadronic molecules in which they can be described as meson-meson bound states interacting via contact interactions and pion exchanges (e.g., X-EFT Ref. [10], heavy meson molecule EFT [11, 12, 13]). Among the theoretical advantages of EFTs, a very interesting one is power counting: we can expand any physical quantity as a power series in terms of the expansion parameter (Q/M), where Q is a typical low energy scale (the inverse of the size of the molecular state, the momenta of the mesons within a molecule or the pion mass, e.g.) and M is a high energy scale at which the EFT description stops being valid (for instance, the inverse size of the hadrons; QCD hadronic mass scale, of the order of the ρ mass, or the center-of-mass momentum necessary for a heavy hadron to excite another).

The heavy hadrons are non-relativistic: thus we can define a hadron-hadron potential that admits a low energy expansion $V_{HH}^{\rm EFT} = V_{HH}^{\rm LO} + V_{HH}^{\rm NLO} + \ldots$, where LO stands for "leading order", NLO for "next-to-leading order" and so on. In addition, the interaction among the heavy hadrons forming a molecule is non-perturbative so that we have to iterate, solving a Schrödinger/Lippmann-Schwinger equation, the EFT potential. Due to the exploratory character of this work and the lack of data, we will not go beyond LO. The contribution of physics at the hard scale M is safely encoded in the counter-terms of the EFT at low energies [14, 15]. The situation is analogous to that of the EFT formulation of the nucleon-nucleon interaction [16, 17], which we use as a template for the EFT of heavy hadronic molecules.

Yet heavy hadrons entail interesting simplifications over nucleons. In addition, we can take advantage that the heavy-light quark content of heavy meson molecules implies a high degree of symmetry. They are subjected to heavy quark symmetries (HQS) [18, 19, 20, 21], which impose interesting constrains in the heavy meson-antimeson interaction [22]. As a consequence, HQS can be used to predict the existence of so far unobserved molecular states [13, 23, 24, 25]. On the other hand, we must not forget the light quark content of heavy meson molecules. If we consider $q = u, d, s$, we expect $SU(3)$-flavour symmetry to hold: we can arrange molecular states within isospin and $SU(3)$ multiplets. Among the manifestations of heavy quark symmetries, we can count heavy quark spin symmetry (HQSS) which implies that molecular states may appear in HQSS multiplets, for instance (but not limited to) the $D_{s0}^*(2317)$ and $D_{s1}^*(2460)$ [26], the $Z_b(10610)$ and $Z_b'(10650)$ [13, 23, 25, 27]. From heavy flavour symmetry (HFS), we know that the interaction among heavy hadrons is roughly independent on whether they contain a charm or a bottom quark. In this regard, the recently discovered $Z_c(3900)$ resonance could very well be a heavy flavour partner of the $Z_b(10610)$. Last, there is a less explored type of heavy quark symmetry, HADS, that is also going to lead to interesting consequences in this work and that explores the existing similarity between a heavy antiquark and a heavy diquark [28].

Due to ongoing experimental efforts, a series of new heavy quarkonium states called XYZ states have been observed in the last decade. Many of them are expected to be of exotic nature; for a comprehensive review we refer to Ref. [29]. Due to the proximity of the masses to certain hadronic thresholds, some of the XYZ states have been proposed to be hadronic molecules, i.e. states that are generated by the interaction between two or more hadrons (they are bound states if they are below the threshold and in the first Riemann sheet, or virtual states and resonances if they are in the second Riemann sheet of the scattering amplitude). Among all of them, the famous $X(3872)$ resonance discovered by the Belle Collaboration [30] deserves special attention as it has opened new perspectives in hadron spectroscopy. The $X(3872)$, even though it clearly contains a $c\bar{c}$ pair, does not fit well within the standard charmonium spectrum. Disentangling its nature requires a more exotic explanation. The discovery of the $X(3872)$ has been followed by the experimental observation of a series of hidden charm resonances above the open-charm threshold. Some of the XYZ states fit well within the charmonium spectrum, most notably the $Z(3930)$, that was identified as the $\chi_{c2}(2P)$ state [31], but others do not and may require, just like the $X(3872)$, non-conventional explanations. A few of them might have a large molecular content: several authors [32, 33, 34] have proposed the $X(3915)$ [35] and $Y(4140)$ [36] to be $D^*\bar{D}^*$ and $D_s^*\bar{D}_s^*$ bound states, respectively. The $Y(4260)$ state [37] might even have a three body structure $(J/\Psi\, K\bar{K})$ [38]. The $Y(4660)$ [39] and $X(4630)$ [40] have been theorized to be $f_0(980)\Psi'$ molecule [41, 42] (they may be the same state [42]). More recently, the Belle collaboration has observed two isovector hidden bottom resonances, the $Z_b(10610)$ and $Z_b(10650)$ [43], located just a few MeV away from the $\mathrm{B}\bar{\mathrm{B}}^*$ and $\mathrm{B}^*\bar{\mathrm{B}}^*$ thresholds, respectively, which are clear candidates to have a molecular nature [13, 23, 44]. In Sect. 1.1 we briefly comment the current status of the hadronic spectrum paying special attention to some observed exotic states, not well understood, and in particular we will focus on those experimental observations which have been used as an

input in this work.

In order to understand the dynamics of these exotic states, in particular their binding mechanisms and discriminate the different models in the literature, it is important to find out methods which can distinguish among different scenarios. Decay patterns are often used for this purpose. Here we will pursue a different approach and we will try to classify these states using Heavy Quark Spin-Flavour Symmetry (HQSFS). Without developing complicated dynamical models, symmetries are often helpful in describing certain aspects of various physical systems. For a system involving a heavy quark whose mass m_Q is much larger than $\Lambda_{\rm QCD}$ (that is, in the limit m_Q going to infinity), flavour and spin symmetries arise, as explicitly discussed in Sect. 2.1 below, and it seems thus natural to explore their consequences. In Sect. 1.2, we briefly describe the approximate underlying QCD symmetries we use to build the EFT employed for the description of the molecular states: HQSFS, HADS and Chiral Symmetry.

Finally, in Sect. 1.3 some remarks on the properties of the scattering T-matrix are given. We pay special attention to its analytical properties, which play a key role in the determination of the properties of bound states and resonances. We also briefly discuss the Lippmann-Schwinger Equation (LSE), which provides a non-perturbative s-channel resummation, that restores exact two-body elastic unitarity.

1.1 Exotic Hadrons

The quark model is a classification scheme for hadrons in terms of their valence quarks, proposed by Murray Gell-Mann and George Zweig in 1964. Its application has been very successful so far and it has allowed us to partially understand the hadronic spectrum. This model relies on the fact that hadrons are not elementary, but complex systems composed of some elementary components called quarks (or antiquarks) which are responsible for their quantum numbers. In the simplest quark model, only combinations of a quark and an antiquark (mesons) and three quarks (baryons) are permitted. The inner quark structure forces a regular distribution for hadrons where only some set of quantum numbers are possible. In Table 1.1, we compile the quantum numbers of several hadrons in the heavy sector of the hadron spectrum taken from the PDG [45]. The mesons are classified in J^{PC} multiplets. The $l = 0$ are the pseudoscalar (0^{-+}) and the vector (1^{--}) states. The orbital excitations $l = 1$ are the scalar (0^{++}), the axial vector (1^{+-} and 1^{++}), and the tensor (2^{++}) states. Quark model assignments for many of the known mesons are also given in Table 1.1. Radial excitations are denoted by the principal quantum number n. The observed experimental spectrum is more complex than the one expected from quark models, which is a strong hint for new physics. Since the wave function of hadrons is the sum of every possible state with the same quantum numbers, it involves those states described within quark models but it might also include some other states, called *Exotic Hadrons*. These exotic hadrons can be glueballs (composed by valence gluons); hybrids (containing both valence quarks and valence gluons); tetraquarks and pentaquarks; molecular bound states... Many experimental exotic hadrons have been proposed, see Refs. [29, 45] for instance, although these lists need to be updated.

Among the exotic hadrons, in this work we are interested in the hadronic molecules that contain a heavy meson and a heavy antimeson. As already mentioned, these molecular states were first theorized in 1976, by Voloshin and Okun [8], and later on by Tornqvist [46]. Tornqvist called these exotic hadrons *deusons* because of the similarities between these molecular states and the deuteron. In the picture of Ref. [46], the forces that bind both the deuteron and the heavy meson-heavy antimeson system could be described as a light meson exchange and, as in the case of the deuteron, the binding energy was expected to be small too. This similarity can

$n^{2s+1}l_J$	J^{PC}	$I=0$ $c\bar{c}$	$I=0$ $b\bar{b}$	$I=\frac{1}{2}$ $c\bar{u};c\bar{d};\bar{c}u;\bar{c}d$	$I=0$ $c\bar{s};\bar{c}s$	$I=\frac{1}{2}$ $b\bar{u};b\bar{d};\bar{b}u;\bar{b}d$	$I=0$ $b\bar{s};\bar{b}s$	$I=0$ $b\bar{c};\bar{b}c$
1^1S_0	0^{-+}	$\eta_c(1S)$	$\eta_b(1S)$	D	$D_s^{\pm}$	B	B_s	$B_c^{\pm}$
1^3S_1	1^{--}	$J/\psi(1S)$	$\Upsilon_b(1S)$	D^*	$D_s^{*\pm}$	B^*	$B_s^{*\pm}$	B_c^+
1^1P_1	1^{+-}	$h_c(1P)$		$D_1(2420)$	$D_{s1}(2536)^{*\pm}$	$B_1(5721)$	$B_{s1}(5830)^{*0}$	
1^3P_0	0^{++}	$\chi_{c0}(1P)$	$\chi_{b0}(1P)$		$D_{s0}^{*\pm\dagger}(2317)$			
1^3P_1	1^{++}	$\chi_{c1}(1P)$	$\chi_{b1}(1P)$		$D_{s1}^{*\pm\dagger}(2460)$			
1^3P_2	2^{++}	$\chi_{c2}(1P)$	$\chi_{b2}(1P)$	$D_2(2460)$	$D_{s2}^{*\pm\dagger}(2573)$	$B_2^*(5747)$	$B_{s2}^{*\pm\dagger}(5840)$	
1^3D_1	1^{--}	$\psi(3770)$			$D_{s1}^*(2700)^{\pm}$			
2^1S_0	0^{-+}	$\eta_c(2S)$		$D(2550)$				
2^3S_1	1^{--}	$\psi(2S)$	$\Upsilon(2S)$					
2^1P_1	1^{+-}		$h_b(2P)$					
$2^3P_{0,1,2}$	$0^{++},1^{++},2^{++}$	$\chi_{c0,1,2}(2P)$	$\chi_{b0,1,2}(2P)$					

Table 1.1: *$q\bar{q}$ quark-model assignments for the observed heavy mesons with established J^{PC} quantum numbers [45]. †The masses of these states are considerably smaller than most theoretical predictions. They have also been considered as tetraquark or molecular states.*

be schematically seen as depicted in Fig. 1.1: Since then, many works about this topic have

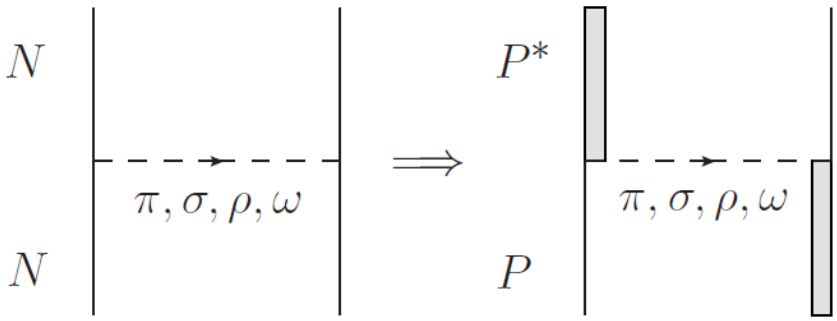

Figure 1.1: *Simple description of the similarities between the deuteron and the bound heavy meson-heavy antimeson systems. P and P^* refer to pseudoscalar and vector mesons, respectively. For the sake of simplicity, the heavy meson-heavy antimeson system has been chosen to be a pseudoscalar-vector system in the figure without any loss of generality.*

become available, see for example the work by De Rújula, Georgi and Glashow in 1977 (only one year later than the theoretical proposal about the existence of these molecular systems) where the $Y(4040)$ was interpreted as a $D^*\bar{D}^*$ [47]. In the light sector, it has also been suggested that the $a_0(980)$ and $f_0(980)$ are also $K\bar{K}$ molecular states. However, according to [48], no other molecular states involving light mesons are expected.

However, in heavier sectors (charm and bottom) many new resonances X,Y and Z without an apparent conventional interpretation have been found. Among all of them, the most important exotic state experimentally observed is the $X(3872)$ resonance, whose molecular interpretation will play a crucial role in this thesis. In the following subsections, we briefly discuss some exotic

resonances whose molecular nature has been assumed in different chapters of this work: the $X(3872)$, the $X(3915)$, the $Y(4140)$ and the $Z_b(10610)/Z_b'(10650)$ resonances.

1.1.1 The $X(3872)$

As already stated, the $X(3872)$ was the first resonance whose molecular interpretation could be appropriated. It has been deeply studied in the last decade (there are more than 550 articles written about it by the time being) but there are many open puzzles not yet understood.

The $X(3872)$ resonance was discovered by the Belle collaboration in 2003 [30] in the $J/\psi\,\pi^+\pi^-$ channel and later confirmed by numerous experiments such as BaBar, CDF or D0 [49, 50, 51, 52]. This resonance has a mass close to the $D\bar{D}^*$ threshold and, due to its radiative decay $X \to J/\psi\gamma$, its quantum numbers had to be $J^{PC} = 1^{++}$ or 2^{-+}, neither one plausible according to the theoretical predictions for charmonium states with that mass. Its isospin structure is complex because the $X(3872) \to J/\psi\ 3\pi$ decay (with $I = 1$) was observed with a decay width comparable to that of the $X(3872) \to J/\psi\ 2\pi$ decay ($I = 0$). Some other decays of this resonance were also observed, being the most important one for this thesis, the $X(3872) \to D^0\bar{D}^0\pi^0$ decay mode that we will study and discuss as a tool to disentangle the properties of this exotic state.

Many different exotic interpretations have been proposed: an excitation of some charmonium state, tetraquarks, hybrids... and, of course, the molecular interpretation based on the closeness to the $D^0\bar{D}^{*0}$ threshold, which favoured the $J^{PC} = 1^{++}$ $D\bar{D}^*$ s-wave interpretation.

Finally, the $J^{PC} = 2^{-+}$ assumption was ruled out by LHCb in 2013 [53]. This result supports the molecular interpretation of the $X(3872)$ that still seems quite solid and compatible with every piece of experimental information collected. In Fig. 1.2 we show the experimental observation of the $X(3872)$ mass and the confirmation of the quantum numbers $J^{PC} = 1^{++}$.

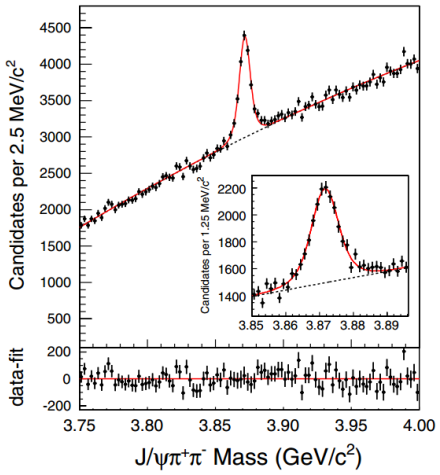

(a) Precise evaluation of the X(3872) mass evaluated from the invariant mass of the $J\psi\pi^+\pi^-$ in the CDF experiment [54].

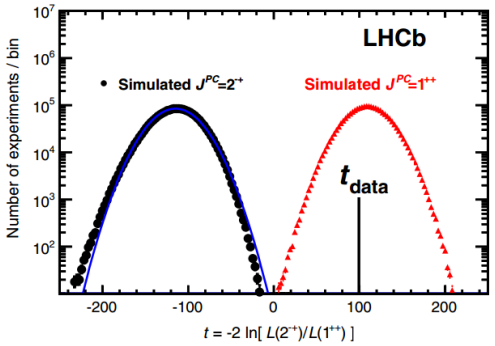

(b) Results of the LHCb experiment in 2013 [53] ruling out the $J^{PC} = 2^{-+}$ quantum numbers for the $X(3872)$.

Figure 1.2: *Experimental information about the* $X(3872)$ *resonance.*

1.1.2 The $X(3915)$

This resonance was first observed by the Belle collaboration in 2004 [55] as a peak in $J/\psi\ \omega$ spectrum in the $B \to K\omega J/\psi$ decays and the $\gamma\gamma \to \omega\ J/\psi$ two-photon fusion reactions. Many theoretical assumptions were made, being the molecular interpretation of the resonance as an isoscalar $D^*\bar{D}^*$ bound state with $J^{PC} = 0^{++}$ one of them. However, it was later suggested by BaBar [56], that this state could be identified with the charmonium $\chi_{c0}(2P)$ state.

Indeed the PDG Summary Table lists the $X(3915)$ as this charmonium state. However, some of its decays raise serious concerns about this assignment [57, 58]. More recently, it has been suggested [59] that the observed properties of this charmonium-like resonance $X(3915)$ can possibly explained if it is an s-wave molecular bound state of a $D_s\bar{D}_s$ molecular pair with binding energy about 18 MeV.

In the meantime, we adopted, in one of the publications that gave origin to this thesis, the $D^*\bar{D}^*$ molecular assumption for this state . Thus, some results depend on this debatable hypothesis.

1.1.3 The $Y(4140)$

The $Y(4140)$ resonance was observed in 2009 by the CDF collaboration [36] in the $J/\psi\phi$ channel. The presence of the hidden strangeness pair in the ϕ meson was the key point for its $D_s^*\bar{D}_s^*$ molecular interpretation with quantum numbers $J^{PC} = 0^{++}$. However, posterior analyses by the Belle [60] and LHCb [61] collaborations did not find this state, thus the current status of this state remains unclear. As in the X(3915) resonance case, some few results of Chapter 3 in this work rely on the molecular nature of this resonance.

1.1.4 The $Z_b(10610)/Z_b'(10650)$

These two resonances were observed at the same time by the Belle collaboration in 2012 [43]. They are very important in the hadronic spectrum because they are the first exotic states found in the bottom sector. The mass of these two states lay, respectively, close to the $B\bar{B}^*$ and $B^*\bar{B}^*$ threshold, similarly to the case of the $X(3872)$ resonance. Besides, it turned out that these states have a well defined isospin $I_{Z_b} = 1$, not compatible with the regular bottomonium spectrum, calling for an exotic interpretation.

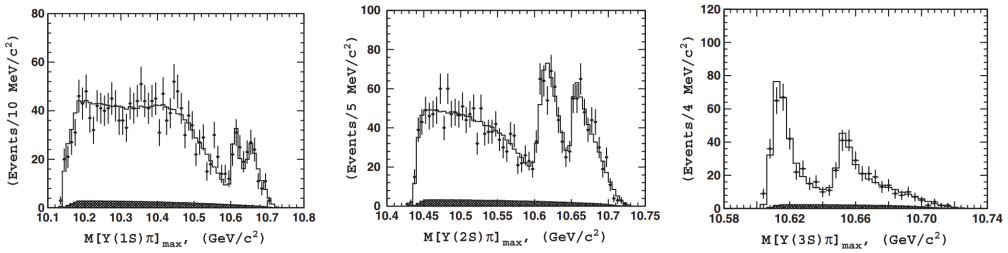

Figure 1.3: *Experimental observation of both the* $Z_b(10610)$ *and the* $Z_b'(10650)$ *resonances in the invariant mass of the* $\Upsilon(1S)\pi$, $\Upsilon(2S)\pi$ *and* $\Upsilon(3S)\pi$ *spectrum, from left to the right [43].*

The angular analyses favour the set of quantum numbers $J^P = 1^+$ for both resonances. On the other hand, theoretical analyses [13, 27] based on Heavy Quark Spin Symmetry predict the existence of two $B\bar{B}^*$ and $B^*\bar{B}^*$ degenerated molecular states with quantum numbers $J^{PC} =$

1^{+-}. Thus, we have assumed in this thesis the $Z_b(10610)/Z_b'(10650)$ to be $B\bar{B}^*$ and $B^*\bar{B}^*$ bound states, respectively, with quantum numbers $J^{PC} = 1^{+-}$ and $I = 1$.

1.2 QCD and its approximate symmetries

The current state-of-the-art of high energy physics is based on the development of Abelian and non-Abelian Gauge Theories. These Quantum Field Theories (QFT) describe the different interactions between elementary particles. The construction of these QFT's relies on the fact that the theory must have definite properties under basic transformations (for instance, Lorentz, parity or charge conjugation transformations, among others). Moreover, the conservation of local gauge symmetries (extra degrees of freedom in the Lagrangian) are imposed as well. Depending on whether these gauge transformations belong to (non-) commutative groups, we talk about (non-) abelian gauge theories. In some cases these local symmetries turn out to be spontaneously broken.

The first success of gauge theories was Quantum ElectroDynamics (QED), where a $U(1)$ local gauge theory is developed (details of this theory can be found in the literature, see for instance [62, 63]). However, weak and strong interactions are assumed to be nonabelian gauge theories; specifically, they are based on the $SU(2)_L \times U(1)_Y$ and $SU(3)_c$ gauge symmetry groups, respectively. This QFT description of the interactions is summarized in the deeply studied Standard Model (see for instance the textbook [63]). The $SU(3)$ nonabelian gauge theory describing the strong interactions is called Quantum ChromoDynamics (QCD) [64, 65]. This name makes reference to the required additional degree of freedom that needs to be added in order to understand the experimental hadron spectrum: the *colour*. The local $SU(3)$ colour gauge symmetry is exact; it is not broken and the strong interactions always preserve colour symmetry.

QCD states that colour, this new degree of freedom, is the basis of strong processes. The force carriers of QCD, called *gluons*, are massless since QCD is a gauge theory. The number of different force carriers are the $SU(3)$ group generators, and thus there are 8 different gluons. The elementary particles that interact via gluon exchanges are called quarks.

Since leptons do not strongly interact, they neither carry a colour charge nor have any quark content. Hadrons, instead, should be composed of quarks. Depending on their valence quark content we can distinguish between mesons ($q\bar{q}$) and baryons (qqq). Despite the inner quarks are *coloured*, the final hadron state is colourless (corresponding to an $SU(3)$ singlet state) since there have not been experimentally observed any coloured particle in a Millikan-like experiment. The analogy with colours that gives name to the theory follows from the following feature. White colour can be obtained from the mixture of three primary colours: red, green and blue. QCD, analogously, imposes that $SU(3)$-singlet final states are *white* while quarks carry a blue/green/red colour charge.

Then, analogously to QED, the QCD Lagrangian is constructed from requiring invariance under local $SU(3)$ colour gauge transformations.

$$\mathcal{L}_{QCD} = \bar{\psi}\left(i\not{D} - m\right)\psi - \frac{1}{4}G^a_{\mu\nu}G^{\mu\nu a}, \tag{1.2.1}$$

being ψ a Dirac spinor that accounts for the quark field, $\not{D}$ the covariant derivative and $G^a_{\mu\nu}$ is the gluon field strength tensor.

However, gauge theories can also manifest other internal *approximate* symmetries; that is, symmetries that only appear in a certain limit and, when this limit is not satisfied, the symmetry is no longer appropriate. In QCD this becomes very useful when solving QCD is not feasible owing to colour confinement and asymptotic freedom. One example of those approximate symmetries

is the famous $SU(3)_L \otimes SU(3)_R$ Chiral Symmetry in the $m_q \to 0$ limit of QCD. The effective field theory based on chiral symmetry, called Chiral Perturbation Theory, has proved itself to be a powerful tool to predict properties of the light hadrons.

In this section, we briefly describe the approximate symmetries of QCD used in this thesis. We classify these symmetries in two different scenarios: those symmetries that appear in the infinity quark mass limit (Heavy Quark Symmetries), and those arising in the massless quark limit (Light Quark Symmetries).

1.2.1 Heavy Quark Symmetries

Since we study heavy mesons (antimesons) in this thesis, we are interested in the $m_Q >> \Lambda_{QCD} \simeq$ 300 MeV limit of QCD. This requirement is well fulfilled by the bottom quark and fine enough for the charm quark. We will show how QCD acquires a new symmetry in this limit and one should expect, in principle, corrections to this approximate symmetry of the order of $\mathcal{O}\left(\frac{\Lambda_{QCD}}{m_Q}\right)$. First we will discuss how the presence of a heavy quark induces a series of simplifications in the QCD Lagrangian. Indeed, in Sect. 2.1 we will explicitly show that in the $m_q \to \infty$ limit, QCD manifests a $SU(2N_h)$ *Heavy Quark Spin Flavour Symmetry (HQSFS)* being N_h the number of flavours infinitely heavy. This QCD limit has been studied for the past decades and many extensive reviews have been written (see, for instance, Refs. [20, 21]).

Here we only review the most important aspects of HQSFS, symmetry that can simplify analyses that involve hadrons containing heavy quarks.

Heavy Quark Spin Flavour Symmetry

Heavy quark dynamics is simpler than the light quark dynamics thanks to the asymptotic freedom of QCD. If the quark is heavy enough, QCD interactions at its Compton's wave length scale are small. However, the light quarks in the hadrons complicate the analysis since asymptotic freedom is no longer enough to describe a bound state composed by a heavy quark (antiquark) and a light antiquark (quark) in the case of mesons; or a heavy quark and two light quarks in the case of single heavy baryons. In these two cases, the size of the hadron is determined by the QCD confinement scale. That is, there is a simple structure associated to the heavy quark and a very complicated structure associated to the light degrees of freedom (Georgi called it the *brown muck* [66]). In this sense, as the heavy quark becomes heavier, the distances to probe the inner structure become smaller. The colour charge of the heavy quark remains the same, because the flux of colour charge is a long distance effect, and therefore mass independent. We will see how other relativistic effects, such as, chromomagnetism becomes negligible as $m_q \to \infty$.

The degrees of freedom of a heavy quark are its spin and its four-velocity (v^μ). This four-velocity is defined, for a given heavy hadron with four-momentum P^μ,

$$P^\mu_{hadron} = m_{hadron}\ v^\mu, \tag{1.2.2}$$

with $v^2 = 1$. If m_Q is large enough, at leading order, we can safely assume

$$m_Q \simeq m_{hadron}, \tag{1.2.3}$$

where the difference does not depend on m_Q, but on a scale determined by the light degrees of freedom in the hadron (Λ_{QCD}, light quark masses, etc.). Therefore, the heavy quark carries the biggest fraction of the four-momentum but there is a small four-momentum q^μ associated to the light degrees of freedom defined as,

$$p^\mu_Q = P^\mu_{hadron} - q^\mu = m_Q v^\mu + k^\mu, \tag{1.2.4}$$

where we have defined the residual momentum $k^\mu = (m_{bound\ state} - m_Q)v^\mu - q^\mu$.

$$\Rightarrow v_Q^\mu = \frac{p_Q^\mu}{m_Q} = v^\mu + \frac{k^\mu}{m_Q}, \tag{1.2.5}$$

which implies that in the infinite quark mass limit,

$$m_Q \to \infty \qquad \Rightarrow \qquad v_Q^\mu \to v^\mu. \tag{1.2.6}$$

This means that QCD interactions do not change the velocity of the heavy quarks, independently of what changes in the hadron are caused by the interaction of the light degrees of freedom. This is the velocity superselection rule: heavy quarks move in straight trajectories in processes mediated by low energy QCD interactions.

On the other hand, as the heavy quark spin only interacts through relativistic effects, *the spin of the heavy quark decouples*, and, in the $m_Q \to \infty$ limit, the configuration of the light degrees of freedom of a heavy hadron that contains a single heavy quark $Q(v, s)$ with spin s and velocity v, does not change if we swap this heavy quark Q with other heavy quark $Q'(v, s')$ with different flavour and/or spin, but same velocity. Both heavy quarks create the same colour static field. It is not even necessary that the two masses m_Q and $m_{Q'}$ are similar. The only important thing is that the masses of the two heavy quarks are large compared to Λ_{QCD}. Hence, if there are N_h flavours of heavy quarks, there is an approximate $SU(2N_h)$ spin-flavour symmetry group.

This symmetry is quite alike to certain atomic properties. For instance, flavour symmetry is analogous to the fact that different isotopes have the same chemical properties, since it is a good approximation to assume that electronic wave functions do not depend on the mass of the nucleus. Spin symmetry is equivalent to assume that atomic hyperfine structure is almost degenerated and, in fact, nuclear spin decouples in the $m_e/m_N \to 0$ limit. These similarities were the basis of the already mentioned Tornqvist's hypothesis of the *deuson*.

Heavy Antiquark-Diquark Symmetry

In this section we introduce another underlying symmetry of QCD (less known than HQSFS) we are calling Heavy Antiquark-Diquark Symmetry (HADS). HADS is a very useful symmetry in the study of doubly heavy-baryons, since HADS relates heavy diquarks with heavy antiquarks. It can be used to establish relations between mesons and baryons, particles with different spin, statistics and baryon number.

The main idea here is that both an antiquark (in mesons) and a colour antisymmetric diquark (in baryons) belong to the same $\bar{3}$ multiplet of the $SU(3)_c$ symmetry group, and form a colour-singlet configuration when they interact with the remaining quark, belonging to the 3 multiplet of $SU(3)_c$. Such relationship was stated in a first place by Miyazawa in the 60s using group theory arguments [67]. However, this symmetry did not experimentally hold since pions and nucleons were supposed to be in the same degenerated multiplet. Later on, when heavy quarks were included in the analysis, the goodness of this symmetry improved, and it was possible to relate properties of hadrons containing a heavy diquark (and a light quark q) to the familiar $\bar{Q}q$ mesons [68]. Next, many other studies in weak decays and computation of matrix elements were also carried out using this argument too [18, 28, 69, 70].

The QCD interaction between two coloured particles forming a colour-singlet, at leading order, only depends on the colour of the two particles, therefore the quark-antiquark interaction in a meson is expected to be the same than the quark-diquark interaction in a baryon. This supposition was confirmed by lattice QCD calculations. The quark-antiquark potential is (approximately) equal to the quark-diquark potential [71]; and the s-wave function of a quark-antiquark pair is the same than the s-wave function of a quark-diquark in a baryon [72].

Nevertheless, this symmetry is naturally broken due to the differences between antiquarks and diquarks. First of all, the antiquark and the corresponding diquark have different masses; therefore their kinematic operators are different. Second, as we have mentioned in the previous section, QCD interactions also include different spin-dependent and velocity-dependent terms (though they are supposed to be suppressed as m_Q increase); and third, while an antiquark is supposed to be point-like (a single quark, clothed by a sea of quark pairs and gluons, does not have to be point-like), the diquark has a finite size. This different finite size might affect the interaction with a quark, especially if the quark-diquark distance is not much larger than the diquark size.

In principle, the presence of heavy quarks should decrease these three effects. In fact, we can estimate the uncertainties due to the latter finite size effects. There are two scales in a quark-diquark system: the quark-diquark distance and the size of the diquark. The size of a heavy diquark can be estimated, assuming a Coulomb-like interaction:

$$V(r) = -\frac{2}{3}\frac{\alpha_s(r)}{r} \qquad \Rightarrow r_{diquark} \simeq \frac{1}{m_Q \alpha_s} \simeq \frac{1}{m_Q v}, \tag{1.2.7}$$

since[1] $\alpha(m_Q) \simeq v$.

On the other hand, the light quark-heavy diquark distance must be much larger, of the order of Λ_{QCD}, and similar to that of a meson composed of a heavy antiquark and a light quark.

Thus, the ratio of the two different scales (the expansion parameter in a hypothetical EFT) in a light quark-heavy diquark system is $\frac{\Lambda_{QCD}}{m_Q v}$. Hence, one expects that the corrections to the relations provided by HADS would be of the order $\mathcal{O}\left(\frac{\Lambda_{QCD}}{m_Q v}\right)$, slightly larger than those arising in HQSS expansions.

1.2.2 Light Quark Symmetries

QCD turned out to be remarkably successful in the understanding of fundamental forces and components. However its characteristic running coupling along with the corresponding confinement problems made impossible to employ perturbative QCD at low energies (of the order of GeV). In fact, neither quarks or gluons seemed to be the appropriate elementary fields of the theory at that scale. Hadronized states are the relevant physical degrees of freedom instead.

This task was partially solved with the development of Chiral Perturbation Theory (ChPT), an adequate EFT that embodies the chiral symmetry properties that spontaneously arise from the QCD Lagrangian in the massless quarks limit. This chiral Lagrangian techniques were first used by Weinberg and Dashen [73, 74] in the late 1960's, and from then many advances in the low energy hadronic spectrum study have been obtained. For a more detailed analysis of the current situation of the theory, see the extensive reports by Scherer [75] and Pich [76], e.g. Here we only comment some important features of the massless quark limit of QCD.

In the relativistic limit of vanishing u, d and s quark masses, the left- and right-handed quark fields q_L and q_R ($q_{R,L} = P_{R,L}q = \frac{1}{2}(1 \pm \gamma_5)\, q$) are decoupled from each other, leading to the chiral limit QCD Lagrangian:

$$\mathcal{L}^0_{QCD} = -\frac{1}{4} G^{\mu\nu}_a G^a_{\mu\nu} + i\bar{q}_L \gamma^\mu D_\mu q_L + i\bar{q}_R \gamma^\mu D_\mu q_R, \tag{1.2.8}$$

being $q = column(u, d, s)$, D_μ the flavour-independent covariant derivative and $G^a_{\mu\nu}$ is the gluon field strength tensor, with a the colour index. For vanishing masses, the operators $P_{R,L}$ project

[1] This relation is derived from the quantization of the angular momentum $\mu v r = \hbar$

onto the positive and negative helicity eigenstates, respectively, what implies identifying chirality and helicity.

The Lagrangian of Eq. (1.2.8) is invariant under independent global $SU(N_f)_L \otimes SU(N_f)_R$ transformations[2].

Despite this chiral symmetry should be good in the light quark sector (u, d, s), it is not experimentally observed in the hadronic spectrum. In fact, there are two important experimental evidences that suggest a spontaneous breaking of this symmetry. The first one is that the masses of the low-lying pseudoscalar mesons are much smaller than the masses of the lightest scalar mesons and the second one is the non-existence of degenerate parity double spectra for the low lying octet baryons. Since the mass of the lightest pseudoscalar mesons is much smaller than the rest of the hadronic spectra, they are candidates for the Goldstone bosons of a spontaneous breaking of the axial symmetry. On the other hand, $SU(3)$ flavour symmetry seems to be reasonably well fulfilled in nature.

Considering all this empirical information, it can be assumed that the global $SU(N_f)_L \otimes SU(N_f)_R$ symmetry spontaneously breaks down to a $SU(N_f)_{L+R} = SU(N_f)_V$ subgroup and, according to the Goldstone theorem, an $SU(N_f)_A$ multiplet of massless Goldstone bosons arises. For three light quarks (u, d, s), the corresponding light pseudoscalar meson octet is:

$$\phi = \sum_{a=1}^{8} \lambda_a \phi^a = \sqrt{2} \begin{pmatrix} \frac{1}{\sqrt{2}}\pi^0 + \frac{1}{\sqrt{6}}\eta & \pi^+ & K^+ \\ \pi^- & -\frac{1}{\sqrt{2}}\pi^0 + \frac{1}{\sqrt{6}}\eta & K^0 \\ K^- & \bar{K}^0 & -\frac{2}{\sqrt{6}}\eta \end{pmatrix}. \tag{1.2.9}$$

Interactions mediated by this pseudoscalar meson octet are constrained by chiral symmetry. On the other hand, the remaining $SU(N_f)_V$ symmetry explains why, in good approximation, hadrons can be grouped in $SU(3)_V$ multiplets. This $SU(3)$-flavour symmetry also guaranties that we can organize not only the heavy meson-antimeson states, but also the molecules formed by them into $SU(3)$-multiplets.

1.3 T-matrix

Before the rise of QCD as the theory that describes the strong interactions, another scheme was widely employed: the S-matrix (or analogously, the T-matrix) formalism. The S-matrix formalism is used to describe scattering processes via unknown short-distance interactions where, long time before and after the interaction, initial and final states can be thought as free particles. The main idea behind the S-matrix formalism is to learn as much as possible of those processes from simple quantum principles and symmetries. The description that follows can be found in the literature, for instance, see Ref [77].

The scattering of an initial state $|i\rangle$ to a final state $|f\rangle$ is described by the probability amplitude S_{fi}, which is the corresponding S-matrix element:

$$S_{fi} = \langle f | S | i \rangle , \tag{1.3.1}$$

being $|i\rangle$ ($|f\rangle$) a vector representing the initial (final) state; and S is the so-called S-matrix, or the evolution operator. Because the total probability of finding the state $|i\rangle$ in any possible final state $|f\rangle$ must be 1, the S operator must be unitary. Thus,

$$SS^\dagger = S^\dagger S = \mathbb{1}, \tag{1.3.2}$$

[2]The Lagrangian of Eq. (1.2.8) has a larger $U(N_f)_L \otimes U(N_f)_R$ global symmetry. However, the $U(1)_A$ part is broken by quantum effects ($U(1)_A$ anomaly), while the quark-number symmetry $U(1)_V$, responsible for the baryon number conservation, is trivially realized in the meson sector.

Since the initial states may not interact, it is also convenient to rewrite the S-matrix:

$$S = \mathbb{1} - iT, \tag{1.3.3}$$

where $\mathbb{1}$ is the identity matrix that accounts for those processes where the initial states do not interact; and T is the T-matrix carrying the information of the interaction. The i factor is placed for later convenience and might be found in a different way in the literature. The requirement of the S-matrix unitarity in Eq. (1.3.2) also imposes further restrictions in the T-matrix:

$$T - T^\dagger = -iT^\dagger T. \tag{1.3.4}$$

We now focus on the scattering of two particles $a + b \to c + d$. The phase space (PS) associated to the process is:

$$PS = \int \frac{d^3\vec{p}_c}{(2\pi)^3 2E_c} \frac{d^3\vec{p}_d}{(2\pi)^3 2E_d} (2\pi)^4 \delta^{(4)}(P - p_c - p_d) = \frac{|\vec{p}\,|}{4\pi E}, \tag{1.3.5}$$

being $p_i = (E_i, \vec{p}_i)$ the four-momentum of the ith-particle, $P = p_a + p_b = p_c + p_d$ is the total four-momentum of the process; E and $|\vec{p}\,|$ are the total energy of the system and the modulus of the three momentum of the particles in the c.m. frame. Then, inserting Eq. (1.3.4) between the $|i\rangle$ and $|f\rangle$ states we get:

$$\langle f|\, T\, |i\rangle - \langle f|\, T^\dagger\, |i\rangle = -i\, \langle f|\, T^\dagger T\, |i\rangle\,, \tag{1.3.6}$$

Including a resolution of the identity $\mathbb{1} = \sum_a (PS\, |a\rangle\, \langle a|)$ in the right hand size, being $|a\rangle$ every possible intermediate state (bound states and continuum states):

$$\langle f|\, T\, |i\rangle - \langle f|\, T^\dagger\, |i\rangle = -i \sum_a PS\, \langle f|\, T^\dagger\, |a\rangle\, \langle a|\, T\, |i\rangle\,, \tag{1.3.7}$$

$$T_{fi} - T^\dagger_{fi} = -i \sum_a T^\dagger_{fa} T_{ai} \frac{|\vec{p}\,|}{4\pi E}. \tag{1.3.8}$$

From here, we can obtain:

$$\frac{|\vec{p}\,|}{8\pi E}\mathbb{1} = -\frac{1}{2i}\left[(T^\dagger)^{-1}(T - T^\dagger)T^{-1}\right] = -\frac{1}{2i}\left(\left(T^{-1}\right)^\dagger - T^{-1}\right) = \mathrm{Im}\left(T^{-1}\right). \tag{1.3.9}$$

This last equation represents the *optical theorem*, which has tremendous consequences in scattering theory. This result establishes that all dynamics of a two-particle scattering process, is contained in the real part of the inverse of the amplitude, since the imaginary part is fixed by unitarity.

We can also relate the T-matrix variable to some quantities such as the phase shifts or the scattering length. Since phase shift analyses are only done in Chapter 4, these relations are discussed there. Here we focus on the analytic properties of the T-matrix and the Lippmann-Schwinger Equation.

1.3.1 Analytic properties of the T-matrix

The T-matrix elements are, in general, a function of the s, t and u Mandelstam variables. These variables are, in principle, restricted to their physical values. Since the physical regions for the s-, t- and u-channels are non-overlapping, there is no reason we cannot define a single amplitude $T(s,t,u)$, whose variables are in three-different disjoint physical regions. We introduce

the hypothesis that this amplitude $T(s,t,u)$ permits an analytic continuation, which (apart from certain specified singularities) allows the amplitude to be defined over the whole s, t and u complex planes. This hypothesis was first suggested by Mandelstam, so it is usually called the Mandelstam hypothesis [78].

The main idea is that the scattering amplitudes have the less singularities as possible, and that the existing singularities are caused by physical reasons. There is a result in complex variable, the Schwarz's reflection principle, which turns out to be very useful here. This principle states that if Γ is a finite segment of the real axis and D a domain of the z complex plane whose intersection with the real axis is Γ then for any function $f(z)$ which is analytic in D and real in Γ, it must be satisfied,

$$f(z^*) = f^*(z), \tag{1.3.10}$$

whenever z and z^* belong to D. It follows from this principle that if the amplitude $T(s,t,u)$ is analytic in a domain extending on both sides of the s-axis on which $\mathrm{ImT}(s,t,u)$ is zero, then $T(s^*,t) = T^*(s,t)$. However we know, from the Optical Theorem, this does not happen for the bound states and the continuum states included in the resolution of the identity, $\mathbb{1} = \sum_a (PS\,|a\rangle\,\langle a|)$. Therefore, the T-matrix cannot be analytic in the entire s-complex plane. There must be a branch cut above the threshold of the process $s_{th} = M_{th}^2$ (also referred as the Right Hand Cut, RHC) and simple poles placed in the mass of the bound states $s_i = M_i^2 < s_{th} = M_{th}^2$.

Since one of the three Mandelstam variables is not independent of the other two, this same analysis can be performed to other channel. The analogous reasoning in the u-channel (for a fixed t-value) states that there should exist a second branch cut (also called Left Hand Cut) below $-t$ and simple poles related to the bound states $s_i = M_i^2$.

For the sake of simplicity, we analyze the situation for a two equal mass (m) particle elastic scattering with one single bound state. The situation is depicted in Fig. 1.4. We can see both the LHC and RHC and the two simple poles derived from a single bound state with mass M.

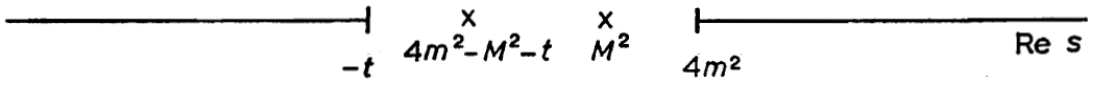

Figure 1.4: *Description of the physically needed singularities of the $T(s,t,u)$ matrix. For this example, a two equal particle elastic scattering is considered. We can observe the two branch cuts, the LHC required for the Optical Theorem in the u-channel and the RHC imposed for unitarity in the s-channel. The two individual poles are required by a bound state with mass M [77].*

Assuming there is no fundamental difference between a bound state and a resonance, other than the matter of stability, we expect that resonances are associated with simple poles of the coupled channel amplitudes. We have just seen, though, that there are not any other singularities in the T-matrix plane beyond bound states, the LHC and RHC. Thus, resonances must appear as simple poles in some unphysical sheet of the s-complex plane. The origin of the unphysical sheet of the s-complex plane is that the mapping between the three-momentum of the particles and s is not unique. This ambiguity is solved using a multivalued definition for the T-matrix elements where the First Riemann Sheet is associated with the physical region while the Second Riemann Sheet is associated with the non-physical one. In this way, we choose:

$$q_I = +\frac{\lambda^{1/2}(s, M_a^2, M_b^2)}{2\sqrt{s}} \tag{1.3.11}$$

$$q_{II} = -\frac{\lambda^{1/2}(s, M_a^2, M_b^2)}{2\sqrt{s}} \tag{1.3.12}$$

with $\lambda(x,y,z) = x^2+y^2+z^2-2xy-2xq-2yz$ the Källén function and q_I and q_{II} the corresponding expression for the three-momentum associated to the s variable in the First (and physical) and Second Riemann Sheet, respectively. Since, above threshold, $T_I(s+i\epsilon) = T_{II}(s-i\epsilon)$ holds, we see that poles close to the real s-axis in the fourth quadrant of the Second Riemann Sheet can have large influence in the physical scattering line.

In conclusion, resonances manifest as simple poles in the unphysical sheet of the T-matrix, above threshold and below the s-axis. Then, we label the resonances with the notation $s_{pole} = s_R - i\Gamma_R\sqrt{s_R}$, where the meaning of s_R and Γ_R becomes obvious when we analyze the probability of a process $|T(s,t,u)|^2$. The T-matrix, in the vicinities of the simple poles (bound states and resonances) can be approximated by,

$$T(s) \simeq \frac{g^2(s_P)}{s - s_P}, \qquad\qquad s \simeq s_P, \tag{1.3.13}$$

where $g(s_P)$ is related to the coupling of the bound state or resonance to the studied channel. If we study $|T(s)|^2$ for resonances we obtain, using $s = E^2$ and $s_P = s_R - i\sqrt{s_R}\ \Gamma_R = E_R^2 - iE_R\Gamma_R$.

$$\begin{aligned} |T(s)|^2 &= \left|\frac{g^2}{E^2 - E_R^2 + i\Gamma_R E_R}\right|^2 = \frac{g^4}{\left(E^2 - E_R^2\right)^2 + E_R^2\Gamma_R^2} \\ &\simeq \frac{\frac{1}{4}\frac{g^4}{E_R^2}}{\left(E - E_R\right)^2 + \frac{1}{4}\Gamma_R^2}, \end{aligned} \tag{1.3.14}$$

which is the form of a Breit-Wigner distribution where $E_R = \sqrt{s_R}$ is the position of the maximum and Γ_R is the half-maximum width. This distribution is depicted in Fig. 1.5.

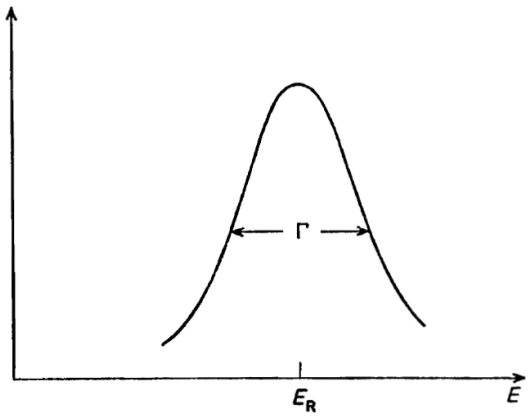

Figure 1.5: *Breit-Wigner shape resonance with half maximum width* Γ *[77].*

As a summary, we have found that the T-matrix is analytic in the physical region of the s complex plane except in the LHC, the RHC and some simple poles whose meaning is related to existence of bound states. Moreover, resonances are present as simple poles in the Second Riemann Sheet of the T-matrix, above threshold and with $\mathrm{Im}\,(T(s)) < 0$.

1.3.2 The Lippmann-Schwinger Equation

In this thesis, we solve the Lippmann-Schwinger Equation (LSE) to compute the T-matrix. The generalization of the LSE for relativistic processes is also found in the literature as the Bethe-Salpeter Equation (BSE). This formalism of the LSE or BSE becomes very useful to supplement perturbative theory in the case of analysis of bound states, since a perturbative series can never generate bound states. The reason for this is that a finite sum of polynomial terms can never present a singularity. This property can intuitively be seen in Eq. (1.3.15), where the singularity only appears when we sum over the infinite terms (*resummation*) of the series.

$$1 + x + x^2 + x^3 + x^4 + ... \simeq \frac{1}{1-x}, \tag{1.3.15}$$

That is the main idea behind solving the LSE, which automatically implements a non-perturbative resummation that could lead to poles in the amplitude. In quantum mechanics, the LSE takes the form (further details can be found in the quantum mechanics textbooks [79, 80]),

$$T(E) = V + VG_0(E)T = V + VG(E)V, \tag{1.3.16}$$

where V represents the potential interaction and $G(G_0)$ is the (free) Green's operator, resolvent or loop function. This equation is equivalent to the Schrödinger Equation with a Hamiltonian $H = H_0 + V$, being H_0 the free Hamiltonian. The free operator $G_0(E)$ is, of course, explicitly known and determined by H_0.

For central potentials, the LSE admits a partial wave decomposition, as discussed in the quantum mechanics textbooks mentioned above. Furthermore, in most cases, the LSE is ill defined in the ultraviolet (UV) limit and it needs to be renormalized. We will address this issue in certain detail in the next chapter.

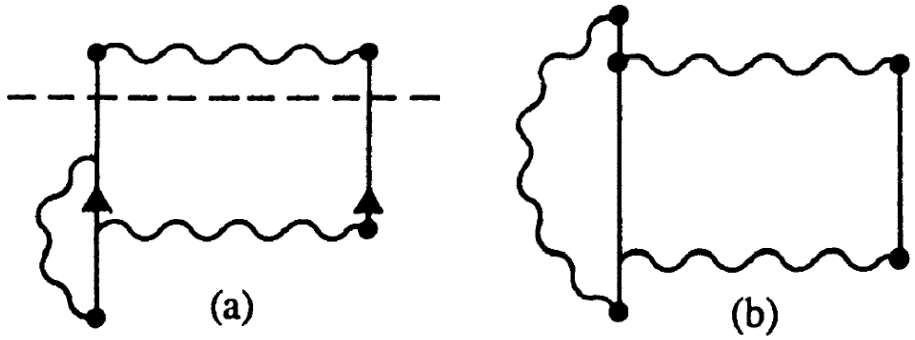

Figure 1.6: *Examples of reducible (left) and irreducible (right) Feynman Diagrams [62].*

A few remarks on the potential V are necessary too. The potential V within an EFT is represented by an infinite sum over Feynman diagrams. The contributing Feynman diagrams are, however, limited by the notion of *reducible interaction kernel*. The reducible interaction kernel is characterized by the fact that these diagrams can be split into two unconnected parts cutting the inner lines. If this cut is not possible, the diagram belongs to the *irreducible interaction kernel*. Examples of both types of diagrams are given in Fig. 1.6. Of course, reducible diagrams can be pictorically obtained from the combination of irreducible diagrams.

For a given order of V in a certain expansion, the LSE leads to a non-perturbative resummation. The scheme is exact and systematically improvable, as long as one computes the kernel V at higher and higher orders in the advocated expansion.

In addition, the solution of the LSE satisfies exact unitarity for any choice of V.

Chapter 2

Heavy Meson-Heavy Antimeson EFT

EFT's are generic theoretical descriptions of low energy phenomena. They become an adequate tool for situations in which a more fundamental description in terms of the underlying dynamics, involving high-energy dynamics, is impractical for whatever reasons. Thus they are very useful for low-energy hadronic processes where quantum chromodynamics (QCD) is not solvable owing to asymptotic freedom and confinement. EFTs include the appropriate degrees of freedom to describe physical phenomena occurring at those regimes, while the ignored substructures and degrees of freedom produce controlled and systematic corrections. In addition, in any EFT there exist certain constrains among the low energy interactions since they must respect the underlying symmetries of the original theory.

In this chapter, we describe the basic elements of our EFT. The key elements in the formulation of the EFT are the effective fields describing the degrees of freedom of the system and the effective interactions that mediate the processes we are interested in. Most of the results displayed in this chapter have already been found in previous works. Here we collect the relevant conclusions we have used in the development of this thesis.

First, we study QCD in the infinite quark mass limit, where the underlying approximate HQSFS manifestly appears. This symmetry is the keystone in the building of the heavy meson-antimeson EFT we are using along this thesis.

In Sect. 2.2, we introduce the meson hyper-fields that include both the pseudoscalar and vector meson (D and D^*) degrees of freedom. There, we will also describe in detail the symmetry transformations (HQSFS, $SU(3)$ light flavour symmetry, charge conjugation...) of these meson (antimeson) hyperfields.

In Sect. 2.3 we discuss the different EFT interactions used to construct the kernel of the Lippmann-Schwinger Equation (LSE), namely, the contact potential and the OPE potential, or that will induce some decays also studied in this work such as radiative interactions. Since these interactions often appear along the thesis, this section is intended to get familiar with some important features of each interaction.

Finally, in Sect. 2.4 we explicitly solve the LSE in some cases. We first discuss (Subsect. 2.4.1) the simplest case, a non-relativistic monochannel diffusion of a momentum-independent potential. A generalization of that analysis with two coupled channels is next considered. In Subsect. 2.4.2, the relations that appear between the cutoff and the contact potential are discussed. Resemblances of these relations to the renormalization group equations of any EFT are stressed. The last Subsect. 2.4.3 is devoted to the solution of the LSE when a $\vec{p}$-dependent potential is employed. In that case, a partial wave analysis and, then, a discretization of the momentum

space to numerically solve the LSE are required.

2.1 Heavy Quark Effective Field Theory

In this section, we describe the simplications that naturally arise in the QCD lagrangian in the infinite quark mass limit. This section can be found more detailed in any review about heavy quark physics such as Refs. [20, 21, 81].

The QCD Lagrangian does not show, explicitly, *Heavy Quark Spin-Flavour Symmetry* when $m_Q \to \infty$. It is sometimes convenient to use an effective field theory for QCD such that HQSFS manifests itself in that limit. This EFT is known as *Heavy Quark Effective Theory* (HQET) and describes the dynamics of hadrons that contain heavy quarks. This theory will only be valid for momenta much smaller than the heavy quark mass.

As pointed out before, the starting point in the construction of HQET is the observation that a very heavy quark bound inside a hadron essentially carries the velocity v ($v^2 = 1$) of the hadron and, therefore, it is almost on-shell. Its momentum can be written as $p = m_Q v + k$, where k is much smaller than $m_Q v$. Interactions of the heavy quark with the light degrees of freedom change this residual momentum by an amount of order $\Delta k \simeq \Lambda_{QCD}$, but the corresponding changes in the heavy quark velocity vanish as $\frac{\Lambda_{QCD}}{m_Q} \to 0$. The usual Dirac propagator for quarks can then be approximated by:

$$i\frac{\not{p} + m_Q}{p^2 - m_Q^2 + i\epsilon} = i\frac{m_Q \not{v} + m_Q + \not{k}}{2m_Q v \cdot k + k^2 + i\epsilon} \to i\frac{1 + \not{v}}{2v \cdot k + i\epsilon} + \mathcal{O}\left(\frac{k}{m_Q}\right), \tag{2.1.1}$$

in the $m_Q \to \infty$ limit. This propagator contains a projection operator P_+, velocity dependent:

$$P_\pm = \frac{1 \pm \not{v}}{2}. \tag{2.1.2}$$

with $P_\pm^2 = P_\pm$ and $P_\pm P_\mp = 0$. It is also convenient to introduce *large* and *small* component fields Q_v and O_v by,

$$Q(x) = e^{-im_Q v \cdot x}\left[Q_v(x) + O_v(x)\right], \tag{2.1.3}$$

being

$$Q_v(x) = e^{im_Q v \cdot x} P_+ Q(x) \qquad O_v(x) = e^{im_Q v \cdot x} P_- Q(x). \tag{2.1.4}$$

The exponential prefactor is introduced so we can subtract the $m_Q v^\mu$ four-momentum of the heavy quark and, in this way, derivatives acting in the fields produce the small residual momentum k. The new fields satisfy (using the anticommutation relation $\gamma^\mu\gamma^\nu + \gamma^\mu\gamma^\nu = 2g^{\mu\nu}$ is straightforward):

$$\begin{cases} \not{v} Q_v = Q_v \\ \not{v} O_v = -O_v \end{cases} \quad \Rightarrow \quad \begin{cases} \bar{Q}_v i\not{D} Q_v = \bar{Q}_v iv \cdot D Q_v \\ \bar{O}_v i\not{D} O_v = -\bar{O}_v iv \cdot D O_v \end{cases}. \tag{2.1.5}$$

where the covariant derivative $D^\mu = \partial^\mu + igT_a A_a^\mu$, and with T_a the Gell-Mann matrices and A_a^μ the gluon field. Substituting these new fields in the QCD Lagrangian:

$$\begin{aligned} \mathcal{L}_Q &= \bar{Q}\left(i\not{D} - m_Q\right)Q = \\ &= e^{im_Q v \cdot x}\left[\bar{Q}_v + \bar{O}_v\right]\left(i\not{D} - m_Q\right)e^{-im_Q v \cdot x}\left[Q_v + O_v\right] = \\ &= \left[\bar{Q}_v + \bar{O}_v\right]\left(i\not{D} - m_Q + m_Q\not{v}\right)\left[Q_v + O_v\right] = \\ &= \bar{Q}_v i\not{D} Q_v + \bar{O}_v(i\not{D} - 2m_Q)O_v + \bar{Q}_v i\not{D} O_v + \bar{O}_v i\not{D} Q_v. \end{aligned} \tag{2.1.6}$$

Using Eq. (2.1.5),

$$\mathcal{L}_Q = \bar{Q}_v iv\cdot DQ_v - \bar{O}_v(iv\cdot D + 2m_Q)O_v + \bar{Q}_v i\not{D}O_v + \bar{O}_v i\not{D}Q_v. \tag{2.1.7}$$

It is also convenient to rewrite the covariant derivative in its parallel and perpendicular components to the velocity v. The perpendicular component to the velocity is given for every four-momentum X^μ by:

$$X^\mu_\perp = X^\mu - X\cdot v\ v^\mu \qquad \Rightarrow \qquad X_\perp \cdot v = 0. \tag{2.1.8}$$

Then, as $\bar{Q}_v v\cdot D\not{v}O_v = 0$ is trivially satisfied, we can substitute $i\not{D} \to i\not{D}_\perp$ in Eq.(2.1.7):

$$\Rightarrow \mathcal{L}_Q = \bar{Q}_v iv\cdot DQ_v - \bar{O}_v(iv\cdot D + 2m_Q)O_v + \bar{Q}_v i\not{D}_\perp O_v + \bar{O}_v i\not{D}_\perp Q_v. \tag{2.1.9}$$

We can now simplify Eq.(2.1.9) using the equation of motion. The Dirac equation for the quark field $Q(x)$ is:

$$(i\not{D} - m_Q)Q(x) = 0. \tag{2.1.10}$$

Rewriting this equation in terms of Q_v and O_v:

$$\begin{aligned} 0 \quad &= (i\not{D} - m_Q)Q = (i\not{D} - m_Q)\left\{e^{-im_Q v\cdot x}\left[Q_v + O_v\right]\right\} = \\ &= (i\not{D} - m_Q + m_Q\not{v})\left[Q_v + O_v\right] = \\ &= (i\not{D} - 2P_- m_Q)\left[Q_v + O_v\right] = \\ &= i\not{D}Q_v + (i\not{D} - 2m_Q)O_v, \end{aligned}$$

Multiplying this equation for $(1-\not{v})$:

$$(1-\not{v})i\not{D}Q_v = -(1-\not{v})(i\not{D} - 2m_Q)O_v. \tag{2.1.11}$$

The left hand side is:

$$\begin{aligned} (1-\not{v})i\not{D}Q_v \quad &= \quad i\left(\not{D} - \not{v}\not{D}\right)Q_v = i\left[\not{D} - (2v\cdot D - \not{D}\not{v})\right]Q_v = \\ &= 2i(\not{D} - v\cdot D)Q_v = \\ &= 2i\not{D}_\perp Q_v. \end{aligned} \tag{2.1.12}$$

And the right hand side:

$$\begin{aligned} -(1-\not{v}) \quad (i\not{D} - 2m_Q)O_v &= -(i\not{D} - 2m_Q - i\not{v}\not{D} + 2m_Q\not{v})O_v = \\ &= -(i\not{D} - 2m_Q - i2v\cdot D + i\not{D}\not{v} + 2m_Q\not{v})O_v = \\ &= -(i\not{D} - 2m_Q - i2v\cdot D - i\not{D} - 2m_Q)O_v = \\ &= 2(iv\cdot D + 2m_Q)O_v. \end{aligned} \tag{2.1.13}$$

Putting everything together, the equation of motion is:

$$i\not{D}_\perp Q_v = (iv\cdot D + 2m_Q)O_v, \tag{2.1.14}$$

thus we can express the O_v field as a function of the field Q_v:

$$O_v = \frac{i\not{D}_\perp}{iv\cdot D + 2m_Q + i\epsilon}Q_v, \tag{2.1.15}$$

and we can conclude that the leading order effects will be caused by $Q_v(x)$ because $O_v(x)$ effects are suppressed by powers of $1/m_Q$. Introducing Eq. (2.1.15) into Eq. (2.1.9):

$$\begin{aligned}\mathcal{L}_Q &= \bar{Q}_v iv\cdot DQ_v + \bar{Q}_v \frac{\left(i\not{D}_\perp\right)\left(i\not{D}_\perp\right)}{-iv\cdot D+2m_Q-i\epsilon}Q_v + \\ &\quad + \bar{Q}_v \frac{i\not{D}_\perp i\not{D}_\perp}{iv\cdot D+2m_Q+i\epsilon}Q_v + \bar{Q}_v \frac{(-1)i\not{D}_\perp i\not{D}_\perp}{-iv\cdot D+2m_Q+i\epsilon}Q_v = \\ &= \bar{Q}_v\left(iv\cdot D - \frac{\not{D}_\perp\not{D}_\perp}{iv\cdot D+2m_Q+i\epsilon}\right)Q_v = \\ &= \bar{Q}_v\left(iv\cdot D - \frac{1}{2m_Q}\not{D}_\perp\not{D}_\perp\right)Q_v + \mathcal{O}\left(\frac{1}{m_Q^2}\right). \end{aligned} \tag{2.1.16}$$

Even more, using $\gamma^\mu\gamma^\nu = \frac{1}{2}\left(\{\gamma^\mu,\gamma^\nu\}+[\gamma^\mu,\gamma^\nu]\right) = g^{\mu\nu}+\frac{1}{2}[\gamma^\mu,\gamma^\nu] = g^{\mu\nu}-i\sigma^{\mu\nu}$,

$$\begin{aligned}\Rightarrow \not{D}_\perp\not{D}_\perp &= D_\perp^2 + \frac{1}{2}[\gamma_\mu,\gamma_\nu]D_\perp^\mu D_\perp^\nu = D_\perp^2 - i\sigma_{\mu\nu}D_\perp^\mu D_\perp^\nu = \\ &= D_\perp^2 - i\sigma_{\mu\nu}\left(\frac{1}{2}[D_\perp^\mu, D_\perp^\nu]\right). \end{aligned} \tag{2.1.17}$$

Introducing this last expression into Eq. (2.1.16):

$$\begin{aligned}\mathcal{L}_Q &= \bar{Q}_v\left(iv\cdot D - \frac{1}{2m_Q}\left(D_\perp^2 - i\sigma_{\mu\nu}\left(\frac{1}{2}[D_\perp^\mu, D_\perp^\nu]\right)\right)\right)Q_v \\ &\quad + \mathcal{O}\left(\frac{1}{m_Q^2}\right). \end{aligned} \tag{2.1.18}$$

We can replace $D_\perp \to D$ in the $\sigma_{\mu\nu}$ term since $\bar{Q}_v\sigma_{\mu\nu}v^\mu Q_v = 0$ and thus we obtain.

$$\begin{aligned}\mathcal{L}_Q &= \bar{Q}_v\left(iv\cdot D - \frac{1}{2m_Q}\left(D_\perp^2 - i\sigma_{\mu\nu}\left(\frac{1}{2}[D^\mu, D^\nu]\right)\right)\right)Q_v + ... = \\ &= \bar{Q}_v\left(iv\cdot D - \frac{1}{2m_Q}\left(D_\perp^2 - \frac{g}{2}\sigma_{\mu\nu}G^{\mu\nu}\right)\right)Q_v + ..., \end{aligned} \tag{2.1.19}$$

being $G^{\mu\nu} = G_a^{\mu\nu}T_a = +\frac{i}{g}[D^\mu, D^\nu]$ the gluon field strength tensor. In the above expression, the terms that will be neglected at leading order can be easily interpreted in the rest frame. The first term:

$$\mathcal{L}_{kin} = \frac{1}{2m_Q}\bar{Q}_v(iD_\perp)^2Q_v \qquad \to \qquad -\frac{1}{2m_Q}\bar{Q}_v(i\vec{D})^2Q_v, \tag{2.1.20}$$

is the gauge covariant extension of the kinetic energy operator that arises from the residual momentum off-shell (k). On the other hand, the second operator is the analogous term to the non-abelian Pauli interacting term describing the heavy quark spin interaction with a gluon.

$$\mathcal{L}_{mag} = \frac{g}{4m_Q}\bar{Q}_v(\sigma_{\mu\nu}G^{\mu\nu})^2Q_v \qquad \to \qquad -\frac{g}{m_Q}\bar{Q}_v(\vec{S}\cdot\vec{B}_c)Q_v, \tag{2.1.21}$$

where the spin operator $\vec{S}$ is defined as:

$$S^i = \frac{1}{2}\begin{pmatrix}\sigma^i & 0\\ 0 & \sigma^i\end{pmatrix} = \frac{1}{2}\gamma_5\gamma^0\gamma^i, \tag{2.1.22}$$

and $B_c^i = -\frac{1}{2}\epsilon^{ijk}G^{jk}$ are the components of the gluon chromomagnetic field. This hyperfine *chromomagnetic* interaction is a relativistic effect which is suppressed by a factor $1/m_Q$. This is the origin of the Heavy Quark Spin Symmetry. As an example, the splitting between the spin 0 and spin 1 heavy-light mesons is small because is suppressed by $\frac{1}{m_Q}$. Furthermore, the decoupling of the heavy quark spin means that in the limit $m_Q \to \infty$, the structure of the light degrees of freedom in the 0^- and 1^- states is identical.

Finally, at leading order, the effective Lagrangian is:

$$\mathcal{L}_Q = \bar{Q}_v(iv \cdot D)Q_v. \tag{2.1.23}$$

This Lagrangian is manifestly independent of both the heavy quark flavour and the heavy quark spin. From this Lagrangian we can obtain the same propagator for the Q_v field than before:

$$\left(\frac{1+\not{v}}{2}\right)\frac{i}{v \cdot k + i\epsilon}. \tag{2.1.24}$$

For a quark-quark-gluon interacting vertex, we obtain at leading order:

$$igT_a\gamma^\mu \to igT_a v^\mu, \tag{2.1.25}$$

If there were N_h heavy quark flavours, the corresponding Lagrangian density would be, at LO:

$$\mathcal{L}_Q^{eff} = \sum_{i=1}^{N_h} \bar{Q}_v^{(i)}\,(iv \cdot D)\,Q_v^{(i)}, \tag{2.1.26}$$

where every heavy quark must have the same velocity v.

This effective Lagrangian density for heavy quarks does not depend neither on the heavy quark flavour nor the heavy quark spin. Hence, it explicitly manifests the spin-flavour $SU(2N_h)$ symmetry. As it can be seen from the derivation, corrections caused by next-to leading order effects are of the order $\mathcal{O}\left(\frac{k}{m_Q}\right) \simeq \mathcal{O}\left(\frac{\Lambda_{QCD}}{m_Q}\right)$.

2.2 Covariant representation of the mesonic fields

The consequences of Heavy Quark Spin Symmetry for the hadronic matrix elements may be derived using the commutation relations of Isgur and Wise [18, 19], or more compactly using the trace-formalism [82]. HQSS implies that the pseudoscalar D (B) meson is degenerate with the vector D^* (B^*) meson; and both mesons should be treated in equal footing. Hence, both pseudoscalar and vector mesons should be part of the non-relativistic superfield used in the effective field theory to account for the heavy-light meson degrees of freedom. The content of this section can be found with more detail in the reviews of Refs. [20, 21, 81].

The Heavy Quark Effective Theory (HQET) eigenstates are "would-be" hadrons composed by a heavy quark and the *brown muck* (meaning everything related to the light degrees of freedom: light quarks, light antiquarks and gluons). In that case, heavy quarks and the *brown muck* have transformation properties well defined under the Lorentz group. Therefore, our mesonic fields must be constructed so they respect those transformation properties.

The fundamental state of a $Q\bar{q}$ meson can be represented by a non-relativistic matrix field $H_v^{(Q)}$ that annihilates mesons (it does not create them since it is a non-relativistic field). This hyperfield behaves as a bilinear under Lorentz transformations [21],

$$H_{v'}^{(Q)'}(x') = D(\Lambda)H_v^{(Q)}(x)D(\Lambda)^{-1}, \tag{2.2.1}$$

where

$$v' = \Lambda v \qquad x' = \Lambda x, \tag{2.2.2}$$

and $D(\Lambda)$ is the matrix representation of the Lorentz transformation Λ in the Dirac space. Equivalently, we have,

$$H_v^{(Q)}(x) \to H_v^{(Q)'}(x) = D(\Lambda) H^{(Q)}_{\Lambda^{-1}v}(\Lambda^{-1}x) D(\Lambda)^{-1}. \tag{2.2.3}$$

The hyperfield $H_v^{(Q)}(x)$ should be a linear combination of the pseudoscalar field $P_v^{(Q)}(x)$ and the vector field $P^{*(Q)}_{v\mu}(x)$. The vector particles have a polarization vector ϵ_μ that satisfies $\epsilon \cdot \epsilon = -1$, and $v \cdot \epsilon = 0$. One of the possible combinations of both fields with the desired transformation properties is:

$$H_v^{(Q)}(x) = \frac{1+\not{v}}{2}\left[\not{P}^{*(Q)}_v - P_v^{(Q)}\gamma_5\right], \qquad v \cdot P^{*(Q)} = 0. \tag{2.2.4}$$

This definition is consistent with $P_v^{(Q)}$ and $P_v^{*(Q)}$ behaving as pseudoscalar and vector fields, respectively; since γ_5 and γ_μ transform pseudoscalars and vectors into bispinors, respectively. The $\frac{1+\not{v}}{2}$ projector retains only the particle components of the heavy quark Q. The sign and relative phase between the P and P^* terms is arbitrary, and it depends on the phase election between pseudoscalar and vector states. The pseudoscalar is multiplied by γ_5 rather than unity, to be consistent with the parity transformation law,

$$H_v^{(Q)}(x) \to \gamma^0 H^{(Q)}_{v_P}(x_P)\gamma^0 \tag{2.2.5}$$

where $x_P = \left(x^0, -\vec{x}\,\right)$ and $v_P = \left(v^0, -\vec{v}\,\right)$. The field $H_v^{(Q)}(x)$ satisfies the constraints,

$$\not{v} H_v^{(Q)} = H_v^{(Q)}, \qquad H_v^{(Q)}\not{v} = -H_v^{(Q)}. \tag{2.2.6}$$

It is also convenient to introduce the conjugated field, which is also transformed as a bispinor under Lorentz transformations:

$$\bar{H}_v^{(Q)}(x) = \gamma^0 H_v^{(Q)\dagger}(x)\gamma^0 = \left[\not{P}^{*(Q)\dagger}_v + P_v^{(Q)\dagger}\gamma_5\right]\frac{1+\not{v}}{2}, \qquad v \cdot P^{*(Q)} = 0. \tag{2.2.7}$$

$$\bar{H}_v^{(Q)}(x) \to \bar{H}_v^{(Q)'}(x) = D(\Lambda)\bar{H}^{(Q)}_{\Lambda^{-1}v}(\Lambda^{-1}x)D(\Lambda)^{-1}, \tag{2.2.8}$$

For mesons containing a heavy antiquark, the corresponding hyperfield is:

$$H_v^{(\bar{Q})}(x) = \left[\not{P}^{*(\bar{Q})}_v - P_v^{(\bar{Q})}\gamma_5\right]\frac{1-\not{v}}{2}, \qquad \bar{H}_v^{(\bar{Q})}(x) = \gamma^0 H_v^{(\bar{Q})\dagger}(x)\gamma^0. \tag{2.2.9}$$

This definition for $H_a^{(\bar{Q})}$ also specifies our convention for charge conjugation, which is $\mathcal{C}P_a^{(Q)}\mathcal{C}^{-1} = P^{(\bar{Q})a}$ and $\mathcal{C}P^{*(Q)}_{a\mu}\mathcal{C}^{-1} = -P^{*(\bar{Q})a}_\mu$, which leads to,

$$\mathcal{C}H_a^{(Q)}\mathcal{C}^{-1} = CH^{a(\bar{Q})T}C^{-1} \qquad \mathcal{C}\bar{H}^{(Q)a}\mathcal{C}^{-1} = C\bar{H}_a^{(\bar{Q})T}C^{-1}, \tag{2.2.10}$$

with C the Dirac space charge conjugation matrix, $C\ \gamma_\mu\ C^{-1} = -\gamma_\mu^T$.

The transformations of $H^{(Q)}$ and $H^{(\bar{Q})}$ under the underlying approximate symmetries of QCD discussed in the previous chapter are:

$$H_a^{(Q)} \to S\left(H^{(Q)}U^\dagger\right)_a, \qquad H^{(\bar{Q})a} \to \left(UH^{(\bar{Q})}\right)^a S^\dagger, \tag{2.2.11}$$

$$\bar{H}^{(Q)a} \to \left(U\bar{H}^{(Q)}\right)^a S^\dagger, \qquad \bar{H}^{(\bar{Q})a} \to S\left(\bar{H}^{(\bar{Q})}U^\dagger\right)^a, \tag{2.2.12}$$

where S is a heavy quark spin transformation and U a light quark flavour rotation whose a index is an $SU(2)$ or $SU(3)$ index depending on whether the strange quark is considered a light quark or not.

It is also important mentioning that in our normalization the heavy meson or antimeson fields, $H^{(Q)}$ or $H^{(\bar{Q})}$ have dimensions of $E^{3/2}$ (see [21] for details). This is because we use a non-relativistic normalization for the heavy mesons, which differs from the traditional relativistic one by a factor $\sqrt{M_H}$. This different normalization causes the inclusion of extra factors in the vertices of the Feynman diagrams.

2.3 Heavy Meson-Heavy Antimeson Effective Lagrangians

As discussed above, the formulation of an EFT to study heavy meson molecules requires the identification of the degrees of freedom and symmetries that are relevant for the low energy dynamics. The EFT description of heavy mesonic molecules involves the adequate hadron fields and the interactions among these degrees of freedom that are compatible with the known low energy symmetries, most notably HQSFS and chiral symmetry. As in the nucleon-nucleon system, the low energy interaction between a pair of heavy mesons is mediated by pion exchanges, which in turn are constrained by chiral symmetry. In content, the nature of the short range interaction remains unknown, but we can parametrize it in terms of contact-range operators between the heavy mesons. A remarkable simplification is that pion exchanges are weaker than in the nuclear case [11, 25] owing to the smaller light quark content of the heavy mesons in comparison to the nucleons. This means that pions produce subleading effects that can be perturbatively treated [11]. A similar feature applies to coupled channel dynamic effects [11, 25].

From this, it is expected that the EFT description of heavy meson molecules will simplify at lowest order to a contact range theory, at least for a certain binding energy window. The EFT approach provides the possibility of constructing generic and systematic descriptions of arbitrary low energy process. To clarify these concepts we reproduce here a part of the discussion outlined in [25]. The EFT idea is simple: we identify the fields and symmetries that are relevant at low energies and construct all possible interactions compatible with them. Even though the number of interactions is infinite, they can be classified according to their importance at low energies by means of power counting, the ordering principle of EFTs. If Q is the soft (low energy) scale of the system we are describing and Λ_0 the hard (high energy) scale, power counting allows us to express any physical quantity as a power series in terms of the small parameter $x_0 = \frac{Q}{\Lambda_0}$.

For illustrating this idea let us consider a physical quantity A that we want to compute in the EFT framework. This quantity receives, in principle, contributions from all the relevant diagrams involving the low energy fields and compatible with the low energy symmetries:

$$A(Q, \Lambda_0) = \sum_D A^{(D)}(Q, \Lambda_0). \tag{2.3.1}$$

However, the different diagrams have different scaling properties that can be used for ordering the sum above. For example, we have the canonical dimension of A, which is defined as,

$$A^{(D)}(\lambda Q, \lambda\Lambda_0) = \lambda^{d_A} A^{(D)}(Q, \Lambda_0) \tag{2.3.2}$$

and is the same for all the EFT contributions to A. But the interesting scaling property is power

counting, which refers to the behaviour under a transformation of the type $Q \to \lambda Q$,

$$A^{(D)}(\lambda Q, \Lambda_0) = \lambda^{\nu_D} A^{(D)}(Q, \Lambda_0), \tag{2.3.3}$$

where ν_D is the order of the contribution D, which is bounded from below (i.e., $\nu_D \geq \nu_0$). The sum of diagrams above can be reorganized as an expansion in terms of increasing scaling dimension:

$$A(Q, \Lambda_0) = \sum_{\nu \geq \nu_0} A^{(\nu)}(Q, \Lambda_0), \tag{2.3.4}$$

where, for simplicity, we suppress the D subscripts and superscripts. For each order ν there is only a finite number of diagrams that contributes to the quantity A. Combining the scaling laws of Eqs.(2.3.2) and (2.3.3) we obtain a well-defined power series for A,

$$A(Q, \Lambda_0) = \Lambda_0^{d_A} \sum_{\nu \geq \nu_0} \left(\frac{Q'}{\Lambda_0}\right)^{\nu} \hat{A}^{(\nu)}\left(\frac{Q}{Q'}\right) = \Lambda_0^{d_A} \sum_{\nu \geq \nu_0} x_0^{\nu} \hat{A}^{(\nu)}\left(\frac{Q}{Q'}\right), \tag{2.3.5}$$

with $\hat{A}^{(\nu)}$ a dimensionless quantity that we expect to be of the order of unity (i.e., Q^0). Notice that $\hat{A}^{(\nu)}$ does not depend on the hard scale Λ_0 and is related to $A^{(\nu)}$ via Eqs. (2.3.2) and (2.3.3). In the formula above, Q' is an auxiliary soft scale we use to express $\hat{A}^{(\nu)}$ as a function of a dimensionless ratio. Provided there is a clear scale separation in the system, that is, $\Lambda_0 \geq Q$, the power series above will be convergent. Not only that, if we consider only contributions from diagrams with $\nu < \nu_{max}$, the error of the EFT calculation will be $x_0^{\nu_{max}+1}$. In this thesis, we will only perform calculations at the lowest order and we expect a relative error of the order of x_0 in the calculations to follow.

If we are interested in the low energy description of heavy meson-antimeson bound states, the relevant physical object we want to expand is the (non-relativistic) potential between the heavy meson and antimeson:

$$V = \sum_{\nu=\nu_0}^{\nu_{max}} V^{(\nu)} + \mathcal{O}\left(x_0^{\nu_{max}+1}\right). \tag{2.3.6}$$

The expansion starts at order $\nu_0 \geq -1$, where x_0 is the ratio between the soft and hard scales of the system. The low energy degrees of freedom we consider are the light structure of the heavy meson and antimeson fields and the pion field. The pion-meson vertices are constrained by chiral symmetry. In turn, HQSS generates strong constraints on the form of the heavy meson-antimeson interactions. This means that the EFT potential includes two kind of contributions: contact range interactions, i.e., four meson vertices, and pion exchanges. The set of soft scales Q includes, in principle, the pion mass m_π and the center-of-mass momenta $\vec{p}$ and $\vec{p}\,'$ of the meson and antimeson. The hard scale Λ_0 can represent the momentum scale at which we expect the low energy symmetries to break down, i.e., the chiral symmetry breaking scale $\Lambda_\chi = 4\pi f_\pi \simeq 1$ GeV (with f_π the pion decay constant) for chiral symmetry and the heavy quark mass m_Q for HQSS, but it can also stand for the momentum scale at which the composite structure of the heavy mesons starts to be resolved.

The existence of bound states implies changes in the power counting of the potential. This can be easily appreciated by considering the bound state equation

$$|\Psi_B\rangle = G_0(E) V |\Psi_B\rangle, \tag{2.3.7}$$

where $|\Psi_B\rangle$ is the wave function of the bound state, $G_0(E) = 1/(E - H_0)$ the resolvent operator and V the non-relativistic potential. If we require the existence of a bound state, then it is

apparent that the successive iterations of G_0V to be of the same order,

$$\mathcal{O}(G_0V) = \mathcal{O}(G_0VG_0V)\,. \tag{2.3.8}$$

If we take into account that $G_0(E)$ is of order Q in loops[1], it is clear that the existence of bound states requires that the EFT potential contains a contribution of order Q^{-1}. Thus the presence of shallow bound states or large scattering lengths in a two-body system requires the non-perturbative treatment of a piece of the effective potential. There exists a problem then: the EFT potential due to OPE and constrained by chiral symmetry starts at order Q^0 and is therefore incompatible with the EFT description of a low energy bound state.

The solution is to redefine power counting by promoting the C_0 contact range operator from order Q^0 to Q^{-1} [83, 84, 85, 86, 87]. This is equivalent to assume that the C_0 operator is contaminated by a low energy scale. If we regularize the EFT potential with a cutoff Λ, and set the value of $C_0(\Lambda)$ to reproduce the position of the bound state, we obtain a generic result,

$$\frac{1}{C_0(\Lambda)} \sim \frac{\mu}{2\pi}\left(\gamma_B - \frac{2}{\pi}\Lambda\right), \tag{2.3.10}$$

where μ is the reduced mass of the two-body system and $\gamma_B = \sqrt{-2\mu E_B}$ the wave number (with E_B the bound state energy) and Λ some UV momenta cutoff. Of course, the exact form of the relation depends on the specific regularization scheme employed, but it will be in line of the previous form.

For a shallow bound state $\gamma_B \sim Q$, it is evident that we can only have $C_0 \sim Q^{-1}$ as long as the UV cutoff Λ scales like $\mathcal{O}(Q)$. Note that this is consistent with our requirement that every momenta involved should be soft and smaller than the charm quark mass to make sense of HQSS. In this case, for the naive identification $\mu \sim \Lambda_0$, we obtain that C_0 should scale as,

$$C_0(Q) \sim \frac{1}{Q\Lambda_0}, \tag{2.3.11}$$

being the wave number γ_B and the momentum cutoff the light scales contaminating C_0.

There is still a significant simplification in the EFT potential that we have not discussed yet. Heavy pseudoscalar and vector mesons P and P^* are only degenerate in the infinite quark mass limit $m_Q \to \infty$. For a finite mass m_Q there is a mass splitting between the heavy hadrons,

$$M_{P^*} - M_P = \Delta_Q, \tag{2.3.12}$$

that scales as $\frac{1}{m_Q}$. As a consequence of this mass gap, the two $H\bar{H}$ thresholds in the 0^{++} ($P\bar{P}$ and $P^*\bar{P}^*$) and 1^{+-} ($P\bar{P}^*$ and $P^*\bar{P}^*$) coupled channels lay at different energies. If we are interested in low lying bound states, the energy difference between the two thresholds may actually be considerably larger than the binding energy of the states within the EFT framework. This means we may very well entitled to ignore the coupled channel effects [25]. The momentum scale associated with each coupled channel is,

$$\Lambda_C(0^{++}) = \sqrt{2\mu(2\Delta_Q)}, \tag{2.3.13}$$

[1]This can be trivially checked by considering the rescaling transformation,

$$\int \frac{d^3\vec{q}}{(2\pi)^3} G_0\left(\lambda^2 E\right) = \lambda \int \frac{d^3\vec{q}}{(2\pi)^3} G_0\left(E\right) \tag{2.3.9}$$

where the energy rescales as λ^2 as we are considering a non-relativistic system.

being $D\bar{D}$ and the $D^*\bar{D}^*$ states the coupled channels and,

$$\Lambda_C(1^{+-}) = \sqrt{2\mu\Delta_Q}, \tag{2.3.14}$$

where the coupled channels are in this case the $D\bar{D}^*$ and the $D^*\bar{D}^*$ states; for the 0^{++} and 1^{+-} cases respectively, where μ is the reduced mass of the $H\bar{H}$ heavy meson system and Δ_Q is the energy gap. The associated momentum scale is similar in the charm and bottom sectors. This can be easily understood if we consider the $m_Q \to \infty$ limit, in which we expect $\mu \sim m_Q$ and $\Delta_Q \sim \frac{1}{m_Q}$, leading to $\Delta_C \sim m_Q^0$. Thus, the suppression of the coupled-channel effects is basically independent of the heavy quark mass. In the particular case of the charm mesons, direct evaluation yields $\Lambda_{C(0^{++})} \sim 750$ MeV and $\Lambda_{C(1^{+-})} \sim 520$ MeV. If we have a 0^{++} $D\bar{D}$ (1^{+-} $D^*\bar{D}$) bound state at threshold, the corresponding 0^{++} $D^*\bar{D}^*$ (1^{+-} $D^*\bar{D}^*$) component will have a wave number at least of the order of the UV cutoff. Thus there is no problem in ignoring the coupled channel structure and treating the two particle channels in the 0^{++} and 1^{+-} cases as independent. From a more formal EFT viewpoint what we are doing is to consider the coupled channel momentum scale as $\Lambda_C \sim \mathcal{O}(Q^0)$, from which we expect the G_0 operator involved in the particle mixing to scale like Q^3. This translates into a suppression of particle coupled channel effects by two orders in the expansion: if we count on the C_0 operator as Q^{-1}, then particle coupled channels do not enter until order Q, that is, at least one order beyond pion exchanges, as we will see.

On the other hand, the influence of three-body $D\bar{D}\pi$ interactions on the properties of the $X(3872)$ was found to be moderate in a Faddeev approach [88].

Hence, at LO, the EFT describing the interaction between a heavy meson and a heavy antimeson is a contact potential. Other effects are next-to-leading-order effects which are accounted in the error of the leading order contribution.

2.3.1 Contact Lagrangian $P^{(*)}\bar{P}^{(*)} \to P^{(*)}\bar{P}^{(*)}$ (hidden heavy sector)

According to the previous arguments, at LO in the EFT expansion the potential only contains energy- and momentum- independent s-wave contact range interactions. To describe the dynamics of s-wave hidden charm or bottom molecules composed of $P^{(*)}\bar{P}^{(*)}$ mesons, one needs, in principle, eight counter-terms for each isospin-strangeness sector (once you take into account C-parity symmetry). However, HQSS reduces the number of independent low energy constants to two, which we call C_A and C_B [22]. As we will see, $SU(3)$ flavour symmetry generates additional relations among the heavy meson-antimeson interactions in sectors with different light content. Indeed, it turns out that four parameters are enough to describe the twenty-four possible s-wave molecular configurations[2].

LO potential mixes the different particle channels but HQSS induces relations among them. The reason is that the P ($\bar{P}$) and P^* ($\bar{P}^*$) mesons (antimesons) can be transformed into each other by means of a flip of the spin of the heavy quark. Nevertheless, the total angular momentum and parity of a heavy meson molecule is conserved.

The most general Lagrangian that can be written involving two and four heavy meson terms is,

$$\mathcal{L} = \mathcal{L}_{2H} + \mathcal{L}_{4H}, \tag{2.3.15}$$

[2]This is the total dimension, without considering the spin-isospin third component multiplicities of the $H\bar{H}$ space ($H = D^+, D^0, D_s^0, D^{*+}, D^{*0}$ and D_s^{*0} in the charm sector) or states that are connected by a C-parity transformation, such as $D_s\bar{D}$ and $\bar{D}_s D$ that are not counted twice.

$\mathcal{L}_{2H}$ is, at LO, already known and takes the form [89, 90, 91]:

$$\begin{aligned}\mathcal{L}_{2H} &= -\mathrm{Tr}\left[\bar{H}^{(Q)}\left(iv\cdot D+\frac{D^2}{2m_Q}\right)H^{(Q)}\right]+\frac{\lambda_2}{m_Q}\mathrm{Tr}\left[\bar{H}^{(Q)}\sigma_{\mu\nu}H^{(Q)}\sigma^{\mu\nu}\right]+\\ &+\frac{ig}{2}\mathrm{Tr}\bar{H}^{(Q)}H^{(Q)}\gamma_\mu\gamma_5\left[\xi^\dagger\partial^\mu\xi-\xi\partial^\mu\xi^\dagger\right]+\text{h.c.}+...,\end{aligned} \tag{2.3.16}$$

where D^μ is the corresponding covariant derivative, $\xi=\exp\left(\frac{i\phi}{\sqrt{2}f_\pi}\right)$ where ϕ is the lightest pseudoscalar meson octet defined in Eq. (1.2.9), $f_\pi=92.3$ MeV is the pion decay constant, g is the $P^*P\pi$ coupling and the dots stand for next-to-leading orders (with more derivatives).

The LO four-body Lagrangian $\mathcal{L}_{4H}$, without taking into account the extra degrees of freedom associated to light degrees of freedom (not relevant in this discussion, but included later on), reads [22]:

$$\begin{aligned}\mathcal{L}_{4H} &= C_A\,\mathrm{Tr}\left[\bar{H}^{(Q)}H^{(Q)}\gamma_\mu\right]\mathrm{Tr}\left[H^{(\bar{Q})}\bar{H}^{(\bar{Q})}\gamma^\mu\right]\\ &+ C_B\,\mathrm{Tr}\left[\bar{H}^{(Q)}H^{(Q)}\gamma_\mu\gamma_5\right]\mathrm{Tr}\left[H^{(\bar{Q})}\bar{H}^{(\bar{Q})}\gamma^\mu\gamma_5\right],\end{aligned} \tag{2.3.17}$$

being C_A and C_B two low-energy constants (LECs) of the EFT. $\mathcal{L}_{4H}$ is invariant under the heavy quark spin rotations introduced in Eqs. (2.2.11) and (2.2.12).

Due to the rotational invariance of this Lagrangian, J is a conserved quantity and, assuming s-wave interactions ($L=0$), heavy meson-heavy antimeson total spin is conserved, and it coincides with J.

Then, expanding the $H^{(Q)}$ hyperfields in terms of the $P^{(*)}$ and $P^{(*)}$ meson fields, as already defined in Subsect. 2.2, we obtain the following Lagrangian,

$$\begin{aligned}\mathcal{L}_{4H} &= -4\,C_A\left[P^{(Q)\dagger}P^{(Q)}P^{(\bar{Q})\dagger}P^{(\bar{Q})}+\left(P^{(Q)*\dagger}\cdot P^{(Q)*}\right)\left(P^{(\bar{Q})*\dagger}\cdot P^{(\bar{Q})*}\right)\right.\\ &\quad\left.-P^{(Q)\dagger}P^{(Q)}\left(P^{(\bar{Q})*\dagger}\cdot P^{(\bar{Q})*}\right)-P^{(\bar{Q})\dagger}P^{(\bar{Q})}\left(P^{(Q)*\dagger}\cdot P^{(Q)*}\right)\right]-\\ &\quad-4\,C_B\left[P^{(Q)}P^{(\bar{Q})}\left(P^{(Q)*\dagger}\cdot P^{(\bar{Q})*\dagger}\right)+P^{(Q)}P^{(\bar{Q})\dagger}\left(P^{(Q)*\dagger}\cdot P^{(\bar{Q})*}\right)\right.\\ &\quad+P^{(Q)\dagger}P^{(\bar{Q})}\left(P^{(Q)*}\cdot P^{(\bar{Q})*\dagger}\right)+P^{(Q)\dagger}P^{(\bar{Q})\dagger}\left(P^{(Q)*}\cdot P^{(\bar{Q})*}\right)+\\ &\quad-i\,\varepsilon^{\rho\sigma\tau\mu}v_\rho P^{(Q)}P_\sigma^{(\bar{Q})*}P_\tau^{(\bar{Q})*\dagger}P_\mu^{(Q)*\dagger}+\\ &\quad-i\,\varepsilon^{\rho\sigma\tau\mu}v_\rho P^{(Q)\dagger}P_\sigma^{(\bar{Q})*}P_\tau^{(\bar{Q})*\dagger}P_\mu^{(Q)*}+\\ &\quad+i\,\varepsilon^{\rho\sigma\tau\mu}v_\rho P^{(\bar{Q})}P_\sigma^{(Q)*\dagger}P_\tau^{(Q)*}P_\mu^{(\bar{Q})*\dagger}+\\ &\quad+i\,\varepsilon^{\rho\sigma\tau\mu}v_\rho P^{(\bar{Q})\dagger}P_\sigma^{(Q)*\dagger}P_\tau^{(Q)*}P_\mu^{(\bar{Q})*}+\\ &\quad+\left(P^{(Q)*}\cdot P^{(\bar{Q})*\dagger}\right)\left(P^{(\bar{Q})*}\cdot P^{(Q)*\dagger}\right)-\\ &\quad-\left.\left(P^{(Q)*}\cdot P^{(\bar{Q})*}\right)\left(P^{(\bar{Q})*\dagger}\cdot P^{(Q)*\dagger}\right)\right],\end{aligned} \tag{2.3.18}$$

with $\varepsilon_{0123}=+1$.

Therefore, projecting onto different spins, we obtain the following potentials V (we use the normalization $V=-\frac{\mathcal{L}}{4}$. Note that the usual non-relativistic normalization factor $\frac{1}{4\sqrt{M_1M_2M_3M_4}}$ is replaced by $\frac{1}{4}$ because of the $\sqrt{M_H}$ normalization of the heavy meson fields.). For $J^P=0^+$, in the $(P\bar{P},P^*\bar{P}^*)$ basis, we get:

$$V(J^P=0^+)=V_0=\begin{pmatrix}C_A & +\sqrt{3}\,C_B\\ +\sqrt{3}\,C_B & C_A-2C_B\end{pmatrix}. \tag{2.3.19}$$

Furthermore, in that case C-parity is even as well. In our convention, the C-parity of a particle-antiparticle system is $C = (-1)^{L+S}$. For $J^P = 1^+$, in the $(P^*\bar{P}, P\bar{P}^*, P^*\bar{P}^*)$ basis, one finds:

$$V(J=1) = V_1 = \begin{pmatrix} C_A & -C_B & \sqrt{2}\,C_B \\ -C_B & C_A & \sqrt{2}\,C_B \\ \sqrt{2}\,C_B & \sqrt{2}\,C_B & C_A - C_B \end{pmatrix}. \tag{2.3.20}$$

As we will discuss below, the above interaction becomes block diagonal when a basis with well-defined C-parity is employed. Finally, for $J = 2$, the only possible channel is the C-parity even state $P^*\bar{P}^*$:

$$V(J=2) = V_2 = C_A + C_B. \tag{2.3.21}$$

Charge conjugation properties have not been considered in the 1^+ sector yet. Since the contact potential in Eq. (2.3.17) commutes with the charge conjugation operator, the elements of the most appropriate basis must be formed by eigenstates of the charge conjugation operator as well. For $J^P = 0^+$ and $J^P = 2^+$, the elements of the respective bases are already charge conjugation eigenstates so the previous expressions for the potential remain unaltered:

$$V_0' = \begin{pmatrix} C_A & +\sqrt{3}\,C_B \\ +\sqrt{3}\,C_B & C_A - 2C_B \end{pmatrix}, \tag{2.3.22}$$

$$V_2' = C_A + C_B, \tag{2.3.23}$$

For $J^P = 1^+$, two of the states in the previous basis are not charge conjugation eigenstates. Using the following charge conjugation eigenstate basis[3] $[\frac{P\bar{P}^* - P^*\bar{P}}{\sqrt{2}}, \frac{P^*\bar{P} + P\bar{P}^*}{\sqrt{2}}, P^*\bar{P}^*]$, the potential V_1' now reads:

$$V_1' = \begin{pmatrix} C_A + C_B & 0 & 0 \\ 0 & C_A - C_B & -2\,C_B \\ 0 & -2\,C_B & C_A - C_B \end{pmatrix}, \tag{2.3.24}$$

which is a block diagonal matrix where each box corresponds to a different charge conjugation sector. As can be seen, the 1^{++} heavy meson-antimeson sector decouples from the dimension two 1^{+-} sector. In addition, the 1^{++} potential $(C_A + C_B)$ is identical to the 2^{++} one. A first trivial consequence is that a 1^{++} heavy meson-antimeson molecule should have a 2^{++} HQSS partner [25].

The same results can be obtained by an alternative, not very known, procedure. Since HQSFS imposes that QCD dynamics is heavy-quark-spin independent, we can build the heavy meson-heavy antimeson wave functions in terms of a different basis, whose elements have well defined the total spin of the $Q\bar{Q}$ quark-antiquark heavy pair (S_Q) and the total spin of the light quark subsystem (s_q) [23]. These wave functions can be obtained from the usual $\left|P^{(*)}\bar{P}^{(*)}\right\rangle$ ones using

[3] We are using a convention where C-parity is isospin-independent, C-parity of a s-wave $D^*\bar{D}^*$ state is $+1$ for $J^P = 0^+, 2^+$, but -1 for $J^P = 1^+$. On the other hand, the $\frac{D\bar{D}^* \pm \bar{D}D^*}{\sqrt{2}}$ states have C-parity $\mp$, respectively.

9-j symbols. One finds,

$$\begin{cases} \left|P\bar{P}, J=0\right\rangle = \frac{1}{2}\left|S_Q=0, s_q=0, J=0\right\rangle + \frac{\sqrt{3}}{2}\left|S_Q=1, s_q=1, J=0\right\rangle \\ \left|P\bar{P}^*, J=1\right\rangle = \frac{1}{2}\left|S_Q=1, s_q=0, J=1\right\rangle - \frac{1}{2}\left|S_Q=0, s_q=1, J=1\right\rangle + \\ \qquad\qquad - \frac{1}{\sqrt{2}}\left|S_Q=1, s_q=1, J=1\right\rangle \\ \left|P^*\bar{P}, J=1\right\rangle = \frac{1}{2}\left|S_Q=1, s_q=0, J=1\right\rangle - \frac{1}{2}\left|S_Q=0, s_q=1, J=1\right\rangle + \\ \qquad\qquad + \frac{1}{\sqrt{2}}\left|S_Q=1, s_q=1, J=1\right\rangle \\ \left|P^*\bar{P}^*, J=0\right\rangle = -\frac{\sqrt{3}}{2}\left|S_Q=0, s_q=0, J=0\right\rangle + \frac{1}{2}\left|S_Q=1, s_q=1, J=0\right\rangle \\ \left|P^*\bar{P}^*, J=1\right\rangle = -\frac{1}{\sqrt{2}}\left(\left|S_Q=1, s_q=0, J=1\right\rangle + \left|S_Q=0, s_q=1, J=1\right\rangle\right) \\ \left|P^*\bar{P}^*, J=2\right\rangle = -\left|S_Q=1, s_q=1, J=2\right\rangle \end{cases}$$

Next, we implement the HQSS constraints in the matrix element of the heavy meson-antimeson potential. To that end, we make use of the Wigner-Eckart theorem,

$$\left\langle S_Q s_q J\right| V \left|S_Q' s_q' J'\right\rangle = \delta_{JJ'}\delta_{S_q S_Q'}\delta_{s_q s_q'} \left\langle V\right\rangle_{s_q} \tag{2.3.25}$$

HQSS implies that the reduced Wigner-Eckart matrix elements $\left\langle V\right\rangle_{s_q}$ depend only on the spin of the light degrees of freedom, which is conserved as it is also conserved the spin of the $Q\bar{Q}$ pair and the total spin J. Defining the following reduced matrix elements:

$$A_0 = \left\langle s_q=0\right| V \left|s_q=0\right\rangle, \tag{2.3.26}$$

$$A_1 = \left\langle s_q=1\right| V \left|s_q=1\right\rangle, \tag{2.3.27}$$

the potentials now read:

$$V(J^P=0^+) = V_0 = \begin{pmatrix} \frac{1}{4}(A_0+3A_1) & \frac{\sqrt{3}}{4}(A_1-A_0) \\ \frac{\sqrt{3}}{4}(A_1-A_0) & \frac{1}{4}(3A_0+A_1) \end{pmatrix}, \tag{2.3.28}$$

$$\begin{aligned} V(J^P=1^+) \quad &= V_1 = \\ &= \begin{pmatrix} \frac{1}{4}(A_0+3A_1) & \frac{1}{4}(A_0-A_1) & \frac{1}{2\sqrt{2}}(-A_0+A_1) \\ \frac{1}{4}(A_0-A_1) & \frac{1}{4}(A_0+3A_1) & \frac{1}{2\sqrt{2}}(-A_0+A_1) \\ \frac{1}{2\sqrt{2}}(-A_0+A_1) & \frac{1}{2\sqrt{2}}(-A_0+A_1) & \frac{1}{2}(A_0+A_1) \end{pmatrix}, \end{aligned} \tag{2.3.29}$$

$$V(J^P=2^+) = V_2 = A_1, \tag{2.3.30}$$

that coincide with Eqs. (2.3.19), (2.3.20) and (2.3.21) with the identifications:

$$A_0 = C_A - 3C_B, \tag{2.3.31}$$

$$A_1 = C_A + C_B, \tag{2.3.32}$$

To recover the full isospin-strangeness dependence of the matrix elements, one of the most important novel points of the thesis (since only $SU(2)$ isospin symmetry was considered before),

we should consider the Lagrangian,

$$\begin{aligned}\mathcal{L}_{4H} &= C_A \,\mathrm{Tr}\left[\bar{H}^{(Q)a} H_a^{(Q)}\gamma_\mu\right]\mathrm{Tr}\left[H^{(\bar{Q})a}\bar{H}_a^{(\bar{Q})}\gamma^\mu\right] \\ &+ C_A^\lambda \,\mathrm{Tr}\left[\bar{H}^{(Q)a}\vec{\lambda}_a^{\,b} H_b^{(Q)}\gamma_\mu\right]\mathrm{Tr}\left[H^{(\bar{Q})c}\vec{\lambda}_c^{\,d}\bar{H}_d^{(\bar{Q})}\gamma^\mu\right] \\ &+ C_B \,\mathrm{Tr}\left[\bar{H}^{(Q)a} H_a^{(Q)}\gamma_\mu\gamma_5\right]\mathrm{Tr}\left[H^{(\bar{Q})a}\bar{H}_a^{(\bar{Q})}\gamma^\mu\gamma_5\right] \\ &+ C_B^\lambda \,\mathrm{Tr}\left[\bar{H}^{(Q)a}\vec{\lambda}_a^{\,b} H_b^{(Q)}\gamma_\mu\gamma_5\right]\mathrm{Tr}\left[H^{(\bar{Q})c}\vec{\lambda}_c^{\,d}\bar{H}_d^{(\bar{Q})}\gamma^\mu\gamma_5\right], \end{aligned} \tag{2.3.33}$$

with $\vec{\lambda}_a^{\,b}$ the Gell-Mann matrices, and $P_a^{(Q)} = \left(Q\bar{u}, Q\bar{d}, Q\bar{s}\right)$. There is only two $SU(3)$ light flavour scalars ($\mathbb{1}$ and $\vec{\lambda}\cdot\vec{\lambda}$) and this symmetry, together with HQSS, provides an enormous simplification: there only appear four LECs in the LO term of $\mathcal{L}_{4H}$, as we anticipated.

2.3.2 $P^{(*)}P^{(*)}\pi$ Interactions and OPE Potential

The $P^{(*)}P^{(*)}\pi$ and $\bar{P}^{(*)}\bar{P}^{(*)}\pi$ couplings needed to construct the OPE potential are determined by the Chiral Symmetry. Indeed, the EFT that describes the interactions of pions (or any Goldstone bosons of the Chiral Symmetry in general) with heavy mesons is called Heavy Meson Chiral Perturbation Theory (see Ref. [81] for a review). The Lagrangian of this theory, at leading order in the chiral expansion, reads [89, 90, 92, 93], see also Eq. (2.3.16).

$$\begin{aligned}\mathcal{L}_{\pi H\bar{H}} &= -\frac{g}{2f_\pi}\left(\mathrm{Tr}\left[\bar{H}^{(Q)j} H_i^{(Q)}\gamma^\mu\gamma_5\right] + \mathrm{Tr}\left[H^{(\bar{Q})j}\bar{H}_i^{(\bar{Q})}\gamma^\mu\gamma_5\right]\right)\cdot \\ &\qquad \cdot (\vec{\tau}\partial_\mu\vec{\phi})_j^{\,i} + \cdots, \end{aligned} \tag{2.3.34}$$

where $\vec{\phi}$ is a relativistic field that describes the pion[4], $g \simeq 0.6$ is the $PP^*\pi$ coupling (fitted to the $D^* \to D\pi$ decay) and $f_\pi \simeq 92.2$ is the pion decay constant. As usual, in this work the pion field has dimensions of energy, while the heavy meson or antimeson fields $H^{(Q)}$ or $H^{(\bar{Q})}$ have dimensions of $E^{3/2}$, as mentioned above. This Lagrangian leads to s-wave single pion exchange potentials that can be, in general, written as:

$$V_{H\bar{H}\pi}(\vec{p},\vec{p'}) = \eta\frac{g^2}{f_\pi^2}\frac{(\vec{a}\cdot\vec{q})\left(\vec{b}\cdot\vec{q}\right)}{\vec{q}^{\,2}+m_\pi^2}, \tag{2.3.35}$$

being $\vec{q} = \vec{p} - \vec{p}'$ the exchanged momentum between the heavy meson-antimeson pair and $\vec{a}$, $\vec{b}$ and η polarization operators and a phase that depend on the corresponding initial and final states. We have approximated $\frac{i}{p^2-m_\pi^2} \simeq \frac{-i}{\vec{p}^{\,2}+m_\pi^2}$ in the pion propagator; that is, we have neglected the transferred energy between the two heavy particles.

The non-relativistic potential for the transition (not necessarily elastic),

$$P^{(*)}(1)\bar{P}^{(*)}(2) \to P^{(*)}(1')\bar{P}^{(*)}(2'), \tag{2.3.36}$$

in terms of the tree level scattering amplitude deduced from the Lagrangian $\mathcal{L}_{\pi H\bar{H}}$ of Eq.(2.3.34), $T_{tree} = \mathcal{V}\,(1+2\to 1'+2')$, where $1, 2$ and $1', 2'$ schematically represent the initial and final state of each particles, that in our case is completely represented by the CM momenta of the initial and final mesons $\vec{p}$ and $\vec{p}'$ and the third component of the spin of each of the particles. Our

[4]We use a convention such that $\phi = \frac{\phi_x - \mathrm{i}\phi_y}{\sqrt{2}}$ creates a π^- from the vacuum or annihilates a π^+, and the ϕ_z field creates or annihilates a π^0.

convention is such that the usual Feynman rules (each vertex contributes with $i\mathcal{L}$, additional i factor for each pion propagator, etc.) provides $-iT$. The relationship between the non-relativistic potential and the invariant scattering amplitude is,

$$\langle \vec{p}\,'; (S_1' m_1')(S_2' m_2') | V | \vec{p}; (S_1 m_1)(S_2 m_2) \rangle = \frac{1}{4} \mathcal{V}(1+2 \to 1'+2'), \tag{2.3.37}$$

where the $|\vec{p}; (S_1 m_1)(S_2 m_2)\rangle$ plane wave states are normalized to the value $(2\pi)^3 \, \delta^3 \, (\vec{p} - \vec{p}\,')$. The OPE potentials are local because they only depend on the transferred momentum $\vec{q} = \vec{p} - \vec{p}\,'$. We take advantage of this feature to obtain the partial wave contribution $V_{JL'L}^{SS'}(\vec{p}, \vec{p}\,')$, defined as the matrix element of the potential between c.m. spherical waves ${}^{2S+1}L_J$, with S, L and J the spin, orbital and total angular momentum of the $P^{(*)}\bar{P}^{(*)}$ pair, respectively (see Eqs. (2.4.68) and (2.4.73) below in Sect. 2.4.3). We take appropriate Fourier transforms and compute the matrix elements in the coordinate space making use of the well known properties,

$$\begin{aligned} \int \frac{d^3\vec{q}}{(2\pi)^3} \frac{(\vec{a}\cdot\vec{q})(\vec{b}\cdot\vec{q})}{\vec{q}^{\,2} + m_\pi^2} e^{-i\vec{q}\cdot\vec{r}} &= -a_i b_j \partial_i \partial_j \left(\frac{e^{-m_\pi r}}{4\pi r} \right) = \\ &= \frac{1}{3} \, \vec{a}\cdot\vec{b} \; \delta^3(\vec{r}) - \left(v_C(r) \vec{a}\cdot\vec{b} + v_T(r) S_{12}(\vec{a}, \vec{b}\,) \right), \end{aligned} \tag{2.3.38}$$

being,

$$S_{12}\left(\vec{a}, \vec{b}\right) = \frac{3\,(\vec{a}\cdot\vec{r}\,)\left(\vec{b}\cdot\vec{r}\right)}{r^2} - \vec{a}\cdot\vec{b}, \tag{2.3.39}$$

$$v_C(r) = \frac{m_\pi^3}{12\pi} \left(\frac{e^{-m_\pi r}}{m_\pi r} \right), \tag{2.3.40}$$

$$v_T(r) = v_C(r) \left(1 + \frac{3}{m_\pi r} + \frac{3}{(m_\pi r)^2} \right). \tag{2.3.41}$$

where $S_{12}\left(\vec{a}, \vec{b}\right)$ is a tensor operator and $v_C(r)$ and $v_T(r)$ the central and tensor pieces of the potential. After some Racah algebra calculation, we obtain (see Sect. 2.4.3 below),

$$V_{JL'L}^{S'S}(p', p) = 4\pi (i^{L-L'}) \int_0^{+\infty} dr \; r^2 j_L(pr) j_{L'}(p'r) \; V_{JL'L}^{S'S}(r), \tag{2.3.42}$$

where

$$V_{JL'L}^{S'S}(r) = \left\{ -\frac{g^2}{12 f_\pi^2} C_{12} \frac{\delta(r)}{4\pi r^2} + \frac{g^2}{4 f_\pi^2} \left[v_C(r) C_{12} + v_T(r) S_{12} \right] \right\} \vec{\tau}_1 \cdot \vec{\tau}_2, \tag{2.3.43}$$

with $\vec{\tau}_1 \cdot \vec{\tau}_2 = 2(\vec{T}^{\,2} - 3/2)$, that takes the values -3 and 1 for total isospin 0 and 1, respectively. The factors C_{12} and S_{12} depend on J, L, L', S and S'. In matrix form (symmetric), they read for each J^{PC} sector[5] [25] (we particularize for the case of the charm sector; the extension to the bottom sector is straightforward),

$$C_{12}(0^{++}) = \begin{pmatrix} 0 & & \\ -\sqrt{3} & 2 & \\ 0 & 0 & -1 \end{pmatrix}, \quad S_{12}(0^{++}) = \begin{pmatrix} 0 & & \\ 0 & 0 & \\ \sqrt{6} & \sqrt{2} & 2 \end{pmatrix},$$
$$\left\{ D\bar{D}({}^1S_0), D^*\bar{D}^*({}^1S_0), D^*\bar{D}^*({}^5D_0) \right\} \tag{2.3.44}$$

[5] We give here expressions only for those sectors accessible for the zero range interaction considered in the previous section.

$$C_{12}(1^{++}) = \begin{pmatrix} -1 & & \\ 0 & -1 & \\ 0 & 0 & -1 \end{pmatrix}, \quad S_{12}(1^{++}) = \begin{pmatrix} 0 & & \\ \sqrt{2} & -1 & \\ \sqrt{6} & \sqrt{3} & 1 \end{pmatrix},$$
$$\left\{[D\bar{D}^*]_2(^3S_1), [D\bar{D}^*]_2(^3D_1), D^*\bar{D}^*(^5D_1)\right\} \tag{2.3.45}$$

$$C_{12}(1^{+-}) = \begin{pmatrix} 1 & & & \\ 0 & 1 & & \\ -2 & 0 & 1 & \\ 0 & -2 & 0 & 1 \end{pmatrix}, \quad S_{12}(1^{+-}) = \begin{pmatrix} 0 & & & \\ -\sqrt{2} & 1 & & \\ 0 & -\sqrt{2} & 0 & \\ -\sqrt{2} & 1 & -\sqrt{2} & 1 \end{pmatrix}$$
$$\left\{[D\bar{D}^*]_1(^3S_1), [D\bar{D}^*]_1(^3D_1), D^*\bar{D}^*(^3S_1), D^*\bar{D}^*(^3D_1)\right\} \tag{2.3.46}$$

$$C_{12}(2^{++}) = \begin{pmatrix} 0 & & & & & \\ 0 & -1 & & & & \\ -\sqrt{3} & 0 & 2 & & & \\ 0 & 0 & 0 & -1 & & \\ 0 & 0 & 0 & 0 & -1 & \\ 0 & 0 & 0 & 0 & 0 & -1 \end{pmatrix}, \tag{2.3.47}$$

$$S_{12}(2^{++}) = \begin{pmatrix} 0 & & & & & \\ 0 & 1 & & & & \\ 0 & 0 & 0 & & & \\ \sqrt{\frac{6}{5}} & -3\sqrt{\frac{2}{5}} & \sqrt{\frac{2}{5}} & 0 & & \\ -2\sqrt{\frac{3}{7}} & \frac{3}{\sqrt{7}} & -\frac{2}{\sqrt{7}} & -\sqrt{\frac{14}{5}} & -\frac{3}{7} & \\ 6\sqrt{\frac{3}{35}} & \frac{12}{\sqrt{35}} & \frac{6}{\sqrt{35}} & 0 & -\frac{12}{7\sqrt{5}} & \frac{10}{7} \end{pmatrix},$$
$$\left\{D\bar{D}(^1D_2), [D\bar{D}^*]_2(^3D_2), D^*\bar{D}^*(^1D_2), D^*\bar{D}^*(^5S_2), D^*\bar{D}^*(^5D_2), D^*\bar{D}^*(^5G_2)\right\}$$

where states with well defined $C-$ parity $\left[D\bar{D}^*\right]_{C=\pm} = \frac{D\bar{D}^* \mp D^*\bar{D}}{\sqrt{2}}$ have been considered. On the other hand, the $\delta(r)$ piece of the OPE potentials can be re-absorbed in the LEC arising from the $\mathcal{L}_{4H}$ Lagrangian of Eq. (2.3.17). Indeed for isospin zero, it amounts to the replacement,

$$C_B \to C_B - \frac{g^2}{4f_\pi^2}. \tag{2.3.48}$$

2.3.3 Effective Lagrangian for Radiative Processes

Radiative processes are very important in the heavy meson phenomenology. Despite not being the most important decay modes of the heavy mesons; radiative Feynman diagrams lead to corrections in chiral calculations which can be important, for instance, to estimate long-distance effects in the calculation of decay constants [94] or chiral couplings [95].

At leading order in the heavy quark expansion, the radiative $D_a^* \to D_a\gamma$ matrix element has the form,

$$\mathcal{M}\left(D_a^* \to D_a\gamma\right) \simeq e\mu_a\, \varepsilon^{\mu\alpha\beta\gamma}\, \varepsilon_\mu^*(\gamma)\, v_\alpha\, k_\beta\, \varepsilon_\lambda\left(D^*\right), \tag{2.3.49}$$

where $\frac{e\mu_a}{2}$ is the transition magnetic moment, k^μ is the photon momentum, $\varepsilon\left(\gamma\right)$ is the polarization of the photon and $\varepsilon\left(D^*\right)$ is the polarization of the D^*. This transition magnetic moment

gets contributions from the photon coupling to the light and the (heavy) charm quark parts of the electromagnetic current $s^\mu_{em} = \frac{2}{3}\bar{u}\gamma^\mu u - \frac{1}{3}\bar{d}\gamma^\mu d - \frac{1}{3}\bar{s}\gamma^\mu s + \frac{2}{3}\bar{c}\gamma^\mu c$.

First, let us start with the contribution of the heavy quark $\mu_{\rm heavy}$. If we had included QED in the derivation of Eq.(2.1.19), we would have obtained the same Lagrangian with an additional term that takes into account the electromagnetic interactions:

$$\mathcal{L}_Q = \bar{Q}_v \left(iv\cdot D - \frac{1}{2m_Q}\left(D_\perp^2 - \frac{g}{2}\sigma_{\mu\nu}G^{\mu\nu} - \frac{eQ'}{2}\sigma_{\mu\nu}F^{\mu\nu}\right)\right) Q_v + \mathcal{O}\left(\frac{1}{m_Q^2}\right),$$

where the covariant derivative is now $D_\mu = \partial_\mu + ig_s A^a_\mu T^a + ieQ'A_\mu$, $e>0$ the proton charge and $Q' = \frac{2}{3}$ the charge of the heavy quark. Besides, $F^{\mu\nu} = \partial^\mu A^\nu - \partial^\nu A^\mu$ is the Maxwell tensor with A^μ the photon field. The last term is the responsible for the charm quark contribution to the transition matrix element of Eq. (2.3.49) and it gives $\mu_{\rm heavy} = \frac{Q'}{m_Q}$. We see that $\mu_{\rm heavy}$ is independent of the light quark flavour and its perturbative $\alpha_S(m_C)$ corrections are of the order $\mathcal{O}\left(\frac{1}{m_C^2}\right)$.

The light quarks also provide another contribution to μ_a. The coupling of the light quarks to the photon is not fixed by HQSS. The light quark current transforms as an octet under $SU(3)$ flavour symmetry. There is only one way to combine a $SU(3)$ octet (electromagnetic current), a $SU(3)$ triplet (light quark in a meson) and a $SU(3)$ antitriplet (light antiquark in the meson) into a $SU(3)$ singlet element. Thus assuming $SU(3)$ light flavour symmetry, $\mu_{\rm light}$ is a function of a single constant β: $\mu_{\rm light} = Q_{ab}\ \beta$; where $Q_{ab} = {\rm diag}\,(2/3, -1/3, -1/3)$ denotes the light quark electric charges. This expression for $\mu_{\rm light}$ includes effects suppressed by powers of $1/m_Q$, since we have only imposed $SU(3)$ light flavour symmetry.

Within our formalism of HQSS, both contributions are taken into account by means of the effective Lagrangian [96, 97]:

$$\begin{aligned}\mathcal{L}_{HH\gamma} &= \frac{e\beta}{4}Q^a_b\left({\rm Tr}\left[\bar{H}^{(Q)b}H^{(Q)}_a\sigma^{\mu\nu}\right] + {\rm Tr}\left[H^{(\bar{Q})b}\bar{H}^{(\bar{Q})}_a\sigma^{\mu\nu}\right]\right)F_{\mu\nu} + \\ &+\frac{eQ'}{4m_Q}\left({\rm Tr}\left[\bar{H}^{(Q)a}\sigma^{\mu\nu}H^{(Q)}_a\right] + {\rm Tr}\left[H^{(\bar{Q})a}\sigma^{\mu\nu}\bar{H}^{(\bar{Q})}_a\right]\right)F_{\mu\nu} + ...\end{aligned} \tag{2.3.50}$$

Q' is the heavy quark electric charge (in units of the proton charge $e=\sqrt{4\pi\alpha}$). For the charm (bottom) quark, we have $Q' = 2/3$ ($Q' = -1/3$). Besides, m_Q is the heavy quark mass and β is the parameter introduced in Ref. [96], as discussed above. These two terms describe the magnetic coupling due to the light quark (preserves HQSS) and the heavy quark (suppressed by $1/m_Q$), respectively. Both terms are needed to understand the observed electromagnetic branching fractions of the D^{*+} and D^{*0} because a cancellation between the two terms accounts for the very small width of the D^{*+} with respect to the D^{*0} width [98].

In the non-relativistic constituent quark model $\beta = 1/m_q \sim 1/330\ {\rm MeV}^{-1}$, where m_q is the light constituent quark mass. Heavy meson chiral perturbation theory provides contributions from Goldstone boson loops (see Fig. 2.1) [21], that provide corrections to β of the order of $\mathcal{O}\left(m^2_{\pi,k}/f^2_{\pi,k}\right)$.

2.4 Computation of the T-matrix

Here we give some details about the solution of the LSE, both for a contact s-wave potential and for a finite range potential, like that corresponding to the OPE. In the latter case, we also give details of the numerical solution of the LSE obtained by discretizing the momentum space. We

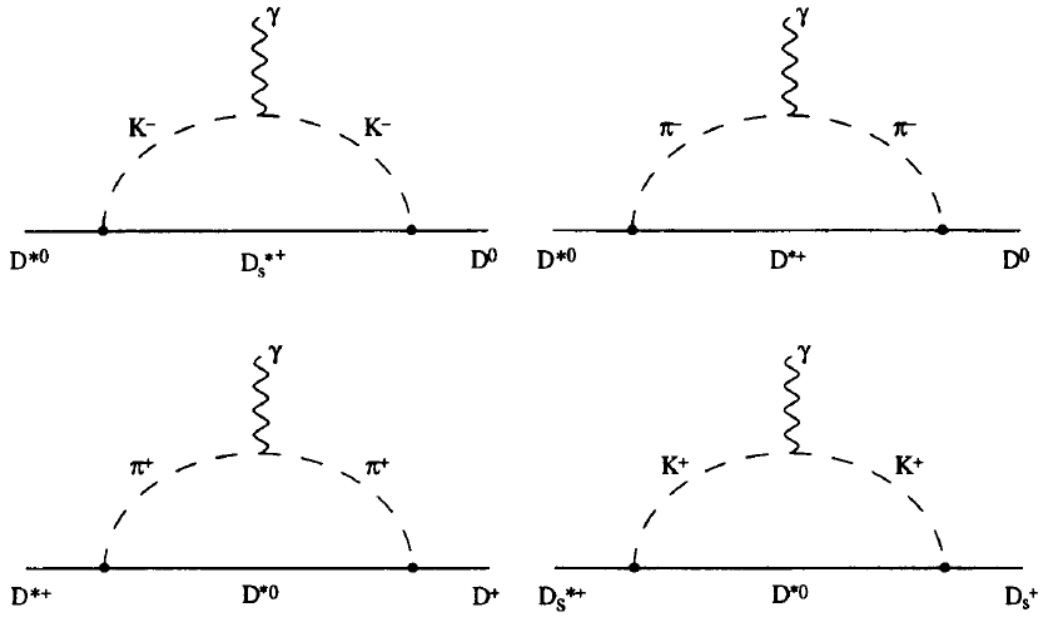

Figure 2.1: *Feynman Diagrams of the leading $SU(3)$ violating contributions.*

also discuss the UV regularization/renormalization scheme employed in this work. The following quantum mechanics properties of the LSE have already been pointed out by other authors in the past. Specifically, Refs. [25, 99] have played a very important role in the preparation of this section.

2.4.1 Monochannel diffusion in a $\vec{p}$-independent potential

Let us study the $1+2 \to 1+2$ scattering, with a c.m. energy E. Our starting point is the LSE:

$$T = V + V\frac{1}{E-H_0}T = V + V\frac{1}{E-H}V, \tag{2.4.1}$$

with H the full hamiltonian and H_0 its kinetic part ($H = H_0 + V$). If we take into account that a bound state satisfies:

$$(E_B - H)\,|\Psi_B\rangle\,, \tag{2.4.2}$$

it is obvious that the T-matrix should show a pole for $E = E_B$, where E_B is the energy of the bound state, below the threshold of the system[6].

The explicit representation of the LSE can only be obtained after a plane-wave projection. Using the normalization:

$$\langle\vec{p}\,|\vec{x}\rangle = e^{-i\vec{p}\cdot\vec{x}} \quad \Rightarrow \quad \int d^3\vec{x}\,|\vec{x}\rangle\,\langle\vec{x}| = \int \frac{d^3\vec{p}}{(2\pi)^3}\,|\vec{p}\rangle\,\langle\vec{p}| = 1, \tag{2.4.3}$$

[6]For continuum states, that is, energies above threshold, the T-matrix shows a *branch cut*, instead of individual poles.

the LSE, in the momentum space, reads:

$$\langle \vec{p}\,|\,T\,|\vec{p}\,'\rangle = \langle \vec{p}\,|V|\vec{p}\,'\rangle + \int \frac{d^3\vec{k}}{(2\pi)^3}\,\frac{\left\langle \vec{p}\,|V|\vec{k}\right\rangle \left\langle \vec{k}|T|\vec{p}\,'\right\rangle}{E-m_1-m_2-\frac{\vec{k}^2}{2\mu}+i\varepsilon}, \tag{2.4.4}$$

with μ the reduced mass of the interacting particles (m_1 and m_2). This equation can be solved for a separable contact potential V such as ($p=|\vec{p}|$ and $p'=|\vec{p}'|$):

$$\langle \vec{p}\,|V|\vec{p}\,'\rangle = V(\vec{p},\vec{p}\,') = \Theta(\Lambda-p)\Theta(\Lambda-p')\;v, \tag{2.4.5}$$

where Θ is a step function with a sharp cutoff regulator Λ that has been included for the treatment of ultraviolet divergences, needed to render finite the LSE. We will first, by its simplicity, discuss the case of a sharp UV cutoff. In this case, there is a semianalytical solution for the LSE using the appropriate *ansatz*:

$$\langle \vec{p}\,|T|\vec{p}\,'\rangle = \Theta(\Lambda-p)\Theta(\Lambda-p')\;t(E) \tag{2.4.6}$$

where $t(E)$ is given by:

$$t(E) = v + vG(E)t(E), \qquad t(E) = \frac{v}{1-vG(E)}, \tag{2.4.7}$$

with G the propagator (loop function) calculated using the UV regulator Λ previously introduced,

$$G(E) = \int \frac{d^3\vec{k}}{(2\pi)^3}\frac{\Theta(\Lambda-k)}{E-m_1-m_2-\frac{\vec{k}^2}{2\mu}+i\varepsilon}, \tag{2.4.8}$$

Once we obtain the T-matrix, we can find the bound states and resonances that are dynamically generated within our model just by looking at its analytical properties. As already discussed, bound states will appear as poles for real energies below the threshold (m_1+m_2) of the first Riemann sheet and resonances will appear as poles in the fourth quadrant of the second Riemann sheet of the T-matrix. Then, the condition for a bound state is:

$$1-vG=0, \tag{2.4.9}$$

for an energy $E_\alpha < m_1+m_2$. This condition also allows us to determine the undetermined LECs of the model from experimental data.

Additionally, one trivially finds,

$$\frac{d}{d\Lambda}(vG)=0, \tag{2.4.10}$$

which is a sort of renormalization group equation and that guaranties that the observables (E_α) is independent of the regulator Λ. Indeed, this equation relates variations in the regulator Λ with variations in the contact potential v. Thus, the position of the pole does not change since the contact potential v absorbs any possible variation in the Λ regulator.

G admits an analytical solution for $E_\alpha < m_1+m_2$,

$$G(E_\alpha) = \frac{1}{(2\pi)^3}\left[-8\pi\mu\left(\Lambda-\gamma\cdot\arctan\left(\frac{\Lambda}{\gamma}\right)\right)\right] \tag{2.4.11}$$

with $\gamma=\sqrt{2\mu E_B^\alpha}$, and $E_B^\alpha = m_1+m_2-E$ the binding energy of the bound state α.

The coupling g of the bound state α to its constituents is defined such that in the vicinity of the pole the scattering matrix behaves as,

$$t = \frac{g^2}{E - E_\alpha} \tag{2.4.12}$$

and hence,

$$g^2 = \lim_{E \to E_\alpha} (E - E_\alpha)\, t = - \left(\frac{dG}{dE} \right)^{-1} \Bigg|_{E=E_\alpha} \tag{2.4.13}$$

The wave function of the state is determined by the Schrödinger equation (see Ref. [99] for further details),

$$H \left| \psi \right\rangle = E \left| \psi \right\rangle \tag{2.4.14}$$

where $|\psi\rangle$ is an eigenfunction of H, the full Hamiltonian. We can write,

$$(H_0 + V) \left| \psi \right\rangle = E \left| \psi \right\rangle \tag{2.4.15}$$

$$\left| \psi \right\rangle = \frac{1}{E - H_0} V \left| \psi \right\rangle \tag{2.4.16}$$

which has the solution

$$\begin{aligned} \langle \vec{p} | \psi \rangle &= \int \frac{d^3\vec{k}}{(2\pi)^3} \int \frac{d^3\vec{k}'}{(2\pi)^3} \langle \vec{p} | \frac{1}{E - H_0} \left| \vec{k}' \right\rangle \left\langle \vec{k}' \right| V \left| \vec{k} \right\rangle \left\langle \vec{k} | \psi \right\rangle = \\ &= v \frac{\Theta(\Lambda - p)}{E - m_1 - m_2 - \frac{p^2}{2\mu}} \int_{k<\Lambda} \frac{d^3\vec{k}}{(2\pi)^3} \left\langle \vec{k} | \psi \right\rangle \end{aligned} \tag{2.4.17}$$

which gives us the wave function. Integrating Eq. (2.4.17) over $d^3\vec{p}$, we obtain,

$$1 - vG(E) = 0, \tag{2.4.18}$$

which is the condition to find a pole. In Eq. (2.4.17), we determined the state wave function up to a constant $\int_{k<\Lambda} \frac{d^3\vec{k}}{(2\pi)^3} \left\langle \vec{k} | \psi \right\rangle$, which can be fixed from the normalization condition. Let $E_\alpha < m_1 + m_2$ be the solution of the above quantization equation, its wave function will satisfy,

$$\int \frac{d^3\vec{p}}{(2\pi)^3} \left| \langle \vec{p} | \psi \rangle \right|^2 = 1 \tag{2.4.19}$$

Note that the wave function can be normalized because we are dealing with a bound state whose energy is below $m_1 + m_2$. From the above equation, one easily finds,

$$1 = v^2 \int_{p<\Lambda} \frac{d^3\vec{p}}{(2\pi)^3} \left(\frac{1}{E_\alpha - m_1 - m_2 - \frac{\vec{p}^2}{2\mu}} \right)^2 \left| \int_{k<\Lambda} \frac{d^3\vec{k}}{(2\pi)^3} \left\langle \vec{k} | \psi \right\rangle \right|^2 \tag{2.4.20}$$

From Eqs. (2.4.13) and (2.4.20), we deduce

$$g = v \int_{k<\Lambda} \frac{d^3\vec{k}}{(2\pi)^3} \left\langle \vec{k} | \alpha \right\rangle, \tag{2.4.21}$$

The value of the wave function at the origin in coordinate space is,

$$\left\langle \vec{x} = \vec{0} | \psi \right\rangle \equiv \psi(\vec{0}) = \int \frac{d^3\vec{k}}{(2\pi)^3} \left\langle \vec{k} | \psi \right\rangle . \tag{2.4.22}$$

We therefore conclude, using Eq. (2.4.17),

$$g = G^{-1}(E_\alpha)\ \psi(\vec{0}). \tag{2.4.23}$$

This is an important result: the couplings, up to a factor $G^{-1}(E_\alpha)$, is a measure of the wave function in coordinate space at the origin.

In EFT treatments, there is no privileged choice of a regulator function. Let us consider a separable potential where we substitute the sharp cutoff by a generic form factor,

$$\langle \vec{p}\,' | \, V \, | \vec{p} \rangle = v \ f\left(\vec{p}\right) f\left(\vec{p}\,'\right) \tag{2.4.24}$$

Now the solution of the LSE would be $\langle \vec{p}\,' | \, T \, | \vec{p} \rangle = t \ f\left(\vec{p}\right) f\left(\vec{p}\,'\right)$ with

$$t(E) = \frac{v}{1 - vG(E)} \tag{2.4.25}$$

and the loop function G is now given by,

$$G(E) = \int \frac{d^3\vec{p}}{(2\pi)^3}\ f^2\left(\vec{p}\right) \frac{1}{E - m_1 - m_2 - \frac{\vec{p}^{\,2}}{2\mu} + i\varepsilon} \tag{2.4.26}$$

and the wave functions are now given by,

$$\langle \vec{p} | \psi \rangle = v \frac{f\left(\vec{p}\right)}{E_\alpha - m_1 - m_2 - \frac{\vec{p}^{\,2}}{2\mu}} \int \frac{d^3\vec{k}}{(2\pi)^3}\ f(\vec{k}) \left\langle \vec{k} | \psi \right\rangle \tag{2.4.27}$$

which upon integration leads to,

$$\int_{p<\Lambda} \frac{d^3\vec{p}}{(2\pi)^3}\ f\left(\vec{p}\right) \langle \vec{p} | \psi \rangle = G(E)\ v \int_{k<\Lambda} \frac{d^3\vec{k}}{(2\pi)^3}\ f(\vec{k}) \left\langle \vec{k} | \psi \right\rangle \tag{2.4.28}$$

which reads,

$$\hat{\psi} = G\ v\ \hat{\psi} \tag{2.4.29}$$

where the bound state condition $1 - vG$ naturally appears again and $\hat{\psi}$ is defined as,

$$\hat{\psi} = \int \frac{d^3\vec{k}}{(2\pi)^3}\ f(\vec{k}) \left\langle \vec{k} | \psi \right\rangle \tag{2.4.30}$$

This redefinition allows us to write Eq. (2.4.27) as,

$$\langle \vec{p} | \psi \rangle = f\left(\vec{p}\right) \frac{1}{E_\alpha - m_1 - m_2 - \frac{\vec{p}^{\,2}}{2\mu}}\ G^{-1}(E_\alpha)\ \hat{\psi} \tag{2.4.31}$$

where we have used $v = G^{-1}(E_\alpha)$ and we again find,

$$g\ G(E_\alpha) = \hat{\psi} \tag{2.4.32}$$

Everything is identical to the sharp cutoff case, but now $\hat{\psi}$ is not, up to a factor, the wave function at the origin (it would be if we removed $f(\vec{p})$ from Eq. (2.4.30)). To see the meaning of $\hat{\psi}$ we write $f(\vec{p})$ in terms of its Fourier transform,

$$f(\vec{p}) = \int d^3\vec{x}\ \hat{f}(\vec{x})\ e^{i\vec{p}\cdot\vec{x}}. \tag{2.4.33}$$

and the wave function of Eq. (2.4.30) also in terms of its Fourier transform,

$$\psi(\vec{p}) = \int d^3\vec{x}\ \psi(\vec{x})\ e^{-i\vec{p}\cdot\vec{x}} \tag{2.4.34}$$

Then upon integrating explicitly over $\vec{k}$ in Eq. (2.4.30) we find,

$$\hat{\psi} = \int d^3\vec{x}\ \hat{f}(\vec{x})\,\psi(\vec{x})\,. \tag{2.4.35}$$

We performed explicit calculations using a Gaussian form for $f(\vec{p})$,

$$f(\vec{p}) = e^{-\vec{p}^{\,2}/\Lambda^2} \qquad \hat{f}(\vec{x}) = \frac{1}{\sqrt{8}\ (2\pi)^{3/2}}\Lambda^3 e^{-(1/4)\vec{x}^2\Lambda^2} \tag{2.4.36}$$

and a Lorentz form,

$$f(\vec{p}) = \frac{\Lambda^2}{\Lambda^2+\vec{p}^{\,2}} \qquad \hat{f}(\vec{x}) = \frac{1}{4\pi}\Lambda^2\frac{e^{-|\vec{x}|\Lambda}}{|\vec{x}|}. \tag{2.4.37}$$

We can see that $\hat{f}(\vec{x})$ has a range of $\frac{1}{\Lambda} \sim 0.2 - 0.3$ fm, a range much smaller than the extension of the wave function. Thus $\hat{\psi}$ gives the average of the wave function in the vicinity of the origin.

In most of the chapters of this thesis we have used the UV Gaussian regulator Λ,

$$\langle\vec{p}|V|\vec{p}\,'\rangle = V(\vec{p},\vec{p}\,') = v\ e^{-\vec{p}^{\,2}/\Lambda^2}\ e^{-\vec{p}^{\,\prime 2}/\Lambda^2}, \tag{2.4.38}$$

so the LSE admits a solution such as:

$$\langle\vec{p}\,|T|\vec{p}\,'\rangle = T(\vec{p},\vec{p}\,') = t\ e^{-\vec{p}^{\,2}/\Lambda^2}\ e^{-\vec{p}^{\,\prime 2}/\Lambda^2} \quad \Rightarrow \quad t = \frac{v}{1-vG}, \tag{2.4.39}$$

and the loop function G is now:

$$\begin{aligned} G(E) &= \int \frac{\mathrm{d}^3\vec{q}}{(2\pi)^3}\frac{e^{-2\vec{q}^{\,2}/\Lambda^2}}{E-m_1-m_2-\vec{q}^{\,2}/2\mu+i\varepsilon} \\ &= \left(-\frac{\mu\Lambda}{(2\pi)^{3/2}}e^{2k^2/\Lambda^2}+\frac{\mu k}{\pi^{3/2}}\phi\left(\sqrt{2}k/\Lambda\right)-i\frac{\mu k}{2\pi}\right)\ e^{-2k^2/\Lambda^2}\ , \end{aligned} \tag{2.4.40}$$

with $\phi(x)$ the Dawson function given by:

$$\phi(x) = \int_0^x e^{y^2}\mathrm{d}y\ . \tag{2.4.41}$$

Note that, the wave number k is a multivalued function of E, with a branch point at threshold $(E = m_1 + m_2)$. The principal argument of $(E - m_1 - m_2)$ should be taken in the range $[0, 2\pi[$. The function $k\phi(\sqrt{2}k/\Lambda)$ does not present any discontinuity for real E above threshold, and $G(E)$ becomes a multivalued function because of the ik term. Indeed, $G(E)$ has two Riemann sheets. In the first one, $0 \leqslant \mathrm{Arg}(E - m_1 - m_2) < 2\pi$, we find a discontinuity $G_I(E+i\epsilon) - G_I(E-i\epsilon) = 2i\,\mathrm{Im}G_I(E+i\epsilon)$ for $E > (m_1+m_2)$. It also guaranties that the $T-$matrix fulfils the optical theorem. For real values of E and below threshold, we have $k = i\sqrt{-2\mu(E-m_1-m_2)}$. In the second Riemann sheet, $2\pi \leqslant \mathrm{Arg}(E-m_1-m_2) < 4\pi$, we trivially find $G_{II}(E-i\epsilon) = G_I(E+i\epsilon)$, for real energies and above threshold.

Generalization for the two coupled channel case.

Here, we study the generalization of the previous analysis of the LSE for two coupled channels. This analysis will be applied in the study of the $X(3872)$ state, for instance, where the neutral $D^0\bar{D}^{*0}$ and charged D^+D^{*-} channels are considered.

As there are two channels involved in the analysis, the potential V and the T-matrix are now 2×2 matrices instead of scalar elements as in the monochannel diffusion case. Introducing a Λ regulator that allows to renormalize the UV divergences, the potential would be now:

$$\langle \vec{p}\,|V|\vec{p}\,'\rangle = f(\vec{p}\,)f(\vec{p}\,')\ v, \tag{2.4.42}$$

so we suggest an *ansatz* for the T-matrix:

$$\langle \vec{p}\,|T|\vec{p}\,'\rangle = f(\vec{p}\,)f(\vec{p}\,')\ t, \tag{2.4.43}$$

with:

$$v = \begin{pmatrix} v_{11} & v_{12} \\ v_{12} & v_{22} \end{pmatrix} \quad , \quad t = \begin{pmatrix} t_{11} & t_{12} \\ t_{12} & t_{22} \end{pmatrix}. \tag{2.4.44}$$

Again, we can choose for the regulator functions $f_\Lambda(\vec{p})$, among other options,

$$f(\vec{p}) = \Theta(\Lambda - p) \qquad , \qquad f(\vec{p}) = e^{-p^2/\Lambda^2}, \tag{2.4.45}$$

for a sharp cutoff and a Gaussian regulator, respectively. The LSE admits the same solution than in the monochannel analysis:

$$T = V + VGT \qquad \Rightarrow \qquad t = (1 - vG)^{-1}v, \tag{2.4.46}$$

where the propagator G is now a 2×2 diagonal matrix:

$$G = \begin{pmatrix} G_{11} & 0 \\ 0 & G_{22} \end{pmatrix}, \qquad G_{ii} = \int \frac{d^3\vec{k}}{(2\pi)^3}\frac{f^2(\vec{k})}{E - M_i - \frac{\vec{k}^2}{2\mu_i} + i\varepsilon}. \tag{2.4.47}$$

where $M_i = m_{1i} + m_{2i}$ is the sum of the masses in the i-th channel and μ_i the corresponding reduced mass.

The bound state and resonance condition (pole of the T-matrix) in a coupled-channel study reads then,

$$\det(1 - vG) = 0. \tag{2.4.48}$$

In order to perform a full study of a molecular state, it is useful the knowledge of the wave function at meson-antimeson short distances. The Schrödinger equation, for a two coupled-channel, takes the form:

$$(H_0 + V)\,|\psi\rangle = E\,|\psi\rangle\,, \tag{2.4.49}$$

where the wave function has two components (one for each channel)

$$|\psi\rangle = \begin{pmatrix} |\psi_1\rangle \\ |\psi_2\rangle \end{pmatrix}. \tag{2.4.50}$$

The solution of the Schrödinger equation is then:

$$|\psi\rangle = \frac{1}{E - H_0}V\,|\psi\rangle\,. \tag{2.4.51}$$

and, after projecting in plane-wave functions,

$$\langle \vec{p}\,|\psi\rangle = \begin{pmatrix} \frac{1}{E-M_1-\frac{\vec{p}^{\,2}}{2\mu_1}+i\varepsilon} & 0 \\ 0 & \frac{1}{E-M_2-\frac{\vec{p}^{\,2}}{2\mu_2}+i\varepsilon} \end{pmatrix} \int \frac{d^3\vec{k}}{(2\pi)^3} \left\langle \vec{p}\,|V|\vec{k}\right\rangle \left\langle \vec{k}\,|\psi\right\rangle, \tag{2.4.52}$$

that is, two coupled equations that only have a non-trivial solution when $\det(1-vG)=0$, the condition of a bound state in the T-matrix. Indeed, for each of the two wave-function components, and using the potential defined in Eq. (2.4.42):

$$\langle \vec{p}\,|\psi_i\rangle = \frac{f(\vec{p})}{E-M_i-\frac{\vec{p}^{\,2}}{2\mu_i}} \sum_j v_{ij} \int \frac{d^3\vec{k}}{(2\pi)^3}\, f(\vec{k}) \left\langle \vec{k}\,|\psi_j\right\rangle, \tag{2.4.53}$$

$$\Rightarrow f(\vec{p})\,\langle \vec{p}\,|\psi_i\rangle = \frac{f^2(\vec{p})}{E-M_i-\frac{\vec{p}^{\,2}}{2\mu_i}} \sum_j v_{ij} \int \frac{d^3\vec{k}}{(2\pi)^3}\, f(\vec{k}) \left\langle \vec{k}\,|\psi_j\right\rangle, \tag{2.4.54}$$

which, after an integration over $d^3\vec{p}$ leads to:

$$\int \frac{d^3\vec{p}}{(2\pi)^3}\, f(\vec{p})\,\langle \vec{p}\,|\psi_i\rangle = G_{ii} \sum_j v_{ij} \int \frac{d^3\vec{k}}{(2\pi)^3}\, f(\vec{k}) \left\langle \vec{k}\,|\psi_j\right\rangle. \tag{2.4.55}$$

We can define a new variable $\hat{\psi}_i$.

$$\hat{\psi}_i = \int \frac{d^3\vec{k}}{(2\pi)^3}\, f(\vec{k}) \left\langle \vec{k}\,|\psi_i\right\rangle. \tag{2.4.56}$$

whose interpretation trivially follows from the discussion above in the monochannel case. Using this vector the bound state equation, Eq. (2.4.55), reads:

$$\hat{\psi}_i = G_{ii} \sum_j v_{ij} \hat{\psi}_j, \tag{2.4.57}$$

and the ratio between the two different wave functions around the origin (very relevant value in the analysis that we will carry out in Chapter 3 for the $X(3872)$) is then given by:

$$\frac{\hat{\psi}_1}{\hat{\psi}_2} = \frac{G_{11}\; v_{12}}{1-G_{11}\; v_{11}} = \frac{1-G_{22}\; v_{22}}{G_{22}\; v_{12}}. \tag{2.4.58}$$

2.4.2 Gaussian cutoff effects and relation to dispersion relations

In this section, the existing correlations between the low energy constant that define the potential and the cutoff is addressed in some detail. We also discuss the relation of our approach to other approaches in which the loop function is calculated from a subtracted dispersion relation.

We recall Eqs. (2.4.38) and (2.4.40) to expand the inverse of the amplitude in powers of $\vec{k}^{\,2}$. For more general purposes, we consider a potential in which the factor that multiplies the Gaussian, $\exp\left(-2\vec{k}^{\,2}/\Lambda^2\right)$, has some energy dependence instead of being constant. That is, we

replace in Eq. (2.4.38) the constant v by an energy dependent function $v(E) = v_1 + v_2 k^2$, that reduces to the original form by setting $v_2 = 0$. We find,

$$\begin{aligned} T^{-1} &= V^{-1} - G\, e^{2\vec{k}^2/\Lambda^2} = \\ &= \frac{1}{v_1} + \frac{\mu\Lambda}{(2\pi)^{3/2}} + \left(-\frac{v_2}{v_1^2} + \frac{2}{v_1\Lambda^2} - \frac{2\mu}{(2\pi)^{3/2}\Lambda} \right) k^2 + i\frac{\mu k}{2\pi} + \mathcal{O}(k^4) \ . \end{aligned} \tag{2.4.59}$$

For model-given values of v_1 and v_2 for an imposed cutoff Λ, one can shift the cutoff to Λ' and have the same T-matrix, up to $\mathcal{O}(k^4)$, by reabsorbing the cutoff shift in the new parameters v_1' and v_2', given by:

$$\frac{1}{v_1'} = \frac{1}{v_1} + \frac{\mu(\Lambda - \Lambda')}{(2\pi)^{3/2}} \ , \tag{2.4.60}$$

$$\frac{v_2'}{v_1'^2} = \frac{v_2}{v_1^2} + \frac{2}{v_1}\frac{\Lambda^2 - \Lambda'^2}{\Lambda^2\Lambda'^2} + \frac{2\mu(\Lambda - \Lambda')^2}{(2\pi)^{3/2}\Lambda\Lambda'^2} \ . \tag{2.4.61}$$

If we insist on a constant potential, $v_2 = v_2' = 0$, we can also reabsorb the cutoff effects in v_1, but this would just be correct up to $\mathcal{O}(k^2)$.

Let us consider an approach in which the amplitude is written in terms of a loop function regularized by means of a once–subtracted dispersion relation (DR),[7]

$$T_{\rm DR}^{-1} = V_{\rm DR}^{-1} - G_{\rm DR} \ , \tag{2.4.62}$$

$$V_{\rm DR} = v \ , \tag{2.4.63}$$

$$G_{\rm DR} = \alpha - i\frac{\mu k}{2\pi} \ , \tag{2.4.64}$$

where v is the potential, analogous to the case of the Gaussian regulator approach, and α is a subtraction constant (a free parameter of the approach). Considering, as before, $v = v_1 + v_2 k^2$, we can expand:

$$V_{\rm DR}^{-1} - G_{\rm DR} = \frac{1}{v_1} - \alpha - \frac{v_2}{v_1^2}k^2 + i\frac{\mu k}{2\pi} + \mathcal{O}(k^4) \ . \tag{2.4.65}$$

We can then reabsorb the effects up to $\mathcal{O}(k^4)$ of an arbitrary shift in the subtraction constant by means of:

$$\frac{1}{v_1'} = \frac{1}{v_1} + \alpha' - \alpha \ , \tag{2.4.66}$$

$$v_2' = \frac{v_1'^2}{v_1^2} v_2 \ . \tag{2.4.67}$$

We see that the effects of the shift can be reabsorbed *exactly* for a constant potential, with the first of the previous equations. However, in the more general case of energy dependent potentials (as the case of chiral potentials, for example), this cannot be made exactly but just up to $\mathcal{O}(k^4)$. We see thus that there are several equivalent ways: one can fit, in the Gaussian regulator case, a constant for the potential and the cutoff, or fix the latter to a reasonable (but otherwise arbitrary) value and fit the LECs that enter in the definition of the interaction. In a dispersion relation, a similar situation is found, where now the subtraction constant plays the equivalent role of the cutoff.

[7] The expression for the loop function can be found by applying the dispersion relation integral, or, in a more handy way, by taking the limit $\Lambda \to \infty$ for the case of the Gaussian regulator loop integral and reabsorbing the infinity in the subtraction constant.

2.4.3 Lippmann-Schwinger Equation in partial waves

To obtain the predictions from OPE heavy meson-heavy antimeson potential requires a partial wave analysis. We consider $^{2S+1}L_J$ partial waves, defined as:

$$|p\,;JMLS\rangle = \frac{1}{\sqrt{4\pi}} \sum_{M_l,M_s} (LSJ|M_L M_S M) \int d\Omega(\hat{p}) Y_{L,M_L}(\hat{p}) |\vec{p}, SM_S\rangle, \tag{2.4.68}$$

with p the modulus of the momentum of the $\mathrm{H\bar{H}}$ pair in their center of mass (c.m.) frame, S, L, J the spin, orbital and total angular momentum and the factor $(LSJ|M_L M_S M)$ a Clebsch-Gordan coefficient. The normalization of these states,

$$\langle p'; J'M'L'S'\,|p\,;JMLS\rangle = (2\pi)^3\, \frac{\delta(p'-p)}{4\pi p^2} \delta_{JJ'}\delta_{MM'}\delta_{LL'}\delta_{SS'}, \tag{2.4.69}$$

is determined by that of the plane wave states, $\langle \vec{p}\,'; S'M'_S\,|\vec{p}\,; SM_S\rangle = (2\pi)^3\,\delta^3(\vec{p}-\vec{p}\,')\delta_{S,S'}\delta_{M_S M'_S}$. In this basis, the LSE for the elastic $1+2\to 1+2$ process reads,

$$\begin{aligned} T^{S'S}_{JL'L}(E;p',p) &= V^{S'S}_{JL'L}(p',p) + \\ &+ \sum_{L'',S''} \int_0^{+\infty} \frac{dqq^2 4\pi}{(2\pi)^3} \frac{V^{S'S''}_{JL'L''}(p',q) T^{S''S}_{JL''L}(E;q,p)}{E-\vec{q}^{\,2}/2\mu - m_1 - m_2 + i\epsilon}. \end{aligned} \tag{2.4.70}$$

with,

$$T^{S'S}_{JL'L}(E;p',p)\delta_{MM'} = \langle p'; JM'L'S'\,|T(E)|p\,;JMLS\rangle, \tag{2.4.71}$$

and a similar expression for the kernel potential $V^{S'S}_{JL'L}(E;p',p)$. The normalization of the scattering amplitude is such that on the mass shell, $p=p'=\sqrt{2\mu(E-m_1-m_2)}\equiv k$, and for diagonal LS transitions, it is related to the phase shifts, $\delta^J_{LS}(k)$, by

$$T^{SS}_{JLL}(E) = -\frac{2\pi}{\mu}\left(\frac{e^{2\mathrm{i}\delta^J_{LS}}-1}{2ik}\right). \tag{2.4.72}$$

We obtain the kernel of the LSE from the Lagrangian of Eq. (2.3.34) as described in Eq. (2.3.37) of Sect. 2.3.2. The matrix elements of the potential between $^{2S+1}L_J$ partial waves, read

$$\begin{aligned} V^{S'S}_{JL'L}(p',p) &\equiv \langle p'; JML'S'\,|V|p\,;JMLS\rangle \\ &= \frac{1}{4\pi}\int d\Omega(\hat{p}) \int d\Omega(\hat{p}') \sum_{M_L M_S M'_L M'_S} (LSJ|M_L M_S M)\times \\ &\quad (L'S'J|M'_L M'_S M) Y^*_{L',M'_L}(\hat{p}') Y_{L,M_L}(\hat{p}) \\ &\times \sum_{m_1 m_2 m'_1 m'_2} (S_1 S_2 S|m_1 m_2 M_S)(S'_1 S'_2 S'|m'_1 m'_2 M'_S)\times \\ &\quad \times \langle \vec{p}\,'; (S'_1 m'_1)(S'_2 m'_2)|V|\vec{p}\,; (S_1 m_1)(S_2 m_2)\rangle\,. \end{aligned} \tag{2.4.73}$$

Note that, thanks to rotational invariance, the above matrix element is independent of the third component of the total angular momentum, M. The partial waves of the potential were given in Eq. (2.3.42) and computed inserting in Eq. (2.4.73) the Fourier transform of the potential,

$$\begin{aligned} &\langle \vec{p}\,'; (S'_1 m'_1)(S'_2 m'_2)|\,V\,|\vec{p}; (S_1 m_1)(S_2 m_2)\rangle = \\ &= \int \frac{d^3\vec{r}}{(2\pi)^3}\, e^{i(\vec{p}-\vec{p}\,')\cdot\vec{r}}\,\langle (S'_1 m'_1)(S'_2 m'_2)|\,V(\vec{r})\,|(S_1 m_1)(S_2 m_2)\rangle\,, \end{aligned} \tag{2.4.74}$$

that is evaluated using Eqs. (2.3.38), (2.3.39), (2.3.40) and (2.3.41). The expressions given in Eq. (2.3.42) are obtained after performing the angular in $d\Omega(\hat{p})$, $d\Omega(\hat{p}')$ integration and $d\Omega(\hat{r})$ and evaluating the sum over the Clebsch-Gordan coefficients.

To deal with the UV divergences, we include a Gaussian regulator,

$$V_{J\ L'L}^{S'S}(p',p) = v_{J\ L'L}^{S'S}(p',p)\, e^{-p'^2/\Lambda^2} e^{-p^2/\Lambda^2}. \tag{2.4.75}$$

The T-matrix in partial waves will have a solution of the form,

$$T_{J\ L'L}^{S'S}(E;p',p) = t_{J\ L'L}^{S'S}(E;p',p)\, e^{-p'^2/\Lambda^2} e^{-p^2/\Lambda^2}, \tag{2.4.76}$$

where $t_{J\ L'L}^{S'S}$ is the solution of the reduced LSE,

$$\begin{aligned} t_{J\ L'L}^{S'S}(E;p',p) &= v_{J\ L'L}^{S'S}(p',p) + \\ &+ \sum_{L'',S''} \int_0^\infty \frac{dq}{(2\pi)^3}\, 4\pi q^2\, \frac{e^{-2q^2/\Lambda^2}}{(E-m_1-m_2)-\frac{q^2}{2\mu}+i\varepsilon} v_{J\ L'L}^{S'S}(p',q)\ t_{J\ L'L}^{S'S}(E;q,p). \end{aligned} \tag{2.4.77}$$

This scheme is similar for any other momentum-dependent potential.

2.4.4 Solution of the LSE in a discretized momentum space

The LSE, in the case of a momentum-dependent potential, does not admit analytical solutions. In this thesis, we have solved the LSE in a momentum grid. Let us consider for simplicity the integral equation,

$$\begin{aligned} t(E;p',p) &= v(p',p) + \\ &+ \int_0^\infty \frac{dq}{(2\pi)^3}\, 4\pi q^2\, \frac{e^{-2q^2/\Lambda^2}}{(E-m_1-m_2)-\frac{q^2}{2\mu}+i\varepsilon} v(p',q)\ t(E;q,p), \end{aligned} \tag{2.4.78}$$

Thus we discretize the momentum space and consider a set of N Gaussian points $(q_i, i = 1, ..., N)$ to replace the integral $\int dq$ by a finite sum. There are two different scenarios depending on the sign of the binding energy $E_B = m_1 + m_2 - E$. bound states with $E_B < 0$ and resonances with $E_B > 0$. The distinction is important because in the latter scenario there might be a pole in the loop integral and, thus, the pole needs to be carefully analyzed.

Bound states

This is the simplest case as $E_B > 0$ and there is not a pole in the integral. Then, the LSE is:

$$t_{ij}(E) = v_{ij} + \sum_{m=1}^{N} w_m \frac{v_{im} g_m t_{mj}}{\gamma^2 - q_m^2}, \tag{2.4.79}$$

being w_m the corresponding Gaussian weights, $g_m = \frac{\mu}{\pi^2} q_m^2 e^{-2q_m^2/\Lambda^2}$ (the exponential appears because of our Gaussian renormalization scheme, the factor might be different in other schemes), $\gamma^2 = 2\mu\,(E - m_1 - m_2) < 0$, $v_{ij} = v(p_i, p_j)$ and an analogous definition for $t(E)$. This expression can be rewritten into,

$$\sum_{m=1}^{N} F_{im}\ t_{mj} = v_{ij} \qquad i,j = 1...N, \tag{2.4.80}$$

where the F-matrix is defined as

$$F_{im} = \delta_{im} - v_{im}\frac{w_m g_m}{\gamma^2 - q_m^2} \qquad i,m = 1...N. \tag{2.4.81}$$

Eq. (2.4.81) is the discretized version of the $(1 - VG)$ factor. Now, bound states will appear as zeros of the determinant of the F-matrix. This condition can also be obtained from the following brief analysis. Taking the determinant in Eq. (2.4.80), we obtain:

$$\det[F(E)]\ \det[t(E)] = \det[v]. \tag{2.4.82}$$

As $\det(v)$ is finite, and, for a bound state, $\det[t(E)] \to \infty$, it is needed that $\det[F(E)] = 0$.

Despite ignoring here particle coupled channels, which are suppressed in the EFT power counting, the inclusion of the OPE interactions induces still some coupled channel effects. For instance, in the $D^*\bar{D}^*$ $J = 2$ sector, the OPE mixes the partial waves ${}^1D_2$, ${}^5S_2$, ${}^5D_2$ and ${}^5G_2$ (sum over L'' and S'' in Eq. (2.4.70)). In this case, we consider dimension $4N$ matrices, where the set of discrete momenta is $q_i = \{q_1, ..., q_N, q_1, ..., q_N, q_1, ..., q_N, q_1, ..., q_N\}$. The matrices v_{ij} or t_{ij} are now constructed out of 16 sub-matrices of dimension N. Each of these sub-matrices correspond to the different partial wave transitions $\{{}^1D_2, {}^5S_2, {}^5D_2, {}^5G_2\} \to \{{}^1D_2, {}^5S_2, {}^5D_2, {}^5G_2\}$.

Resonances

As we have already mentioned, the discrete analysis of resonances involves a pole in the integral in Eq. (2.4.78), which can be rewritten as,

$$\begin{aligned} t(E;p',p) &= v(p',p) + \mathcal{P}\int_0^\infty \frac{dq}{(2\pi)^3}\ 4\pi q^2\ \frac{v(p',q)e^{-2q^2/\Lambda^2}t(E;q,p)}{(E - m_1 - m_2) - \frac{q^2}{2\mu}} - \\ &\mp i\gamma\frac{\mu}{2\pi}e^{-2\gamma^2/\Lambda^2}v(p',\gamma)t(E;\gamma,p), \end{aligned} \tag{2.4.83}$$

being $\gamma^2 = 2\mu(E - m_1 - m_2) > 0$. The $(\mp)$ factor determines the first and the second Riemann sheets, respectively. The first Riemann sheet is important if we are interested in phase shifts while the second sheet is useful if we are interested in the position of the resonances, determined by the position of the pole.

Now, making use of the identity $\mathcal{P}\int_0^\infty \frac{dq}{\gamma^2 - q^2} = 0$, we can re-express Eq. (2.4.83) as,

$$\begin{aligned} t(E;p',p) &= v(p',p) \mp i\gamma\frac{\mu}{2\pi}e^{-2\gamma^2/\Lambda^2}v(p',\gamma)\ t(E;\gamma,p) \\ &+\mathcal{P}\int_0^\infty \frac{dq}{(2\pi)^3}\ 4\pi\left[q^2\ \frac{v(p',q)e^{-2q^2/\Lambda^2}t(E;q,p)}{(E - m_1 - m_2) - \frac{q^2}{2\mu}} - \gamma^2\frac{v(p',\gamma)e^{-2\gamma^2/\Lambda^2}t(E;q,\gamma)}{(E - m_1 - m_2) - \frac{q^2}{2\mu}}\right], \end{aligned} \tag{2.4.84}$$

but thanks to the subtraction we can get rid of the principal value symbol.

In the discretization of the momentum space we now include an additional extra point $q_{N+1} = \gamma$ (the scattering point), thus we obtain:

$$\begin{aligned} t_{ij}(E) &= v_{ij} + \sum_{m=1}^{N+1} w_m \frac{v_{im}g_m t_{mj}(E) - v_{i,N+1}g_{N+1}t_{N+1,j}(E)}{\gamma^2 - q_m^2} \mp \\ &\mp i\gamma\frac{\mu}{2\pi}e^{-2\gamma^2/\Lambda^2}v_{i,N+1}\ t_{N+1,j}, \qquad i,j = 1,...,N+1 \end{aligned} \tag{2.4.85}$$

with the same definitions than in the previous subsection devoted to the bound state scenario, but imposing $w_{N+1} = 0$. Then, we obtain,

$$\Rightarrow \sum_{m=1}^{N+1} F_{im}\ t_{mj} = v_{ij} \qquad i,j = 1,...,N+1 \tag{2.4.86}$$

with,

$$F_{im} = \delta_{im} - v_{im}\frac{w_m g_m}{\gamma^2 - q_m^2} \qquad \text{for } m = 1...N$$

$$F_{i,N+1} = \delta_{i,N+1} + v_{i,N+1}\left(\pm i\frac{\pi}{2\gamma} + \sum_{l=1}^{N}\frac{w_l}{\gamma^2 - q_l^2}\right) g_{N+1}.$$

Again, the condition $\det F = 0$ determines the position of poles in the T-matrix and, therefore, the position of the resonances of the system.

Chapter 3

Heavy meson-heavy antimeson molecules in the charm sector

3.1 Introduction

In this chapter, we predict the possible existence of some molecular states in the hidden charm meson-antimeson molecular spectrum. The chapter is based on Ref. [1], and the results are derived from a natural extension of the work done in [25]. In [25], heavy meson-heavy antimeson molecules, with hidden charm, were described using the EFT model approach based on HQSS and $SU(2)$ light flavour symmetry discussed in the previous chapters. Since the authors in [25] were only interested in the isoscalar molecules without hidden strangeness, no isospin degrees of freedom were needed and, thus, they used the following effective Lagrangian (see Eq. (2.3.17)).

$$\begin{aligned}\mathcal{L}_{4H} &= C_A \,\mathrm{Tr}\left[\bar{H}^{(Q)a} H_a^{(Q)} \gamma_\mu\right] \mathrm{Tr}\left[H^{(\bar{Q})a} \bar{H}_a^{(\bar{Q})} \gamma^\mu\right] \\ &+ C_B \,\mathrm{Tr}\left[\bar{H}^{(Q)a} H_a^{(Q)} \gamma_\mu \gamma_5\right] \mathrm{Tr}\left[H^{(\bar{Q})a} \bar{H}_a^{(\bar{Q})} \gamma^\mu \gamma_5\right] \end{aligned} \tag{3.1.1}$$

The two undetermined LECs were then fitted to reproduce the position of two experimental isoscalar resonances whose molecular nature was assumed (namely, the $X(3872)$ and the $X(3915)$). Within this approach, a series of isoscalar molecular states, not yet observed, were predicted in [25]. We compile, in Table 3.1, the most relevant results of Ref. [25]. We see that, from the molecular interpretation of these two resonances, the existence of another four isoscalar molecular resonances was predicted. Among them, the possible existence of a partner of the $X(3872)$, with $J^{PC} = 2^{++}$ (called $X(4012)$), seemed to be a robust prediction of HQSS since, at LO, the contact interaction in the $X(3872)$ ($J^{PC} = 1^{++}$) and the 2^{++} sectors is identical as we already discussed in the Subsect. 2.3.

In addition, the role of coupled channels and the inclusion of OPE potentials in the dynamics of these molecular states were also discussed and numerically computed. We again collect here the most relevant results obtained in this reference for those effects (Tables 3.2 and 3.3, respectively). What can be observed in these tables is that the OPE and coupled channel effects are numerically small since they only lead to very small deviations from the results in Table 3.1. Moreover, these effects are accounted for the expected HQSS uncertainties displayed in Table 3.1. Then, both effects are thought to be subleading and compatible with the errors owing to the HQSS expansion.

J^{PC}	$H\bar{H}$	V_c	E ($\Lambda = 0.5$ GeV)	E ($\Lambda = 1$ GeV)
0^{++}	$D\bar{D}$	C_{0a}	3706 ± 10	3712^{+13}_{-17}
1^{++}	$D\bar{D}^*$	$C_{0a} + C_{0b}$	Input	Input
1^{+-}	$D\bar{D}^*$	$C_{0a} - C_{0b}$	3814 ± 17	3819^{+24}_{-27}
0^{++}	$D^*\bar{D}^*$	$C_{0a} - 2C_{0b}$	Input	Input
1^{+-}	$D^*\bar{D}^*$	$C_{0a} - C_{0b}$	3953 ± 17	3956^{+25}_{-28}
2^{++}	$D^*\bar{D}^*$	$C_{0a} + C_{0b}$	4012 ± 3	4012^{+4}_{-9}

Table 3.1: *Predicted masses (in MeV) of the $X(3872)$ and $X(3915)$ isoscalar partners for two different values of the Gaussian cutoff using as input 3871.6 MeV and 3917.4 MeV for the mass of these two resonances, respectively. Errors are obtained by varying the strength of the contact interaction in each channel by $\mp 15\%$, which corresponds to the expected violation of HQSS at the charm quark scale (see Ref. [25] for details).*

These conclusions are crucial in the formalism of the EFT used in this thesis. Those numerical results confirm the theoretical findings of Ref. [11].

Next, we extend the work of Ref. [25] introducing two main modifications. On one hand, we use $SU(3)$ light quark flavour symmetry (instead of the former $SU(2)$) what allows us to explore and relate different isospin sectors, including those with explicit and hidden strangeness. The main consequence of this extension is that our LO effective Lagrangian now contains four undetermined LECs that can be used to describe up to 16 different channels with 24 different states. As we will see, the inclusion of a third resonance -the $X(4140)$- in the input to fit one of the two additional LECs will be needed. On the other hand, we also assume in this chapter, and in practically the rest of this thesis, that the $X(3872)$ resonance does not have a well-defined isospin, but instead, it is a state composed of an admixture of isospin 0 and isospin 1. Within this scheme, it is possible to explain its puzzling experimental decays. This latter assumption is detailed below in Sect. 3.2. We will see that this new approach allows to fit the four undetermined LEC of the theory.

This chapter is structured as follows. In Sect. 3.2, we consider the isospin violating decay of the $X(3872)$ into $J/\psi\ \rho$ and $J/\psi\ \omega$, which can be used to obtain information about the interaction of the $D\bar{D}^*$ pair in the isovector channel. Next, in Sect. 3.3, we present the extension to three light flavours of the EFT Lagrangian previously used in Ref. [25] and identify the four undetermined LECs that will be later fitted. In this Sect. 3.3, we calculate the location of the $SU(3)$-flavour and HQSS partners of the $X(3872)$, $X(3915)$ and $X(4140)$ resonances. A brief summary of the obtained results is finally given in Sect. 3.4.

3.2 Isospin violation in the $X(3872)$ decays

The generalization of the Lagrangian of Eq. (2.3.17) to $SU(3)$-flavour symmetry is straightforward, as discussed in Sect. 2.3.1. Thus, taking $P_a^{(c)} = \left(c\bar{u}, c\bar{d}, c\bar{s}\right) = \left(D^0, D^+, D_s^+\right)$ and using

J^{PC}	$H\bar{H}$	$^{2S+1}L_J$	E ($\Lambda = 0.5$ GeV)	E ($\Lambda = 1$ GeV)
0^{++}	$D\bar{D}$	$^1S_0$	3708	3720
1^{++}	$D\bar{D}^*$	$^3S_1, ^3D_1$	Input	Input
1^{+-}	$D\bar{D}^*$	$^3S_1, ^3D_1$	3816	3823
0^{++}	$D^*\bar{D}^*$	$^1S_0, ^5D_2$	Input	Input
1^{+-}	$D^*\bar{D}^*$	$^3S_1, ^3D_1$	3954	3958
2^{++}	$D^*\bar{D}^*$	$^1D_2, ^5S_2, ^5D_2, ^5G_2$	4015	4014

Table 3.2: *Predicted masses (in MeV) of the $X(3872)$ and $X(3915)$ partners when OPE potentials are included in the dynamics. Counter-terms are fixed to reproduce the same input than in Table 3.1. Note that small deviations of the order of few MeVs are obtained with respect to the previous predictions, presented in 3.1. The $^{2S+1}L_J$ partial waves considered in the analysis are collected in the third column. The inclusion of the OPE potential produces a larger change in the C_B coupling than in the C_A one, and actually, it was found that the bulk of the change in C_B was given by the size of the contact piece of OPE: $C_B \to C_B - \frac{g^2}{2f_\pi^2}$, as discussed in Sect. 2.3.2 (see Eq. (2.3.48)).*

the two $SU(3)$ Casimir operators $\mathbb{1}$ and $\vec{\lambda}\cdot\vec{\lambda}$, we could write,

$$\begin{aligned}
\mathcal{L}_{4H} &= C_A \,\mathrm{Tr}\left[\bar{H}^{(Q)a} H_a^{(Q)} \gamma_\mu\right] \mathrm{Tr}\left[H^{(\bar{Q})a} \bar{H}_a^{(\bar{Q})} \gamma^\mu\right] \\
&+ C_A^\lambda \,\mathrm{Tr}\left[\bar{H}^{(Q)a} \vec{\lambda}_a^{\,b} H_b^{(Q)} \gamma_\mu\right] \mathrm{Tr}\left[H^{(\bar{Q})c} \vec{\lambda}_c^{\,d} \bar{H}_d^{(\bar{Q})} \gamma^\mu\right] \\
&+ C_B \,\mathrm{Tr}\left[\bar{H}^{(Q)a} H_a^{(Q)} \gamma_\mu\gamma_5\right] \mathrm{Tr}\left[H^{(\bar{Q})a} \bar{H}_a^{(\bar{Q})} \gamma^\mu\gamma_5\right] \\
&+ C_B^\lambda \,\mathrm{Tr}\left[\bar{H}^{(Q)a} \vec{\lambda}_a^{\,b} H_b^{(Q)} \gamma_\mu\gamma_5\right] \mathrm{Tr}\left[H^{(\bar{Q})c} \vec{\lambda}_c^{\,d} \bar{H}_d^{(\bar{Q})} \gamma^\mu\gamma_5\right], \qquad (3.2.1)
\end{aligned}$$

There are still four counter-terms that are related to the four possible spin-$SU(3)$ flavour configurations of the light degrees of freedom in the $P^{(*)}\bar{P}^{(*)}$ system: spin 0,1 and flavour $SU(3)$ singlet or octet. The counter-terms C_A, C_A^λ, C_B and C_B^λ that appear in Eq. (3.2.1) can be easily rewritten[1] in terms of C_{0a}, C_{0b}, C_{1a} and C_{1b} introduced in the $\mathcal{L}_{4H}$ of Eq. (2.3.17). If we are able to determine the value of the counter-terms of the LO $SU(3)$ EFT, we can calculate the location of the molecular partners of the $X(3872)$. These four parameters describe the twenty-four different JIS sectors where possible s-wave molecules can be dynamically generated (sectors connected by C-parity transformations are not counted twice). Isoscalar molecules ($I = 0$, $S = 0$) without hidden strangeness can be described with C_{0a} and C_{0b}. Isospinor ($I = 1/2$, $S = \pm 1$) and isovector ($I = 1$, $S = 0$) states are in turn determined by C_{1a} and C_{1b}. Finally, for molecular states with hidden strangeness, the contact range interactions turn out to be the average of the isoscalar and isovector ones.

The effective interaction of Eq. (3.2.1) does not produce isospin violations, since it respects the symmetry of the underlying interaction, QCD, in the $m_u = m_d$ limit. This means that the

[1] $C_{0a} = C_A + \frac{10}{3}C_A^\lambda$, $C_{0b} = C_B + \frac{10}{3}C_B^\lambda$, $C_{1a} = C_A - \frac{2}{3}C_A^\lambda$ and $C_{1b} = C_B - \frac{2}{3}C_B^\lambda$

J^{PC}	$H\bar{H}$	E ($\Lambda = 0.5$ GeV)	E ($\Lambda = 1$ GeV)
0^{++}	$D\bar{D}, D^*\bar{D}^*$	3690	3694
1^{++}	$D\bar{D}^*$	Input	Input
1^{+-}	$D\bar{D}^*, D^*\bar{D}^*$	3782	3782
0^{++}	$D\bar{D}, D^*\bar{D}^*$	$3939 - \frac{i}{2}12$	$3939 - \frac{i}{2}31$
1^{+-}	$D\bar{D}^*, D^*\bar{D}^*$	$3984 - \frac{i}{2}17$	$3982 - \frac{i}{2}29$
2^{++}	$D^*\bar{D}^*$	4012	4012

Table 3.3: *Predicted pole positions (in MeV) of the $X(3872)$ partners when particle coupled channel effects are considered. The local contact interaction terms are fixed to the values used in Table 3.1, adjusted to reproduce the $X(3872)$ and $X(3915)$ masses neglecting coupled channel effects (see details in Ref.[25]). Again small differences are found with respect to the results in Table 3.1.*

eigenstates of this effective theory are expected to have a well-defined isospin. However, the $X(3872)$ has been experimentally observed in two different isospin channels [100],

$$B_X = \frac{\mathcal{B}(X(3872) \to J/\psi\ \pi^+\pi^-\pi^0)}{\mathcal{B}(X(3872) \to J/\psi\ \pi^+\pi^-)} \simeq 0.8 \pm 0.3. \tag{3.2.2}$$

The ratio of these two branching fractions is expected to be zero (or infinite) if isospin were a good quantum in the decay. We expect the 2π and 3π decays to happen via an intermediate ρ and ω meson, respectively. The first of these two decays is mediated by an intermediate ω meson:

$$X(3872) \to J/\psi\ \omega \to J/\psi\ \pi^+\pi^-\pi^0, \tag{3.2.3}$$

which is consistent with an isoscalar $X(3872)$ state. The other decay mode, analogously, would be mediated by a ρ meson:

$$X(3872) \to J/\psi\ \rho \to J/\psi\ \pi^+\pi^-, \tag{3.2.4}$$

where the isospin of the final state is one. This situation suggests two different scenarios: either the decay of the resonance violates isospin symmetry (something difficult to match with QCD processes) or the resonance does not have a well defined isospin quantum number. Along this work, we will adopt the latter perspective. The $X(3872)$ resonance is placed a few tens of keV from the $D^0\bar{D}^{*0}$ threshold and thus its binding energy is much smaller than the energy difference between the charged (D^+D^{*-}) and neutral ($D^0\bar{D}^{*0}$) channels, around 8 MeV. Owing to this mass splitting, despite the potential V in the Hamiltonian conserves isospin, the kinetic operator does not, and the whole Hamiltonian does not commute with the isospin operator. Therefore, eigenstates of the Hamiltonian do not have to be eigenstates of the isospin operator (required condition to have a defined isospin) and, thus, isospin symmetry breaking is expected at long distances.

Now, considering that the $X(3872)$ is a coupled $D\bar{D}^*$ molecular system[2] with quantum numbers $J^{PC} = 1^{++}$, where we distinguish between the neutral ($D^0\bar{D}^{*0}$) and charged (D^+D^{*-})

[2]When we refer to $D^0\bar{D}^{*0}$, D^+D^{*-}, or in general $D\bar{D}^*$, we are actually referring to the combination of these states with their charge conjugate ones in order to form a state with well-defined C-parity. In the case of the $X(3872)$, the C-parity is $+$.

components of the wave function, the two decays of Eq. (3.2.3) and (3.2.4) can be described similarly by the Feynman diagram depicted in Fig. 3.1:

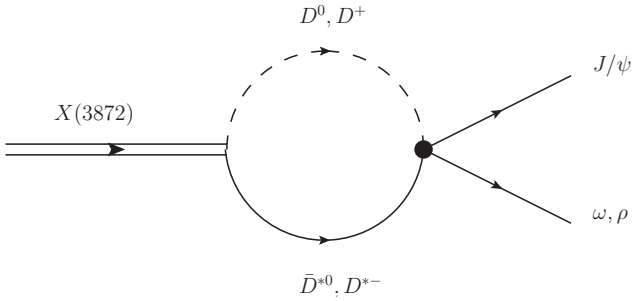

Figure 3.1: *Decay mechanisms of the $X(3872)$ decay into J/ψ $\omega(\rho)$ assuming a $D\bar{D}^*$ molecular nature of the resonance.*

To compute these Feynman diagrams, one needs the $D\bar{D}^* \to J/\psi\ \omega$ and $D\bar{D}^* \to J/\psi\ \rho$ amplitudes. We define these amplitudes as,

$$\mathcal{M}_\omega(D\bar{D}^*(I=0) \to J/\psi\ \omega) = g_\omega, \tag{3.2.5}$$

$$\mathcal{M}_\rho(D\bar{D}^*(I=1) \to J/\psi\ \rho) = g_\rho, \tag{3.2.6}$$

for on-shell particles. On the other hand, the isospin $D\bar{D}^*$ states are related to the charged and neutral ones by,

$$\left|D^0\bar{D}^{*0}\right\rangle = \frac{1}{\sqrt{2}}\left(|I=0\rangle + |I=1\rangle\right), \tag{3.2.7}$$

$$\left|D^+D^{*-}\right\rangle = \frac{1}{\sqrt{2}}\left(|I=0\rangle - |I=1\rangle\right), \tag{3.2.8}$$

which leads to the following amplitudes for the $X(3872) \to J/\psi\ \rho$ and $X(3872) \to J/\psi\ \omega$ transitions,

$$\mathcal{M}\left(X(3872) \to J/\psi\ \omega\right) = \frac{1}{\sqrt{2}}\left(g_1 G_{11}^\alpha + g_2 G_{22}^\alpha\right) g_\omega \tag{3.2.9}$$

$$\mathcal{M}\left(X(3872) \to J/\psi\ \rho\right) = \frac{1}{\sqrt{2}}\left(g_1 G_{11}^\alpha - g_2 G_{22}^\alpha\right) g_\rho \tag{3.2.10}$$

where $E_\alpha = M(X(3872))$ is the mass of the bound state. The $D^0\bar{D}^{*0}$ and $D^+\bar{D}^{*-}$ are the channels 11 and 22 respectively. Besides, g_1 and g_2 are the couplings of the $X(3872)$ resonance to the neutral and charged channels, respectively. They are defined, as discussed in the previous chapter, from the residue of the non-relativistic T-matrix at the pole (see Eq. (2.4.12)). The non-relativistic propagators read,

$$G_{ii}^\alpha = \int \frac{d^3\vec{q}}{(2\pi)^3} \frac{f^2(q)}{E_\alpha - m_{1i} - m_{2i} - \frac{\vec{q}^2}{2\mu_{ii}}}, \qquad \mu_{ii}^{-1} = m_{1i}^{-1} + m_{2i}^{-1} \tag{3.2.11}$$

Note that we have been able to factorize the propagator defined in Eq. (3.2.11) because there appears two insertions of the UV regulator, $f(q)$, in the computation of the Feynman diagram. The first one accounts for the off-shellness of the $D\bar{D}^*$ mesons in the $X(3872)$ vertex, while the

second one appears because we have taken a factor $\frac{f(q)}{f(k)}$ for the off-shell extrapolation of the amplitudes of Eqs. (3.2.5) and (3.2.6)[3].

On the other hand, from Subsect. 2.4, we have,

$$g_i G_{ii} = \hat{\psi}_i = \int \frac{d^3p}{(2\pi)^3} f(p) \langle \vec{p} | \psi_i \rangle = \int d^3x \psi_i(x) \hat{f}(x) \tag{3.2.12}$$

where $\hat{\psi}$ is the UV weighted average of the i-th component of the wave function in a region around the origin (zero separation distance between the D and $\bar{D}^*$ mesons). This is natural, since the strong interaction is of short range and the D and $\bar{D}^*$ mesons should be close enough to be reconverted in a charmonium state plus a light vector meson. In this way, the ratio can be rewritten as,

$$R_X = \frac{\mathcal{M}(X(3872) \to J/\psi\ \rho)}{\mathcal{M}(X(3872) \to J/\psi\ \omega)} = \frac{g_\rho}{g_\omega} \left(\frac{\hat{\psi}_1 - \hat{\psi}_2}{\hat{\psi}_1 + \hat{\psi}_2} \right) \tag{3.2.13}$$

It is interesting to notice the analysis of Hanhart et al., of Ref. [101], where the branching ratio quoted in Eq. (3.2.2) is used to estimate the amplitude ratio R_X once the different decay widths of the intermediate mesons ρ, ω are taken into account. The analysis of Ref. [101] leads to,

$$R_X = 0.26^{+0.08}_{-0.05}. \tag{3.2.14}$$

The amplitude ratio R_X is equivalent to the experimental branching ratio B_X, provided we assume the quantum numbers of the $X(3872)$ to be $J^{PC} = 1^{++}$. In particular, the experimental errors in B_X are completely accounted for by the errors in R_X.

The only parameter we cannot determine in our EFT formalism is the ratio between the unknown on-shell couplings g_ρ and g_ω. Nonetheless, taking advantage of $SU(3)$ light flavour symmetry, we can relate these two couplings. Using the tables computed in [102] and using an appropriate basis we can describe the states in terms of $SU(3)$ light degrees of freedom. Thus, in the $|M; S; I\rangle$ basis, being M the $SU(3)$ multiplet, S the strangeness and I the isospin quantum numbers, the $D\bar{D}^*$ states can be written:

$$\left| D\bar{D}^*, I = 0 \right\rangle = -\frac{1}{\sqrt{3}} \left(\sqrt{2} \left| 1; 0; 0 \right\rangle + \left| 8; 0; 0 \right\rangle \right), \tag{3.2.15}$$

$$\left| D\bar{D}^*, I = 1 \right\rangle = \left| 8; 0; 1 \right\rangle. \tag{3.2.16}$$

The light final state mesons read,

$$\rho = -\left| 8; 0; 1 \right\rangle, \tag{3.2.17}$$

$$\omega = \frac{1}{\sqrt{3}}\ \omega_8 + \sqrt{\frac{2}{3}}\ \omega_1, \tag{3.2.18}$$

$$\phi = -\sqrt{\frac{2}{3}}\ \omega_8 + \frac{1}{\sqrt{3}}\ \omega_1, \tag{3.2.19}$$

where $\omega_{1,8}$ are the $SU(3)$ $|1; 0; 0\rangle$ and $|8; 0; 0\rangle$ states. Besides, the J/ψ is a pure charmonium state. Since the QCD Hamiltonian is invariant under $SU(3)$ light flavour rotations, states belonging to different $SU(3)$ multiplets cannot be connected, meaning that:

$$g_\rho = \langle J/\psi\ \rho | H_{QCD} \left| D\bar{D}^*, I = 1 \right\rangle = -H_8, \tag{3.2.20}$$

[3]Note that in the computation of the Feynman diagram of Fig. 3.1, it appears the residue of the T-matrix, but it together with the factor $\frac{1}{\hat{f}(k)}$ (with k the on-shell momentum), it gives rise to the residue of the reduced t-matrix used in Eqs. (3.2.9), (3.2.10) and (3.2.12).

$$g_\omega = \langle J/\psi\ \omega|\, H_{QCD}\, \big|D\bar{D}^*, I=0\big\rangle = -\frac{2}{3}H_1 - \frac{1}{3}H_8, \tag{3.2.21}$$

$$g_\phi = \langle J/\psi\ \phi|\, H_{QCD}\, \big|D\bar{D}^*, I=0\big\rangle = -\frac{\sqrt{2}}{3}H_1 + \frac{\sqrt{2}}{3}H_8, \tag{3.2.22}$$

where $H_{1,8}$ is the QCD Hamiltonian in the singlet and octet representation, respectively.

$$\Rightarrow g_\omega - g_\rho = \sqrt{2}g_\phi. \tag{3.2.23}$$

Finally, assuming that the OZI selection rule holds (quark-antiquark pair creation is suppressed) $g_\rho, g_\omega >> g_\phi$, we can conclude that[4]

$$g_\omega \simeq +g_\rho \tag{3.2.24}$$

and that the R_X ratio simplifies to,

$$R_X \simeq \left(\frac{\hat{\psi}_1 - \hat{\psi}_2}{\hat{\psi}_1 + \hat{\psi}_2}\right) = 0.26^{+0.08}_{-0.05}, \tag{3.2.25}$$

and thus it only depends on the values of the neutral and charged channel wave function around the origin. As mentioned above, this result should not be surprising since it might seem natural that, using short-range operators (as those mediating strong processes), the ratio of the studied transitions should only involve the wave function at short distances.

To evaluate R_X, we have to compute the wave functions around the origin first. That calculation requires a coupled channel $\left\{D^0\bar{D}^{0*}, D^+D^{*-}\right\}$ potential. If the contact potential V were of the type,

$$V = \begin{pmatrix} V_0 & V_0 \\ V_0 & V_0 \end{pmatrix}, \tag{3.2.26}$$

equivalent to assume that the $I=1$ components of the $D\bar{D}^*$ system do not interact (as assumed in [99, 103] from a $SU(4)$ flavour extended hidden gauge model in which the value of the counterterms are determined from meson exchange saturation), then:

$$\hat{\psi}_1 = aG_{11} \qquad \hat{\psi}_2 = aG_{22}, \tag{3.2.27}$$

where a is an scalar constant. G_{11} and G_{22} only depend on the masses of the neutral and charged D and $\bar{D}^*$ mesons and the mass of the $X(3872)$ resonance, then R_X is totally fixed by the binding energy of the $X(3872)$,

$$R_X = \left(\frac{G_{11} - G_{22}}{G_{11} + G_{22}}\right) \sim 0.13. \tag{3.2.28}$$

This result obtained in Refs. [99, 103] is close to the fitted value from experimental data in [101], $R_X \simeq 0.26^{+0.08}_{-0.05}$, but in principle there is room for improvement. Indeed, we can use the experimental determination of R_X to constrain the interaction in the isovector channel. For that purpose, we use the interaction deduced from $\mathcal{L}_{4H}$ in Eq. (3.2.1) where the interaction in the isospin $I=1$ channel is no longer neglected. Our potential in the coupled channel space is then,

$$V = \frac{1}{2}\begin{pmatrix} C_{0X} + C_{1X} & C_{0X} - C_{1X} \\ C_{0X} - C_{1X} & C_{0X} + C_{1X} \end{pmatrix}, \tag{3.2.29}$$

[4]Of course, there are deviations from the result above coming from the approximate nature of the OZI rule and, to a lesser extend, to SU(3) breaking effects. However, estimating the size of these deviations is not straightforward and therefore we have not attempted to systematically include this error source in the calculations to come. In this regard we simply note that owing to the large relative error in R_X (20-30%), smaller relative deviations from $g_\rho/g_\omega \simeq 1$ (e.g. 10-20%), for which our results turn out to be little sensitive, will be inconsequential as the two errors are independent and thus are added quadratically.

being $C_{0X} = C_{0a} + C_{0b}$ and $C_{1X} = C_{1a} + C_{1b}$, the interaction for well defined isospin $I = 0$ and $I = 1$ states, respectively. The couplings C_{0X} and C_{1X} (or equivalently $C_{0a}+C_{0b}$ and $C_{1a}+C_{1b}$) can be then determined from the $X(3872)$ mass and the experimental ρ/ω ratio R_X.

We solve the LSE using as a kernel of the equation the LO potential of Eq. (3.2.29). We regularize the LSE with a Gaussian regulator function (see for instance Eq. (2.4.38) for further details) and use a cutoff Λ in the range $0.5 - 1.0\,\text{GeV}$. We obtain the values[5]

$$C_{0X} = -1.693^{+0.036}_{-0.023}\,\text{fm}^2 \qquad (-0.731^{+0.008}_{-0.005}\,\text{fm}^2)\,, \tag{3.2.30}$$

$$C_{1X} = -0.08^{+0.42}_{-0.41}\,\text{fm}^2 \qquad (-0.373^{+0.089}_{-0.090}\,\text{fm}^2)\,, \tag{3.2.31}$$

for $\Lambda = 0.5\,\text{GeV}$ ($1\,\text{GeV}$). The errors displayed take into account the asymmetric errors in the ratio R_X. Here, we have not considered the error on the $X(3872)$ mass. The couplings indicate that the strength of the interaction in the isovector channel is weaker than in the isoscalar one. In particular, we will show that the isovector coupling C_{1X} is not strong enough to generate a second bound state, the (mostly) isovector partner of the $X(3872)$.

We find it worth commenting the comparison of our results for the counter-terms with the hidden gauge model of Gamermann et al. [99, 103], discussed above in Eqs. (3.2.26)-(3.2.28). The hidden gauge model predicts $C_{1X} = 0$ (as the contributions from the ρ and ω mesons cancel out) and $R_X = 0.136$ (for a sharp cutoff regulator and $\Lambda = 653\,\text{MeV}$, see Ref. [99] for details), we obtain a small (yet important) contribution to C_{1X}. As can be seen, this small contribution is necessary to fine tune the isospin violating branching ratio of the $X(3872)$ decays to its exact value.

3.3 The SU(3) and HQSS Partners

We fix two of the counter-terms that appeared in $\mathcal{L}_{4H}$ of Eq. (3.2.1) from the location of the $X(3872)$ resonance and its isospin breaking branching ratio, as explained in the previous section. The remaining two LECs require the identification of two partners of the $X(3872)$. We have chosen the $X(3915)$ [35] as a 0^{++} isoscalar $D^*\bar{D}^*$ molecule and the $Y(4140)$ [36] as a 0^{++} $D_s^*\bar{D}_s^*$ molecule, guided by its apparently dominant decay into $J/\Psi\phi$. We notice that these identifications were proposed for the first time in Refs. [32, 33, 34].

The 0^{++} assignment for the quantum numbers of the $X(3915)$ and $Y(4140)$ deserves some discussion. On one hand, the 2^{++} option is excluded: HQSS fixes the location of the isoscalar 2^{++} $D^*\bar{D}^*$ partner of the $X(3872)$ in the vicinity of $4012\,\text{MeV}$, far away from the $3915\,\text{MeV}$ region. If we additionally consider the isospin breaking decays of the $X(3872)$, we can determine that the isovector 2^{++} $D^*\bar{D}^*$ and the isoscalar 2^{++} $D_s^*\bar{D}_s^*$ molecules do not exist. On the other the 1^{+-} option can also be discarded from the decays of the $X(3915)$ and $Y(4140)$ into $J/\Psi\,\omega$ and $J/\Psi\,\phi$, requiring a positive C-parity state. Thus we are only left with $J^{PC} = 0^{++}$.

However, the choice of the $X(3915)$ and $Y(4140)$ states as input is not entirely free of problems. The first is the binding energy of the $X(3915)$, approximately $100\,\text{MeV}$. Around this binding there is power counting transition – one pion exchange changes from perturbative to non-perturbative – though the critical binding energy that marks this transition is not known exactly and can happen at larger bindings than expected [11]. In this regard, the investigations of Ref. [25] discussed at the beginning of this chapter, shows (by performing the explicit calculations) that we are still in the perturbative regime for the $X(3915)$ and we can employ a contact theory to describe it at LO. The $Y(4140)$, with a binding energy of $80\,\text{MeV}$, is not affected by

[5] In this chapter based on Ref.[1], we have used the experimental information available in 2013, $M_{X(3872)} = 3871.68 \pm 0.17$ MeV and the neutral threshold $m_{D^0} + m_{D^{*0}} = 3871.84 \pm 0.20$ MeV. Since then, both experimental values have slightly changed.

this issue because the $D_s^* \bar{D}_s^*$ system cannot exchange a single pion. The second problem is the debatable experimental status of the $Y(4140)$. After its first and only observation by the CDF Collaboration [36], subsequent experiments have failed to find it [60, 61]. This means that the consequences derived from the assumption that the $Y(4140)$ exists and that it has a molecular structure should be taken with a grain of salt.

Now we fix the counter-terms to the location of the $X(3915)$ and $Y(4140)$. For convenience we first define the linear combinations of counter-terms:

$$C_2 = C_{0a} - 2C_{0b}\,, \tag{3.3.1}$$

$$C_3 = \frac{1}{2}\left((C_{0a} - 2C_{0b}) + (C_{1a} - 2C_{1b})\right)\,, \tag{3.3.2}$$

where C_2 / C_3 is a convenient way to write the LO potential of the $X(3915)$ / $Y(4140)$ channel. We obtain

$$C_2 = -6.710\ \text{fm}^2 \qquad (-1.611\,\text{fm}^2)\,, \tag{3.3.3}$$

$$C_3 = -5.915\ \text{fm}^2 \qquad (-1.459\,\text{fm}^2)\,, \tag{3.3.4}$$

for a Gaussian regulator $\Lambda = 0.5\,\text{GeV}$ (1 GeV). We can transform the values of the combinations above (and the corresponding ones for C_{0X} and C_{1X}) to the standard counter-term representation, yielding

$$C_{0a} = -3.366^{+0.024}_{-0.015}\,\text{fm}^2 \qquad (-1.024^{+0.005}_{-0.003}\,\text{fm}^2)\,, \tag{3.3.5}$$

$$C_{0b} = +1.673^{+0.012}_{-0.008}\,\text{fm}^2 \qquad (+0.293^{+0.004}_{-0.002}\,\text{fm}^2)\,, \tag{3.3.6}$$

$$C_{1a} = -1.76^{+0.29}_{-0.29}\,\text{fm}^2 \qquad (-0.684^{+0.064}_{-0.063}\,\text{fm}^2)\,, \tag{3.3.7}$$

$$C_{1b} = +1.68^{+0.15}_{-0.15}\,\text{fm}^2 \qquad (+0.311^{+0.033}_{-0.033}\,\text{fm}^2)\,, \tag{3.3.8}$$

for $\Lambda = 0.5\,\text{GeV}$ (1 GeV), where the error comes from the uncertainty in R_X (a negligible effect in the isoscalar channels, but important in the isovector ones).

We notice that there are two additional error sources: the violations of HQSS due to the finite charm quark mass and the breaking of light flavour symmetry. The first of these effects can be taken into account by noticing that the EFT potential has a relative uncertainty of the order of

$$V^{\text{LO}}_{(m_Q=m_c)} = V^{\text{LO}}_{(m_Q\to\infty)}\,(1 \pm \frac{\Lambda_{QCD}}{m_c})\,, \tag{3.3.9}$$

with respect to the exact heavy quark limit. Taking a value of around 1.5 GeV for the charm quark mass and $\Lambda_{\text{QCD}} \sim 200$ MeV, we should expect a 15% violation of HQSS for the LO contact range potentials[6].

The second error source affects molecules containing strange quarks[7], where we expect the contact range potential to deviate slightly from the pure $SU(3)$ prediction, that is

$$V^{\text{LO}}_{(s-quark)} = V^{\text{LO}}_{SU(3)}\,(1 \pm \delta_{SU(3)})\,. \tag{3.3.10}$$

In the expression above $\delta_{SU(3)}$ is the relative size of the $SU(3)$-breaking effects, which can be estimated from the ratio of the kaon and pion decay constants $f_K/f_\pi \sim 1.2$, yielding $\delta_{SU(3)} = 0.2$.

[6] Actually, the 15% violation represents the full expected deviation from the heavy quark limit in the charm sector. Even though heavy quark symmetry involves heavy flavour symmetry as well as HQSS, only the later one is relevant for our purposes. Thus, when we are talking about HQSS violations, it is merely language abuse for heavy quark symmetry violations in general.

[7] We do not consider isospin breaking effects for the potential, as their size will be negligible.

This uncertainty also affects the determination of the C_3 counter-term from the mass of the $Y(4140)$ state. Thus we can assume a 20% relative error in the value we give for this parameter in Eq. (3.3.4). In turn, this will translate into an additional error in the isovector counter-terms C_{1a} and C_{1b}, see Eq. (3.3.2) for details. Actually, their errors are fully anti-correlated to ensure that the linear combination $C_1 = C_{1a} + C_{1b}$ is free from the $SU(3)$ uncertainties of C_3. For simplicity and due to the exploratory nature of the study presented on this chapter we have neglected these correlations. Instead we have substituted the correlated error in C_{1X} by an uncorrelated error in C_{1a}[8], a choice that overestimates the size of the errors in the molecular masses.

At this point we find it worth mentioning that the three error sources we have considered – the experimental error in R_X plus the breaking of HQSS and $SU(3)$ light flavour symmetry – are independent: we can compute the total error by adding the partial errors in quadratures.

Finally, we emphasize that the choice of a regulator is inessential in EFT calculations. It does not matter which regulator we have chosen, as far as the cutoff window is sensible enough. We have explicitly tested this assumption by calculating the full molecular spectrum with other regulators. In general we find small changes in the central location of the states that are compatible with the cutoff uncertainty we already find in Tables 3.4-3.7, i.e. around 10 MeV for the most tightly bound cases. For instance, the location of the 1^{+-} isoscalar molecule we predict in Table 3.4 changes from 3955 MeV (3958 MeV) for a Gaussian regulator to 3954 MeV (3957 MeV) with a sharp cutoff, 3965 MeV (3964 MeV) with a monopolar regulator and 3960 MeV (3961 MeV) with a dipolar regulator, in all cases with a cutoff $\Lambda = 0.5\,\text{GeV}$ (1.0 GeV)[9].

3.3.1 The SU(2) Isoscalar ($I = 0$) Partners

We begin with the $SU(2)$ isoscalar sector, in which we ignore the hidden strange components. The states are determined by the counter-terms C_{0a} and C_{0b}. We do not take into account particle coupled channel effects since they are subleading, as explicitly checked in Ref. [25]. There is one exception though, the 1^{++} and 2^{++} channels, where the mass gap between the neutral and charged channels (8 and 6 MeV in each case) is similar in size to the binding energy in the isospin symmetric limit (4 and 5 MeV). This suggests that we may treat the neutral and charged channels as explicit degrees of freedom of the theory. We note that the inclusion of isospin violation is the only difference with respect to the previous analysis of Ref. [25]. The spectrum of molecular states is presented in Table 3.4. As can be seen, isospin violation is a small perturbation over the former predictions of Ref. [25] and presented in Tables 3.1-3.3 (though it is still crucial to describe isospin violating decays properly).

We, however, would like to make a few remarks. The first one concerns the 2^{++} state. The central values of the counter-terms as given in Eqs. (3.3.5)–(3.3.8) predict that the 2^{++} state lies very close (less than 1 MeV) to the lowest energy threshold, i.e. $D^{*0}\bar{D}^{*0}$. When we decrease the strength of the potential to account for the uncertainties of our approach, the pole reaches the neutral threshold and then bounces back into the second Riemann sheet. That is, the state becomes virtual (instead of bound). In any case, the existence of the pole will strongly influence the amplitude at threshold.

[8] Note that we can rewrite C_3 as $\frac{1}{2}C_2 - C_{1X} + \frac{3}{2}C_{1a}$. The isoscalar part of the interaction C_2 and the isovector C_1 are fixed by the $X(3872)$ and $X(3915)$ inputs, meaning that all the error can be transferred to C_{1a}. As a matter of fact the decomposition is not unique: we could transfer the error to C_{1b} instead.

[9] Actually, one should take into account that the optimal cutoff window depends on the choice of a regulator. In particular, for the monopolar regulator we should use larger cutoffs than for the sharp cutoff and Gaussian cases. However, for the purposes of the current discussion we can ignore this effect and take the same cutoff value for all the regulators we have considered.

J^{PC}	$\mathrm{H}\bar{\mathrm{H}}$	$^{2S+1}L_J$	V_C	E ($\Lambda = 0.5$ GeV)	E ($\Lambda = 1$ GeV)	Exp [45]	Threshold [MeV]
0^{++}	$D\bar{D}$	$^1S_0$	C_{0a}	3709^{+9}_{-10}	3715^{+12}_{-15}	–	3734.5*
1^{++}	$D^*\bar{D}$	$^3S_1$	Eq. (3.2.29)	Input	Input	3871.6	3871.8/3879.9
1^{+-}	$D^*\bar{D}$	$^3S_1$	$C_{0a} - C_{0b}$	3815^{+16}_{-17}	3821^{+23}_{-26}	–	3875.9*
0^{++}	$D^*\bar{D}^*$	$^1S_0$	$C_{0a} - 2\,C_{0b}$	Input	Input	3917	4017.3*
1^{+-}	$D^*\bar{D}^*$	$^3S_1$	$C_{0a} - C_{0b}$	3955^{+16}_{-17}	3958^{+24}_{-27}	3942	4017.3*
2^{++}	$D^*\bar{D}^*$	$^5S_2$	Eq. (3.2.29)	$4013^{\dagger\dagger}_{-9}$	$4013^{\dagger\dagger}_{-12}$	–	4014.0/4020.6

Table 3.4: *Predicted masses (in MeV) of the $SU(2)$ isoscalar HQSS partners of the $X(3872)$ resonance for two different values of the Gaussian cutoff. We use as input 3871.6 MeV, 3917.4 MeV and 4140 MeV for the $X(3872)$, $X(3915)$ and $Y(4140)$, respectively. In the last column, we also give the thresholds for the different charge combination channels ($P^0\bar{P}^0/P^+P^-$) or the threshold value that results when we neglect isospin breaking effects and we employ charge averaged masses. In this latter case, we mark it with an asterisk (*). Errors in the predicted masses are obtained by adding in quadratures the uncertainties stemming from the two sources of systematic errors discussed at the end in Subsect. 3.3: errors in our determination of the LO counter-terms in Eqs. (3.3.5)–(3.3.8) and variations obtained by modifying the strength of the contact interaction in each channel by ±15%, which corresponds to the expected violations of HQSS for the charm quark mass. †† : the upper error of the 2^{++} state mass deserves a detailed discussion that can be found in the text (Subsect. 3.3.1).*

The second comment is about the 0^{++} $D\bar{D}$ channel. As can be seen in the Table 3.4, this state is bound by about 20-25 MeV. For simplicity, we have used in this channel the isospin symmetric limit. Yet the $D^0\bar{D}^0 - D^+D^-$ threshold gap is around 9 MeV, and it might make sense the explicit consideration of isospin breaking in this channel. However, as in the $X(3872)$ and $X(4012)$ cases, the effect is rather small, justifying the validity of the isospin symmetric limit for the spectroscopy problem.

Finally, there is a remark concerning the possible effect of hidden strange channels in the dynamics of the $X(3915)$ state. As we will see, there is a 0^{++} $D_s\bar{D}_s$ state at 3925 MeV (see Table 3.7) that in principle can mix with the $X(3915)$. However, explicit calculations show that the influence of the hidden strange channel is numerically marginal: it moves the position of the predicted molecular states by a small fraction of a MeV (usually $\Delta M \sim 0.1 - 0.2$ MeV), a tiny effect compared to other error sources. The reason lies in the transition potential between the isoscalar 0^{++} $D^*\bar{D}^*$ and $D_s\bar{D}_s$ channels:

$$\langle D^*\bar{D}^*|V^{\mathrm{LO}}(0^{++})|D_s\bar{D}_s\rangle = \sqrt{\frac{3}{2}}(C_{0b} - C_{1b})\,, \tag{3.3.11}$$

which turns out to be numerically quite small, since we accidentally find $C_{0b} \simeq C_{1b}$, see Eqs. (3.3.5)–(3.3.8).

3.3.2 The Isospinor ($I = \frac{1}{2}$) Partners

The isospinor molecules are different in the sense that they have not well-defined C-parity, as they are not bound states of a heavy meson and its antimeson. In general this poses no problem (the formalism is identical to the one in the previous case) except for the 1^+ $D_s\bar{D}^*$ and $D\bar{D}_s^*$ molecules. The $D_s\bar{D}^*$ and $D\bar{D}_s^*$ thresholds are separated by only 2 MeV and require a coupled

J^{PC}	$\mathrm{H}\bar{\mathrm{H}}$	$^{2S+1}L_J$	V_C	E ($\Lambda = 0.5$ GeV)	E ($\Lambda = 1$ GeV)	Exp [45]	Threshold [MeV]
0^+	$D_s^+\bar{D}^-$	$^1S_0$	C_{1a}	$3835.8^{+2.3}_{-7.3}$	$3837.7^{+0.4}_{-8.1}$	–	3838.1
1^+	$D_s\bar{D}^*$,$D_s^*\bar{D}$	$^3S_1$	Eq. (3.3.12)	3949^{+20}_{-21}	3957^{+22}_{-32}	–	$3977.15^\dagger, 3979.55^\dagger$
0^+	$D_s^*\bar{D}^*$	$^1S_0$	$C_{1a} - 2\,C_{1b}$	4056^{+31}_{-35}	4061^{+45}_{-54}	–	$4120.9^\dagger$
1^+	$D_s^*\bar{D}^*$	$^3S_1$	$C_{1a} - C_{1b}$	4091^{+19}_{-22}	4097^{+24}_{-33}	–	$4120.9^\dagger$
2^+	$D_s^*\bar{D}^*$	$^5S_2$	$C_{1a} + C_{1b}$	–	–	–	

Table 3.5: Predicted masses (in MeV) of the isospinor ($I = \frac{1}{2}$) HQSS partners of the $X(3872)$ resonance, for two different values of the Gaussian cutoff. The meaning of the quoted errors in the table is the same as in Table 3.4. We also give the relevant thresholds (in MeV) for each channel. We use isospin third component averaged masses for those cases marked with a † symbol. Note that as we decrease the strength of the potential, the $D_s^+\bar{D}^-$ state becomes virtual (see discussion in Subsect. 3.3.2).

J^{PC}	$\mathrm{H}\bar{\mathrm{H}}$	$^{2S+1}L_J$	V_C	E ($\Lambda = 0.5$ GeV)	E ($\Lambda = 1$ GeV)	Exp [45]	Threshold [MeV]
0^{++}	$D^+\bar{D}^0$	$^1S_0$	C_{1a}	$3732.5^{+2.0}_{-6.9}$	$3734.3^{+0.2}_{-6.9}$	–	3734.5
1^{++}	$D^*\bar{D}$	$^3S_1$	Eq. (3.2.29)	–	–	–	
1^{+-}	$D^*\bar{D}$	$^3S_1$	$C_{1a} - C_{1b}$	3848^{+15}_{-17}	3857^{+15}_{-22}	–	3875.9*
0^{++}	$D^*\bar{D}^*$	$^1S_0$	$C_{1a} - 2\,C_{1b}$	3953^{+24}_{-26}	3960^{+31}_{-37}	–	4017.3*
1^{+-}	$D^*\bar{D}^*$	$^3S_1$	$C_{1a} - C_{1b}$	3988^{+15}_{-17}	3995^{+17}_{-23}	–	4017.3*
2^{++}	$D^*\bar{D}^*$	$^5S_2$	Eq. (3.2.29)	–	–	–	

Table 3.6: Predicted masses (in MeV) of the $SU(2)$ isovector HQSS partners of the $X(3872)$ resonance for two different values of the Gaussian cutoff. The meaning of the quoted errors in the table is the same as in Table 3.4. We also give the relevant thresholds (in MeV) for each channel. For the $D^*\bar{D}$ and $D^*\bar{D}^*$ cases, we give the threshold that would correspond to the zero isospin third component and calculated with charge averaged masses. Note that as we decrease the strength of the potential, the $D^+\bar{D}^0$ state becomes virtual. The upper errors for the mass of this state just account for the distance between its central mass value and the threshold.

channel treatment. The LO potential reads

$$V^{\mathrm{LO}} = \begin{pmatrix} C_{1a} & -C_{1b} \\ -C_{1b} & C_{1a} \end{pmatrix}, \tag{3.3.12}$$

where channel 1 (2) corresponds to $D_s\bar{D}^*$ ($D_s^*\bar{D}$). We find that this coupled channel potential only leads to one bound state (of a maximum of two). We list this and the other isospinor molecules in Table 3.5, where we have considered only the strangeness one states. The spectrum is identical for the strangeness minus one sector. We also notice that the error bands are bigger as they include the additional $SU(3)$ breaking effects at the level of the contact range interaction.

There is a total of four states, one of them – the 0^+ $D_s\bar{D}$ molecule – almost at threshold. Actually, there exists a small violation of the third component of isospin, because of the different masses of the D^- (D^{*-}) and $\bar{D}^0$ ($\bar{D}^{*0}$) mesons. In general the isospin splitting is smaller than the other errors in the calculations and we ignore it. The exception is the 0^+ $D_s\bar{D}$ molecule: in Table 3.5 we only report the $I_3 = -1/2$ component of the molecule, which is being formed

J^{PC}	$H\bar{H}$	$^{2S+1}L_J$	V_C	E ($\Lambda = 0.5$ GeV)	E ($\Lambda = 1$ GeV)	Exp [45]	Threshold [MeV]
0^{++}	$D_s\bar{D}_s$	$^1S_0$	$\frac{1}{2}(C_{0a}+C_{1a})$	3924^{+10}_{-13}	3928^{+9}_{-19}	–	3937.0
1^{++}	$D_s^*\bar{D}_s$	$^3S_1$	$\frac{1}{2}(C_{0a}+C_{1a}+C_{0b}+C_{1b})$	–	–	–	
1^{+-}	$D_s^*\bar{D}_s$	$^3S_1$	$\frac{1}{2}(C_{0a}+C_{1a}-C_{0b}-C_{1b})$	4035^{+23}_{-25}	4040^{+33}_{-39}	–	4080.8
0^{++}	$D_s^*\bar{D}_s^*$	$^1S_0$	$\frac{1}{2}(C_{0a}+C_{1a}-2\,C_{0b}-2\,C_{1b})$	Input	Input	4140	4224.6
1^{+-}	$D_s^*\bar{D}_s^*$	$^3S_1$	$\frac{1}{2}(C_{0a}+C_{1a}-C_{0b}-C_{1b})$	4177^{+23}_{-25}	4180^{+35}_{-40}	–	4224.6
2^{++}	$D_s^*\bar{D}_s^*$	$^5S_2$	$\frac{1}{2}(C_{0a}+C_{1a}+C_{0b}+C_{1b})$	–	–	–	

Table 3.7: *Predicted masses (in MeV) of the hidden strange isoscalar HQSS partners of the $X(3872)$ resonance for two different values of the Gaussian cutoff. The meaning of the quoted errors is the same as in Table 3.4. We also give the relevant thresholds (in MeV) for each channel.*

by the $D_s^+D^-$ interaction[10]. Similarly to what happens with the isoscalar 2^{++} state, with the central values of the counter-terms in Eq. (3.3.5)–(3.3.8) we predict a 0^+ state that lies very close to threshold. When we decrease the strength of the potential, the molecule approaches the threshold and finally becomes a virtual state, at least within our simple scheme[11]. In the real world, it might well happen that in this situation the state could become a narrow resonance, placed very close to threshold, and decaying into the $D_s^+\bar{D}^-$ pair instead of a becoming a virtual state. In any case, we predict the existence of some structure close to threshold. The upper errors for the mass of this state, as quoted in Table 3.5, just account for the distance between its central mass value and the $D_s^+\bar{D}^-$ threshold.

3.3.3 The Isovector ($I = 1$) Partners

The spectrum of the isovector molecules is similar to the isospinor one. The reason is that the LO potential is identical in both cases, with the exception of the 1^{++} and 2^{++} molecules owing to isospin violation, as we commented previously. We find four molecular states of a possible total of six that we list in Table 3.6. The location of the states is similar to the isoscalar sector, only that they are a bit less bound. The two missing states would correspond to the isovector partners of the $X(3872)$ and $X(4012)$.

We also mention that there is a complication with the isovector 0^{++} $D\bar{D}$ molecule, which lies very close to the $D\bar{D}$ threshold. This implies that explicit isospin breaking should be taken into account. However, we notice that this is only necessary for the $I_3 = 0$ component of the isospin triplet, where the neutral ($D^0\bar{D}^0$) and charged (D^+D^-) channels are to be found. If we consider instead the $I_3 = \pm 1$ states (corresponding to the particle channels $D^+\bar{D}^0$ and D^0D^-), there is no mixing with the isoscalar components and no need for coupled channel dynamics. Thus, for simplicity, we have decided to report only the $I_3 = +1$ state in Table 3.6.

3.3.4 The Hidden Strange Partners

Finally, we consider the molecules with hidden strangeness. In this sector the strength of the LO potential is the arithmetic mean of the isoscalar and isovector one. This means that if there

[10] The dynamics of the other state member of the isospin doublet is similar, being its mass just shifted by about 5 MeV. This shift is due to the mass difference between the $D_s^+D^-$ and the $D_s^+\bar{D}^0$ pairs.

[11] A resonance state in one channel is usually associated to a barrier in coordinate space which is not reproduced by a constant (in energy) potential. The situation may be different when we have coupled channels [104], in which case one of the channels can decay into the other.

is a bound state in the isoscalar and isovector sector, we can be confident about the existence of a heavy meson molecule containing a $s\bar{s}$ quark-antiquark pair. Conversely, if we consider the $X(3872)$ and $X(4012)$ molecules, the fact that they have no isovector partners is a strong hint that there will be no hidden strange partner either. The four states we obtain are listed in Table 3.7.

3.4 Conclusions

In this chapter we have shown how the heavy quark spin and light $SU(3)$ flavour symmetries constrain the charmed meson-antimeson interaction ($H\bar{H} \to H\bar{H}$, being $H = D^+, D^0, D_s^0, D^{*+}, D^{*0}$ and D_s^{*0}). This has been done within the EFT framework, where the heavy meson interactions can be easily arranged from more to less relevant thanks to power counting, the ordering principle behind EFT. The bottom line of the EFT approach is that contact interactions (i.e. four meson vertices) dominate the low energy dynamics of heavy meson molecules. In turn, $SU(3)$ flavour symmetry and HQSS reduce the number of contact interactions from twenty four to only four. The approach we advocate is actually an extension of the ideas of Ref. [25] for the $SU(2)$ isoscalar channel to the isospinor, isovector and hidden strange sectors.

The four counter-terms can be determined as follows: we fix three of them by identifying the $X(3915)$, $Y(4140)$ and $X(3872)$ resonances as molecular states. In particular we consider the $X(3915)$ and $Y(4140)$ to be a 0^{++} isoscalar $D^*\bar{D}^*$ and $D_s^*\bar{D}_s^*$ molecules respectively, while the $X(3872)$ is a 1^{++} isospin admixture $D\bar{D}^*$ state. Finally, the fourth counter-term is determined from the isospin breaking branching ratio of the $X(3872)$ into $J/\Psi\,2\pi$ and $J/\Psi\,3\pi$. We notice that the $X(3872)$ is weakly bound (~ 0.2 MeV) and lies extremely close to the $D^0\bar{D}^{0*}$ threshold. Its binding energy is much smaller than the mass splitting between the charged and neutral components of the $X(3872)$ (~ 8 MeV). Hence, we have taken into account these degrees of freedom explicitly. We work within a scheme where all interactions are isospin invariant, but where the $X(3872)$ does not have a well defined isospin[12] as a consequence of the mass and kinetic terms of the $D\bar{D}^*$ Hamiltonian [99, 103]. The isospin breaking of the masses naturally explains the appearance of an isospin violation (and its quantity) in the decays of the $X(3872)$, as pointed out in Refs. [99, 103] for the first time. However, in the aforementioned works the experimental branching ratio [100]

$$\frac{\Gamma(X(3872) \to J/\Psi\,\pi^+\pi^-\pi^0)}{\Gamma(X(3872) \to J/\Psi\,\pi^+\pi^-)} = 0.8 \pm 0.3\,,$$

is not perfectly reproduced [13]. The reason is that the authors of Refs. [99, 103] assume that the isovector $D\bar{D}^*$ interaction vanishes. Here, we improve on that and take advantage of the experimental ratio to constraint the non-vanishing interaction in the isovector channel.

Once we have fixed the counter-terms, we have established the existence and the location of up to a total of 15 molecular partners of the $X(3915)$, $Y(4140)$ and $X(3872)$ states, see Tables 3.4 - 3.7. These predictions are subjected to a series of uncertainties, in particular the approximate nature of HQSS (especially in the charm sector). We have estimated the size of these corrections and concluded that the HQSS pattern of molecular states is stable, though the exact location of the states can change by a few tens of MeV in certain cases.

[12] The isospin mixing depends on the relative distance between the pseudoscalar and vector mesons.

[13] Notice, however, that Refs. [99, 103] used an older experimental determination of the branching ratio ($1.0 \pm 0.3 \pm 0.4$) with much larger errors. It is only with the updated branching ratio that their explanation fails at the fine quantitative level.

Actually, the family of $D^{(*)}\bar{D}^{(*)}$ states we theorize depends on the assumption that the $X(3872)$, $X(3915)$ and $Y(4140)$ resonances are molecular. While in the $X(3872)$ case the molecular interpretation is compelling and widely accepted, the $X(3915)$ and $Y(4140)$ states are merely compatible with it. Regarding the $X(3915)$, it is interesting to notice that the size of the decay width of this resonance is difficult to conciliate with the hypothesis that it is a charmonium [58]. This observation enhances the prospects that the $X(3915)$ may be a molecule after all. However, with the $Y(4140)$ we have a more serious problem: this resonance is far from being confirmed experimentally. Thus not all the states we predict are equally likely. Predictions derived from the $X(3872)$ should be regarded as more solid than those depending on the $X(3915)$, which in turn are less speculative that the ones obtained from the $Y(4140)$. In this regard, as stressed in Ref. [25], the 2^{++} $\mathrm{D}^*\bar{\mathrm{D}}^*$ isoscalar partner of the $X(3872)$ is still the most reliable prediction of the present work, followed by the other isoscalar states. If in the future we count with clearer molecular candidates than the $X(3915)$ and, particularly, the $Y(4140)$ resonances, they could be included in the current scheme instead of the later ones, helping to achieve more robust predictions. Conversely, the observation of any of the states predicted here can serve as proof of the molecular nature of the previously mentioned resonances.

Finally, we find it interesting to compare our results with those of the hidden gauge formalism, another theoretical approach for the study of hidden charm states. While the spectrum of the isoscalar molecules in the hidden gauge is similar to the one we obtain (with the notable exception of the 2^{++} state), fewer poles are reported in the $I = 1/2$, $I = 1$ and hidden strange sectors [105, 106, 107]. If we consider the case of two heavy pseudoscalar mesons, Gamermann et al. [105] predict an isoscalar 0^{++} $\mathrm{D}\bar{\mathrm{D}}$ state in the vicinity of 3700 MeV. We can identify this state with the $X(3710)$ $\mathrm{D}\bar{\mathrm{D}}$ molecule we obtain in the present work. However, they do not predict the existence of the isospinor, isovector and hidden strangeness partners of the $X(3710)$. The reason is that in Ref. [105] the interaction in the isovector channel is zero. The same comments apply to the extension of the hidden gauge formalism to pseudoscalar-vector molecules [106], where it is found a counterpart of the 1^{+-} $\mathrm{D}\bar{\mathrm{D}}^*$ isoscalar molecule that we obtain at 3820 MeV at a slightly higher energy (3840 MeV) but no $I = 1/2$, $I = 1$ or hidden strangeness states. Last, in the case of two heavy vector mesons the hidden gauge predicts a series of isoscalar 0^{++}, 1^{+-} and 2^{++} $\mathrm{D}^*\bar{\mathrm{D}}^*$ states, plus a few non-isoscalar ones [107]. In the isoscalar sector, the 0^{++} and 1^{+-} $\mathrm{D}^*\bar{\mathrm{D}}^+$ resonances are located in the region around 3943 and 3945 MeV respectively, not very different to the masses we use (3917 and 3955 MeV). However, there is a striking difference in the mass of the 2^{++} $\mathrm{D}^*\bar{\mathrm{D}}^*$ isoscalar state, which in Ref. [107] happens at 3922 MeV (instead of 4013 MeV). The reason for this value, which is incompatible with HQSS, is the remarkably strong vector-vector interaction that is obtained in the hidden gauge model. Probably as a result of this strong interaction, Ref. [107] also reports the existence of broad 2^{++} isovector $D^*\bar{D}^*$ and hidden strange $D_s^*\bar{D}_s^*$ resonances, with widths above 100 MeV, and masses of around 3910 and 4160 MeV, respectively. These states are difficult to accommodate within our HQSS scheme.

Chapter 4

Hidden-charm molecules in a finite volume

4.1 Introduction

Lattice QCD (LQCD) is a well-established non-perturbative approach to solve the quantum chromodynamics theory of quarks and gluons. The idea is to formulate QCD on a grid (or lattice) of points in space and time. When the size of the lattice is taken infinitely large and its points infinitesimally close to each other, the continuum QCD is recovered [108].

Analytic or perturbative solutions in low-energy QCD are hard or impossible due to the highly nonlinear nature of the strong force. This formulation of QCD in discrete rather than continuous space-time naturally introduces a momentum cutoff at the order $1/a$, where a is the lattice spacing, which regularizes the theory. As a result, lattice QCD is mathematically well-defined, but the number of degrees of freedom becomes very large, being then possible the use of MonteCarlo methods. Most importantly, lattice QCD provides a framework for investigation of non-perturbative phenomena such as confinement and quarkgluon plasma formation, which are unsolvable by means of analytic field theoretical methods. For a more detailed description of LQCD, see for instance the report in Ref. [109].

The determination of the hadron spectrum from lattice QCD calculations is attracting many efforts and one can get an overview on the different methods used and results in a recent review by Fodor and Hoelbling [110]. One of the tools becoming gradually more used is the analysis of lattice levels in terms of the Lüscher method [111, 112]. This method converts binding energies of a hadron-hadron system in the finite box into phase shifts of the hadron-hadron interaction from levels above threshold, or binding energies from levels below threshold [113, 114, 115]. From the phase shifts one can get resonance properties, and there are several works that have recently applied these techniques to study the ρ resonance [116, 117, 118, 119, 120, 121, 122, 123, 124]. There exist other resonances far more difficult to get with this approach like the $a_1(1260)$, which was also attempted in [123] (the properties of this resonance in a finite box were also studied in Ref. [125], starting from an effective field theory approach for the infinite volume case). Scalar mesons have also been searched for with this method [126, 127, 128, 129] and gradually some calculations are being performed for systems in the charm sector [130, 131, 132, 133, 134, 135, 136]. From another field theoretical perspective, finite volume calculations have also been devoted to this sector in [137, 136]. In [137] the $\bar{K}D$, ηD_s interaction is studied

in finite volume with the aim of learning about the nature of the $D_{s0}^*(2317)$ resonance from lattice data. The infinite volume model used in [137] was derived in [105], where the $D_{s0}^*(2317)$ resonance appears dynamically generated from the interaction of $\bar{K}D$, ηD_s and other less relevant channels. In this latter work, a scalar hidden charm state coming from the $D\bar{D}$ interaction with other coupled channels was also found, which qualifies basically as a $D\bar{D}$ quasi-bound state (decaying into pairs of lighter pseudoscalars). Although not reported experimentally, support for this state has been found in [138] from the analysis of the data of the $e^+e^- \to J/\psi D\bar{D}$ reaction of [139]. From the effective field theory point of view, this state has also been reported in [25] and Chapter 3 as well, using light $SU(3)$-flavour and heavy quark spin symmetries to describe charmed meson-antimeson interactions.

The purpose of the present chapter is to study the interaction of $D\bar{D}$ and $D^*\bar{D}^*$ using a field theoretical approach in finite volume in order to evaluate energy levels in the finite box which might be compared with future LQCD calculations. This work also presents a strategy to better analyze future lattice results in order to get the best information possible about bound states and phase shifts in the infinite volume case from these lattice data. For this purpose we shall use the HQSS EFT based model introduced in Chapter 3, although most of the results and the basic conclusions are independent of which model is used.

As to the method to obtain the finite volume levels and the inverse problem of obtaining the results in the real world, phase shifts and binding energies, we shall follow the method of [140] where a reformulation of Lüscher approach is done based on the on-shell factorization of the scattering matrix that one uses in the chiral unitary approach [141]. This method is conceptually and technically very easy and introduces improvements for the case of relativistic particles. Some works using this formalism can be found in Refs. [125, 137, 142, 143, 144].

The structure of this chapter is as follows: in Sect. 4.2 we briefly recall the most important features of the formalism in infinite volume (already described in previous chapters) laying emphasis on the derivation of the phase shifts from the T-matrix. In Sect. 4.3 we extend the formalism to analyze the finite volume effects and results are collected in Sect. 4.4, where the inverse problem is also discussed in detail. Finally, the conclusions and remarks are given in Sect. 4.5.

4.2 Formalism: infinite volume

In our normalization (see Sect. 2.4), the S-matrix[1] for an elastic $H\bar{H}'$ scattering process reads,

$$S(E) \equiv e^{2i\delta(E)} = 1 - i\frac{\mu k}{\pi} T(E) \ , \tag{4.2.1}$$

where the modulus of the momentum $k = |\vec{k}|$ is given by $k^2 = 2\mu(E - m_1 - m_2)$, and μ is the reduced mass of the system of two particles with masses m_1 and m_2. In Eq. (4.2.1), δ is the phase shift, and we can write:

$$T = -\frac{2\pi}{\mu k} \sin\delta \ e^{i\delta} \ , \tag{4.2.2}$$

$$T^{-1} = -\frac{\mu k}{2\pi} \cot\delta + i\frac{\mu k}{2\pi} \ . \tag{4.2.3}$$

[1] We always consider $s-$wave meson-antimeson interactions, and thus the spin of the molecule always coincides with the total spin of the meson-antimeson pair. The partial waves ${}^{2S+1}L_J$ are then ${}^{2S+1}S_{J=S}$. For simplicity in what follows, we drop all references to the L, S and J quantum numbers, both in the S and T matrices.

The expression for the T-matrix is given again by the LSE:

$$T^{-1}(E) = V^{-1}(E) - G(E) \ , \tag{4.2.4}$$

with V the potential (two-particle irreducible amplitude) and G a one-loop two-point function. The UV divergent loop function G accounts for unitarity (Right-Hand Cut, RHC); while the contribution of the left-hand cut (LHC) should be included in the potential V. We will approximate V by its LO contribution in the $1/m_Q$ expansion derived in the previous chapters. Thus, we are completely neglecting the LHC; we will come over this point below.

The loop function G needs to be regularized in some way to treat the UV divergences. Here, we follow the approach of Ref. [25] and Chapter 3 in which the loop function is regularized with a Gaussian regulator. For an arbitrary energy E, we recall Eq. [2.4.40],

$$\begin{aligned} G(E) &= \int \frac{\mathrm{d}^3\vec{q}}{(2\pi)^3} \frac{e^{-2(\vec{q}^{\,2}-k^2)/\Lambda^2}}{E - m_1 - m_2 - \vec{q}^{\,2}/2\mu + i0^+} \\ &= -\frac{\mu\Lambda}{(2\pi)^{3/2}} e^{2k^2/\Lambda^2} + \frac{\mu k}{\pi^{3/2}} \phi\left(\sqrt{2}k/\Lambda\right) - i\frac{\mu k}{2\pi} \ , \end{aligned} \tag{4.2.5}$$

Notice that in this chapter we use for the propagator $G(E)$ a different definition with respect to Eq. (2.4.40) in Chapter 2, since in Eq. (4.2.5) we have included the Gaussian factor $e^{2\vec{q}^{\,2}/\Lambda^2}$ to guaranty $\mathrm{Im}T^{-1} = -\mathrm{Im}G$. The definition of the loop function in Eq. (2.4.40) is related to the reduced T-matrix t, introduced in Eq.(2.4.39). Indeed, the Gaussian form factor enters Eq. (4.2.5) in a way that is unity for on-shell momenta, and hence the optical theorem $\mathrm{Im}T^{-1} = \mu k/(2\pi)$ is automatically fulfilled.

It should be noted that the omission of the LHC contribution is in general a minor problem in the scattering of hadrons in the chiral unitary approach or related problems. The reason is that its contribution to the dispersion relation in the physical region of interest is small to begin with, and even then, what matters is not its absolute value but its energy dependence. If one studies a region of energies where the contribution of the mechanisms that give rise to the LHC is practically constant, this contribution can be absorbed in the models by a suitable change in the cutoff Λ or in the subtraction constant. In the heavy-quark sector, this result is even more accurate. The bulk of the potential comes from contact terms that effectively account for the exchange of mesons heavier than the pion[2] or, in a picture like the local hidden gauge approach, from the exchange of vector mesons. Because of the large mass of the vector mesons, the LHC is at unphysical energies very far below the threshold of the channels and its energy dependence in the moderate ranges of energies that we study here is completely negligible. In the case of our EFT, the most relevant contribution to the LHC would be that stemming from OPE, but its contribution is subleading in the power counting of the EFT [11], where the OPE potential was derived for these systems, and its quantitative effects discussed. The contributions of multipion exchanges (MPE) would be even more suppressed. Another possible contribution to the LHC would arise from the $t-$ or $u-$ channel loops with two heavy mesons running in the loop. However, this cut is located at $E = 0$, i.e., far away from the energies considered in this work. As discussed above, its energy dependence would be completely negligible in our study.

Then, the potential V is taken as

$$V(E) = e^{-2k^2/\Lambda^2} C(\Lambda) \ , \tag{4.2.6}$$

where C is the proper combination of the four different counter-terms for each considered channel $H\bar{H}'$. Explicit expressions were given in Chapter 2. The dependence of the counter-term on the

[2]We should note here that one can find in the literature other models (see for instance Refs. [46, 145, 146], where the $X(3872)$ is bound solely by OPE.

ultraviolet (UV) cutoff Λ should cancel that of the loop function G, such that $G(E_B)V(E_B)$ becomes independent of Λ, when E_B is the energy of the bound state used to determine the counter-term. For other energies, there will exist a remaining, unwanted/unphysical, dependence of the T matrix on the cutoff. This is due to the truncation of the perturbative expansion (see discussion in Ref. [25]).

Up to this point, we have discussed only the case of uncoupled channels, but the generalization to coupled channels is straightforward.[3]

Finally, above threshold the effective range expansion reads:

$$k \cot \delta = -\frac{1}{a} + \frac{1}{2} r k^2 + \cdots \ , \tag{4.2.7}$$

where a and r are, respectively, the scattering length and the effective range. From Eqs. (4.2.3) and (4.2.4) we can calculate the theoretical predictions for these effective range parameters, obtaining:

$$a_{\rm th} = \ \frac{\mu}{2\pi} \left(\frac{1}{C} + \frac{\mu \Lambda}{(2\pi)^{3/2}} \right)^{-1} \ , \tag{4.2.8}$$

$$r_{\rm th} = -\frac{8\pi}{\mu \Lambda^2} \left(\frac{1}{C} - \frac{\mu \Lambda}{(2\pi)^{3/2}} \right) . \tag{4.2.9}$$

4.3 Formalism: finite volume

In this section, we follow the steps of Ref. [140] to write the amplitude in a finite box of size L with periodic boundary conditions, denoted by $\tilde{T}$. Since the potential does not depend on L, one only has to replace the loop function G with its finite volume version, $\tilde{G}$, in which the integral over momentum $\vec{q}$ is replaced by a discrete sum over the allowed momenta,

$$\tilde{T}^{-1}(E) = V^{-1}(E) - \tilde{G}(E) \ , \tag{4.3.1}$$

$$\tilde{G}(E) = \frac{1}{L^3} \sum_{\vec{q}} \frac{e^{-2(\vec{q}^{\,2} - k^2)/\Lambda^2}}{E - m_1 - m_2 - \vec{q}^{\,2}/2\mu} \ , \tag{4.3.2}$$

where the (quantized) momentum is given by:

$$\vec{q} = \frac{2\pi}{L} \vec{n} \ , \quad \vec{n} \in \mathbb{Z}^3 \ . \tag{4.3.3}$$

Now, the energy levels in the box are given by the poles of the $\tilde{T}$-matrix, $V^{-1} = \tilde{G}$. For the energies of these levels in the box, the amplitude in the infinite volume is recovered as:

$$T^{-1}(E) = V^{-1}(E) - G(E) = \tilde{G}(E) - G(E) = \delta G(E) \ . \tag{4.3.4}$$

Since the G function is regularized (either in the box or in the infinite volume) with a Gaussian regulator, the difference above depends explicitly on the cutoff Λ. This remaining non-physical dependence on Λ quickly disappears as the volume increases. Indeed, we find that it is exponentially suppressed and that it dies off as $\exp\left(-L^2\Lambda^2/8\right)$ (see Subsect. 4.3.1). Thus, it is clear that in this context, we can end up the renormalization program just by sending the UV cutoff to

[3] One just has to rewrite the T-matrix as $T = (\mathbb{1} - VG)^{-1} V$, where V and G are now matrices in the coupled channels space.

infinity. This will allow us to obtain the physical $T-$matrix, independent of any renormalization scale, for the energy levels found in the lattice Monte Carlo simulation (finite box).

For the practical calculations that we will show in what follows, the Λ dependence is already negligible when $\Lambda \gtrsim 1$ GeV even for the smallest volumes considered in this work (the limit $\Lambda \to \infty$ is effectively achieved for such values). In this limit, Eq. (4.3.4) becomes the Lüscher equation [111, 112], as we discuss in certain detail later in Subsect. 4.3.1. These results also show that the inclusion of a Gaussian regulator is a quite efficient technique, from the computational point of view, to evaluate the Lüscher function $\mathcal{Z}_{00}(1, \hat{k}^2)$ used in [112]. Finally, from Eqs. (4.2.3) and (4.3.4), we can write:

$$k \cot \delta = -\frac{2\pi}{\mu} \lim_{\Lambda \to \infty} \mathrm{Re} \left(\tilde{G}(E) - G(E) \right) \ . \tag{4.3.5}$$

We have previously discussed that the LHC can be safely neglected in the study of the $H\bar{H}'$ interactions in the infinite-volume case. With respect to the finite-volume case, we recall that the most relevant contribution (although subleading in the power counting of the EFT) to the LHC arises from the OPE mechanism. But the OPE potential does not depend on the L, since it does not involve any loop function in the infinite-volume case. The first volume-dependent contributions to the LHC would be those of MPE and crossed $t-$ or $u-$channel loops with heavy mesons in the loop. In the infinite-volume case, however, these are even more suppressed in the power counting than the contribution of OPE, and so one should expect their contributions to the LHC to be negligible. The relevance of the LHC in the case of $\pi\pi$ interactions (note that in this case the LHC is located close to threshold) in finite volumes has been studied in Refs.[144, 147]. There, it was found that the LHC contribution is, in fact, negligible (exponentially suppressed) for $Lm_\pi \geq 1.5$. In summary, although the volume-dependent contributions to the potential would be certainly present in an actual lattice calculation, these are sufficiently small so that they can be safely neglected, at least in an exploratory study. In the end, that is the assumption of most of the works that study unitarized effective field theories in a finite volume, e.g., Ref.[143].

4.3.1 Gaussian regulator and relation to Lüscher formula

In this subsection, we discuss the details of Eq. (4.3.5) within a Gaussian regularization scheme. We also study the dependence of the function $\delta G(E)$, that appeared in Eq. (4.3.4), on the UV cutoff Λ. For convenience, we re-write $\delta G(E)$ as

$$\begin{aligned} \delta G(E;\Lambda) = \tilde{G}(E) - G(E) = \qquad\qquad\qquad\qquad\qquad\qquad\qquad\qquad\qquad\qquad (4.3.6) \\ = \overbrace{\frac{1}{L^3} \sum_{\vec{q}} \frac{e^{-2(\vec{q}^2 - k^2)/\Lambda^2} - 1}{E - m_1 - m_2 - \frac{\vec{q}^2}{2\mu}} - \int \frac{\mathrm{d}^3 \vec{q}}{(2\pi)^3} \frac{e^{-2(\vec{q}^2 - k^2)/\Lambda^2} - 1}{E - m_1 - m_2 - \frac{\vec{q}^2}{2\mu} + i0^+}}^{\delta G_A} \\ + \underbrace{\frac{1}{L^3} \sum_{\vec{q}} \frac{1}{E - m_1 - m_2 - \frac{\vec{q}^2}{2\mu}} - \int \frac{\mathrm{d}^3 \vec{q}}{(2\pi)^3} \frac{1}{E - m_1 - m_2 - \frac{\vec{q}^2}{2\mu} + i0^+}}_{\delta G_L} \end{aligned}$$

The function δG explicitly depends on the cutoff Λ, and this dependence is carried by the δG_A term. On the other hand, the term δG_L is well defined, and it is related to the Lüscher function [140] (see discussion below). In the strict $\Lambda \to \infty$ limit, only the second term survives, which justifies our approach in Sec. 4.3. Still, for practical purposes, the limit $\Lambda \to \infty$ can only be achieved by taking Λ large enough, and then it is necessary to study the dependence of δG

with Λ. Let us note that δG_A has no poles, and hence it is exponentially suppressed with L according to the regular summation theorem [111, 112]. For $k^2 > 0$, $E > m_1 + m_2$, δG_L is not exponentially suppressed for $L \to \infty$ (because of the pole in the integral) and, in this case, δG_L clearly dominates over δG_A.

However for $k^2 < 0$, δG_L is also exponentially suppressed as L increases, and therefore one needs to explicitly calculate the dependence of δG_A on ΛL.

Let us calculate the derivative of δG with respect to Λ. Only δG_A depends on Λ, and this latter function does it through the exponential function $\exp[-2(\vec{q}^2 - \vec{k}^2)/\Lambda^2]$. The derivative brings down a factor $(\vec{q}^2 - \vec{k}^2)$ that cancels out the denominators. This greatly simplifies the calculation of both the sum and the integral. The latter one is trivial and it only amounts to the integration of a Gaussian function, while the former one, up to constant factors, now reads

$$\frac{1}{L^3}\sum_{\vec{q}} e^{-2\vec{q}^2/\Lambda^2} = \left(\frac{1}{L}\sum_{n=-\infty}^{+\infty} e^{-2\left(\frac{2\pi}{L}\right)^2\frac{n^2}{\Lambda^2}}\right)^3 = \left[\frac{\theta_3(0, e^{-\frac{8\pi^2}{\Lambda^2 L^2}})}{L}\right]^3 , \tag{4.3.7}$$

where we have used $\vec{q}^2 = q_x^2 + q_y^2 + q_z^2$ and that the exponential of a sum is the product of the exponentials. This latter property allows to relate the sum in three dimensions to the cube of the sum in one dimension. In Eq. (4.3.7), $\theta_3(u, \alpha)$ is a Jacobi elliptic theta function [148]. It satisfies [149],

$$\frac{\theta_3(0, e^{-\pi x^2})}{\theta_3(0, e^{-\pi/x^2})} = \frac{1}{x} . \tag{4.3.8}$$

This allows us to write then:

$$\frac{\partial\ \delta G}{\partial \Lambda} = -\frac{\mu}{(2\pi)^{3/2}} e^{2k^2/\Lambda^2}\left(\left[\theta_3(0, e^{-\Lambda^2 L^2/8})\right]^3 - 1\right) . \tag{4.3.9}$$

We note that this equation is exact. The above equation converges rapidly to zero as the Gaussian cutoff increases, which shows that the limit $\Lambda \to \infty$ is effectively quickly achieved. To proceed further, we note that:

$$[\theta_3(0, \alpha)]^3 = 1 + 6\alpha + 12\alpha^2 + \cdots = \sum_{m=0}^{\infty} c_m \alpha^m , \tag{4.3.10}$$

and the coefficients c_m are nothing but the multiplicities of $m = \vec{n}^2$, $\vec{n} \in \mathbb{Z}^3$. Since $\alpha = e^{-\Lambda^2 L^2/8}$, we can find the leading term in Eq. (4.3.9),

$$\frac{\partial\ \delta G}{\partial \Lambda} = -\frac{6\mu}{(2\pi)^{3/2}} \exp\left(\frac{2k^2}{\Lambda^2} - \frac{\Lambda^2 L^2}{8}\right)\ \left(1 + \mathcal{O}\left(e^{-\Lambda^2 L^2/8}\right)\right) . \tag{4.3.11}$$

Given that $\delta G = \delta G_L$ for $\Lambda \to \infty$, we find keeping just the leading term:

$$\begin{aligned}\delta G(E;\Lambda) &= \delta G_L(E) + \frac{6\mu}{(2\pi)^{3/2}}\int_{\Lambda}^{\infty} \mathrm{d}\Lambda' \exp\left(\frac{2k^2}{\Lambda'^2} - \frac{\Lambda'^2 L^2}{8}\right) \\ &= \delta G_L(E) + \frac{3\mu}{2\pi L}\left[e^{ikL}\mathrm{erfc}\left(\frac{\Lambda L}{2\sqrt{2}} + i\frac{\sqrt{2}k}{\Lambda}\right) + \right. \\ &\qquad \left. + e^{-ikL}\mathrm{erfc}\left(\frac{\Lambda L}{2\sqrt{2}} - i\frac{\sqrt{2}k}{\Lambda}\right)\right] ,\end{aligned} \tag{4.3.12}$$

and, then, its asymptotic behaviour is:

$$\delta G(E;\Lambda) = \delta G_L(E) + \frac{24\mu}{(2\pi)^{3/2}} \frac{e^{-\frac{\Lambda^2 L^2}{8}}}{\Lambda L^2} \left[1 + \frac{2(k^2L^2-2)}{L^2\Lambda^2} + \mathcal{O}\left(\Lambda^{-4}\right)\right] + \cdots \,, \tag{4.3.13}$$

where $\mathcal{O}(\Lambda^{-4})$ refers to $(k/\Lambda)^4$, $(k^2/L^2)/\Lambda^4$ and $1/(L\Lambda)^4$, and the ellipsis stands for terms that are more exponentially suppressed (the next one would take the form $e^{-\Lambda^2 L^2/4}$). Given the form of the L suppression, the Gaussian regularization scheme does not introduce any spurious terms that would dominate over[4] the physical contribution δG_L, as long as Λ is sufficiently large. Indeed, one can efficiently compute the regularized Lüscher function by means of the Gaussian regulated δG loop function. The Lüscher function[5] is related to the loop functions by means of [140]:

$$\sqrt{4\pi}\mathcal{Z}_{00}(1,\hat{k}^2) = -\frac{L}{2\pi}\frac{(2\pi)^3}{2\mu}\delta G_L(E), \quad \hat{k}^2 = \frac{k^2L^2}{(2\pi)^2} \,. \tag{4.3.14}$$

Thus, for a mildly large value of Λ, $\delta G_L(E)$ can be approximated by the Gaussian regulated $\delta G(E,\Lambda)$ function, up to corrections suppressed by the exponential factor $e^{-\frac{\Lambda^2 L^2}{8}}$ (see Eq. (4.3.13)),

$$\sqrt{4\pi}\mathcal{Z}_{00}(1,\hat{k}^2) = -\frac{L}{2\pi}\frac{(2\pi)^3}{2\mu}\left(\delta G(E,\Lambda) + \mathcal{O}\left(e^{-\frac{\Lambda^2 L^2}{8}}\right)\right) \tag{4.3.15}$$

which in turn provides $\mathcal{Z}_{00}(1,\hat{k}^2)$ with enough accuracy in a computationally easy way.

4.4 Results

We present in this section the results obtained with the formalism outlined in Sect. 4.3. We first discuss the results obtained by putting the model of Chapter 3 directly in the box. That is, we study the volume dependence of the molecules found in chapter 3, predicting thus the existence of sub-threshold levels (asymptotically different of threshold) for the different channels, which have a clear correspondence with the hidden charm molecules reported back in Chapter 3. This is done in Subsec. 4.4.1.

Our purpose in Subsecs. 4.4.2, 4.4.3 and 4.4.4 is to simulate a realistic situation in a LQCD study, where one would obtain different energy levels (one or two) for different sizes, L, of the box. To do so, we generate "synthetic data" from the exact levels that we obtain from the model of chapter 3. We take five different values of L_i, in the range $Lm_\pi = 1.5$ to 3.5. From the calculated levels, we obtain randomly shifted levels (in a range of 5 MeV), and assign an error of 10 MeV to each of these points (this is an educated guess based on the assumption that, in the near future charmonium physics LQCD simulations will reduce the statistical fluctuations of the measured excitation energies at the level of ten percent). Next we use a Monte Carlo simulation, to estimate the errors on the determination of observables (the phase shifts, for instance) when the energy levels are obtained with a certain statistical error. Specifically, we study in these subsections the $I = 0$ $J^{PC} = 0^{++}$ $D\bar{D}$ channel.

In Subsec. 4.4.2, the Lüscher formalism to study the phase shifts calculated from Eq. (4.3.5) is applied to the synthetic levels above threshold that we find for the different studied channels.

[4] As already mentioned, for $k^2 > 0$ δG_L is not exponentially suppressed for $L \to \infty$, while for $k^2 < 0$, we expect δG_L to decrease as $\exp(-|k|L)$.

[5] It satisfies [112],

$$e^{2i\delta} = \frac{k\cot\delta + ik}{k\cot\delta - ik} = \frac{\mathcal{Z}_{00}(1,\hat{k}^2) + i\pi^{\frac{3}{2}}\hat{k}}{\mathcal{Z}_{00}(1,\hat{k}^2) - i\pi^{\frac{3}{2}}\hat{k}}.$$

From these phase shifts, we calculate the effective range expansion parameters, and use them to determine the masses of the bound states. In Subsec. 4.4.3 we adopt another strategy to extract information from the generated levels. Namely, we consider a potential whose parameters are then fitted to reproduce the synthetic levels (above and below threshold, simultaneously). With this potential, we can make predictions in the infinite volume case, and thus we end up with another determination of the masses of the predicted bound states. We shall see that this method allows one to obtain better results (better central value and smaller errors) for the mass of the bound state than the previous one. We then analyze in detail the differences between both approaches. In Subsec. 4.4.4 another method is proposed, in which the effective range approximation is retained for the inverse of the T-matrix amplitude, but fitting the energy levels directly instead of the phase shifts, and studying simultaneously the levels above and below threshold. In this case, then, we notice that the precision achieved for the mass of the bound state is similar to that obtained with the potential analysis.

In Subsec. 4.4.5, we analyze in a more quantitative way, the qualitative arguments given in Subsec. 4.4.1, where the behaviour of the sub-threshold levels is discussed. We offer a method to discriminate between those levels that produce bound states in the limit $L \to \infty$ and those that do not, and hence tend to threshold in the infinite volume limit. This method allows the extraction of the mass and the coupling of the bound state in the infinite volume limit.

All these methods are applied in Subsec. 4.4.6 to the bound state present in the $I = 0$ $J^{PC} = 2^{++}$ $D^*\bar{D}^*$ channel. The difference with respect to the case used as an example in the previous subsections is that the state is now weakly bound (the binding energy is only around 2–3 MeV), so that we can compare how the methods exposed above work for this case.

4.4.1 The model of Chapter 3 in a finite box

In Figs. 4.1 and 4.2 we present the dependence of the energy levels on the size of the finite box, as calculated from Eqs. (4.3.1) and (4.3.2), for the different channels studied in Chapter 3. We have fixed the potential in the different channels by means of the central values given in this reference for the various counter-terms given by Eq. (3.3.5). When needed, we have also implemented in the finite box a coupled channel formalism. The solid lines correspond to the case $\Lambda = 1$ GeV, whereas the dot-dashed lines to $\Lambda = 0.5$ GeV. For comparison, we also show, with the horizontal dashed lines, the involved threshold energies. We just show those energy levels that can be identified with bound states ($k^2 < 0$) in the infinite volume case. That is, their asymptotic $L \to \infty$ value approaches the bound energies given in Chapter 3, and thus they are different from threshold. Of course, one has this latter piece of information from the calculations of the model in an infinite volume, but this would not be the case in a lattice simulation. Let us focus, for simplicity, on the $I = 0$ case, shown in the left panel of Fig. 4.1. The large L asymptotic behaviour can be well appreciated in some cases like the 0^{++} $D\bar{D}$ or 1^{+-} $D^*\bar{D}$ molecules. However in other cases, it might be difficult to discriminate between a real bound state and a threshold level, even for quite large values of the box size L. Clear examples are the 1^{++} $D^*\bar{D}$ or the 2^{++} $D^*\bar{D}^*$ molecules (similar examples can be found in the different isospin-strangeness channels), which in the infinite volume case are loosely bound.[6] Thus, we see a well known result from Quantum Mechanics; the smaller the binding energies, the larger

[6] The first one corresponds to the $X(3872)$ resonance that has been observed close to the $D^0\bar{D}^{0*}$ threshold [30] (see also a recent determination and discussion of other experiments in Ref. [150]) and it has been a hot topic for both the experimental and theory communities since its discovery. The 2^{++} state is a HQSS partner of the $X(3872)$ molecule which dynamics, at LO in the heavy quark expansion, is being determined by precisely the same combination of counter-terms that appear in the $X(3872)$ channel. Given the discovery of the $X(3872)$ resonance, the existence of the 2^{++} state, either as a bound state or a resonance, is therefore a quite robust consequence of HQSS, see Ref. [25] and Chapter 3.

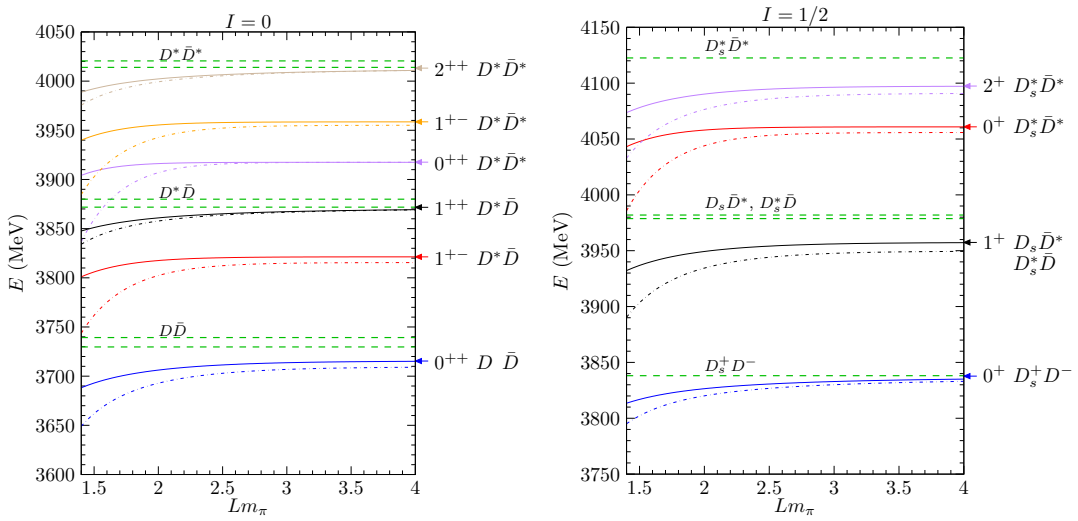

Figure 4.1: *Volume dependence of the $I = 0$ (left) and $I = 1/2$ (right) molecules predicted in Chapter 3. The horizontal dashed lines show the different thresholds involved (when the charge is not explicitly given, we are displaying the thresholds associated to the different charge channels). The solid lines correspond to the levels found in the box for $\Lambda = 1$ GeV, whereas the dot-dashed ones stand for those obtained with $\Lambda = 0.5$ GeV. Over the right axis we mark with arrows the masses of the bound states as predicted in the infinite volume case and $\Lambda = 1$ GeV. The J^{PC} quantum numbers of the different channels are indicated beside the arrows.*

the L values needed to reach the asymptotic behaviour become. From this study, we conclude that in a lattice simulation, when dealing with states that are at least bound by some tens of MeV, one might safely discriminate them by using box sizes of the order of $Lm_\pi \simeq 3$. However, the lattice study of other states less bound (binding energies below 4 or 5 MeV, as in the case of the $X(3872)$ or the 2^{++} resonances) might require significantly larger volumes. To achieve more accurate predictions for the former and solve the problem for the latter ones, we follow different approaches in the following subsections.

Finally, we note that some of the levels in Figs. 4.1 and 4.2 are not realistic, in the sense that they would mix with other levels generated by channels with the same quantum numbers, but lower thresholds. That is the case, for example in $I = 0$, of the 0^{++} $D^*\bar{D}^*$ at $E \simeq 3920$ MeV, that would mix with some higher levels of the $D\bar{D}$ channel. Indeed, it is to be expected that these bound states would acquire some width due to the coupled channel dynamics. Still, it is possible that these states could appear as more or less stable energy levels.[7]

4.4.2 Inverse analysis: phase shifts

Here we start discussing the case of the isoscalar 0^{++} $D\bar{D}$ interaction. Some levels found from the model of Chapter 3 in a finite box,[8] obtained as the zeros of Eq. (4.3.1), are shown with a

[7] In Ref. [107] the $D^*\bar{D}^*$, $D_s^*\bar{D}_s^*$ states are studied with the interaction taken from the extrapolation of the local hidden gauge approach to the charm sector, which also respects HQSS. The coupling to $D\bar{D}$ and $D_s\bar{D}_s$ is allowed and generates a width of about 50 MeV for the most bound state, the one with $I = 0$ and $J^{PC} = 2^{++}$.

[8] In what follows we will use an UV cutoff $\Lambda = 1$ GeV when presenting results deduced from the model of Chapter 3, both for finite boxes and in the infinite volume case. Other cutoffs compatible with the effective theory designed in [25] and Chapter 3 give rise to similar results.

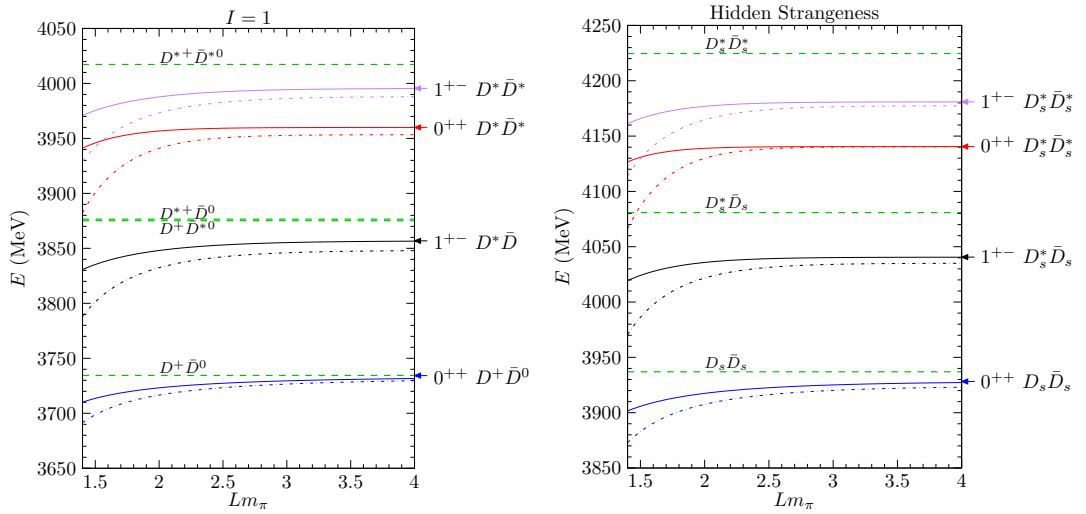

Figure 4.2: *The same as in Fig. 4.1 for the $I = 1$ (left) and hidden strangeness (right) molecules predicted in Chapter 3.*

(red) solid line in Fig. 4.3. The synthetic levels generated from them and our choice for their errors are shown with points. Recall that we give an error of ± 10 MeV to these points trying to simulate a realistic situation in a LQCD study, where these levels will be determined with some statistical uncertainties. From the upper level and the Lüscher's formula, Eq. (4.3.5), we find the phase shifts shown with points in Fig. 4.4. The errors in the phase shifts in this figure are determined by recalculating them, through Eq. (4.3.5), with different values of the upper level energy, E, randomly taken within the error intervals displayed for each of the synthetic data points in Fig. 4.3.

We could also obtain the scattering length and the effective range parameters either from the determined phase shifts, or from Eqs. (4.2.7) and (4.3.5). Actually, combining these two latter equations we have,

$$\mathrm{Re}\,\delta G_L = \lim_{\Lambda\to\infty} \mathrm{Re}\left(\tilde{G}(E) - G(E)\right) \;= -\frac{2\pi}{\mu}\left(-\frac{1}{a} + \frac{1}{2}rk^2 + \cdots\right) \tag{4.4.1}$$

for the upper energy levels, E, determined in finite boxes of different sizes. We have obtained $1/a$ and r from a χ^2-linear fit to the five data points generated for $\mathrm{Re}\,\delta G_L$ using the five synthetic upper energy levels[9] shown in Fig. 4.3. We find

$$\frac{1}{a} = 0.62 \pm 0.25 \text{ fm}^{-1}, \qquad r = 0.53 \pm 0.18 \text{ fm} \tag{4.4.2}$$

with a linear Gaussian correlation coefficient $R = 0.83$. From the above result, we find

$$a = 1.6^{+1.0}_{-0.5} \text{ fm} \,. \tag{4.4.3}$$

These values are to be compared with those obtained in the infinite volume model, Eqs. (4.2.8) and (4.2.9), with parameter $C = C_{0a}(\Lambda = 1 \text{ GeV}) = -1.024$ fm^2, which turn out to be:

$$a_{\rm th} = 1.38 \text{ fm} \,, \quad r_{\rm th} = 0.52 \text{ fm} \,. \tag{4.4.4}$$

[9]To estimate the errors in $\mathrm{Re}\,\delta G_L$ for each of the synthetic energy levels considered, we follow a procedure similar to that outlined above for the phase shifts. Thus, we let the synthetic energy level vary within the error interval displayed in Fig. 4.3 and find the range of variation of $\mathrm{Re}\,\delta G_L$.

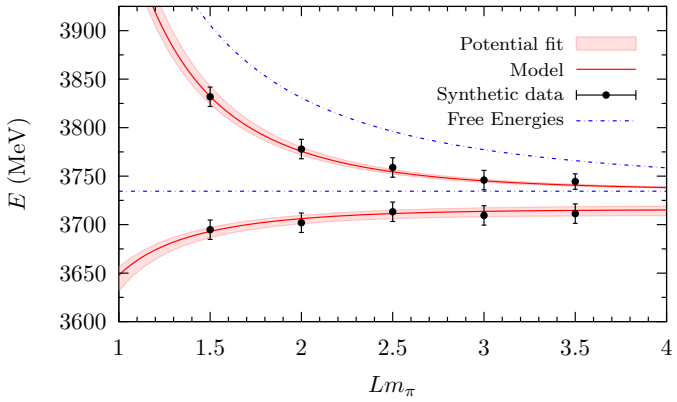

Figure 4.3: *Some energy levels for the $I = 0$, $J^{PC} = 0^{++}$ $D\bar{D}$ interaction as a function of the box size L. The levels obtained with the model of Refs.[25] and Chapter 3 in a box for $\Lambda = 1$ GeV are shown with (red) solid lines, while the generated levels for some particular values of L (synthetic data points, see the text for details), together with their assigned errors are displayed with black circles. The non-interacting energies ($m_1 + m_2 + (2\pi/L)^2 n^2/2\mu$ with $n = 0, 1$) are shown with (blue) dash-dotted lines. The error bands around the solid lines are obtained from the fit to a potential discussed in Subsec. 4.4.3. They have been obtained by considering pairs of fitted parameters $(1/C_{0a}, \Lambda)$ that provide values of χ^2 that differ from the minimum one by less than one unit ($\chi^2 \leqslant \chi^2_{min} + 1$).*

Our fitted values are compatible with the theoretical ones, but have sizable errors, although the correlation is large. Performing a standard analytical continuation of Eqs. (4.2.3) and (4.2.7) below the $D\bar{D}$ threshold, we estimate the position of the $X(3715)$ bound state,

$$E = 3721^{+10}_{-25} \text{ MeV} , \tag{4.4.5}$$

whereas the value found in Chapter 3 is $E = 3715^{+12}_{-15}$ MeV.[10] The binding energy, $B < 0$, is obtained from Eqs. (4.2.3) and (4.2.7), upon changing $k \to i\kappa$, and imposing $T^{-1} = 0$,

$$B = \frac{\kappa^2}{2\mu} , \qquad \kappa = \frac{1 \pm \sqrt{1 - 2r/a}}{r} . \tag{4.4.6}$$

To estimate the uncertainties in Eq. (4.4.5), we have performed a Monte Carlo simulation taking into account the existing statistical correlations between $1/a$ and r. We quote a 68% confident interval (CL), but with some caveats as we explain next. Note that $2r/a$ is not far from unity and within errors it can be even bigger, which means that we can get some events in the Monte Carlo runs (around 25%) with $1 - 2r/a < 0$, for which we set the square root to zero. Thus, the lower error quoted in Eq. (4.4.5) is somehow uncertain, since the above procedure tends to accumulate events around 3695 MeV. On the other hand, for the cases with $1 - 2r/a > 0$, but small, the two roots of κ in Eq. (4.4.6) are not so different, and hence there is some ambiguity in the binding energy B (we choose the smallest value of κ). Note that, although the value of E obtained with its errors seems quite accurate, when one considers it relative to the binding energy B, we find a large dispersion, since the $D\bar{D}$ threshold is at around 3734 MeV.

Finally, if we decrease the error of the synthetic energy levels from 10 MeV to 5 MeV, then the errors of the phase shifts as well as those of the threshold parameters are also reduced

[10] The errors calculated for finite volume quantities in this work refer to the statistical uncertainties we generate in the synthetic data. The errors quoted from Chapter 3 refer instead to the uncertainties in the determination of the constants appearing in the potential.

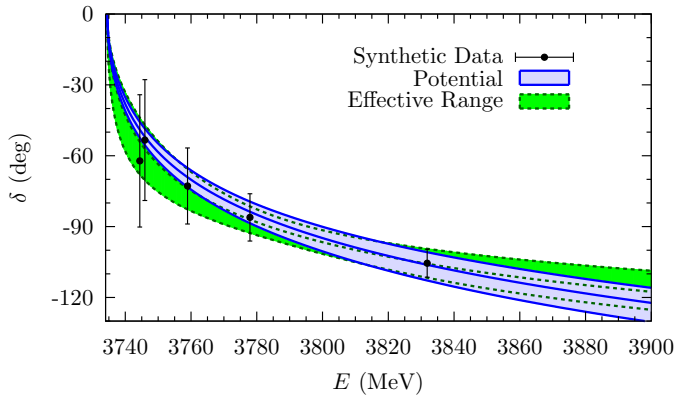

Figure 4.4: *Phase shifts obtained for $I = 0$ $J^{PC} = 0^{++}$ $D\bar{D}$ interaction. The points stand for the phase shifts calculated from the synthetic energy levels displayed in Fig. 4.3 using Eq.* (4.3.5)*. The green dashed line and its associated error band corresponds to the effective range analysis of Subsec. 4.4.2, while the blue solid line and its error band stand for the results obtained by fitting a potential discussed in Subsec. 4.4.3. The phase shifts in the infinite volume are very similar to the latter ones, so we do not show them. In both cases, the error bands have been obtained by considering pairs of fitted parameters [$(1/a, r)$ for the effective range fit and $(1/C_{0a}, \Lambda)$ for the case of the potential fit] that provide values of χ^2 that differ from the minimum one by less than one unit (points included in the dark blue $\chi^2 \leqslant \chi^2_{min}+1$ ellipse displayed in Fig. 4.5).*

approximately to half of their previous values, and the predicted mass is more accurate, $E = 3723^{+5}_{-11}$ MeV (and now $1 - 2r/a$ becomes negative for only around 6% of the Monte Carlo events). This should give an idea of the precision needed in the determination of the energy levels in order to have an appropriate determination of the mass.

In the next sections we discuss different alternatives that allow to achieve a better precision.

4.4.3 Inverse analysis: fit to a potential

We now consider another approach to analyze/use the synthetic levels that we generated in the previous section. Here again we aim to falsifying real data obtained from LQCD Monte Carlo simulations for various finite volumes. The analysis of phase shifts in the previous subsection necessarily takes into account only the level above threshold in Fig. 4.3. It is then convenient to develop an approach that could simultaneously make use of all available levels. Thus, we propose to describe all levels using a potential, Eqs. (4.2.6) and (4.3.1), fitting its parameters for such purpose. We adopt here an approach where we fit a counter-term $C = C_{0a}$ defining the potential and the UV cutoff Λ, involved in the finite-box loop function and in the potential (see Eq. (4.2.6)) to the synthetic energy levels shown in Fig. 4.3. Thus, the χ^2 function is then given by:

$$\chi^2 = \sum_{i=1}^{5} \frac{\left(E^{(0)}_{\rm thV}(L_i) - E^{(0)}_i\right)^2}{\left(\Delta E^{(0)}_i\right)^2} + \sum_{i=1}^{5} \frac{\left(E^{(1)}_{\rm thV}(L_i) - E^{(1)}_i\right)^2}{\left(\Delta E^{(1)}_i\right)^2} \ , \tag{4.4.7}$$

where $E^{(0,1)}_{\rm thV}(L_i)$ are the first two energy levels calculated from the HQSS potential, with parameters C_{0a} and Λ, in a finite box of size L_i. On the other hand, $E^{(0,1)}_i$ and $\Delta E^{(0,1)}_i$ are the synthetic levels, that we have generated, together with their assigned errors. Here, the superscript $j = 0, 1$

refers to the two levels shown in Fig. 4.3. The fit parameters, $1/C_{0a}$ and Λ, obtained in the best fit are

$$\frac{1}{C_{0a}} = -0.93 \pm 0.20 \text{ fm}^{-2}, \qquad \Lambda = 970 \pm 130 \text{ MeV} , \tag{4.4.8}$$

with a linear Gaussian correlation coefficient $R = -0.98$. These errors, and the correlation coefficient, are calculated from the hessian of χ^2 at the minimum. However, since the fit is not linear, these errors are slightly different from those obtained requiring $\chi^2 \leqslant \chi^2_{\rm min}+1$. This latter requirement gives the following non-symmetrical errors:

$$\frac{1}{C_{0a}} = -0.93^{+0.18}_{-0.27} \text{ fm}^{-2}, \qquad \Lambda = 970^{+180}_{-120} \text{ MeV} \ . \tag{4.4.9}$$

From Eq. (4.4.8), we find $C_{0a} = -1.08^{+0.19}_{-0.29}$ fm^2. The central values of both, the counter-term and the UV cutoff, agree well with those of the original model of Chapter 3, $C_{0a} = -1.024$ fm^2 and $\Lambda = 1$ GeV, used to generate the synthetic levels. However, as expected, the two parameters are strongly correlated. This was further discussed in Subsec 2.4.2. A contour plot of the χ^2 function in the $(1/C_{0a}, \Lambda)-$plane is shown in Fig. 4.5, that manifestly shows the correlation.

On the other hand, the fitted parameters of Eq. (4.4.8) predict a value for the mass of the bound state of $E = 3715^{+3}_{-6}$ MeV (68% CL, obtained from a Monte Carlo Gaussian simulation keeping the statistical correlations) in the infinite volume case. The central value agrees remarkably well with the value obtained from the model of Chapter 3, $E = 3715$ MeV, and certainly much better than the one obtained with the phase shift analysis carried out in the previous subsection ($E = 3721^{+10}_{-25}$ MeV). The errors found now are also significantly smaller.

The (blue) dashed lines in Fig. 4.3 show the energy levels obtained with the best fit parameters of Eq. (4.4.8). Note that they hardly differ from those deduced from the exact model (red solid line). Finally, we have calculated error bands for the predicted finite box levels and phase shifts by quantifying the variations that are produced in these observables when one randomly considers pairs $(1/C_{0a}, \Lambda)$ of parameters that provide $\chi^2 \leqslant \chi^2_{\rm min}+1$ (points included in the dark blue ellipse displayed in Fig. 4.5). These error bands are shown in Figs. 4.3 and 4.4, respectively.

We now discuss the dependence of this analysis on the regulator scheme. Naively, one could think that, having generated the synthetic levels with an amplitude regularized with a Gaussian regulator, it is a tautology that analyzing them with the same form of the amplitude gives good results. Then, it is clearly useful to analyze the synthetic levels with other regulator schemes, so that one can be sure that the procedure followed is reliable. For such a purpose, we consider two approaches. In the first one, we consider a non-relativistic amplitude regulated with a Lorentz (instead of Gauss) form-factor, that is:

$$V(E) = C(\Lambda') \left(\frac{\Lambda'^2}{\Lambda'^2 + k^2} \right)^2 , \tag{4.4.10}$$

$$\begin{aligned} G(E) &= \int \frac{\mathrm{d}^3 \vec{q}}{(2\pi)^3} \frac{1}{E - m_1 - m_2 - \vec{q}^{\,2}/2\mu + i0^+} \left(\frac{\Lambda'^2 + k^2}{\Lambda'^2 + \vec{q}^{\,2}} \right)^2 = \\ &= \mu \frac{k^2 - \Lambda'^2}{4\pi\Lambda'} - i\frac{\mu k}{2\pi} \ . \end{aligned} \tag{4.4.11}$$

In the second approach, a relativistic amplitude is considered, with the relativistic loop function G given by a once subtracted dispersion relation, and the potential given also in terms of the relativistic momentum, $\bar{k} = \sqrt{E^2/4 - m^2}$ (in the case of equal masses, $m_1 = m_2 = m$, which is

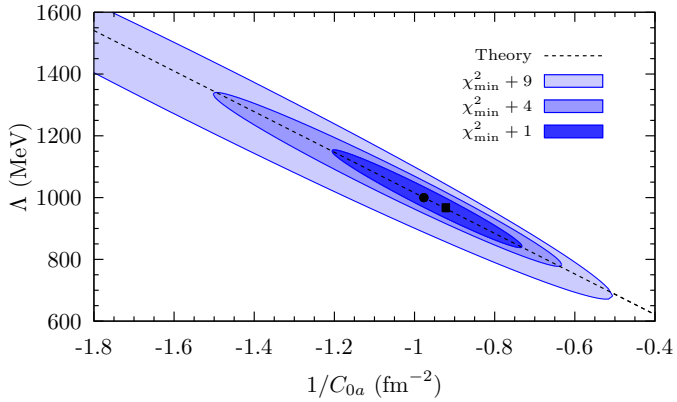

Figure 4.5: *Contour plots for the χ^2 function defined in Eq.* (4.4.7) *for the $I = 0$ $J^{PC} = 0^{++}$ $D\bar{D}$ channel. The dashed line shows the correlation predicted from the model of Chapter 3, Eq.* (2.4.60)*. The circle represents the central value taken for that model, $C_{0a} = -1.024$ fm^2 and $\Lambda = 1$ GeV, while the square stands for the results of the best fit of Eq.* (4.4.8)*. We already see from this figure that Λ and $1/C_{0a}$ are strongly correlated, and that the correlation is of the form given in Eq.* (2.4.60)*. Indeed, the dashed line in the plot, that lies close to the axis of the error ellipse, is Eq.* (2.4.60) *using the central values of the cutoff and the potential given in Chapter 3, $\Lambda = 1000$ MeV and $C_{0a} = -1.024$ fm^2. We also infer that the correlation is stronger for higher values of the cutoff, since the quadratic terms in Eq.* (2.4.60) *become less important as Λ increases.*

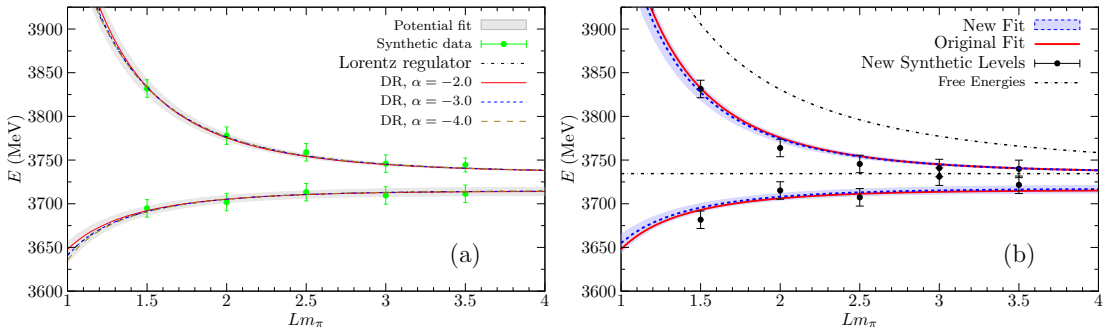

Figure 4.6: *Energy levels for the $I = 0$, $J^{PC} = 0^{++}$ $D\bar{D}$ interaction as a function of the box size L. (a) Comparison of the energy levels obtained with the Gaussian regulator analysis with those obtained with other regularization schemes. For clearness, we just show the error bands in the case of the Gaussian regulator (identical to those already displayed in Fig. 4.3). The dash-dotted line represents the levels obtained with the amplitude regularized with a Lorentz form factor. The solid, short-dashed and long-dashed lines are the energy levels obtained with the relativistic amplitude with $\alpha(\nu = m) = -2, -3$ and -4, respectively. The dot-dashed and short-dashed lines are almost indistinguishable in the range of L considered. (b) Potential results (blue dashed line) obtained from a fit to a new set of synthetic data points (black circles). These data points have been generated assuming a larger Gaussian random shift of 10 MeV (instead of the 5 MeV used through all this work) with respect to the position of the exact levels. A common error of 10 MeV has been assigned to all synthetic data points and the error bands around the blue dashed lines have been obtained as in Fig. 4.3. Finally and for comparison, the red solid lines stand for the original potential fit, displayed in Fig. 4.3, to the original 5 MeV shift synthetic data.*

the one studied in the $I = 0$ $J^{PC} = 0^{++}$ $D\bar{D}$ channel). The explicit expressions are:

$$V(E) = c_1 + c_2 \vec{k}^{\,2} \ , \tag{4.4.12}$$

$$G(E) = \frac{m^2}{4\pi^2}\left(\alpha(\nu) + \log\frac{m^2}{\nu^2} - \sigma(E)\log\frac{\sigma(E)-1}{\sigma(E)+1}\right) \ , \tag{4.4.13}$$

being $\sigma(E) = \sqrt{1-4m^2/E^2} = 2k/E$, $\alpha(\nu)$ a subtraction constant and ν an arbitrary scale (note that the only relevant parameter is α, since the quantity $\alpha(\nu) + \log\frac{m^2}{\nu^2}$ does not depend on ν). The finite volume version of this loop function is calculated as in Ref. [137].

For the first approach, we fit the counter-term C and the cutoff[11] Λ' to the synthetic levels obtained before. For the second approach, we fit the parameters of the potential, c_1 and c_2, for three different values of the subtraction constant $\alpha = -2, -3, -4$ (we take here $\nu = m$). In Fig. 4.6(a), we compare the energy levels (displayed by curves) obtained with the best fit of these parameters with those levels obtained originally with the amplitude regularized with a Gaussian form factor. We note that the four lines almost overlap for $Lm_\pi \geqslant 1.5$ (the region in which the synthetic data are located), whereas the differences are a bit larger, but still hardly visible, for $Lm_\pi \simeq 1$. More importantly, all of them lie well within the error bands obtained with the analysis at the beginning of this section. We have focused here on the energy levels obtained with the different regulator schemes, but similar conclusions are obtained for other quantities, like the phase shifts and, importantly, for the binding energy of the state. The value obtained with these two new approaches for the latter (including the error analysis) are very similar to that obtained with the Gaussian regulator amplitude. Namely, for the case of the relativistic amplitude with $\alpha = -2$ we obtain $E = 3714$ MeV, whereas for the other cases (Lorentz regulator amplitude and relativistic amplitude with $\alpha = -3$ and -4) the value obtained is $E = 3715$ MeV. We conclude that our approach, consisting in the simultaneous analysis of the energy levels by means of a potential and a loop function (being both suitably regularized), is quite reliable and independent of the regularization scheme.

At the beginning of this Section we explained how the synthetic energy levels have been generated. For some values of the box size L, the theoretical energy levels are randomly shifted within a range of ± 5 MeV. Then, a statistical error of ± 10 MeV is given to each of these points. It would be also useful to investigate the effect of increasing the range of the shift, and we now perform the same analysis that led to the fit in Eq. (4.4.8) by considering a range of ± 10 MeV (*i.e.*, we now assume a larger Gaussian random shift of 10 MeV, instead of the 5 MeV previously used, with respect to the position of the exact levels). We still assign a common error of 10 MeV to all synthetic data points. The parameters obtained from the fit to this new set of synthetic data (shown in Fig. 4.6(b)) turn out to be:

$$\frac{1}{C_{0a}} = -1.16 \pm 0.33 \text{ fm}^{-2}, \qquad \Lambda = 1120 \pm 210 \text{ MeV}, \tag{4.4.14}$$

with a linear Gaussian correlation coefficient $R = -0.99$. These new parameters agree, within errors, with those in Eq. (4.4.8), and also with the theoretical values. The energy levels calculated with these parameters, as well as the associated error bands, are shown in Fig. 4.6(b) with blue dashed lines. For comparison, we also show with red solid lines the original fit (given by Eq. (4.4.8) and shown in Fig. 4.3). The difference between both predictions for the energy levels is small. Moreover, we see that the original curves lie well within the new error bands. In what respects the mass of the bound state, we find $E = 3717^{+4}_{-6}$ MeV, which also agrees within errors with that obtained from the original fit and the theoretical value. Thus, given the number of synthetic

[11] Note that this new cutoff is not equal to that of the Gaussian regulator.

data that we consider in the fit, the obtained results turn out to be reasonably stable against this variation of the initial energy shift. Obviously, predictions will become more and more stable as the number of the considered data points increases.

4.4.4 Inverse analysis: effective range

We have seen in Subsecs. 4.4.2 and 4.4.3 that the fit of the synthetic energy levels with a potential leads to better results for the mass of the bound state than those obtained from the fit to the phase shifts (deduced from the upper level) with the effective range expansion. We believe that the reasons for this improvement are basically three. First, the potential fit takes into account both levels, above and below threshold, while the phase shifts analysis takes into account just the upper level. Second, in the potential fit, the "observables" are the energy levels, while, in the phase shifts analysis, the quantity that enters in the χ^2 function is $k \cot \delta$, and the propagation of errors can lead thus to worse determinations of the parameters. Third, the analytical structure of the inverse of the amplitude is different in both approaches. In the effective range approach, one truncates a series up to k^2, while in the potential fit one is effectively including further terms beyond the latter ones. Indeed, the full loop function G is taken into account. To study the importance of the first two points, we follow here another approach, in which we shall keep the effective range approximation for the amplitude, but fit the energy levels (above and below threshold) instead of the phase shifts obtained from the above threshold level.

The effective range expansion for the inverse of the T-matrix is written from Eqs. (4.2.3) and (4.2.7):

$$T^{-1}(E) = \begin{cases} -\frac{\mu}{2\pi}\left(-\frac{1}{a} + \frac{r}{2}k^2 - ik\right) \ , & , \ E > m_1 + m_2 \\ -\frac{\mu}{2\pi}\left(-\frac{1}{a} - \frac{r}{2}\gamma^2 + \gamma\right) \ , & , \ E < m_1 + m_2 \end{cases} \ . \tag{4.4.15}$$

with $k = \sqrt{2\mu(E - m_1 - m_2)}$ and $\gamma = \sqrt{2\mu(m_1 + m_2 - E)}$, respectively. Now, the energy levels in the box are found for given values of a and r, by means of Eq. (4.3.4). It is to say, by numerically solving $T^{-1}(E) = \delta G_L(E)$, similarly as it is done in the case of the potential, but now using Eq. (4.4.15) to model the $T-$matrix both above and below threshold. We will denote the levels obtained in this manner as $E^{(j)}_{\rm thEF}$. To determine the best values of a and r, we consider thus a χ^2 function as Eq. (4.4.7), where the $E^{(j)}_i$ are still the synthetic levels we have generated, but replacing the $E^{(j)}_{\rm thV}$ by $E^{(j)}_{\rm thEF}$, calculated as explained above. The values of the best parameters are:

$$\frac{1}{a} = 0.70 \pm 0.07 \text{ fm}^{-1}, \qquad r = 0.56 \pm 0.07 \text{ fm} \ , \tag{4.4.16}$$

with a linear Gaussian correlation coefficient $R = -0.6$.[12] Hence, we obtain:

$$a = 1.43^{+0.16}_{-0.13} \text{ fm} \ . \tag{4.4.17}$$

The errors calculated in this way are clearly smaller than those displayed in Eq. (4.4.2) with the phase shifts analysis carried out in Subsec. 4.4.2. Also, the central value of the scattering length agrees better with the theoretical one, Eq. (4.4.4). These improvements have a clear impact in the determination of the mass of the bound state, which is now $E_B = 3716^{+4}_{-5}$ MeV (68% CL), with smaller errors and better central value than those obtained with the phase shifts analysis in Eq. (4.4.5). In Fig. 4.7 we show a comparison of the ellipses in the $(1/a, r)$ parameter space

[12] In this case, the errors calculated from the requirement $\chi^2 \leqslant \chi^2_{\rm min} + 1$ almost coincided with those given here in Eq. (4.4.16).

determined by the condition $\chi^2 \leqslant \chi^2_{\rm min} + 1$ for the fits of Eqs. (4.4.2) and (4.4.16). There, it can be clearly appreciated the significant improvement achieved by fitting directly to both, lower and upper energy levels, instead of fitting to the phase shifts deduced from the latter levels. Finally, we must point out that the determination of the energy levels obtained with this method are very similar to those obtained in Subsec. 4.4.3 by introducing of a potential, and shown in Fig. 4.3. Actually, the differences between the upper and lower energy level curves (and their error bands) deduced from both methods would not be easily appreciated in Fig. 4.3. For this reason, we have not shown in this figure the results obtained from the method discussed in this subsection.

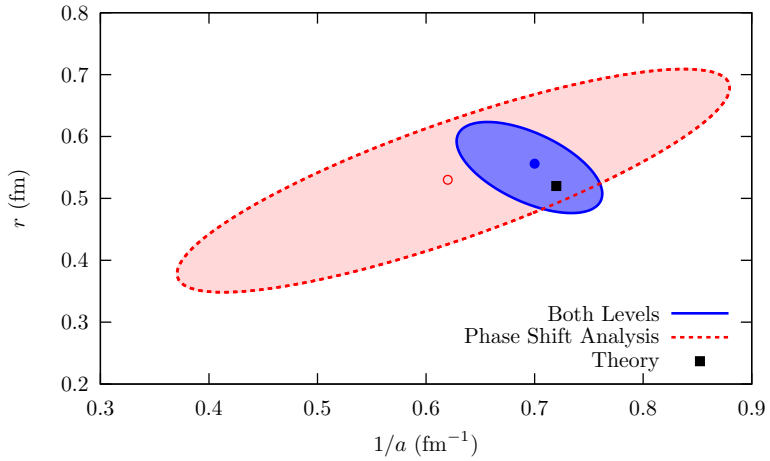

Figure 4.7: *Comparison of the determination of the effective range parameters, $1/a$ and r, with the methods explained in Subsecs. 4.4.2 (red dashed line) and 4.4.4 (solid blue line). The ellipses are obtained from the condition $\chi^2 \leqslant \chi^2_{min} + 1$ in each case. The central values of each fit are represented with points. We also show, for comparison, the theoretical values of the parameters, as given in Eq.* (4.4.4)*, with a black square.*

4.4.5 Inverse analysis: bound state fit

We have discussed in Subsec. 4.4.1 the volume dependence of the sub-threshold levels that arise when we put the model in a finite box. For cases with $V < 0$, the potential is attractive, and hence, a bound state in the infinite volume case may arise. Whether it is bound or not in the infinite volume case, there would appear a sub-threshold level for finite volumes. It was argued in Subsec. 4.4.1 that it may be not very clear, at first sight, if these levels tend to the threshold energy or to a bound state in the $L \to \infty$ limit. To circumvent this problem, we suggest here a method to study this volume dependence. By subtracting Eqs. (4.2.4) and (4.3.1), we can write the amplitude in the finite box as [151]:

$$\tilde{T}^{-1} = T^{-1} - \delta G_L, \qquad \delta G_L = \lim_{\Lambda\to\infty} \delta G = \lim_{\Lambda\to\infty} \left(\tilde{G} - G\right) \ . \tag{4.4.18}$$

A bound state with mass E_B appears as a pole in the T-matrix, thus in the vicinity of the pole, we can approximate:

$$T(E \simeq E_B) = \frac{g^2}{E - E_B} + \dots \ , \tag{4.4.19}$$

where the ellipsis denote regular terms in the Laurent series of the amplitude. The coupling can also be calculated analytically,

$$g^2 = \lim_{E\to E_B}(E-E_B)T(E) \quad \text{or} \quad \frac{1}{g^2} = \left.\frac{\mathrm{d}T^{-1}(E)}{\mathrm{d}E}\right|_{E=E_B} . \tag{4.4.20}$$

The volume dependence of the sub-threshold level in the finite box, given by the equation $\tilde{T}^{-1}(E)=0$ is then dominated by this bound state, and hence:

$$\tilde{T}^{-1}(E) \simeq \frac{E-E_B}{g^2} - \delta G_L(E) = 0 , \tag{4.4.21}$$

from where one can write:

$$E(L) = E_B + g^2 \delta G_L\left[E(L), L\right] . \tag{4.4.22}$$

This equation is a reformulation of a similar result obtained in Refs. [113, 114, 115].[13] The coupling g obtained here is related to Z_ψ of Ref. [115]. Note, however, that Eq. (4.4.22) is appropriate as long as Eq. (4.4.19) is sufficiently accurate to describe the infinite volume $T-$matrix for the energy levels found in the lattice simulation (i.e., energies for which $\tilde{T}^{-1}$ vanishes). Hence, the larger the box sizes, the better Eq. (4.4.22) will perform.[14] We extract the mass and the coupling of the bound state from a fit to the sub-threshold level in Fig. 4.3 with the following χ^2 function,

$$\chi^2 = \sum_{i=1}^{5} \frac{\left(E(L_i) - E_i^{(0)}\right)^2}{\left(\Delta E_i^{(0)}\right)^2} \tag{4.4.23}$$

where $E(L)$ is given by Eq. (4.4.22).[15] The best χ^2 is $\chi^2_{\rm min}=0.5$, and the parameters so obtained are:

$$E_B = 3712 \pm 6 \text{ MeV} , \qquad g^2 = (2.8 \pm 2.1) \text{ GeV}^{-1} , \tag{4.4.24}$$

to be compared with those obtained with the model in the infinite volume case, $E_B = 3715$ MeV and $g^2 = 2.6$ GeV^{-1}.

It could be that, for the case of weakly bound states, the error bars on the energies overlap with the threshold and it is difficult to determine if one has a bound state or not. A weak attractive potential that does not bind in the infinite volume case, still provides a level below threshold for finite volumes, and the energies go to threshold as $L\to\infty$. For this case we proceed

[13] In the same line as in those references, but using boosted reference frames, in Ref. [152] linear combinations of energy levels are suggested to reduce the volume dependence. Our method does not rely upon the analytical form of the volume dependence to make extrapolations since for every L considered, the exact L dependence is provided by $\delta G_L(E(L),L)$.

[14] On the other hand, for very small binding energies, some subtleties appear, because the coupling g^2 tends to zero as the mass of the bound state approaches the threshold [99, 153, 154]. We will discuss this issue at length in Subsec. 4.4.6.

[15] It is worth noting the following technical detail. In principle, $E(L)$ should be extracted for each L_i as the implicit solution in Eq. (4.4.22) for given E_B and g^2. For practical purposes, though, it is more convenient to obtain $E(L)$ by plugging into the right-hand side of this equation the values of $E_i^{(0)}$ and L_i that we are fitting to. If Eq. (4.4.19) is accurate enough, both methods are equivalent, as long as the effects in Eq. (4.4.22) of the statistical fluctuations of the measured lattice levels are sufficiently small. In that case, the results for E_B and g^2 should not be very different, as we have checked. Indeed, the best fit results given in Eq. (4.4.24) have been obtained within this approximation. However, this approximation cannot be safely used when the bound state is placed close to threshold, because then δG_L rapidly changes and statistical fluctuations in the determined lattice energy levels induce large variations in the right-hand side of Eq. (4.4.22).

as follows. The volume dependence of this level would be given by:

$$\begin{aligned}\tilde{T}^{-1} = 0 = T^{-1} - \delta G_L = \\ &= -\frac{\mu}{2\pi}\left(-\frac{1}{a} + \frac{r}{2}k^2 + \cdots\right) - \frac{2\mu}{L^3}\frac{1}{k^2} - \alpha - \beta k^2 + \cdots \\ &= -\frac{2\mu}{L^3 k^2} + \frac{\mu}{2\pi a} - \alpha + \left(-\frac{\mu r}{4\pi} - \beta\right)k^2 + \cdots\end{aligned}$$

with some coefficients α and β, disregarding exponentially suppressed terms. In the above equation, we have explicitly separated the threshold singularity of δG_L,

$$\frac{1}{L^3}\frac{1}{E - m_1 - m_2} = \frac{2\mu}{L^3 k^2} \ .$$

Hence, the general behaviour of this level would be:

$$k^2 = \frac{2\mu}{L^3}\frac{1}{A + Bk^2} \ . \tag{4.4.25}$$

Now, this expression could be used in a χ^2 function as in Eq. (4.4.23) (with $k^2 < 0$ for the level below threshold). We have checked that, if we try to fit the energies of the lower level of Fig. 4.3 with this formula, we get a much worse χ^2 value, discarding the possibility that there is not a bound state in the infinite volume.

We have seen then that the method outlined in this subsection allows for a safe discrimination between those levels that correspond to bound states in the infinite volume and those that do not, and it also gives a precise determination of the mass. It is also worth noting that the errors for the mass of the bound state are similar to those obtained with the analysis from a potential in Subsec. 4.4.3, and smaller than those calculated with the phase shift analysis in Subsec. 4.4.2.

4.4.6 The case of the $I = 0$ $J^{PC} = 2^{++}$ channel

We repeat the same analyses carried out above but now for the case of the bound state present in the $I = 0$ $J^{PC} = 2^{++}$ $D^*\bar{D}^*$ channel. As already mentioned, the 2^{++} state is a HQSS partner of the $X(3872)$ molecule whose dynamics, at LO in the heavy quark expansion, is determined by precisely the same combination of counter-terms that appear in the $X(3872)$ channel. The existence of the 2^{++} state, either as a bound state or a resonance, is a quite robust consequence of HQSS, see [25] and Chapter 3, and it can be certainly subject to experimental detection. It is also worth discussing this channel in this context because, contrary to the case analyzed before, we have here a very weakly bound state. In the calculation of Chapter 3, and also in the results of Subsec. 4.4.1, shown in the left panel of Fig. 4.1, charged and neutral coupled channels were studied, because the gap between both thresholds is indeed larger than the binding energy of the bound state. The mass of the bound state is $E_B = 4013.2$ MeV, whereas the neutral and charged thresholds are located at 4014.0 MeV and 4020.6 MeV, respectively. Here, however, in order to discuss the problem in simpler terms, we will consider only an uncoupled channel problem with $I = 0$, and use isospin average masses, keeping the relevant counter-term, C_{0X} in the nomenclature of Chapter 3, to the same value, namely, $C_{0X} = -0.731$ fm^2. In this way, the threshold is located at 4017.3 MeV, whereas the mass of the bound state now becomes $E_B = 4014.6$ MeV. The first two energy levels obtained with this simplified model are shown with (red) solid lines in Fig. 4.8. As before, for the following statistical analyses we consider the synthetic levels shown in this figure with points. The centroid of these points is randomly shifted in the range ± 5 MeV, and they are given an error of ± 10 MeV. With the points of the upper

level, we generate the phase shifts shown in Fig. 4.9 with points, through Eq. (4.3.5). We can now obtain the scattering length and effective range as in Subsec. 4.4.2, that turn out to be

$$\frac{1}{a} = 0.41 \pm 0.30 \text{ fm}^{-1} , \quad r = 0.67 \pm 0.19 \text{ fm} , \tag{4.4.26}$$

with a linear Gaussian correlation $R = 0.81$. From the above fitted value for $1/a$, we find

$$a = 2.4^{+2.4}_{-1.2} \text{ fm (68\% CL)} , \tag{4.4.27}$$

while the theoretical values, obtained from Eqs.(4.2.8) and (4.2.9), are

$$a_{\text{th}} = 3.0 \text{ fm} , \quad r_{\text{th}} = 0.58 \text{ fm} , \tag{4.4.28}$$

which agree with the above determinations, within errors. The phase shifts obtained with these parameters, and the associated error bands, are shown in Fig. 4.9 with (green) dashed lines, and they satisfactorily reproduce the synthetic data. The mass of the bound state turns out to be then $E_B = 4013^{+4}_{-18}$ MeV. Recall that the caveats raised in Subsec. 4.4.2 apply here.

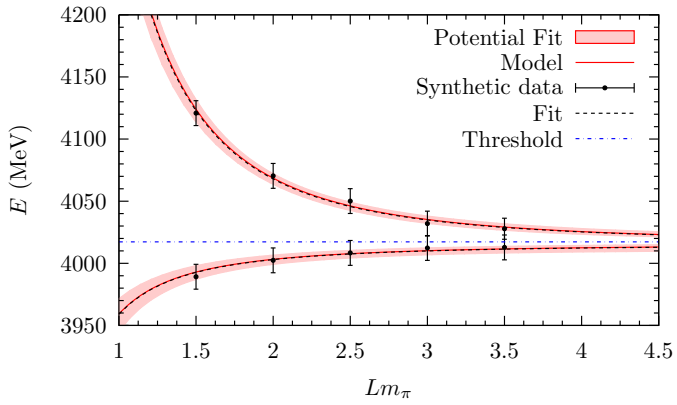

Figure 4.8: *Same as in Fig. 4.3, but for the* $I = 0$ 2^{++} $D^*\bar{D}^*$ interaction.

The next step is to consider a potential fit, as in Subsec. 4.4.3, where the free parameters are C_{0X} and Λ. From a best fit, as described in Subsec. 4.4.3, we find

$$\frac{1}{C_{0X}} = -1.4 \pm 0.5 \text{ fm}^{-2} , \quad \Lambda = 1020 \pm 240 \text{ MeV} , \tag{4.4.29}$$

with a linear Gaussian correlation coefficient $R = -0.97$. The non-symmetrical errors given by the condition $\chi^2 \leqslant \chi^2_{\text{min}} + 1$ are instead

$$\frac{1}{C_{0X}} = -1.4^{+0.4}_{-0.7} \text{ fm}^{-2} , \quad \Lambda = 1020^{+360}_{-190} \text{ MeV} . \tag{4.4.30}$$

The energy levels obtained with these parameters are shown in Fig. 4.8 with a (black) dashed line, although they are so similar to those of the exact model that they mostly overlap. Also shown in the figure are the error bands generated from the errors of the parameters, as described previously in Fig. 4.3. With this potential, we can also calculate the phase shifts, which are shown in Fig. 4.9 with (blue) solid lines, and also the associated error band. The quality of both descriptions, that of the effective range and that of the potential, are very similar, and

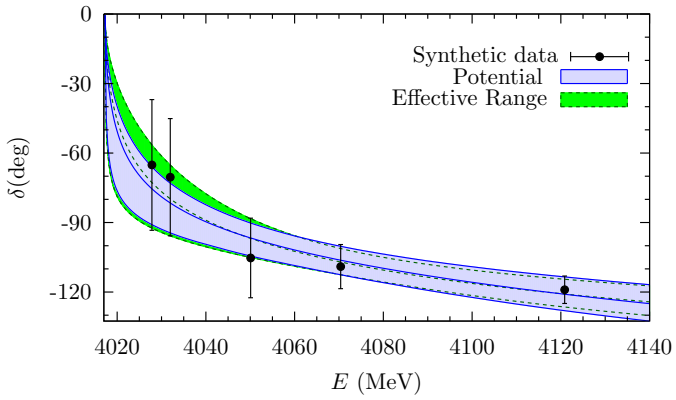

Figure 4.9: *Phase shifts for the $I = 0$ $J^{PC} = 2^{++}$ $D^*\bar{D}^*$ channel interaction. The points stand for the synthetic phase shifts generated from the upper energy level of Fig. 4.8. The (green) dashed line corresponds to the effective range fit, while the (blue) solid line corresponds to the potential fit. The associated error bands are obtained by considering randomly chosen pair of parameters [$(1/a, r)$ and $(1/C_0, \Lambda)$ for the effective range and potential fits, respectively] that satisfy $\chi^2 \leqslant \chi^2_{min} + 1$.*

indeed both lines are very similar to the one of the exact model, and hence we do not show the latter. The value of C_{0X} deduced from Eq. (4.4.29) is $C_{0X} = -0.71^{+0.19}_{-0.39}$ fm^2 (68% CL), in good agreement with the one of the infinite volume model, $C_{0X} = -0.73$ fm^2. Finally, the mass of the bound state is given by $E_B = 4014.3^{+2.3}_{-5.4}$ MeV. We must stress again that the errors obtained with this method are smaller than those obtained with the phase shifts analysis.

Now, we consider the method of Subsec. 4.4.4, in which the effective range expansion is used to study the levels below and above threshold. In this case, the best fit values that we obtain for the scattering length and effective range parameters are

$$\frac{1}{a} = 0.35 \pm 0.15 \text{ fm}^{-1} , \qquad r = 0.64 \pm 0.15 \text{ fm} , \tag{4.4.31}$$

with a linear Gaussian correlation coefficient $R = 0.3$. The non-symmetric errors stemming from the condition $\chi^2 \leqslant \chi^2_{\text{min}} + 1$ turn out to be

$$\frac{1}{a} = 0.35^{+0.13}_{-0.21} \text{ fm}^{-1} , \qquad r = 0.64^{+0.14}_{-0.16} \text{ fm} . \tag{4.4.32}$$

Propagating the correlated Gaussian errors of Eq. (4.4.31), we find

$$a = 2.9^{+2.0}_{-0.9} \text{ fm} . \tag{4.4.33}$$

We note that here, as it also occurred for the $I = 0$, $J^{PC} = 2^{++}$ case, the central values obtained with this method agree better with the theoretical ones, Eq. (4.4.28), than those obtained with the phase shift description, Eq. (4.4.26), and have smaller errors than the latter ones. The mass of the bound state obtained is $E_B = 4014.2^{+2.3}_{-4.8}$ MeV, which is better determined than that obtained by means of the phase shifts analysis, and very similar to the one obtained with the potential method.

Finally, we should proceed now with the analysis performed in Subsec. 4.4.5. However, there is a major difference in this case, namely, that the bound state is very close to the threshold in this case. It is known that, in this case, the coupling of the state tends to zero [99, 153, 154, 155, 156],

and so additional terms in the Laurent series, Eq. (4.4.19), are relevant for energies not very far from the bound state mass.[16] Further, since we are considering an error of ± 10 MeV in the energy levels, and we are trying to reproduce a bound state of binding energy of $2-3$ MeV, we should expect a greater qualitative impact on the lower energy levels, which are the only ones considered in this method (note that the other methods examined above use always the upper levels as well). These considerations explain why, when performing such analysis, we obtain very bad results for the bound state mass and the coupling. Hence, we must conclude that this method can only be applied safely in the case of bound states that are not very loosely bound. On the other hand, including a background term would increase the number of free parameters, and so, the errors stemming from a best fit would be even larger. At this stage, the approaches in Subsecs. 4.4.2 to 4.4.4 would be more useful for cases like this one, in which the bound state is very close to threshold.

4.5 Conclusions

In this chapter we have addressed the interaction of heavy charmed mesons in the hidden charm sector where several bound states are produced using an interaction that is based on heavy quark spin symmetry, following the formalism derived for an infinite volume in Chapter 3.

The interaction is then studied in a finite box and the levels expected from a lattice QCD calculation are evaluated for the $D\bar{D}$, $D\bar{D}^*$, $D^*\bar{D}^*$ states and their $SU(3)$ partners. With this analysis we are able to reproduce the predictions listed in the previous chapter. This calculation serves as a test of the validity of this finite volume formalism employed.

Then the inverse problem is faced, generating "synthetic data" from the levels obtained and using different procedures to obtain the relevant magnitudes in the infinite space, phase shifts and binding energies for the bound states. Particular emphasis is done in the error analysis to establish the accuracy of the different methods. We use two levels for different values of the box size L, one below threshold and the closest one above threshold. One strategy is to use the Lüscher formula to get phase shifts for each energy of the level above threshold. Another strategy is to use the effective range approximation, but fitting the scattering length and effective range to both levels (above and below threshold). The two methods work, but the latter one gives better determinations of the parameters (scattering length and effective range), but also of the mass of the bound state. Yet, the method that proves most efficient[17] is to parameterize a potential and a regularizing UV cutoff for the meson-meson loops and carry a fit to the data. Once the potential and the UV cutoff are determined one can evaluate the phase shifts and binding energies with much better precision than the one assumed in the "synthetic data".

We also devoted particular attention to the case of weakly bound states, where special care must be taken. For this purpose we have analyzed the $J^{PC}=2^{++}$ HQSS partner of the $X(3872)$ resonance, whose binding energies are similar.

Finally, as a byproduct we present an efficient method to obtain the Lüscher function, supported by an analytical study that allows one to truncate the sum by means of a Gaussian form factor and estimate the error induced by the truncation.

[16] As an example, consider a background term in the amplitude in Eq. (4.4.19), so that $T = g^2/(E-E_B)+\beta+\cdots$. From the theoretical model, one can calculate $g^2 = 0.58\cdot 10^{-3}$ MeV^{-1} and $\beta = -0.68\cdot 10^{-4}$ MeV^{-2}. For energies $E \simeq 3990$ MeV, as we find for the lower level in Fig. 4.8 for $Lm_\pi = 1.5$, we have $\left|g^2/(E-E_B)\right| < |\beta|$.

[17] As one moves far away from threshold, any method based on the effective range approximation becomes less appropriated.

Chapter 5

Extension to the bottom and bottom-charm sectors

5.1 Introduction

The bottom sector provides very interesting probes of the dynamics of the Standard Model. Many experiments (related to flavour physics or CP Violation, e.g.) are currently being carried out in several B-factories (such as Belle or BaBar) and there are collaborations devoted to b-physics (LHCb) since the experimental measurements in the bottom sector are more precise than in the charm sector. Therefore, the understanding of the hadronic spectrum in the bottom sector becomes crucial. In principle, due to Heavy Flavour Symmetry (already introduced in Sect. 1.2.1), a high degree of similarity between the charm and bottom sectors is expected since the dynamics must be the same (up to corrections of the order $\mathcal{O}(1/m_Q)$) in both sectors. Indeed, the spectrum of the charmonium and bottomonium, displayed in Fig. 5.1, are quite similar. However and despite having similar dynamics, the bottomonium states have a significantly larger binding energy than its corresponding counterparts in the charm sector. This is easily understood if one takes into account a dominant hydrogen-like interaction and the fact that the reduced mass is larger in the bottomonium than in the charmonium system.

As a consequence of this large experimental research program, many heavy quarkonium states have been observed in the bottom sector. Owing to the similarities with the charm sector, some of those new states are expected to be difficult to accommodate on conventional quark model spectrum, such as those we have studied in the previous chapters: heavy-light meson heavy-light antimeson molecular systems. Some experimental resonances that seem likely to fit into this description are the isovector $Z_b^{\pm,0}(10610)$ and $Z_b^{\pm}(10650)$ resonances reported by the Belle Collaboration [43, 158] which have been considered to be $B\bar{B}^*$ and $B^*\bar{B}^*$ hadronic molecules, respectively [27]. This was motivated because they lie very close to those thresholds. It is worth noting that since these resonances have isospin $I = 1$, their quark content must be of, at the very least, four quarks, and therefore, they cannot be described within a conventional constituent quark model. They were the first experimental resonances with a mandatory exotic interpretation.

In this chapter, we will study the consequences of HQSFS in the spectrum of hadronic molecules in the bottom sector, and we will also study hybrid bottom-charm systems.

First, we will review the constrains in the LO potential deduced from heavy flavour and

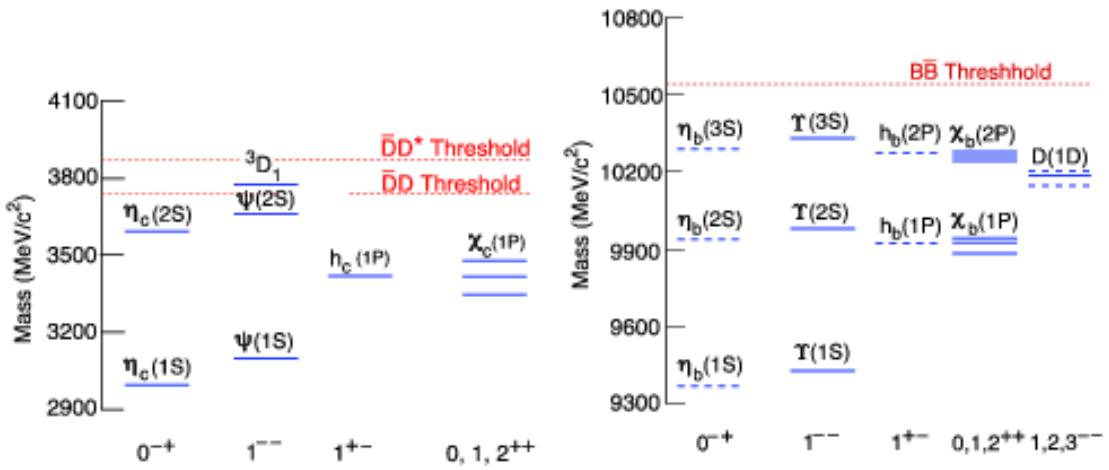

Figure 5.1: *Experimental quarkonium ($Q\bar{Q}$) spectrum in the charm and bottom sectors taken from Ref. [157]. The vertical scales are the same, offset to align the ground states.*

spin symmetry in these systems and employ the same scheme used in Chapter 3. Thus, we will fix some counter-terms thanks again to the identification of some resonances as heavy meson molecules. Since the identification of the $X(3915)$ and the $X(4140)$ as hidden-charm meson-antimeson molecules could be subject of some founded doubts, here we will use two very-close-to-threshold resonances: the $X(3872)$ and $Z_b^{\pm,0}(10610)/Z_b^{\pm}(10650)$ resonances to fix the counter-terms of the 4H LO HQSFS local interaction. These resonances are located very close to $P^{(*)}\bar{P}^{(*)}$ thresholds and their identification as loosely bound states seems much more robust. The novelty is that we employ simultaneously inputs from the charm ($X(3872)$) and bottom sectors ($Z_b^{\pm,0}(10610)/Z_b^{\pm}(10650)$). In Sect. 5.2, we will discuss how these inputs allow us to fix only two[1] of the four undetermined LECs. Thus, the predicted set of states derived from HQSFS is more limited. These results are presented in Table 5.2. Despite OPE is considered a subleading effect in the charm sector, things could be unclear in the bottom sector due to the large masses of the bottom mesons [11]. Thus in Subsect. 5.3, we estimate the numerical effect of OPE in the dynamics of the isoscalar states in the bottom sector. Finally, some conclusions are given in Sect. 5.4.

5.2 Heavy spin-flavour molecular partners of the $X(3872)$ and $Z_b(10610)$ states

We are mainly interested in two manifestations of heavy quark symmetry: heavy quark spin symmetry (HQSS) and heavy flavour symmetry (HFS). Their role can be easily illustrated in the heavy meson-antimeson system with a series of examples. We begin with HQSS as applied to the Z_b and Z_b', where we assume that they are 1^{+-} $B\bar{B}^*$ and $B^*\bar{B}^*$ isovector molecules, respectively. HQSS implies that the LO non-relativistic isovector heavy meson-antimeson potential is identical

[1] In this chapter, we will not consider the $X(3872)$ isospin mixing scenarios, discussed in Chapter 3

in both cases [13, 23, 27]

$$V^{\rm LO}_{B\bar{B}^*}(1^{+-}) = V^{\rm LO}_{B^*\bar{B}^*}(1^{+-})\,, \tag{5.2.1}$$

where we have indicated the particle channel in the subscript. This explains why the energy shift of the Z_b/Z_b' states relative to the $B\bar{B}^*/B^*\bar{B}^*$ thresholds is almost the same. For a further example we can consider the $X(3872)$ — the X_c from now on — as a 1^{++} $D\bar{D}^*$ molecule. HQSS then predicts that the potential in the X_c channel is the identical to that of the 2^{++} $D^*\bar{D}^*$ channel [11, 25]:

$$V^{\rm LO}_{D\bar{D}^*}(1^{++}) = V^{\rm LO}_{D^*\bar{D}^*}(2^{++})\,, \tag{5.2.2}$$

meaning that we can expect the existence of a 2^{++} HQSS partner of the $X(3872)$. Explicit calculations indicate that its mass should be in the vicinity of 4012 MeV, see Ref. [25]. Following the previous naming pattern, we will call this state the X_{c2} resonance. We have already discussed these HQSS relations in Chapters 2 and 3.

As can be appreciated, the exciting feature about heavy meson molecules is their high degree of symmetry. This is even more evident when we consider HFS. According to HFS, the interactions involving heavy mesons do not depend on the heavy quark flavour. This means that the heavy meson-antimeson potential is not able to distinguish the D/D^* mesons from the B/B^* ones. If we apply this idea to the X_c, we find

$$V^{\rm LO}_{D\bar{D}^*}(1^{++}) = V^{\rm LO}_{B\bar{B}^*}(1^{++})\,, \tag{5.2.3}$$

and the same is true for the potentials in the X_{c2}, Z_b and Z_b' channels. The consequence of HFS is that heavy meson molecules should appear in flavour multiplets. A resonance in the charm sector might have a counterpart in the bottom sector and viceversa. However, there is a catch. As already said, the formation of bound states does not only depend on the strength of the potential, but also on the reduced mass of the two-body system. A higher reduced mass translates into a stronger binding. If the X_c binds, it is more than likely that the X_b — the bottom counterpart of the X_c — binds too. Searching for such a state may even be regarded as a test of the hadronic molecular hypothesis of the $X(3872)$. On the contrary, the shallow nature of the Z_b and Z_b' indicates that their charm counterparts could be probably unbound. Yet the Z_c and Z_c' might survive as virtual states or resonances. As we will see, this is indeed the case.

We compute in this chapter then the expected location of the HQSS and HFS partners of the X_c, Z_b and Z_b'. For that purpose, we notice that at LO the EFT potential is simply a contact-range interaction of the type

$$\langle \vec{p}|V_X^{\rm LO}|\vec{p}\,'\rangle = C_{0X}\,, \tag{5.2.4}$$
$$\langle \vec{p}|V_Z^{\rm LO}|\vec{p}\,'\rangle = C_{1Z}\,, \tag{5.2.5}$$

where the subscripts indicate the isospin and whether we are considering an X- or Z-like channel (see Table 5.1). For finding bound state solutions we iterate this potential in the LSE, as we described in Sect. 2.4. At this point, we find it worth commenting again that the contact-range potential is singular and requires a regularization and renormalization procedure. In this thesis, we employ a standard Gaussian regulator with a cutoff $\Lambda = 0.5 - 1\,\text{GeV}$, where we have chosen the cutoff window according to the following principles: Λ must be bigger than the wave number of the states, but at the same time must be small enough to preserve heavy quark symmetry and prevent that the theory might become sensitive to the specific details of short distance dynamics. The dependence of the results on the cutoff, when it varies within this window, provides an

$I(J^{PC})$	C_{0X}	$I(J^{PC})$	C_{1Z}
$0(1^{++})$	$\frac{1}{\sqrt{2}}\left(P\bar{P}^* - P^*\bar{P}\right)$	$1(1^{+-})$	$\frac{1}{\sqrt{2}}\left(P\bar{P}^* + P^*\bar{P}\right)$
$0(2^{++})$	$P^*\bar{P}^*$	$1(1^{+-})$	$P^*\bar{P}^*$
$0(2^{+})$	D^*B^*	$1(1^{+})$	D^*B^*

Table 5.1: *Various combinations having the same contact term as the $X(3872)$ (left) and $Z_b(10610)$ (right). Here P and P^* represent $D, \bar{B}$ and $D^*, \bar{B}^*$, respectively.*

Table 5.2: *Heavy meson–heavy antimeson combinations having the same contact term as the $X(3872)$ and $Z_b(10610)$, and the predictions of the pole positions, which are understood to correspond to bound states except if we write "V" in parenthesis for denoting a virtual state. When we increase the strength of the potential to account for the various uncertainties, in one case (marked with † in the table) the virtual pole evolves into a bound state. The masses are given in units of MeV.*

V_C	$I(J^{PC})$	States	Thresholds	Masses ($\Lambda = 0.5$ GeV)	Masses ($\Lambda = 1$ GeV)	Measurements
C_{0X}	$0(1^{++})$	$\frac{1}{\sqrt{2}}(D\bar{D}^* - D^*\bar{D})$	3875.87	3871.68 (input)	3871.68 (input)	3871.68 ± 0.17 [45]
	$0(2^{++})$	$D^*\bar{D}^*$	4017.3	4012^{+4}_{-5}	4012^{+5}_{-12}	?
	$0(1^{++})$	$\frac{1}{\sqrt{2}}(B\bar{B}^* - B^*\bar{B})$	10604.4	10580^{+9}_{-8}	10539^{+25}_{-27}	?
	$0(2^{++})$	$B^*\bar{B}^*$	10650.2	10626^{+8}_{-9}	10584^{+25}_{-27}	?
	$0(2^{+})$	D^*B^*	7333.7	7322^{+6}_{-7}	7308^{+16}_{-20}	?
C_{0Z}	$1(1^{+-})$	$\frac{1}{\sqrt{2}}(B\bar{B}^* + B^*\bar{B})$	10604.4	10602.4 ± 2.0 (input)	10602.4 ± 2.0 (input)	10607.2 ± 2.0 [43]
						10597 ± 9 [160]
	$1(1^{+-})$	$B^*\bar{B}^*$	10650.2	10648.1 ± 2.1	$10648.1^{+2.1}_{-2.5}$	10652.2 ± 1.5 [43]
						10649 ± 12 [160]
	$1(1^{+-})$	$\frac{1}{\sqrt{2}}(D\bar{D}^* + D^*\bar{D})$	3875.87	3871^{+4}_{-12} (V)	3837^{+17}_{-35} (V)	$3899.0 \pm 3.6 \pm 4.9$ [161]
						$3894.5 \pm 6.6 \pm 4.5$ [162]
	$1(1^{+-})$	$D^*\bar{D}^*$	4017.3	4013^{+4}_{-11} (V)	3983^{+17}_{-32} (V)	4026.3 ± 2.6 [163].
	$1(1^{+})$	D^*B^*	7333.7	$7333.6^{\dagger}_{-4.2}$ (V)	7328^{+5}_{-14} (V)	?

estimate of the expected size of subleading corrections. For a more complete discussion on the choice of the cutoff in nucleon-nucleon systems, see for instance Ref. [159].

For the numerical calculations, we work in the isospin symmetric limit and use the averaged masses of the heavy mesons, which are $M_D = 1867.24$ MeV, $M_{D^*} = 2008.63$ MeV, $M_B = 5279.34$ MeV and $M_{B^*} = 5325.1$ MeV. The value of C_{0X} is determined from reproducing the central value of the Particle Data Group averaged mass of the $X_c(3872)$, 3871.68 ± 0.17 GeV [45][2]. The resulting value is $C_{0X} = -1.94$ fm^2 for $\Lambda = 0.5$ GeV and -0.79 fm^2 for $\Lambda = 1$ GeV [25], where the uncertainties coming from the error in the mass of the X_c are negligible. At this point, one may argue that isospin breaking is important for the X_c, owing to its closeness to the $D^0\bar{D}^{0*}$ threshold, but concrete calculations indicate that the effect is tiny for spectroscopy (see the results of Chapter 3). Neglecting isospin breaking effects prevents to extract any information on the C_{1X}

[2]Since the inclusion of the interaction of the isovector components of the $X(3872)$ resonance hardly varies the predictions for its scalar "partners"; for the sake of simplicity we are neglecting the $I = 1$ component of the $X(3872)$ resonance in this analysis.

counter-term. In turn, the value of C_{1Z} may be fixed using the $Z_b(10610)$ mass. The mass of the $Z_b(10610)$ measured in the $\Upsilon(nS)\pi, h_b(nP)\pi$ distribution 10607.2 ± 2.0 MeV [43] is $1.3\,\sigma$ above the $B\bar{B}^*$ threshold, while the value measured in the $\Upsilon(5S) \to B\bar{B}^*\pi$ decay 10597 ± 9 MeV [160] overlaps with the $B\bar{B}^*$ threshold. However, these estimations are based on parameterizing the Z_b and Z_b' poles as Breit-Wigner. The analysis of Ref. [44], which overcomes this limitation, suggests that the Z_b and Z_b' are slightly below threshold and have a binding energy of $\sim 4.7\,\text{MeV}$ and $\sim 0.1\,\text{MeV}$ respectively. In line with the estimates of Ref. [44], we assume the Z_b binding energy to be $2.0 \pm 2.0\,\text{MeV}$, yielding $C_{1Z} = -0.75^{+0.15}_{-0.28}$ fm^2 for $\Lambda = 0.5$ GeV and $-0.30^{+0.03}_{-0.07}$ fm^2 for $\Lambda = 1$ GeV.

With these values, we can make predictions by solving the LSE, as previously commented. We summarize our results in Table 5.2. The uncertainties that are listed correspond to taking into account that HQSS and HFS are not exact, but approximate. We expect a Λ_{QCD}/m_Q deviation of the C_{0X} and C_{1Z} value from the heavy quark limit. Taking 300 MeV for Λ_{QCD} [45], and 1.5 GeV and 4.5 GeV for m_c and m_b, respectively, this translates into a relative 20% error in the charm sector and 7% in the bottom one. Actually, the errors are dominated by the uncertainty in the charm sector. When we compute the X_b and X_{b2}, the relative error of C_{0X} is rather 20% than 7% as its value has been determined from the $X_c(3872)$. We remind that the uncertainties coming from the errors in the mass of the $X_c(3872)$ are negligible in comparison. For the states derived from the Z_b's, we sum the Λ_{QCD}/m_Q and the binding energy errors in quadrature, where the binding error dominates. Some of the states — the partners of the Z_b/Z_b' — are not bound, but virtual. We indicate this with a "V".

Among the predicted states, the 2^{++} ones can decay into two heavy pseudoscalar mesons in a d-wave, which would introduce a width of order $\mathcal{O}(10\text{ MeV})$ (this decay mode is studied in Chapter 9). The predicted mass of the $D^*\bar{D}^*$ bound state is higher than the $\chi_{c2}(2P)$ with a mass of 3927.2 ± 2.6 MeV [45], and might be searched for in the same process as the $\chi_{c2}(2P)$, i.e. $\gamma\gamma \to D\bar{D}$. The data collected at both Belle and BaBar [31, 164] in that range do not have enough statistics for concluding the existence of such a state.

The most robust prediction would be the $B\bar{B}^*$ bound state with $I(J^{PC}) = 0(1^{++})$, to be called $X_b(10580)$, the analogue of the $X_c(3872)$ in the bottom sector. This state should be narrow since the decay into the $B\bar{B}$ is forbidden. It would decay dominantly into a bottomonium and light mesons. Moreover, the difference between the charged and neutral $B\bar{B}^*$ threshold is tiny, and negligible now when compared with the binding energy. Therefore, unlike the $X_c(3872)$, whose decays exhibit a large isospin breaking, the $X_b(10580)$ would decay into $\Upsilon(nS)\pi\pi\pi$ ($n = 1, 2$) rather than $\Upsilon(nS)\pi\pi$. It can also decay into $\chi_{bJ}(nP)$ and pions. It is worth emphasizing that the existence of such a state is a consequence of HFS and the assumption of the $X_c(3872)$ being a $D\bar{D}^*$ bound state. Searching for it would shed light on the nature of the $X_c(3872)$.

The Z_c and Z_c' appear as virtual states, not very far away from their respective thresholds. However, the uncertainties of the LO calculation are large, of the order of tens of MeV, as indicated by the difference between the results with different cutoff values. From this point of view, the new charged structure $Z_c(3900)$ observed by the BESIII Collaboration [161], confirmed by the Belle Collaboration [162] and an analysis using the CLEO data [165], is a natural candidate for the partner in the charm sector of the $Z_b(10610)$. Analogously, we expect the recent $Z_c(4025)$ [163] to be the partner of the $Z_b(10650)$.

Therefore, we are tempted to identify the $Z_c(3870)$ and $Z_c(4010)$ states reported in Table 5.2 with the observed $Z_c(3900)$ and $Z_c(4025)$. We observe that the actual Z_c and Z_c' physical states are not necessarily virtual: there are subleading order dynamics that can easily move the states above threshold. Most notably, at next-to-leading order, the EFT potential can develop a short range repulsive barrier. Thus, the LO uncertainty also encompasses the possibility that the states might be resonant. There are also corrections coming from coupled channel dynamics, but, in

Table 5.3: *Masses (MeV units) of the isoscalar heavy meson–heavy antimeson molecules when, in addition to the local potential, OPE contributions are taken into account. In all cases, the local potential is C_{0X}, for which we use -1.48 fm^2 and -0.29 fm^2 for $\Lambda = 0.5$ GeV and 1.0 GeV, respectively [25]. In parenthesis we collect the predictions given in Table 5.2 that did not include the OPE potential.*

$I(J^{PC})$	States	Thresholds	Masses ($\Lambda = 0.5$ GeV)		Masses ($\Lambda = 1$ GeV)	
$0(1^{++})$	$\frac{1}{\sqrt{2}}(B\bar{B}^* - B^*\bar{B})$	10604.4	10582	(10580^{+9}_{-8})	10546	(10539^{+25}_{-27})
$0(2^{++})$	$B^*\bar{B}^*$	10650.2	10627	(10626^{+8}_{-9})	10586	(10584^{+25}_{-27})
$0(2^{+})$	D^*B^*	7333.7	7323	(7322^{+6}_{-7})	7309	(7308^{+16}_{-20})

general, they are at least next-to-next-to-leading order and hence their impact is modest at best. For instance, the Z_c and Z_c' channels couple with each other and with the nearby $h_c(2P)\pi$ and $\psi(2S)\pi$ channels, though in the latter case we do not know the location of these charmonia. Their impact could be enhanced if they are close enough to the Z_c/Z_c' poles (yet they will continue to be subleading). All this indicates that the Z_c and Z_c' are promising candidates to explain the recently observed $Z_c(3900)$ and $Z_c(4025)$ resonances, though further theoretical effort is still required.

5.3 Estimation of the OPE effects in the isoscalar bottom and charm-bottom sectors

We discussed in Chapter 3 that in heavy meson-heavy antimeson interactions, pion exchanges are in general perturbative [10, 11], in contrast to nuclear physics where they are not [166], and produce small effects. The only exception could be the isoscalar bottom sector where the pions might be nonperturbative due to the large masses of bottom mesons [11, 13][3]. One may worry about the stability of the results in this sector against including the pion exchange effects.

For this purpose, we have computed the numerical effect of OPE in the results presented in Table 5.2 for the isoscalar sector. We have added the OPE potential defined in Eq. (2.3.34) to the contact interaction, thus we now have:

$$V = V_{contact} + V_{OPE}, \tag{5.3.1}$$

$$V_{OPE} = \frac{2g^2}{f_\pi^2} \frac{(\vec{a}\cdot\vec{q})\left(\vec{b}\cdot\vec{q}\right)}{\vec{q}^{\,2} + m_\pi^2}, \tag{5.3.2}$$

with $g \simeq 0.6$, $f_\pi = 92.2$ MeV and $\vec{a}$ and $\vec{b}$ the corresponding tensor operators (see Sect. 2.3.2). The OPE provides a momentum-dependent potential and the resolution of the LSE involves the momentum space discretization procedure outlined in Sect. 2.4.4. Poles of the T-matrix correspond to the isoscalar heavy meson-heavy antimeson bound states. The counter-term $C_{0X} = C_{0a} + C_{0b}$ was fixed in [25] with the inclusion of OPE effects. It was fitted to the mass of the $X(3872)$, neglecting isospin mixing effects, as also done here, and it was found $C_{0X} =$

[3]Because the isospin factor in the isovector case is only 1/3, in absolute value, of that in the isoscalar case, the pions are perturbative again in the isovector bottom sector.

-1.48 (-0.29) fm^2 for $\Lambda = 0.5$ (1.0) GeV. The results showed in Table 3.2 were obtained with these values of the counter-terms. In Table 5.3, we show the results obtained with these LECs for the two UV cutoffs, including the OPE potential, together with the predictions obtained without the inclusion of OPE effects (in parentheses). We see that the inclusion of OPE effects also leads to small modifications of the predicted masses of the molecules in the bottom and charm-bottom sector, and that they are still well accounted for the error provided by HQSFS breaking effects.

5.4 Conclusions

To summarize, in this work we have argued that in addition to HQSS, HFS can be used to predict new heavy meson molecules. We have also considered the uncertainties due to the finite mass of the heavy quarks. The predictions are important for understanding the newly observed hadrons in the heavy quarkonium mass region in the sense that, if the XYZ states are hadronic molecules, they will probably have heavy flavour partners that should be searched for. Note that HFS is a symmetry in the Lagrangian of the interaction (this is to say, the heavy meson potentials), and not a symmetry of the binding energies, since the kinetic term of the Lagrangian breaks the symmetry. Particularly, we studied in detail the new states that can be derived from the hypothesis that the $X(3872)$ and $Z_b(10610)$ are $D\bar{D}^*$ and $B\bar{B}^*$ hadronic molecules, respectively[4]. Searching for the isoscalar 1^{++} $B\bar{B}^*$ bound state in the $\Upsilon(1S,2S)\pi^+\pi^-\pi^0$ channel at hadron colliders or photon-photon collisions would provide valuable information on the structure of the $X(3872)$. In addition, we find promising isovector 1^{+-} $D\bar{D}^*$ and $D^*\bar{D}^*$ virtual states near threshold that could very well be identified with the newly discovered $Z_c(3900)$ [161] and $Z_c(4025)$ [163].

We have also estimated the OPE effects in the isoscalar bottom and charm-bottom sectors. This contribution was already found negligible in the charm sector. We find that the OPE potential produces also small deviations in these sectors, which allows us to keep the OPE interaction as a subleading effect in further analysis. In the isovector channel, these contributions are even smaller (a factor 3) owing to the isospin factor.

[4]We notice that approaches involving phenomenological (i.e. model-dependent) ingredients – but usually incorporating heavy quark symmetry – can lead to other conclusions: while the X_b is usually predicted, the Z_c is not [24, 46, 167].

Chapter 6

Heavy Antiquark-Diquark Symmetry and triply heavy exotic baryons

6.1 Introduction

Up to now, we have only studied meson molecular states (with integer spin). Baryonic states have a half-integer spin instead, and as a consequence, they are composed of three quarks, at least. This extra quark makes studying baryons a more difficult task. Numerous approaches to the study of baryons have been proposed. Conventional quark models describe baryons using three quark configurations. The scheme is successful and the properties of many of the low-lying baryon states can be addressed within these schemes. However, the description of some exotic states require the consideration of additional degrees of freedom, namely gluons, quark-antiquark pairs, etc.

In this chapter, we study molecular baryonic states that might appear as bound states of a doubly heavy baryon and a heavy-light meson. We relate these exotic baryonic states with the hidden charm (and bottom) meson molecular states studied in the previous chapters. This is done by using the Heavy Antiquark-Diquark Symmetry (HADS) introduced in Chapter 1.

HADS states that the two heavy quarks within a doubly heavy baryon behave approximately as a heavy antiquark. The heavy diquark component of the baryon forms a colour anti-triplet with a characteristic length scale of $1/(m_Q v)$, where m_Q is the mass of the heavy quarks and v their velocity. The length scale of the diquark is smaller than the typical QCD length scale $1/\Lambda_{\rm QCD}$ and hence we can treat the diquark as point-like if the quarks are heavy enough. The consequence is that the light-quark cloud surrounding the heavy diquark in a heavy baryon would be similar to the one around the heavy antiquark in a heavy antimeson. We expect violations of the order of $\Lambda_{\rm QCD}/(m_Q v)$, instead of $\Lambda_{\rm QCD}/m_Q$ as in HQSS and HFS cases. This translates into a $30-40\%$ uncertainty in the charm sector and $15-20\%$ in the bottom one. Yet even with this limitation, HADS can be useful in suggesting the possibility of new charmed molecules (see also Ref. [168] for a discussion of this symmetry in the charm sector), while for bottom ones concrete predictions can be made, as we will show in what follows.

We consider the interaction between doubly-heavy baryons $\Xi_{Q_1Q_2}$, $\Xi^*_{Q_1Q_2}$ ($Q_{1,2}=c,b$, total spin of the heavy pair $s_{Q_1Q_2}=1$ and $J^P=\frac{1}{2}^+$ and $\frac{3}{2}^+$, respectively) or the $J^P=\frac{1}{2}^+$ Ξ'_{bc} ($s_{bc}=0$), and a heavy meson $P^{(*)}$. HADS allows us to write the LO $\Xi^{(*)}_{Q_1Q_2}P^{(*)}$ potential in

Table 6.1: *LO potentials and quantum numbers for various doubly-heavy baryon–heavy meson systems.*

States	$\Xi_{Q_1Q_2}P$	$\Xi_{Q_1Q_2}P^*$	$\Xi_{Q_1Q_2}P^*$	$\Xi^*_{Q_1Q_2}P$	$\Xi^*_{Q_1Q_2}P^*$	$\Xi^*_{Q_1Q_2}P^*$	$\Xi^*_{Q_1Q_2}P^*$	$\Xi'_{bc}P$	$\Xi'_{bc}P^*$	$\Xi'_{bc}P^*$
J^P	$\frac{1}{2}^-$	$\frac{1}{2}^-$	$\frac{3}{2}^-$	$\frac{3}{2}^-$	$\frac{1}{2}^-$	$\frac{3}{2}^-$	$\frac{5}{2}^-$	$\frac{1}{2}^-$	$\frac{1}{2}^-$	$\frac{3}{2}^-$
$V^{\rm LO}$	C_{Ia}	$C_{Ia}+\frac{2}{3}C_{Ib}$	$C_{Ia}-\frac{1}{3}C_{Ib}$	C_{Ia}	$C_{Ia}-\frac{5}{3}C_{Ib}$	$C_{Ia}-\frac{2}{3}C_{Ib}$	$C_{Ia}+C_{Ib}$	C_{Ia}	$C_{Ia}-2C_{Ib}$	$C_{Ia}+C_{Ib}$

terms of the same counter-terms C_{Ia} and C_{Ib} that appear in the LO meson-antimeson potential.

6.2 Heavy-Light Meson-Doubly Heavy Baryon Interactions

According to HQSFS, the dynamics of a heavy hadron system depends neither on the spin nor on the flavour configuration of its heavy quark subsystem. Indeed, the dynamics turns out to be fully determined by the spin-flavour configuration of the light degrees of freedom.

Heavy-light meson $(Q\bar{l})$-heavy-light antimeson $(\bar{Q}'l')$ and heavy-light meson $(Q\bar{l})$-doubly heavy baryon $(Q'Q''l')$ systems contain both a light $\bar{l}l'$ quark-antiquark pair. The total spin $\mathcal{L}$ of the light subsystem can take two values, $\mathcal{L}=0,1$. Thus, at LO, with the Wigner Eckart theorem (see Eq. (2.3.25)), for each light flavour configuration, there exist two undetermined LECs, A_0 and A_1, which can be related to the C_A and C_B counter-terms that appear in the LO description of the local $P^{(*)}\bar{P}^{(*)}\to P^{(*)}\bar{P}^{(*)}$ interactions (see Lagrangian of Eq.(2.3.17)). Actually, as we discussed in Sect. 2.3, it turns out that $A_0=C_A-3C_B$ and $A_1=C_A+C_B$ (Eqs. (2.3.31) and (2.3.32)).

The idea is to express the doubly heavy baryon-heavy antimeson states in terms of the elements of a basis where the total spin of heavy subsystem ($\mathcal{S}$) and the total spin of the light quarks ($\mathcal{L}$) are well defined. This is the basis introduced in Sect. 2.3, and its elements are of the form $|\mathcal{S},\mathcal{L},J,\alpha,\alpha_H\rangle$, where $\alpha(\alpha_H)$ stands for other quantum numbers of the light (heavy) subsystem. The crucial observation is that the matrix element of the hamiltonian in this basis enormously simplifies and reads,

$$\langle \mathcal{S},\mathcal{L},J,\alpha,\alpha_H|\,H_{QCD}\,|\mathcal{S}',\mathcal{L}',J',\alpha',\alpha'_H\rangle=\delta_{\mathcal{S}\mathcal{S}'}\delta_{\mathcal{L}\mathcal{L}'}\delta_{\alpha\alpha'}\delta_{\alpha_H\alpha'_H}\delta_{JJ'}\,\langle H_{QCD}\rangle_{\mathcal{L},\alpha} \tag{6.2.1}$$

where the reduced matrix elements $\langle H_{QCD}\rangle_{\mathcal{L},\alpha}$ only depends on the light degrees of freedom, the light spin $\mathcal{L}$ and α (isospin, strangeness, etc.). Thus these reduced matrix elements are A_0^α and A_1^α; and hence they are given in terms of the LECs C_{0a},C_{0b},C_{1a} and C_{1b} introduced to describe the LO $P^{(*)}\bar{P}^{(*)}\to P^{(*)}\bar{P}^{(*)}$ local interactions.

The analysis of the light quark components in the heavy baryon-meson system leads to the potentials listed in Table 6.1, from which we can derive the spectrum of triply heavy exotic baryon molecules. Note that we have also made use of HFS which guaranties that the previous potentials do not depend, in the heavy quark limit, on the flavour of the heavy quarks contained in the system.

6.3 Heavy-Light meson - Doubly heavy baryon spectrum

To estimate the binding energies of the exotic baryon molecules we solve the LSE and look for poles as we have described in the previous chapters. The EFT potential produces singularities when it is iterated, and therefore the amplitudes need to be regularized and renormalized[1].

[1]We employ the usual approach in this thesis: a Gaussian regulator with the cutoffs $\Lambda=0.5\,\text{GeV}$ and $1\,\text{GeV}$. For the meson masses, we take isospin averaged values $M_D=1867.24$ MeV, $M_{D^*}=2008.63$ MeV, $M_B=$

The doubly charmed baryons were only reported by the SELEX Collaboration [169, 170, 171]. However, the measured masses are lower than expectations in most of the model and lattice calculations, and the observed isospin splittings seem too large to be accommodated in QCD [172]. Thus, we will use a recent lattice calculation for the masses, $M_{\Xi_{cc}} = 3606 \pm 22$ MeV and $M_{\Xi^*_{cc}} = 3706 \pm 28$ MeV [173]. For the doubly bottom baryons, there is no experimental observation yet, and the lattice QCD predictions are $M_{\Xi_{bb}} = 10127 \pm 13^{+12}_{-26}$ MeV and $M_{\Xi^*_{bb}} = 10151 \pm 14^{+16}_{-25}$ MeV [174]. Their central values will be used. Furthermore, we take constituent quark model predictions for the Ξ'_{bc} and Ξ^*_{bc} masses, 6958 and 6996 MeV, respectively [175][2]. Predictions will be made for the binding energies instead of masses to avoid introducing the lattice QCD errors of the baryon masses into the results. Finally, the HQSS/HFS uncertainty in the counter-terms is assumed to be 20%(7%) in the charm (bottom sector), while for HADS we use 40% (20%). They are assumed to be uncorrelated. We will also use a 30% HADS uncertainty for the Ξ'_{bc} systems.

We begin by considering the $X(3872)$ as a pure isoscalar 1^{++} $D\bar{D}^*$ molecule as in [25]. The LO potential is given by the counter-term combination $C_{0X} \equiv C_{0a} + C_{0b}$, which is identical to the one appearing in the family of $\Xi^*_{Q_1Q_2}P^*$ with $J = \frac{5}{2}^-$ and the $\Xi'_{bc}P^*$ systems with $J^P = \frac{3}{2}^-$. We have $C_{0X} = -1.94\,(-0.79)\,\text{fm}^2$ for $\Lambda = 0.5\,(1.0)\,\text{GeV}$ [25]. Bound state solutions are found in all the considered systems, though the $\Xi^*_{cc}D^*$ system can be very loosely bound due to the large uncertainty of the LO potential, and the predictions can be found in Table 6.2. In addition, it is more than probable that the isoscalar $\Xi^{(*\prime)}_{bc}B^*$ and $\Xi^*_{bb}\bar{B}^*$ molecules require non-perturbative OPE owing to their heavy reduced mass. Though the non-perturbative OPE will modify the binding energies, we expect that these systems will remain bound. In principle, the predicted isoscalar hadronic molecules could mix with the normal triply-heavy (QQQ) baryons. Because of the different parity, mixing with the triply heavy baryon ground states are forbidden. Moreover, the lowest lying states are typically around 1 GeV below the molecular states presented here. See for instance Table I of Ref. [176], where predicted triply heavy baryon ground state masses from several schemes (lattice-QCD, QCD-sum rules, bag model, relativistic and non-relativistic constituent three quark models, perturbative-non-relativistic QCD, Regge, ...) are compiled. Thus, only an eventual mixing between highly excited triply heavy baryon states and the molecular states studied here might play a certain role. However, a quantitative calculation of such a mixing effect requires models for both, the high excited part of the normal triply baryon spectrum, and the creation and annihilation of a light quark antiquark pair. This is beyond the scope of this preliminary work and will not be discussed herein.

Now we continue with what can be deduced from the $Z_b^{(\prime)}$ as isovector 1^{+-} $B^{(*)}\bar{B}^*$ molecular states. As can be seen from Table 6.1, there is no exact match among the LO potential for the Z_b's, $C_{1Z} \equiv C_{1a} - C_{1b}$, and the six possible $\Xi^{(*)}_{Q_1Q_2}P^{(*)}$ configurations. Yet, the $\frac{3}{2}^-$ $\Xi^*_{Q_1Q_2}P^*$ configuration has coupling: $C_{1a} - \frac{2}{3}C_{1b} = C_{1Z} + \frac{1}{3}C_{1b}$. As far as the relative contribution of the C_{1b} coupling is not excessive, a hadronic molecule, either as a bound or virtual state, looks probable. Other two interesting configurations are the $\frac{1}{2}^-$ $\Xi^*_{Q_1Q_2}P^*$ and $\frac{3}{2}^-$ $\Xi_{Q_1Q_2}P^*$ systems, for which the couplings read $C_{1Z} \mp \frac{2}{3}C_{1b}$. Depending on the sign and size of C_{1b} at least one of the two configurations should bind.

5279.34 MeV, $M_{B^*} = 5325.1$ MeV and $M_X = 3871.68\,\text{MeV}$ [45]. We assume that the binding energy of the Z_b is $2.0 \pm 2.0\,\text{MeV}$, as in Chapter 5.

[2] In fact, the precise values of the input doubly-heavy baryon masses are not important. This can be seen from a comparison of the binding energies of the $\Xi^*_{cc}D^*$ and $\Xi^*_{bb}D^*$. The interaction is the same in these two channels, and the only difference arises from the masses of the baryons. As one can see from the first and third rows in Table 6.2, the difference in the binding energies is only a few MeV for $\Lambda = 0.5$ GeV, and slightly more for $\Lambda = 1$ GeV.

Table 6.2: *Predictions of the doubly-heavy baryon–heavy meson molecules. The isoscalar states are related to the $X(3872)$, and the error in their binding energies is a consequence of the approximate nature of HADS. The isovector states are determined by the $Z_b(10610, 10650)$ and the isovector component of the X. In this part, different error sources have been taken into account: the uncertainty in the Z_b binding, in the isospin breaking decays of the X and in the HADS breaking. For simplicity, we only show a unique error obtained by adding in quadratures all the previous ones. Here, $M_{\rm th}$ represents the threshold, and all masses are given in units of MeV. When we decrease the strength of the potential to account for the various uncertainties, in some cases (marked with † in the table) the bound state pole reaches the threshold and the state becomes virtual. The cases with a virtual state pole at the central value are marked by [V], for which †† means that the pole evolves into a bound state one and N/A means that the pole is far from the threshold with a momentum larger than 1 GeV so that it is both undetectable and beyond the EFT range.*

State	$I(J^P)$	$V^{\rm LO}$	Thresholds	Mass ($\Lambda = 0.5$ GeV)	Mass ($\Lambda = 1$ GeV)
$\Xi^*_{cc}D^*$	$0(\frac{5}{2}^-)$	$C_{0a} + C_{0b}$	5715	$(M_{\rm th} - 10)^{+10}_{-15}$	$(M_{\rm th} - 19)^{\dagger}_{-44}$
$\Xi^*_{cc}\bar{B}^*$	$0(\frac{5}{2}^-)$	$C_{0a} + C_{0b}$	9031	$(M_{\rm th} - 21)^{+16}_{-19}$	$(M_{\rm th} - 53)^{+45}_{-59}$
$\Xi^*_{bb}D^*$	$0(\frac{5}{2}^-)$	$C_{0a} + C_{0b}$	12160	$(M_{\rm th} - 15)^{+9}_{-11}$	$(M_{\rm th} - 35)^{+25}_{-31}$
$\Xi^*_{bb}\bar{B}^*$	$0(\frac{5}{2}^-)$	$C_{0a} + C_{0b}$	15476	$(M_{\rm th} - 29)^{+12}_{-13}$	$(M_{\rm th} - 83)^{+38}_{-40}$
$\Xi'_{bc}D^*$	$0(\frac{3}{2}^-)$	$C_{0a} + C_{0b}$	8967	$(M_{\rm th} - 14)^{+11}_{-13}$	$(M_{\rm th} - 30)^{+27}_{-40}$
$\Xi'_{bc}\bar{B}^*$	$0(\frac{3}{2}^-)$	$C_{0a} + C_{0b}$	12283	$(M_{\rm th} - 27)^{+15}_{-16}$	$(M_{\rm th} - 74)^{+45}_{-51}$
$\Xi^*_{bc}D^*$	$0(\frac{5}{2}^-)$	$C_{0a} + C_{0b}$	9005	$(M_{\rm th} - 14)^{+11}_{-13}$	$(M_{\rm th} - 30)^{+27}_{-40}$
$\Xi^*_{bc}\bar{B}^*$	$0(\frac{5}{2}^-)$	$C_{0a} + C_{0b}$	12321	$(M_{\rm th} - 27)^{+15}_{-16}$	$(M_{\rm th} - 74)^{+46}_{-51}$
$\Xi_{bb}\bar{B}$	$1(\frac{1}{2}^-)$	C_{1a}	15406	$(M_{\rm th} - 0.3)^{\dagger}_{-2.5}$	$(M_{\rm th} - 12)^{+11}_{-15}$
$\Xi_{bb}\bar{B}^*$	$1(\frac{1}{2}^-)$	$C_{1a} + \frac{2}{3}\,C_{1b}$	15452	$(M_{\rm th} - 0.9)[{\rm V}]^{\rm N/A}_{\dagger\dagger}$	$(M_{\rm th} - 16)^{+14}_{-17}$
$\Xi_{bb}\bar{B}^*$	$1(\frac{3}{2}^-)$	$C_{1a} - \frac{1}{3}\,C_{1b}$	15452	$(M_{\rm th} - 1.2)^{\dagger}_{-2.9}$	$(M_{\rm th} - 10)^{+9}_{-13}$
$\Xi^*_{bb}\bar{B}$	$1(\frac{3}{2}^-)$	C_{1a}	15430	$(M_{\rm th} - 0.3)^{\dagger}_{-2.4}$	$(M_{\rm th} - 12)^{+11}_{-13}$
$\Xi^*_{bb}\bar{B}^*$	$1(\frac{1}{2}^-)$	$C_{1a} - \frac{5}{3}\,C_{1b}$	15476	$(M_{\rm th} - 8)^{+8}_{-7}$	$(M_{\rm th} - 5)^{\dagger}_{-8}$
$\Xi^*_{bb}\bar{B}^*$	$1(\frac{3}{2}^-)$	$C_{1a} - \frac{2}{3}\,C_{1b}$	15476	$(M_{\rm th} - 2.5)^{\dagger}_{-3.6}$	$(M_{\rm th} - 9)^{+9}_{-11}$
$\Xi^*_{bb}\bar{B}^*$	$1(\frac{5}{2}^-)$	$C_{1a} + C_{1b}$	15476	$(M_{\rm th} - 4.3)[{\rm V}]^{\rm N/A}_{+3.3}$	$(M_{\rm th} - 18)^{+17}_{-19}$

All this indicates that the isospin-1 doubly-heavy baryon–meson molecules are probable, but a further assessment requires the determination of both C_{1a} and C_{1b}. From the Z_b's, we obtain (see Chapter 5) $C_{1Z} = C_{1a} - C_{1b} = -\left(0.75^{+0.15}_{-0.28}\right)$ $[-\left(0.30^{+0.03}_{-0.07}\right)]\,{\rm fm}^2$ for $\Lambda = 0.5\,{\rm GeV}$ $[1.0\,{\rm GeV}]$, where the errors come from the uncertainties in the binding energy. But for disentangling the C_{1a} and C_{1b} couplings a second source of information is necessary. For that we will use the isospin symmetry breaking of the $X(3872)$, which offers a window into the interaction in the isovector 1^{++} $D\bar{D}^*$ channel, see the discussion in Chapter 3. The decay of the $X(3872)$ into the isovector $J/\psi 2\pi$ channel indicates that the X is not a pure isoscalar state, but contains a small isovector component. The branching ratio of the isovector $J/\psi 2\pi$ to the isoscalar $J/\psi 3\pi$ decays constrains the size of this component and hence the strength of the interaction in the isovector

channel. Following Chapter 3, the ratio of the decay amplitudes

$$R_X = \frac{\mathcal{M}(X \to J/\Psi\rho)}{\mathcal{M}(X \to J/\Psi\omega)}, \tag{6.3.1}$$

is related to C_{0X} and C_{1X} and using the value $R_X = 0.26^{+0.08}_{-0.05}$ extracted in Ref. [101] as input, we find $C_{1X} = -(0.13 \pm 0.40)\,[-(0.39 \pm 0.09)]\,\mathrm{fm}^2$ for $\Lambda = 0.5\,\mathrm{GeV}\,[1\,\mathrm{GeV}]$, where the errors reflect the experimental uncertainty in the branching ratio.[3] Using the formulas $C_{1a} = (C_{1X} + C_{1Z})/2$ and $C_{1b} = (C_{1X} - C_{1Z})/2$, we obtain $C_{1a} = -(0.44 \pm 0.24)\,[-(0.35 \pm 0.06)]\,\mathrm{fm}^2$ and $C_{1b} = (0.31 \pm 0.24)\,[-(0.05 \pm 0.06)]\,\mathrm{fm}^2$ (the errors shown are for guidance only and have been obtained by adding in quadratures those quoted for C_{1X} and C_{1Z}). We see that C_{1b} is either positive or, if negative, extremely small and that $|C_{1b}| < |C_{1a}|$, which already contains a lot of information about the possible molecular states. We show the predictions in Table 6.2, where the uncertainties in the binding energies come from the errors in C_{1X} and C_{1Z}, the additional HQSS/HFS 20% error (as part of the information comes from the charm sector) and from the expected 20% violation of HADS. Notice that coupled channels exist for most of the predicted isovector states. For instance, all the three states with quantum numbers $I(J^P) = 1(\frac{1}{2}^-)$ can couple to each other. Yet, the coupled-channel effects were studied in the case of interaction between a heavy meson and an antiheavy meson in Ref. [25]. It turns out that the results without coupled channels are only slightly modified by the coupled-channel effects. Since the systems are quite similar here, we can conclude that the coupled-channels effects will neither remove the existence of hadronic molecules, nor significantly change the predicted masses, and will be neglected in this work[4].

In the isovector sector, all configurations are plausible molecular candidates. However, when we take into account the various uncertainties of the current approach, we cannot discard in all cases the appearance of virtual states instead of proper bound molecules. The most promising predictions are the $\frac{1}{2}^-$ and $\frac{3}{2}^-$ $\Xi^*_{bb}\bar{B}^*$ molecules, for which binding is moderately robust against the different error sources.

To confirm these states from the theoretical side we need to pinpoint the value of C_{1b} more accurately. This could be done either by more accurate measurements of the X isospin breaking ratio or, better yet, by the eventual discovery of HQSS partners of the Z_b's, the W_b states proposed in Ref. [23]. Notice that all the isospin-1 triply-heavy molecules are very interesting in the sense that they have a non-trivial pentaquark component. We point out that though heavy pentaquarks have been predicted in the literature on the basis of several arguments [177, 178, 179], this is the first prediction of a triply heavy one.

6.4 Conclusions

To summarize this chapter, we have studied the implications of HADS (plus HQSS and HFS) for heavy hadronic molecules. As a consequence of this symmetry, we can be confident about the existence of doubly-heavy baryon–heavy meson (and eventually doubly-heavy baryon–antibaryon: $\Xi^{(*)}_{Q_1Q_2}$–$\Xi^{(*)}_{\bar{Q}_1\bar{Q}_2}$) partners of heavy meson–antimeson molecules. From the assumption that the $X(3872)$ and the $Z_b(10610/10650)$ are molecular states we can predict the existence of the exotic pentaquark-like partners of these states. We notice that phase space forbids any of the predicted molecules to decay through the strong decays of their components. One of the possible strong decay channels is a triply-heavy baryon plus one or more pions. Such a decay involves exchanging

[3] The central value of C_{1X} differs from that quoted in Chapter 3 by an amount that is around 10% of its error. This is because of the use of different values for the X resonance mass.

[4] Coupled channel effects are for instance also neglected in the context of the $Z(10610)$ and $Z(10650)$ molecular states in Ref. [23].

a heavy quark and a light quark so that it would have a small partial width. The $\Xi_{Q_1Q_2}P$ in a D wave could be the dominant decay channel of the $\Xi^*_{Q_1Q_2}P^*$ states with $J^P = \frac{3}{2}^-$ and $\frac{5}{2}^-$. However, if the binding energy is so small that the binding momentum is much smaller than the pion mass, the predicted state should be quite stable. It would be intriguing if any of the predicted states can be found in high-energy hadron colliders and heavy ion collisions.

Chapter 7

Correlation Functions for heavy-light meson-heavy-light antimeson systems

7.1 Introduction

In this chapter we study the $X(3872)$ and its partners in the heavy quark limit from a completely different point of view: QCD correlation functions. As Feynman once said, *"every theoretical physicist who is any good knows six or seven different theoretical representations for exactly the same physics."*! Thus, we propose interpolating currents for the $X(3872)$ state and show that, in the heavy quark limit of QCD, the $X(3872)$ state should have degenerate partners, independent of its internal structure. We will also discuss magnitudes of possible $I = 0$ and $I = 1$ components of the $X(3872)$.

Correlation functions are fundamental objects in quantum field theory studies of hadron physics. They are constructed out of the time-ordered product of hadronic interpolating currents and can be written in terms of hadronic properties. These Green functions are the main object of interest in many non-perturbative methods such as QCD sum rules or Lattice QCD.

The Shifman-Vainshtein-Zakharov (SVZ) sum rules [180] relate hadronic parameters, such as meson masses and coupling constants, baryon magnetic moments, etc., to few characteristics of quantum chromodynamics (QCD): gluon and quark condensates, etc. The method is based on Wilson's operator product expansion which was adapted by the authors to QCD in the mid-1970s. Quark confinement is assumed rather than proved. The SVZ method was applied, with remarkable success, for (approximate) calculations of a large variety of properties of all low-lying hadronic states. In the 1980s the SVZ method was developed in various directions shifting the emphasis from calculation of masses and coupling constants of "classic" resonances to such problems as magnetic moments, form factors at intermediate momentum transfers, weak decays, structure functions of deep inelastic scattering at intermediate values of the Bjorken variable x , heavy quarkonium systems, and many others.

The basic idea lying behind the SVZ method [180] is as follows. In the states comprising the low-lying part of the hadronic spectrum, both mesonic (e.g. ρ) and baryonic (e.g. p or n), quarks are not asymptotically far from each other, on average. Under these circumstances, the string-like long chromoelectric flux tubes have no chance to be developed. The valence quarks injected in the vacuum by means of the current, in a sense, perturb it only slightly. Then one does not need the full QCD string theory to approximately obtain the properties of the hadronic

states. Their basic features depend on how the valence quarks, of which they are built, interact with typical vacuum field fluctuations.

It was suggested (and then established) that the QCD vacuum is sufficiently characterized by a number of condensates [180]: the gluon condensate $\langle G^2_{\mu\nu}\rangle$, the quark condensate $\langle\bar{q}q\rangle$, the mixed condensate $\langle\bar{q}\sigma Gq\rangle$, the four-quark condensate, and few others.

The theoretical basis of any calculation within the SVZ method is the Wilson's Operator Product Expansion (WOPE) for correlation functions of two or more currents. WOPE allows one to consistently separate the large and short distance contributions. The former are then represented by the vacuum condensates while the latter are accounted for in the coefficient functions. In constructing WOPE one must introduce a somewhat artificial boundary, μ , usually referred to as normalization point. All fluctuations with frequencies higher than μ are supposed to be hard and are included in the coefficient functions. Those with frequencies lower than μ are soft. Only soft modes are to be retained in the condensates. Thus, the separation principle of WOPE is "soft versus hard." Both, the WOPE coefficients and condensates are explicitly μ dependent. However, all physical quantities are μ independent; the normalization point dependence of the condensates is compensated by that of the coefficient functions.

The SVZ method uses numerical values of the condensates and then determine, with sufficient accuracy, parameters of a large number of mesons and baryons. Without invoking the entire infinite set of condensates one can capture only gross features of the hadron systems. Correspondingly, any calculation of the hadronic parameters based on the SVZ method is approximate in nature. The usefulness of the method lies in its analytic capabilities: analytic analyses become possible in a wide range of problems from hadronic physics

Several models have been proposed to study the properties of $X(3872)$ using the heavy quark effective field theory approach (see [25, 181] and Chapter 3). One of the results obtained in Chapter 3, using heavy quark spin symmetry, states that if $X(3872)$ is a bound state of a D and a $\bar{D}^*$, then it should have degenerate partners in the heavy quark limit. In this chapter, the question of partners of the $X(3872)$ meson will be addressed directly using QCD in the heavy quark limit. In Sect. 7.2, an interpolating current for the $X(3872)$ is proposed, and its correlator is studied to prove that there should be three other degenerate partners of the $X(3872)$. Sect. 7.3 is devoted to the study of isospin mixing in the $X(3872)$ mesons, and finally in Sect. 7.4, our results are summarized.

7.2 $X(3872)$ Partners

As mentioned above, the fundamental object to study the properties of hadrons in a field theory framework is a correlation function of the form

$$\Pi = i\int d^4x\; e^{ipx}\langle 0|\mathcal{T}j(x)j^\dagger(0)|0\rangle, \tag{7.2.1}$$

where $j(x)$ is a suitably chosen interpolating current that can create the hadron of interest from the vacuum, p is the momentum of the state created by $j(x)$, and $\mathcal{T}$ is the time ordering operator.

In the molecular representation of $X(3872)$ as a bound state of D and D^*, the $J^{PC} = 1^{++}$ combination can be written as

$$|X(3872)\rangle = \frac{1}{\sqrt{2}}\left(|D\bar{D}^*\rangle - |\bar{D}D^*\rangle\right), \tag{7.2.2}$$

In the heavy quark spin symmetry basis introduced in Subsect. 2.3.1, one can express this state as

$$|X(3872)\rangle = |(S_{c\bar{c}} = 1; S_{q\bar{q}} = 1)J = 1\rangle, \tag{7.2.3}$$

i.e., the c and $\bar{c}$ quarks and q and $\bar{q}$ quarks, each combine in a spin-1 state, and the two pairs combine to give a state with overall $J = 1$. Motivated by the latter picture, one can choose a current of the form

$$j^q_{\alpha\beta} = \bar{Q}^a \gamma_\alpha Q^b \bar{q}^b \gamma_\beta q^a, \tag{7.2.4}$$

where Q is a heavy quark (c in the case of $X(3872)$), q is any quark different from Q, a and b are colour indices written in a way to assure colourless D and D^* states. Note that one can rewrite the colour factors of the $q\bar{q}$ and $Q\bar{Q}$ as

$$\bar{Q}^a \gamma_\alpha Q^b = \left(\bar{Q}^a \gamma_\alpha Q^b - \frac{\delta^{ab}}{3} \bar{Q}^c \gamma_\alpha Q^c \right) + \frac{\delta^{ab}}{3} \bar{Q}^c \gamma_\alpha Q^c, \tag{7.2.5}$$

and a similar expansion for the other quark-antiquark current. Here the first term is a colour octet combination and the last term is a colour singlet. In this form it can be seen that this current also has a non-trivial coupling to the $J/\Psi\omega$ and/or $J/\Psi\rho$ component of the $X(3872)$ state [145].

In the following discussion, we will drop the superscript q until Sect. 7.3. The current in Eq. (7.2.4) has $C = +1$. (An alternative current with $C = +1$ is $j_{\alpha\beta} = \bar{Q}^a \sigma_{\alpha\delta} Q^b \bar{q}^b \sigma^\delta{}_\beta q^a$. This current yields the same final results.) The product of two vector currents can be written as a sum of irreducible representations of the Lorentz group upon using the projection operators:

$$\mathcal{P}^2_{\mu\nu;\bar{\mu}\bar{\nu}} = \frac{1}{2} \left(g_{\mu\bar{\mu}} g_{\nu\bar{\nu}} + g_{\mu\bar{\nu}} g_{\nu\bar{\mu}} - \frac{1}{2} g_{\mu\nu} g_{\bar{\mu}\bar{\nu}} \right), \tag{7.2.6}$$

$$\mathcal{P}^1_{\mu\nu;\bar{\mu}\bar{\nu}} = \frac{1}{2} \left(g_{\mu\bar{\mu}} g_{\nu\bar{\nu}} - g_{\mu\bar{\nu}} g_{\nu\bar{\mu}} \right), \tag{7.2.7}$$

$$\mathcal{P}^0_{\bar{\mu}\bar{\nu}} = g_{\bar{\mu}\bar{\nu}}, \tag{7.2.8}$$

as

$$j^2_{\mu\nu} = \mathcal{P}^2_{\mu\nu;\bar{\mu}\bar{\nu}} j^{\bar{\mu}\bar{\nu}}, \tag{7.2.9}$$

$$j^1_{\mu\nu} = \mathcal{P}^1_{\mu\nu;\bar{\mu}\bar{\nu}} j^{\bar{\mu}\bar{\nu}}, \tag{7.2.10}$$

$$j^0 = \mathcal{P}^0_{\bar{\mu}\bar{\nu}} j^{\bar{\mu}\bar{\nu}}, \tag{7.2.11}$$

where the superscript denotes the largest spin that a particle that couples to the corresponding current can have.

Let us first consider the correlation function constructed from the current given in Eq. (7.2.4):

$$\begin{aligned} \Pi_{\alpha\beta;\gamma\delta} &= i \int d^4x e^{ipx} \langle 0 | \mathcal{T} j_{\alpha\beta}(x) j^\dagger_{\gamma\delta}(0) | 0 \rangle \\ &= i \int d^4x e^{ipx} \langle 0 | \mathcal{T} \bar{Q}^a(x) \gamma_\alpha Q^b(x) \bar{q}^b(x) \gamma_\beta q^a(x) \\ &\qquad \bar{Q}^d(0) \gamma_\gamma Q^e(0) \bar{q}^e(0) \gamma_\delta q^d(0) | 0 \rangle. \end{aligned} \tag{7.2.12}$$

In the heavy quark limit, the momentum of the state created by the current can be written as $p = 2m_Q v + k$, where v is the common velocity of the heavy quarks and k is the residual momentum of the system. The field corresponding to the quark Q can be decomposed as:

$$Q(x) = e^{-im_Q x} h^{(+)}_Q(x) + e^{im_Q x} h^{(-)}_{\bar{Q}}(x), \tag{7.2.13}$$

where $h_Q^{(+)}(x)(h_{\bar{Q}}^{(-)}(x))$ contains the positive (negative) frequency components, i.e. $h_Q^{(+)}(x)$ contains the annihilation operators for the quark and $h_{\bar{Q}}^{(-)}(x)$ contains the creation operators for the antiquark. Substituting Eq. (7.2.13) into Eq. (7.2.12), and taking the heavy quark limit, the correlation function becomes:

$$\Pi_{\alpha\beta;\gamma\delta} = i\int d^4x e^{ikx}\langle 0|\mathcal{T}\overline{h_{\bar{Q}}^{(-)a}}(x)\gamma_\alpha h_Q^{(+)b}(x)\bar{q}^b(x)\gamma_\beta q^a(x) \overline{h_Q^{(+)d}}(0)\gamma_\gamma h_{\bar{Q}}^{(-)e}(0)\bar{q}^e(0)\gamma_\delta q^d(0)|0\rangle, \tag{7.2.14}$$

Note that in obtaining Eq. (7.2.14), terms that contain and exponential factor with infinite oscillation frequency (m_Q) are neglected.

In the heavy quark limit, the spin of the heavy quark decouples from the theory. Hence all the gamma matrices multiplying the heavy quarks can be factored out of the correlation function:

$$\begin{aligned}\Pi_{\alpha\beta;\gamma\delta} &= \mathrm{Tr}\left[\gamma_\alpha\frac{1+\not{v}}{2}\gamma_\gamma\frac{1-\not{v}}{2}\right](\mathcal{R}_1 g_{\beta\delta}+\mathcal{R}_2 v_\beta v_\delta)\\ &= 2\left(g_{\alpha\gamma}-v_\alpha v_\gamma\right)(\mathcal{R}_1 g_{\beta\delta}+\mathcal{R}_2 v_\beta v_\delta),\end{aligned} \tag{7.2.15}$$

where the most general decomposition of the remaining part of the correlation function is written in terms of Lorentz invariant functions $\mathcal{R}_1$ and $\mathcal{R}_2$. Applying the projection operators Eqs. (7.2.6-7.2.8), the correlation functions for the currents given in Eqs. (7.2.9-7.2.10) can be obtained as (we will not need the correlation function for the current given in Eq. (7.2.11)):

$$\begin{aligned}\Pi^2_{\mu\nu;\bar{\mu}\bar{\nu}} &= 2\mathcal{P}_{2\mu\nu;\bar{\mu}\bar{\nu}}\mathcal{R}_1 - \frac{1}{8}\mathcal{R}_1\left(g_{\mu\nu}-4v_\mu v_\nu\right)\left(g_{\bar{\mu}\bar{\nu}}-4v_{\bar{\mu}}v_{\bar{\nu}}\right)\\ &\quad+\frac{1}{2}(\mathcal{R}_2-\mathcal{R}_1)\left[v_\nu v_{\bar{\nu}}\left(g_{\mu\bar{\mu}}-v_\mu v_{\bar{\mu}}\right)+v_{\bar{\mu}}v_\nu\left(g_{\mu\bar{\nu}}-v_\mu v_{\bar{\nu}}\right)\right.\\ &\quad\left.+v_\mu v_{\bar{\nu}}\left(g_{\bar{\mu}\nu}-v_{\bar{\mu}}v_\nu\right)+v_\mu v_{\bar{\mu}}\left(g_{\nu\bar{\nu}}-v_\nu v_{\bar{\nu}}\right)\right],\end{aligned} \tag{7.2.16}$$

$$\begin{aligned}\Pi^1_{\mu\nu;\bar{\mu}\bar{\nu}} &= \mathcal{R}_1\left(g_{\mu\bar{\mu}}g_{\nu\bar{\nu}}-g_{\mu\bar{\nu}}g_{\nu\bar{\mu}}\right)\\ &\quad-\frac{1}{2}(\mathcal{R}_1-\mathcal{R}_2)\left(v_\nu v_{\bar{\nu}}g_{\mu\bar{\mu}}-v_{\bar{\mu}}v_\nu g_{\mu\bar{\nu}}-v_\mu v_{\bar{\nu}}g_{\nu\bar{\mu}}+v_\mu v_{\bar{\mu}}g_{\nu\bar{\nu}}\right),\end{aligned} \tag{7.2.17}$$

To calculate the expression for the correlation function in terms of the hadronic states, note the $j^1_{\mu\nu}$ current, being anti-symmetric under its indices, couples only to $J^P=1^+$ and $J^P=1^-$ states, whereas the $j^2_{\mu\nu}$ current couples to states with $J^P=2^+$, $J^P=0^+$ and $J^P=1^-$ spin-parity.

The matrix element of the $j^1_{\mu\nu}$ current between the $J^P=1^+$ and $J^P=1^-$ particles and the vacuum can be written as

$$\begin{aligned}\langle 0|j^1_{\mu\nu}|1^-\rangle &= A\left(v_\mu\epsilon_\nu-v_\nu\epsilon_\mu\right),\\ \langle 0|j^1_{\mu\nu}|1^+\rangle &= A'\epsilon_{\mu\nu\alpha\beta}v_\alpha\epsilon'_\beta,\end{aligned} \tag{7.2.18}$$

where $A(A')$ and $\epsilon^{(\prime)}$ are the coupling strength and the polarization vector of the (axial) vector particle. Summing over the polarizations of the (axial) vector using

$$\sum_{polarization}\epsilon_\mu\epsilon^*_\nu = -\left(g_{\mu\nu}-v_\mu v_\nu\right), \tag{7.2.19}$$

it is seen that the correlation function reads,

$$\begin{aligned}\Pi^1_{\mu\nu;\bar{\mu}\bar{\nu}} &= -\frac{A^2}{kv-\Lambda_{1^+}}\left[(v_\mu v_{\bar{\mu}} g_{\nu\bar{\nu}} - v_\mu v_{\bar{\nu}} g_{\nu\bar{\mu}} - v_\nu v_{\bar{\mu}} g_{\mu\bar{\nu}} + v_\nu v_{\bar{\nu}} g_{\mu\bar{\mu}})\right] + \\ &+ \frac{A'^2}{kv-\Lambda_{1^-}}\cdot \\ &\cdot\left[(g_{\mu\bar{\mu}} g_{\nu\bar{\nu}} - g_{\mu\bar{\nu}} g_{\nu\bar{\mu}}) - (v_\nu v_{\bar{\nu}} g_{\mu\bar{\mu}} - v_{\bar{\mu}} v_\nu g_{\mu\bar{\nu}} - v_\mu v_{\bar{\nu}} g_{\nu\bar{\mu}} + v_\mu v_{\bar{\mu}} g_{\nu\bar{\nu}})\right],\end{aligned} \tag{7.2.20}$$

$$\Rightarrow \Pi^1_{\mu\nu;\bar{\mu}\bar{\nu}} = \frac{A'^2}{kv-\Lambda_{1^+}}\left(g_{\mu\bar{\mu}} g_{\nu\bar{\nu}} - g_{\mu\bar{\nu}} g_{\nu\bar{\mu}}\right) - \tag{7.2.21}$$

$$-\left(\frac{A^2}{kv-\Lambda_{1^-}} + \frac{A'^2}{kv-\Lambda_{1^+}}\right)\left(v_\nu v_{\bar{\nu}} g_{\mu\bar{\mu}} - v_{\bar{\mu}} v_\nu g_{\mu\bar{\nu}} - v_\mu v_{\bar{\nu}} g_{\nu\bar{\mu}} + v_\mu v_{\bar{\mu}} g_{\nu\bar{\nu}}\right),$$

where a sum over all particles with $J^P = 1^+$ and $J_P = 1^-$ should be understood. Comparing with Eq. (7.2.17), the $\mathcal{R}_1$ and $\mathcal{R}_2$ functions can be identified as:

$$\begin{aligned}\mathcal{R}_1 &= \frac{A'^2}{kv-\Lambda_{1^+}}, \\ \mathcal{R}_1 - \mathcal{R}_2 &= 2\frac{A^2}{kv-\Lambda_{1^-}} + 2\frac{A'^2}{kv-\Lambda_{1^+}}.\end{aligned} \tag{7.2.22}$$

One can find an expression for the functions $\mathcal{R}_1$ and $\mathcal{R}_2$ using the current $j^2_{\mu\nu}$ and its correlator given in Eq. (7.2.16). The coupling of the $J^P = 2^+$, $J^P = 0^+$ and $J^P = 1^-$ states to the $j^2_{\mu\nu}$ currents can be written as

$$\begin{aligned}\langle 0|j^2_{\mu\nu}|2^+\rangle &= D\epsilon_{\mu\nu}, \\ \langle 0|j^2_{\mu\nu}|0^+\rangle &= C\left(g_{\mu\nu} - 4v_\mu v_\nu\right), \\ \langle 0|J^2_{\mu\nu}|1^-\rangle &= F\left(\epsilon_\mu v_\nu + \epsilon_\nu v_\mu - \frac{1}{2}g_{\mu\nu}\epsilon\cdot v\right),\end{aligned} \tag{7.2.23}$$

where ϵ_μ and $\epsilon_{\mu\nu}$ are the polarizations of the vector and tensor particles respectively, satisfying $v^\mu\epsilon_\mu = 0$, $\epsilon_\mu\epsilon^{\mu*} = -1$, $v^\mu\epsilon_{\mu\nu} = 0$, $\epsilon_{\mu\nu} = \epsilon_{\nu\mu}$, $\epsilon_{\mu\nu}g^{\mu\nu} = 0$, $\epsilon_{\mu\nu}\epsilon^{\mu\nu*} = 1$.

Inserting a complete set of these states into the correlation function and summing over the polarizations upon using Eq. (7.2.19) for vector particles and

$$\begin{aligned}\sum_{polarization}\epsilon_{\mu\nu}\epsilon^*_{\alpha\beta} &= \frac{1}{2}\Big[\left(g_{\mu\alpha} - v_\mu v_\alpha\right)\left(g_{\nu\beta} - v_\nu v_\beta\right) + \\ &+ \left(g_{\nu\alpha} - v_\nu v_\alpha\right)\left(g_{\mu\beta} - v_\mu v_\beta\right) - \frac{2}{3}\left(g_{\mu\nu} - v_\mu v_\nu\right)\left(g_{\alpha\beta} - v_\alpha v_\beta\right)\Big],\end{aligned} \tag{7.2.24}$$

for tensor particles, the correlation function Eq. (7.2.16) can be written as

$$\begin{aligned}\Pi^2_{\mu\nu;\bar{\mu}\bar{\nu}} &= \frac{D^2}{kv-\Lambda_{2^+}}\mathcal{P}^2_{\mu\nu;\bar{\mu}\bar{\nu}} + \\ &+\left(\frac{C^2}{kv-\Lambda_{0^+}} - \frac{D^2}{12(kv-\Lambda_{2^+})}\right)\left(g_{\mu\nu} - 4v_\mu v_\nu\right)\left(g_{\bar{\mu}\bar{\nu}} - 4v_{\bar{\mu}}v_{\bar{\nu}}\right) - \\ &-\left(\frac{D^2/2}{kv-\Lambda_{2^+}} + \frac{F^2}{kv-\Lambda_{1^-}}\right)\left[v_\nu v_{\bar{\nu}}\left(g_{\mu\bar{\mu}} - v_\mu v_{\bar{\mu}}\right) + v_\nu v_{\bar{\mu}}\left(g_{\mu\bar{\nu}} - v_\mu v_{\bar{\nu}}\right) + \right. \\ &\left. + v_\mu v_{\bar{\nu}}\left(g_{\nu\bar{\mu}} - v_\nu v_{\bar{\mu}}\right) + v_\mu v_{\bar{\mu}}\left(g_{\nu\bar{\nu}} - v_\nu v_{\bar{\nu}}\right)\right].\end{aligned} \tag{7.2.25}$$

Comparing with Eq. (7.2.16), we find now

$$\begin{aligned}
\mathcal{R}_1 &= \frac{D^2/2}{kv-\Lambda_{2^+}}, \\
\mathcal{R}_1 &= -8\frac{C^2}{kv-\Lambda_{0^+}}+\frac{2}{3}\frac{D^2}{kv-\Lambda_{2^+}}, \\
\mathcal{R}_1-\mathcal{R}_2 &= \frac{D^2}{kv-\Lambda_{2^+}}+\frac{2F^2}{kv-\Lambda_{1^-}}.
\end{aligned} \tag{7.2.26}$$

Note that, requiring the consistency of the two expressions for $\mathcal{R}_1$ in Eq. (7.2.26), one arrives at the equalities $\Lambda_{0^+}=\Lambda_{2^+}$ and $D^2=48C^2$. Furthermore, Eqs. (7.2.22) and (7.2.26) are consistent only if $A^2=F^2$, $2A'^2=D^2$, and $\Lambda_{2^+}=\Lambda_{1^+}$. Hence, there should be two more states, with $J^{PC}=0^{++}$ and 2^{++}, degenerate with $X(3872)$ resonance.

We would like to stress here that the degeneracy obtained in this section does not make any assumption about the nature of the two quark fields q appearing in the current given in Eq. (7.2.4). Hence, these degeneracies also hold for states with $I=0$ (with or without hidden strange flavour), $I=1$ and $I=1/2$.

The obtained degeneracies will be broken by finite mass effects. In Chapter 3, we have derived an effective field theory scheme to describe $D^{(*)}\bar{D}^{(*)}$ molecules implementing leading order heavy quark spin symmetry constraints on the dynamics. It is shown that the dynamics of the 2^{++} and 1^{++} channels are identical. However the predicted 2^{++} and 1^{++} ($X(3872)$) states are not degenerate because of the D^*-D mass difference, which is a consequence of the finite value of the charm quark mass.

On the other hand, in the scheme of Chapter 3, there appears also a 0^{++} state degenerate with the 1^{++} and 2^{++} states mentioned above in the infinite quark mass limit. This new state is a result of the $D\bar{D}$ and $D^*\bar{D}^*$ coupled channel dynamics (see Eqs. (18-21) of Ref. [25] and Eqs. (2.3.22-2.3.24) in Chapter 2). This state is similar to the 1^{++} and 2^{++} states in the sense that in this state the heavy quarks are coupled to spin-1 and the light quark are coupled to spin-1 as shown in Eq. (7.2.3). However, for finite charm quark masses, coupled channel effects are subleading in the expansion proposed in [25] and Chapter 3. When these effects are neglected, the dynamics of the 0^{++} state predicted in [25] and Chapter 3 is different to that governing the 1^{++} and 2^{++} sectors.

Up to now, the discussion has been limited to the $C=+1$ states. In [25] and Chapter 3, it was also observed that there is another state with the same binding energy as the 0^{++}, 1^{++} and 2^{++} states and with the quantum numbers $J^{PC}=1^{+-}$ (see Eqs. (18-21) in Ref. [25] and Eqs. (2.3.22-2.3.24) in Chapter 2). To study this state, a possible current that can be used is:

$$j^q_{\alpha\beta}=\bar{Q}^a\gamma_\alpha\gamma_5 Q^b\bar{q}^b\gamma_\beta q^a \tag{7.2.27}$$

where a γ_5 is inserted into the heavy quark sector so as to change the C-parity to $C=-1$ (it also changes the P-parity). The analysis of this $C=-1$ current is similar to the analysis of the $C=+1$ current. In the heavy quark limit, the correlation function using this current can be written as:

$$\tilde{\Pi}_{\alpha\beta;\gamma\delta} = \mathrm{Tr}\left[\gamma_\alpha\gamma_5\frac{1+\not{v}}{2}\gamma_\gamma\gamma_5\frac{1-\not{v}}{2}\right](\mathcal{R}_1 g_{\beta\delta}+\mathcal{R}_2 v_\beta v_\delta) \tag{7.2.28}$$

where the functions $\mathcal{R}_1$ and $\mathcal{R}_2$ are identical to the functions appearing in Eq. (7.2.15). This follows due to the fact that, the currents used for the $C=+1$ and $C=-1$ cases differ only in the structure of the heavy degrees of freedom and are identical in the light degrees of freedom.

Carrying out steps similar to the analysis of the $C = +1$ case leads to the result that $\mathcal{R}_1$ has poles when kv is equal to binding energy of the 1^{+-} state, and $\mathcal{R}_1 + \mathcal{R}_2$ has poles when kv is equal to the binding energy of the 0^{--} state. Comparing with the results presented in Eq. (7.2.26), it is seen that $\Lambda_{0^{++}} = \Lambda_{1^{++}} = \Lambda_{2^{++}} = \Lambda_{1^{+-}}$ and also $\Lambda_{0^{--}} = \Lambda_{1^{-+}}$.

To study the $C = -1$ states, one can also use the current

$$j_{\alpha\beta} = \bar{Q}^a \gamma_\alpha Q^b \bar{q}^b \gamma_\beta \gamma_5 q^a \tag{7.2.29}$$

i.e. γ_5 is inserted into the light sector. As the structure of the light degrees of freedom is modified, the correlation function of this current cannot be expressed in terms of the functions $\mathcal{R}_1$ and $\mathcal{R}_2$. Nevertheless, since the decomposition given in Eq. (7.2.15) only uses the structure of the heavy degrees of freedom, a similar decomposition can also be made for this current using different Lorentz invariant functions. In the identification of the spectrum of particles created by this current, the only difference will be that the particles will have the opposite C and P parities. Hence, the results of the previous analysis can be immediately applied to this case: $\Lambda_{0^{--}} = \Lambda_{1^{--}} = \Lambda_{2^{--}}$. To compare with states of positive C parity, the current

$$j_{\alpha\beta} = \bar{Q}^a \gamma_\alpha \gamma_5 Q^b \bar{q}^b \gamma_\beta \gamma_5 q^a \tag{7.2.30}$$

can be used, leading to the degeneracies $\Lambda_{0^{--}} = \Lambda_{1^{-+}}$ and also $\Lambda_{0^{++}} = \Lambda_{1^{+-}}$ (when comparing results from the currents defined in Eqs. (7.2.29) and (7.2.30) that involve the same structure in the light sector). Note that the last degeneracy corresponds to the 0^{++} and 1^{+-} states in Eqs. (18-19) of [25], which are not degenerate with the 1^{++} and 2^{++} states. The distinction between the 0^{++} and 1^{+-} states that are degenerate with the 1^{++} and 2^{++} is in the light quarks. The states degenerate with 1^{++} and 2^{++} have their light quarks in a state with quantum numbers $J^{PC} = 1^{--}$. The others have their light quarks in the state with quantum numbers 0^{-+}. In the choice of the currents, $\bar{q}\gamma_\alpha\gamma_5 q$ can create a quark-anti-quark pair in the $J^{PC} = 0^{-+}$ state whereas $\bar{q}\gamma_\alpha q$ creates a pair in the 1^{--} state. For the same reason, the 0^{--} and 1^{-+} states related to the currents of Eqs. (7.2.29) and (7.2.30) do not correspond to those discussed for the currents of Eqs. (7.2.4) and (7.2.27).

7.3 $I = 0$ and $I = 1$ Components of $X(3872)$

In this section, possible $I = 1$ admixture of the $X(3872)$ will be analyzed using the method outlined in [182], which is briefly sketched below.

Let us denote the normalized I=0 and I=1 components of $X(3872)$ state by $|X(0)\rangle$ and $|X(1)\rangle$. The currents that couple to the isospin states $|X(0)\rangle$ and $|X(1)\rangle$ can be written as

$$\begin{aligned} j^{I=0} &= \frac{1}{\sqrt{2}}\left(j^u + j^d\right), \\ j^{I=1} &= \frac{1}{\sqrt{2}}\left(j^u - j^d\right), \end{aligned} \tag{7.3.1}$$

respectively, where j^q is any of the currents given in Eqs. (7.2.9) and (7.2.10). Let us define the correlation functions

$$\begin{aligned} \Pi^{qq'} &= i\int d^4x e^{ipx}\langle 0|\mathcal{T} j^q(x) j^{q'\dagger}(0)|0\rangle, \\ \Pi^{II'} &= i\int d^4x e^{ipx}\langle 0|\mathcal{T} j^I(x) j^{I'\dagger}(0)|0\rangle. \end{aligned} \tag{7.3.2}$$

Then

$$\begin{aligned}
\Pi^{00} &= \frac{1}{2}\left(\Pi^{uu} + \Pi^{dd} + \Pi^{ud} + \Pi^{du}\right), \\
\Pi^{11} &= \frac{1}{2}\left(\Pi^{uu} + \Pi^{dd} - \Pi^{ud} - \Pi^{du}\right), \\
\Pi^{10} &= \frac{1}{2}\left(\Pi^{uu} - \Pi^{dd} + \Pi^{ud} - \Pi^{du}\right), \\
\Pi^{01} &= \frac{1}{2}\left(\Pi^{uu} - \Pi^{dd} - \Pi^{ud} + \Pi^{du}\right).
\end{aligned} \tag{7.3.3}$$

Since isospin is not an exactly conserved quantity, the states $X(0)$ and $X(1)$ cannot be eigenstates. Hence, they can evolve into one another, i.e., oscillate. This is reflected in the fact that the off diagonal correlation functions are not zero: $\Pi^{10} \neq 0$ and $\Pi^{01} \neq 0$.

The physical $X(3872)$ and its orthogonal state can be written as:

$$\begin{aligned}
|X(3872)\rangle &= \cos\theta|X(0)\rangle + \sin\theta|X(1)\rangle, \\
|X_\perp\rangle &= -\sin\theta|X(0)\rangle + \cos\theta|X(1)\rangle,
\end{aligned} \tag{7.3.4}$$

where any possible relative phase can be absorbed in the definition of the states. The respective interpolating currents are given by:

$$\begin{aligned}
j_{X(3872)} &= \cos\theta j^{I=0} + \sin\theta j^{I=1}, \\
j_{X_\perp} &= -\sin\theta j^{I=0} + \cos\theta j^{I=1}.
\end{aligned} \tag{7.3.5}$$

Being physical eigenstates $|X(3872)\rangle$ and $|X_\perp\rangle$ should not oscillate, i.e.

$$\begin{aligned}
i\int d^4x\; e^{ipx}\langle 0|\mathcal{T} j_{X(3872)}(x) j^\dagger_{X_\perp}(0)|0\rangle \quad + \\
+ i\int d^4x\; e^{ipx}\langle 0|\mathcal{T} j_{X_\perp}(x) j^\dagger_{X(3872)}(0)|0\rangle = 0,
\end{aligned} \tag{7.3.6}$$

the solution of which gives

$$\tan 2\theta = \frac{\Pi^{10} + \Pi^{01}}{\Pi^{00} - \Pi^{11}} = \frac{\Pi^{uu} - \Pi^{dd}}{\Pi^{ud} + \Pi^{du}}. \tag{7.3.7}$$

In our case, in this expression, the correlation functions that appear are either $\mathcal{R}_1$ or $\mathcal{R}_2$, and it should be understood that the contributions of states other than $X(3872)$ are subtracted, and hence Π's contain only the contribution from $X(3872)$. Note that the numerator is non-zero only if isospin is violated, and the denominator receives contributions only from annihilation diagrams. In the annihilation diagrams, the $u(d)$ quark inserted into the vacuum by the current annihilates into gluons or the photon which then form $d(u)$ quarks that are annihilated by the other current. Such annihilation diagrams are usually omitted in sum rules and lattice calculations since they are considered to be small. From Eq. (7.3.7), it is seen that if the annihilation diagrams are negligible and/or much smaller then isospin breaking effects, the mixing of the $I = 0$ and $I = 1$ components in $X(3872)$ can be large (in the limiting case, if one neglects the annihilation diagrams, one obtains maximal mixing as long as there exist isospin symmetry breaking independent of how small the breaking is)

To obtain an order of magnitude estimate of the mixing angle θ, let us first consider the numerator. The numerator receives contributions only from isospin breaking effects. There are

two important sources of isospin breaking: the mass differences of the u and d quarks, and electromagnetic interactions. Note also that, the mass dimension of the correlation function is eight. Hence, from dimensional analysis, one would expect $\Pi^{uu} - \Pi^{dd}$ to be of the order of $(m_u - m_d)\Lambda^7$ or $\alpha\Lambda^8$ where α is the electromagnetic coupling and Λ, in the framework of QCD sum rules, is the Borel mass, which, in the heavy quark limit is of the order of the binding energy of the $X(3872)$ meson, i.e. $\Lambda \sim m_X - 2m_c = 1.32$ GeV. For such a value of Λ, $\alpha\Lambda \sim (m_u - m_d)$. Hence, both sources give the same order of magnitude contribution to the numerator. Considering the denominator in Eq. (7.3.7), there is no a priori symmetry limit in which it vanishes. Hence, the denominator is $\mathcal{O}(\Lambda^8)$. Note that, the denominator is also responsible for the difference of the correlation functions Π^{10} and Π^{01}, i.e. it is the term responsible for the mass difference between the $I = 0$ and $I = 1$ states. Hence, if this mass difference is zero, then the denominator should also be zero. Therefore, the denominator can be estimated as $\beta\Lambda^8$ where β is a parameter that measures the splitting between the $I = 0$ and $I = 1$ states. Inserting such a factor β is also consistent with the fact that in the hypothetical limit where the splitting between the $I = 0$ and $I = 1$ states would go to infinity, the mixing angle would go to zero.

Explicit calculation of the parameter β for $X(3872)$ is beyond the scope of this chapter, but an estimate of it can be obtained from the ρ/ω system. In the currents that are used, the light quarks (which are responsible for the splitting between the $I = 0$ and $I = 1$ states) are put in a vector configuration, just like in the ρ and ω mesons. Hence, an estimate of the β parameter can be obtained as

$$\beta \sim \frac{m_\omega - m_\rho}{m_\omega + m_\rho} = 0.0046. \tag{7.3.8}$$

Combining the estimates for the denominator and numerator, one would estimate that

$$\tan 2\theta = \frac{m_u - m_d}{\beta\Lambda} \simeq 0.56 \longrightarrow \theta \simeq 15^\circ, \tag{7.3.9}$$

and hence,

$$|X(3872)\rangle = 0.96|X(0)\rangle + 0.25|X(1)\rangle. \tag{7.3.10}$$

In the models where $X(3872)$ are dominantly a DD^* molecule, the $|X(0)\rangle$ and $|X(1)\rangle$ components can be written as

$$\begin{aligned} |X(0)\rangle &= \frac{1}{\sqrt{2}}\left(|D^0\bar{D}^{*0}\rangle + |D^+D^{*-}\rangle\right), \\ |X(1)\rangle &= \frac{1}{\sqrt{2}}\left(|D^0\bar{D}^{*0}\rangle - |D^+D^{*-}\rangle\right), \end{aligned} \tag{7.3.11}$$

where a $C = +1$ combination is implied. Inserting these into Eq. (7.3.10), it is obtained that the probability of observing a molecule of neutral D and D^* meson is 75%, whereas the probability is 25% for the charged channel, which are consistent with the bulk part of the results obtained in [183]. [1]

In [99] also, $X(3872)$ is described as a $D\bar{D}^*$ molecule. In the notation of [99] (see the Subsect. 2.4.1 of Chapter 2), the mixing angle θ can be written as

$$\tan^2\theta = \frac{\int d^3\vec{r}|\Psi_1(\vec{r}) - \Psi_2(\vec{r})|^2}{\int d^3\vec{r}|\Psi_1(\vec{r}) + \Psi_2(\vec{r})|^2} = 0.64, \tag{7.3.12}$$

[1] Note that, in [183], a possible $c\bar{c}$ component of $X(3872)$ is also considered.

which gives a mixing angle of $\theta \simeq 39^\circ$, which is twice as large as the order of magnitude estimated in Eq. (7.3.9) and quite close to maximal mixing $\theta_{max} = 45^\circ$.

Note that, the observed isospin violation in the decays $X(3872) \to \rho J/\Psi$, and $X(3872) \to \omega J/\Psi$ is not determined only by the mixing angle, but also by the relative magnitudes of the aptitudes $\langle J/\Psi\rho|H|X(1)\rangle$ and $\langle J/\Psi\omega|H|X(0)\rangle$ where we neglect possible isospin violation in decay. The ratio of the amplitudes will be given by[2]

$$\begin{aligned}\frac{A(X(3872) \to J/\Psi\rho)}{A(X(3872) \to J/\Psi\omega)} &= \tan\theta \frac{\langle J/\Psi\rho|H|X(1)\rangle}{\langle J/\Psi\omega|H|X(0)\rangle} \\ &= \left(\frac{\hat{\psi}_1 - \hat{\psi}_2}{\hat{\psi}_1 + \hat{\psi}_2}\right), \end{aligned} \tag{7.3.13}$$

where in the last equality, we used the result of [99], also derived in Sect. 2.4.1 and $\hat{\psi}$ is a weighted average of the wave function $\psi(\vec{r})$ with a weight that is strongly peaked at the origin (zero relative distance between the two mesons). Isospin plays a relevant role in strong processes which are sensitive to short distance dynamics. In the molecular picture of $X(3872)$, at short distances, the dynamics of the $X(3872)$ is such that the probability amplitudes of both the neutral and charged meson channels are very similar. This suggests that, when dealing with strong processes, only isospin $I = 0$ component will be relevant. The observed isospin breaking in the amplitudes will be small even if the probability to find the $D^0\bar{D}^{*0}-$c.c. component in the full space is much larger than that for the $D^+D^{*-}-$c.c. component. In [99], it is shown that this ratio is consistent with the experimental value.

Although the strong decays of $X(3872)$ will mainly be determined by the wave function at the origin, and hence conceal the large isospin violation, the largeness of the mixing angle θ can lead to significant contributions from the isospin-1 component of $X(3872)$ to processes that are sensitive to large separation between the D mesons making the $X(3872)$ state. Electromagnetic decays such as $X \to \gamma\Psi(2S)$ which is observed with a branching ratio larger than 3% [45], will be sensitive to physics at distances of the order of the size of the D-mesons that form the $X(3872)$ state. Possible weak decays of $X(3872)$ in which the c-quark decays weakly into an s-quark, will be sensitive to even larger separations of the D mesons in the molecular picture. If these weak decays are semi-leptonic, they will also conserve isospin.

7.4 Conclusions

In this chapter, even C-parity currents given in Eqs. (7.2.9) and (7.2.10) that can be used to study the $X(3872)$ meson have been proposed. These currents can be used in the future for more quantitative analysis of these mesons and a QCD SR analysis is under way. Compared to other currents used in the literature to study the $X(3872)$ resonance (see e.g. [184, 185]), the proposed currents have the advantage that they can also be used to study the partners of the $X(3872)$ meson on an equal footing.

Using the proposed currents, it is proven that the states that couple to them form degenerate triplets with the quantum numbers $J^{PC} = 2^{++}$, $J^{PC} = 1^{++}$, and $J^{PC} = 0^{++}$. Note that since the results are exact in the heavy quark limit, this conclusion holds for *any* state that couples to the currents independent of its internal structure. One such triplet is the triplet of mesons χ_{c0}, χ_{c1} and χ_{c2}. The masses of these particles differ from their average by at most 80 MeV. Another example is the χ_{b0}, χ_{b1} and χ_{b2}. In this case, the variation is less than 30 MeV, consistent

[2] To evaluate the ratio of the widths, one should also take into account the phase space of the ρ decaying into two pions and ω decaying into three points [99, 101].

with an $1/m_Q$ effect. Taking this deviation as a measure of the possible $1/m_Q$ effects, $X(3872)$ should have spin-0 and spin-2 partners that have a mass that differs by ~ 100 MeV from the mass of $X(3872)$. We have also analyzed odd C-parity currents and ended up with a degeneracy spectrum compatible with that derived in the molecular picture of Chapter 3 and [25].

Possible existence of a $I = 1$ component in the state $|X(3872)\rangle$ is also discussed. It is shown that the mixing angle between the $I = 0$ and $I = 1$ components can be large and even close to maximal [99]. But, it might not be reflected in its strong decays. Nevertheless, this mixing can be important in decays of the $X(3872)$ resonance which are not strong.

Chapter 8

Detecting the long-distance structure of the X(3872)

8.1 Introduction

In this chapter, based on Ref. [5], we start studying the decays of the exotic molecular states that we have dynamically generated in the previous chapters. Decay channels are one of the most important pieces of empirical information. The different decay channels of a resonance provide the quantum numbers of the state and, beyond, they might serve as a test of the different theoretical interpretations. Since the most famous candidate to fit a molecular description is the $X(3872)$, it seems natural to start studying the decays of that state. In particular, we study the $X(3872) \to D^0\bar{D}^0\pi^0$ decay that might be sensitive to the long-distance structure of the $X(3872)$ resonance.

The most discussed decay channels of the $X(3872)$ are those with a charmonium in the final state, which include the $J/\psi\pi\pi$, $J/\psi 3\pi$, $J/\psi\gamma$ and $\psi'\gamma$. In the hadronic molecular picture, these decays occur through the mechanism depicted in Fig. 8.1. Thus, the charm and anti-charm mesons only appear in the intermediate (virtual) state, and the amplitude of such decays is proportional to the appropriate charged or neutral $D\bar{D}^*$ loop integrals [103]. Because the quarks in the two mesons have to recombine to get the charmonium in the final state, the transition from the charm–anti-charm meson pair into the J/ψ plus pions (or a photon), occurs at a distance much smaller than both the size of the $X(3872)$ as a hadronic molecule ($\sim$ few fm's)[1] and the range of forces between the D and $\bar{D}^*$ mesons which is of the order of $1/m_\pi \sim 1.5$ fm. In this case, if this transition matrix t in Fig. 8.1 does not introduce any momentum dependence, the loop integral reduces to the wave function of the $X(3872)$ at the origin, $\Psi(\vec{0})$,[2] (more properly, around the origin, since the needed ultraviolet regulator, for which we do not give details here, would smear the wave functions) [99][3],

[1] This is approximately given by $1/\sqrt{2\mu\epsilon_X}$ fm where μ is the reduced mass of the D and $\bar{D}^*$ pair and $\epsilon_X = M_{D^0} + M_{D^{*0}} - M_{X(3872)} = 0.16 \pm 0.26$ MeV [45].

[2] The relative distance between the two mesons is zero in the wave function at the origin.

[3] For related discussions in case of the two-photon decay width of a loosely bound hadronic molecule, see Ref. [186].

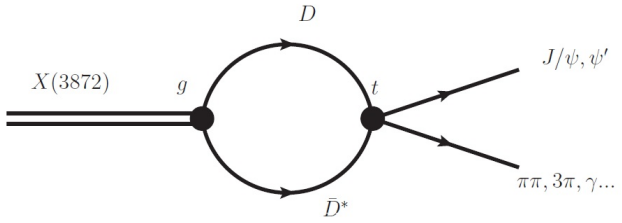

Figure 8.1: *Mechanism for the decays of the $X(3872)$ into $J/\psi\pi\pi$, $J/\psi 3\pi$, $J/\psi\gamma$, $\psi'\gamma$ ... assuming the $X(3872)$ to be a $D\bar{D}^*$ molecule. The charge conjugated channel is not plotted.*

$$\begin{aligned}\langle f|X(3872)\rangle &= \int d^3\vec{q}\ \underbrace{\langle f|D\bar{D}^*(\vec{q})\rangle}_{t}\underbrace{\langle D\bar{D}^*(\vec{q})|X(3872)\rangle}_{\Psi(\vec{q})} = \\ &= t\int d^3\vec{q}\ \Psi(\vec{q}) = t\,\Psi(\vec{0}) = t\,\hat{g}G,\end{aligned} \tag{8.1.1}$$

where $\hat{g}$ is the coupling of the $X(3872)$ to the $D\bar{D}^*(\vec{q})$ pair and G is the diagonal loop function for the two intermediate D and $\bar{D}^*$ meson propagators, with the appropriate normalizations that are discussed below. The last equality follows from the expression of the momentum space wave function [99]

$$\Psi(\vec{q}) = \frac{\hat{g}}{M_X - M_D - M_{D^*} - \vec{q}^{\,2}/(2\mu)}, \tag{8.1.2}$$

where μ is the reduced mass of the D and $\bar{D}^*$. This can be easily derived from the Schrödinger equation assuming the coupling of the $X(3872)$ to $D\bar{D}^*$ to be a constant, which is valid since the $X(3872)$ is very close to the threshold (see the related discussion of Sect. 2.4). Thus, one can hardly extract information on the long-distance structure of the $X(3872)$ from these decays.

In general, to be sensitive to the long-distance part of the wave function of a hadronic molecule, it is better to investigate the decay processes with one of the constituent hadrons in the final state and the rest of the final particles being products of the decay of the other constituent hadron of the molecule. For instance, for the case of the $X(3872)$ as a $D\bar{D}^*$ molecule, we should use the $X(3872) \to D^0\bar{D}^0\pi^0$ or $X(3872) \to D\bar{D}\gamma$ modes to study the long-distance structure. In these processes, the relative distance between the $D\bar{D}^*$ pair can be as large as allowed by the size of the $X(3872)$ resonance, since the final state is produced by the decay of the $\bar{D}^*$ meson instead of a rescattering transition. These decay modes have been addressed in some detail in different works, e.g., Refs. [10, 88, 187, 188, 189, 190, 191]. The $D^0\bar{D}^0\pi^0$ mode has already been observed by the Belle Collaboration [192, 193], which triggered the virtual state interpretation of the $X(3872)$ [194], and it is studied in detail in this chapter.

As we have mentioned at length in the previous chapters, as long as the hadrons are not too tightly bound, they will not probe the specific details of the interaction binding them at short distances. Moreover, each of the constituent heavy hadrons will be unable to see the internal structure of the other heavy hadron. This separation of scales can be used to formulate an EFT description of hadronic molecules compatible with the approximate nature of HQSS. We have seen that at LO the EFT is particularly simple and it only involves energy-independent contact range interactions. As explained in Chapter 3, the $X(3872)$ mass and its puzzling isospin violating decays into $J/\psi\ 2\pi$ and $J/\psi\ 3\pi$ can be used to fix the linear combination of LECs:

$(C_{0a} + C_{0b})$ and $(C_{1a} + C_{1b})$ that in turn determine the $X(3872)$ coupling to the neutral and charged $D\bar{D}^*$ pairs, input needed to compute the decay width $\Gamma(X(3872) \to D^0\bar{D}^0\pi^0)$. However, the interaction between a D and a $\bar{D}$ is different. It depends on a different combination of LECs (compare Eqs. (2.3.22) and (2.3.24) in Sect. 2.3.1). This interaction will be important to address $D\bar{D}$ Final State Interactions (FSI) effects, that will affect the $\Gamma(X(3872) \to D^0\bar{D}^0\pi^0)$ width.

Thus, the $X(3872) \to D^0\bar{D}^0\pi^0$ decay, on one hand, detects the long-distance structure of the $X(3872)$; on the other hand, it provides the possibility to constrain the $D\bar{D}$ s-wave interaction at very low energies. The effect of the $D\bar{D}$ s-wave FSI in the $X(3872) \to D^0\bar{D}^0\pi^0$ decay can be very large because of the possible existence of a sub-threshold isoscalar state in the vicinity of 3700 MeV [25, 105]. It will be discussed in detail in this chapter.

As mentioned above, this $X(3872)$ decay channel has been previously studied. The first calculation was carried out in Ref. [188] using effective-range theory. In Ref. [10], using an EFT, the results of Ref. [188] was reproduced at LO, and the size of corrections to the LO calculation was estimated. These next-to-leading-order (NLO) corrections to the decay width include effective-range corrections as well as calculable non-analytic corrections from π^0 exchange. It was found that non-analytic calculable corrections from pion exchange are negligible and the NLO correction was dominated by contact interaction contributions. The smallness of these corrections confirms one of the main points raised in [10], namely, that pion exchange can be dealt with using perturbation theory[4]. However, the $D\bar{D}$ FSI effects we are including here were not considered in these two works.

The chapter is structured as follows: in Section 8.2, we briefly discuss the $X(3872)$ resonance within the hadronic molecular picture and the s-wave low-energy interaction between a charm and an anti-charm mesons. The decay $X(3872) \to D^0\bar{D}^0\pi^0$ is discussed in detail in Section 8.3 with the inclusion of the $D\bar{D}$ FSI. Section 8.4 presents a brief summary.

8.2 The $X(3872)$ and the heavy meson s-wave interaction

The basic assumption is that the $X(3872)$ exotic charmonium is a $D\bar{D}^* - D^*\bar{D}$ bound state with quantum numbers $J^{PC} = 1^{++}$. For the sake of completeness we briefly discuss again in this section the formalism used to describe this resonance, which is based on the solution of the Lippmann-Schwinger equation (LSE) with a kernel constrained by HQSS. More specific details can be found in previous chapters.

As argued in previous chapters, for loosely bound states, the interaction between a charm and anti-charm meson can be accurately described just in terms of a contact-range potential, as a function of four LECs (C_{0a}, C_{0b} and C_{1a}, C_{1b}) which stand for the counter-terms in the isospin $I = 0$ and $I = 1$ channels, respectively. The LSE, with a kernel constructed out of a contact interaction, shows an ill-defined ultraviolet behaviour, and requires a regularization and renormalization procedure. We employ a standard Gaussian regulator

$$\langle \vec{p}|V|\vec{p}\,'\rangle = C_{I\phi}\; e^{-\vec{p}^{\,2}/\Lambda^2}\; e^{-\vec{p}^{\,\prime 2}/\Lambda^2}, \tag{8.2.1}$$

with $C_{I\phi}$ the corresponding counter-term. We will take cutoff values $\Lambda = 0.5 - 1$ GeV, as in the rest of the chapters in this thesis. Pion exchange and coupled-channel effects are not considered at LO. This is justified since both effects were shown to be small by the explicit calculation carried out in [25] and the power counting arguments established in [11].

[4]This result has been also confirmed in Refs. [11, 25, 88]. In the latter reference, the range of center-of-mass momenta, for which the tensor piece of the one pion exchange potential is perturbative, is studied in detail, and it is also argued that the effect of coupled channels is suppressed by at least two orders in the EFT expansion.

Bound states correspond to poles of the T-matrix below threshold on the real axis in the first Riemann sheet of the complex energy. If we assume that the $X(3872)$ state and the isovector $Z_b(10610)$ states are $\left(D\bar{D}^* - D^*\bar{D}\right)/\sqrt{2}$ and $\left(B\bar{B}^* + B^*\bar{B}\right)/\sqrt{2}$ bound states, respectively, and use the isospin breaking information of the decays of the $X(3872)$ into the $J/\psi\pi\pi$ and $J/\psi\pi\pi\pi$, we can determine three linear combinations among the four LECs C_{0a}, C_{0b}, C_{1a} and C_{1b} with the help of heavy quark spin and flavour symmetries (see chapters 3 and 5 for all sort of details). We consider both the neutral $\left(D^0\bar{D}^{*0} - D^{*0}\bar{D}^0\right)$ and charged $(D^+D^{*-} - D^{*+}D^-)$ components in the $X(3872)$. The coupled-channel potential is given by Eq.(3.2.29)

$$V_{X(3872)} = \frac{1}{2}\begin{pmatrix} C_{0X}+C_{1X} & C_{0X}-C_{1X} \\ C_{0X}-C_{1X} & C_{0X}+C_{1X} \end{pmatrix}, \tag{8.2.2}$$

where $C_{0X} \equiv C_{0a}+C_{0b}$ and $C_{1X} \equiv C_{1a}+C_{1b}$. Using $M_{X(3872)} = (3871.68\pm0.17)$ MeV, the isospin violating ratio of the decay amplitudes for the $X(3872) \to J/\psi\pi\pi$ and $X(3872) \to J/\psi\pi\pi\pi$, $R_{X(3872)} = 0.26 \pm 0.07$ [101],[5] and the mass of the $Z_b(10610)$ (we assume, as in Chapter 5, that its binding energy is 2.0 ± 2.0 MeV [44]) as three independent inputs, we find

$$\begin{aligned} C_{0X} &= -1.71^{+0.06}_{-0.04}\ (-0.73^{+0.02}_{-0.01})\,\text{fm}^2, \\ C_{1X} &= -0.13^{+0.53}_{-0.41}\ (-0.39 \pm 0.09)\,\text{fm}^2, \\ C_{1Z} \equiv C_{1a} - C_{1b} &= -0.75^{+0.24}_{-0.14}\ (-0.30^{+0.03}_{-0.03})\,\text{fm}^2 \end{aligned} \tag{8.2.3}$$

for $\Lambda = 0.5(1.0)$ GeV. Errors were obtained from a Monte Carlo (MC) simulation assuming uncorrelated Gaussian errors for the three inputs and using 1000 samples. Note that the values of the different LEC's are natural, $\sim \mathcal{O}(1\ \text{fm}^2)$, as one would expect.

The $X(3872)$ coupling constants to the neutral and charged channels, g_0^X and g_c^X, respectively, are determined by the residues of the T-matrix elements at the $X(3872)$ pole

$$\begin{aligned} \left(g_0^X\right)^2 &= \lim_{E\to M_{X(3872)}} \left[E - M_{X(3872)}\right] \times T_{11}(E), \\ g_0^X g_c^X &= \lim_{E\to M_{X(3872)}} \left[E - M_{X(3872)}\right] \times T_{12}(E), \end{aligned} \tag{8.2.4}$$

where T_{ij} are the matrix elements of the T-matrix solution of the UV regularized LSE. Their values are slightly different. Using the central values of C_{0X} and C_{1X}, we get,

$$\begin{aligned} g_0^X &= 0.35^{+0.08}_{-0.18}\,(0.34^{+0.07}_{-0.18})\ \text{GeV}^{-1/2}, \\ g_c^X &= 0.32^{+0.07}_{-0.16}\,(0.26^{+0.05}_{-0.14})\ \text{GeV}^{-1/2}, \end{aligned} \tag{8.2.5}$$

where, again, the values outside and inside the parentheses are obtained with $\Lambda = 0.5$ and 1 GeV, respectively. To obtain the central values and the errors of Eq. (8.2.5), we used $B = 160\pm170$ keV, and a Monte Carlo simulation was performed to propagate errors[6]. In the simulation, we rejected $X(3872)$ binding energies values smaller than 10 keV, and those values were set to this minimum value. This effectively amounts to consider $B = 160^{+170}_{-150}$ keV, since the Gaussian distribution of binding energies was truncated. We slightly decreased the lower error to guaranty a bound state with a CL larger than 68%, since the scheme followed here only allows the computation of the width when the $X(3872)$ state is bound. Note that when the position of the $X(3872)$ resonance approaches the $D\bar{D}^*$ threshold, both couplings g_0^X and g_c^X tend to zero. This is because for very small binding energies, all the couplings of a bound state tend to zero when the mass of

[5] We have symmetrized the errors provided in [101] to use Gaussian distributions to estimate errors.

[6] The error on the threshold energy ($M_{D^0} + M_{D^{*0}}$), $\sim$120 keV, has not been taken into account.

the bound state gets closer to the lowest threshold [155]. For the case of the $X(3872)$, this was re-derived in [99] and explicitly shown that both the neutral $X(3872)D^0\bar{D}^{*0}$ (g_0^X) and charged $X(3872)D^+\bar{D}^{*-}$ couplings scale as $B^{\frac{1}{4}}$.

Within this model, we will account for the $D\bar{D}$ FSI effects to the $X(3872) \to D^0\bar{D}^0\pi^0$ decay width. The s-wave interaction in the $D\bar{D}$ system with $J^{PC} = 0^{++}$ is not entirely determined by C_{0X}, C_{1X} and C_{1Z}. Indeed, considering again both the neutral and charged channels $D^0\bar{D}^0$ and D^+D^-, the potential is given by[7]

$$V_{D\bar{D}} = \frac{1}{2}\begin{pmatrix} C_{0a}+C_{1a} & C_{0a}-C_{1a} \\ C_{0a}-C_{1a} & C_{0a}+C_{1a} \end{pmatrix}. \tag{8.2.6}$$

Thus, this interaction is not completely determined from what we have learned from the $X(3872)$ and $Z_b(10610)$ states. Even if we use heavy quark spin and flavour symmetries, the value of C_{0a} is still unknown. Depending on the value of C_{0a}, there can be a $D\bar{D}$ s-wave bound state or not. For instance, considering the case for $\Lambda = 0.5$ GeV and taking the central value for $C_{1a} = -0.44$ fm^2, if $C_{0a} = -3.53$ fm^2, then one finds a bound state pole in the $D\bar{D}$ system with a mass 3706 MeV (bound by around 25 MeV); if $C_{0a} = -1.65$ fm^2, there will be a $D\bar{D}$ bound state at threshold; if the value of C_{0a} is larger, there will be no bound state any more. Therefore, the information of C_{0a} will be crucial in understanding the $D\bar{D}$ system and other systems related to it through heavy quark symmetries. Conversely, as we will see, the $X(3872) \to D^0\bar{D}^0\pi^0$ decay width could be used to extract information on the fourth LEC, C_{0a}, thanks to the FSI effects.

8.3 $X(3872) \to D^0\bar{D}^0\pi^0$ decay

Here, we discuss the decay of the $X(3872)$ into the $D^0\bar{D}^0\pi^0$ mode. This decay can take place directly through the decay of the constituent D^{*0} or $\bar{D}^{*0}$ as shown in Fig. 8.2(a). After emitting a pion, the vector charm meson transits into a pseudoscalar one, and it can interact with the other constituent in the $X(3872)$ as shown in Fig. 8.2(b). Figure 8.2(c) presents another possibility, namely the decay can also occur through the decay of the charged vector charm meson, and the virtual charged D^+D^- pair then rescatter into $D^0\bar{D}^0$.

We will use the relevant term in the LO Lagrangian of heavy meson chiral perturbation theory to describe the $D^*D\pi$ coupling, already discussed in Eq.(2.3.34),

$$\begin{aligned}\mathcal{L}_{\pi HH} &= -\frac{g}{2f_\pi}\left(\mathrm{Tr}\left[\bar{H}^{(Q)b}H_a^{(Q)}\gamma_\mu\gamma_5\right] + \mathrm{Tr}\left[H^{(\bar{Q})b}\bar{H}_a^{(\bar{Q})}\gamma^\mu\gamma_5\right]\right) \\ &\qquad (\vec{\tau}\partial_\mu\vec{\phi})_b^a + \cdots\end{aligned} \tag{8.3.1}$$

with $\vec{\phi}$ a relativistic field that describes the pion[8], $g \simeq 0.6$ is the $PP^*\pi$ coupling and $f_\pi = 92.2$ MeV the pion decay constant. Note that in our normalization, the pion field has a dimension of energy, while the heavy meson or antimeson fields $H^{(Q)}$ or $H^{(\bar{Q})}$ have dimensions of $E^{3/2}$, as we already mentioned.

[7] The reason for using particle basis, where the interaction is not diagonal, instead of isospin basis is because for some values of the LEC's, a $D\bar{D}$ bound state close to threshold might be generated. If its binding energy is smaller or comparable to the $D^0\bar{D}^0 - D^+D^-$ threshold difference, as it happens in the case of the $X(3872)$ resonance, then it will become necessary to account for the mass difference among the neutral and charged channels.

[8] We use a convention such that $\phi = \frac{\phi_x - \mathrm{i}\phi_y}{\sqrt{2}}$ creates a π^- from the vacuum or annihilates a π^+, and the ϕ_z field creates or annihilates a π^0.

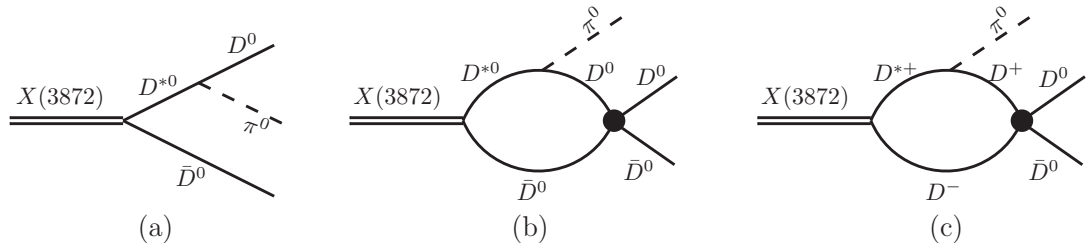

Figure 8.2: *Feynman diagrams for the decay $X(3872) \to D^0\bar{D}^0\pi^0$. The charge conjugate channel is not shown but included in the calculations.*

8.3.1 Tree Level Approximation

For the process in question, the charm mesons are highly non-relativistic, thus we can safely neglect higher order terms in $\vec{p}_{\bar{D}^{*0},D^{*0}}/M_{D^*}$. Taking into account the contributions from both the $D^0\bar{D}^{*0}$ and $D^{*0}\bar{D}^0$ components of the $X(3872)$, the tree-level amplitude is given by

$$\mathcal{T}_{\text{tree}} = -2i\frac{gg_0^X}{f_\pi}\sqrt{M_X}M_{D^{*0}}M_{D^0}\vec{\epsilon}_X\cdot\vec{p}_\pi\left(\frac{1}{p_{12}^2-M_{\bar{D}^{*0}}^2}+\frac{1}{p_{13}^2-M_{\bar{D}^{*0}}^2}\right), \tag{8.3.2}$$

where $\vec{\epsilon}_X$ is the polarization vector of the $X(3872)$, $\vec{p}_\pi$ is the three-momentum of the pion, p_{12} and p_{13} are the four momenta of the π^0D^0 and $\pi^0\bar{D}^0$ systems, respectively[9]. We have neglected the D^{*0} and $\bar{D}^{*0}$ widths in the above propagators because their inclusion only leads to small numerical variations in the $X(3872) \to D^0\bar{D}^0\pi^0$ decay rate of the order of 0.1 keV. As we will see below in Eq. (8.3.7), uncertainties on the predicted width induced by the errors in the coupling g_0^X and the mass of the $X(3872)$ resonance, turn out to be much larger (of the order of few keV).

Note that we have approximated the $X(3872)D^0\bar{D}^{*0}$ vertex by g_0^X. It could have some dependence on the momentum of the mesons, which can be expanded in powers of momentum in the spirit of EFT. For the process in question, the momenta of the charm mesons are much smaller than the hard energy scale of the order of the cutoff, we can safely keep only the leading constant term.

Since the amplitude of Eq. (8.3.2) depends only on the invariant masses $m_{12}^2 = p_{12}^2$ and $m_{23}^2 = (M_X^2 + m_{\pi^0}^2 + 2M_{D^0}^2 - m_{12}^2 - p_{13}^2)$ of the final π^0D^0 and $D^0\bar{D}^0$ pairs, respectively, we can use the standard form for the Dalitz plot [45]

$$d\Gamma = \frac{1}{(2\pi)^3}\frac{1}{32M_X^3}\overline{|\mathcal{T}|}^2 dm_{12}^2 dm_{23}^2, \tag{8.3.3}$$

[9]To obtain the amplitude, we have multiplied by factors $\sqrt{M_{D^{*0}}M_{D^0}}$ and $\sqrt{8M_XM_{D^{*0}}M_{D^0}}$ to account for the normalization of the heavy meson fields and to use the coupling constant g_0^X, as defined in Eq. (8.2.4) and given in Eq. (8.2.5), for the $X(3872)D^0\bar{D}^{*0}$ and $X(3872)D^{*0}\bar{D}^0$ vertices.

and thus, we readily obtain

$$\begin{aligned}\Gamma_{\rm tree} &= \frac{g^2}{192\pi^3 f_\pi^2}\left(g_0^X \frac{M_{D^0}M_{D^{*0}}}{M_X}\right)^2 \\ &\times \int_{(M_{D^0}+m_\pi^0)^2}^{(M_X-M_{D^0})^2} dm_{12}^2 \int_{(m_{23}^2)_{(\rm min)}}^{(m_{23}^2)_{(\rm max)}} dm_{23}^2 \\ &\qquad \left[\left(\frac{1}{p_{12}^2-M_{D^{*0}}^2}+\frac{1}{p_{13}^2-M_{D^{*0}}^2}\right)^2 |\vec{p}_\pi|^2\right],\end{aligned} \tag{8.3.4}$$

with

$$|\vec{p}_\pi| = \frac{\lambda^{1/2}(M_X^2, m_{23}^2, m_{\pi^0}^2)}{2M_X}, \tag{8.3.5}$$

the pion momentum in the $X(3872)$ center of mass frame [$\lambda(x,y,z) = x^2+y^2+z^2-2(xy+yz+xz)$ is the Källén function]. In addition, for a given value of m_{12}^2, the range of m_{23}^2 is determined by its values when $\vec{p}_D$ is parallel or anti-parallel to $\vec{p}_{\bar{D}}$ [45]:

$$\begin{aligned}(m_{23}^2)_{(\rm max)} &= (E_D^*+E_{\bar{D}}^*)^2-(p_D^*-p_{\bar{D}}^*)^2, \\ (m_{23}^2)_{(\rm min)} &= (E_D^*+E_{\bar{D}}^*)^2-(p_D^*+p_{\bar{D}}^*)^2,\end{aligned} \tag{8.3.6}$$

with $E_D^* = (m_{12}^2-m_{\pi^0}^2+M_{D^0}^2)/2m_{12}$ and $E_{\bar{D}}^* = (M_X^2-m_{12}^2-M_{D^0}^2)/2m_{12}$ the energies of the D^0 and $\bar{D}^0$ in the m_{12} rest frame, respectively, and $p_{D,\bar{D}}^*$ the moduli of their corresponding three momenta.

Using the couplings given in Eq. (8.2.5), the partial decay width for the three-body decay $X(3872) \to D^0\bar{D}^0\pi^0$ at tree level is predicted to be

$$\Gamma(X(3872)\to D^0\bar{D}^0\pi^0)_{\rm tree} = 44.0^{+2.4}_{-7.2}\left(42.0^{+3.6}_{-7.3}\right)\ \text{keV}, \tag{8.3.7}$$

where the values outside and inside the parentheses are obtained with $\Lambda = 0.5$ and 1 GeV, respectively, and the uncertainty reflects the uncertainty in the inputs ($M_{X(3872)}$ and the ratio $R_{X(3872)}$ of decay amplitudes for the $X(3872)\to J/\psi\rho$ and $X(3872)\to J/\psi\omega$ decays). We have performed a Monte Carlo simulation to propagate the errors.

Before studying the effects of the $D\bar{D}$ FSI, we would like to make two remarks:

1. Within the molecular wave-function description of the $X(3872) \to D^0\bar{D}^0\pi^0$ decay, the amplitude of Fig. 8.2(a) reads[10]

$$\begin{aligned}\mathcal{T}_{\rm tree} &\sim \int d^3\vec{q}\ \underbrace{\langle D^0\bar{D}^{*0}(\vec{p}_{D^0})|D^0\bar{D}^{*0}(\vec{q})\rangle}_{\propto\delta^3(\vec{q}-\vec{p}_{D^0})} \times \\ &\qquad \times\langle D^0\bar{D}^{*0}(\vec{q})|X(3872)\rangle\mathcal{T}_{\bar{D}^{*0}(\vec{p}_{\bar{D}^{*0}})\to\bar{D}^0\pi^0} \\ &= \Psi(\vec{p}_{D^0})\mathcal{T}_{\bar{D}^{0*}(\vec{p}_{\bar{D}^{0*}})\to\bar{D}^0\pi^0},\end{aligned} \tag{8.3.8}$$

   with $\vec{p}_{\bar{D}^{0*}} = -\vec{p}_{D^0}$ in the laboratory frame. Note that this description is totally equivalent to that of Eq. (8.3.2) because the $D^0\bar{D}^{*0}$ component of the non-relativistic $X(3872)$ wave-

[10] For simplicity, we omit the contribution to the amplitude driven by the $D^{*0}\bar{D}^0$ component of the $X(3872)$ resonance, for which the discussion will run in parallel.

function is given by [99]

$$\Psi(\vec{p}_{D^0}) = \frac{g_0^X}{E_{D^0} + E_{\bar{D}^{*0}} - M_{D^0} - M_{D^{*0}} - \vec{p}^{\,2}_{D^0}/2\mu_{D^0D^{*0}}} = \\ = \frac{g_0^X}{E_{\bar{D}^{*0}} - M_{D^{*0}} - \vec{p}^{\,2}_{\bar{D}^{*0}}/2M_{D^{*0}}}, \tag{8.3.9}$$

with $\mu^{-1}_{D^0D^{*0}} = M^{-1}_{D^0} + M^{-1}_{D^{*0}}$. In the last step, we have used that the D^0 meson is on-shell and therefore $\left(E_{D^0} - M_{D^0} - \vec{p}^{\,2}_{D^0}/2M_{D^0}\right) = 0$. Thus, the wave function in momentum space turns out to be proportional to the coupling g_0^X times the non-relativistic reduction, up to a factor $2M_{D^{*0}}$, of the $\bar{D}^{*0}$ propagator that appears in Eq. (8.3.2).

The amplitude in Eq. (8.3.8) involves the $X(3872)$ wave function at a given momentum, $\vec{p}_{D^0}$, and the total decay width depends on the wave function in momentum space evaluated only for a limited range of values of $\vec{p}_{D^0}$ determined by energy-momentum conservation. This is in sharp contrast to the decay amplitude into charmonium states, as shown in Fig. 8.1, in Eq. (8.1.1), where there is an integral over all possible momenta included in the wave function. Such an integral can be thought of as a Fourier transform at $\vec{x} = 0$, and thus gives rise to the $X(3872)$ wave function in coordinate space at the origin. This is to say, the width is proportional to the probability of finding the $D\bar{D}^*$ pair at zero (small in general) relative distance within the molecular $X(3872)$ state. This result is intuitive, since the $D\bar{D}^*$ transitions to final states involving charmonium mesons should involve the exchange of a virtual charm quark, which is only effective at short distances. However, in the $X(3872) \to D^0\bar{D}^0\pi^0$ process, the relative distance of the $D\bar{D}^*$ pair can be as large as allowed by the size of the $X(3872)$ resonance, since the final state is produced by the one body decay of the $\bar{D}^*$ meson instead of by a strong two body transition. Thus, this decay channel might provide details on the long-distance part of the $X(3872)$ wave function. Indeed, it follows from Eq. (8.3.8) that a future measurement of the $d\Gamma/d|\vec{p}_{D^0}|$ distribution might provide valuable information on the $X(3872)$ wave-function $\Psi(\vec{p}_{D^0})$.

2. So far, we have not made any reference to the isospin nature of the $X(3872)$ resonance. We have just used the coupling, g_0^X, of the resonance to the $D^0\bar{D}^{0*}$ pair. In addition to the $J/\Psi\pi^+\pi^-\pi^0$ final state, the $X(3872)$ decay into $J/\Psi\pi^+\pi^-$ was also observed [195, 196], pointing out to an isospin violation, at least, in its decays [145]. In the $D\bar{D}^*$ molecular picture, the isospin breaking effects arise due to the mass difference between the $D^0\bar{D}^{*0}$ pair and its charged counterpart, the $D^+\bar{D}^{*-}$ pair, which turns out to be relevant because of the closeness of the $X(3872)$ mass to the D^0D^{*0} threshold [99, 103, 145]. The observed isospin violation in the decays $X(3872) \to \rho J/\psi$, and $X(3872) \to \omega J/\psi$ depends on the probability amplitudes of both the neutral and charged meson channels near the origin which are very similar [99]. This suggests that, when dealing with these strong processes, the isospin $I = 0$ component will be the most relevant, though the experimental value of the isospin violating ratio, $R_{X(3872)}$, of decay amplitudes could be used to learn details on the weak $D\bar{D}^*$ interaction in the isovector channel (C_{1X} in Eq. (8.2.2)). The $X(3872) \to D^0\bar{D}^0\pi^0$ decay mode can shed more light into the isospin dynamics of the $X(3872)$ resonance, since it can be used to further constrain the isovector sector of the $D\bar{D}^*$ interaction. This is already the case at tree level because the numerical value of the coupling g_0^X is affected by the interaction in the isospin one channel, C_{1X}.

We should also stress that in absence of FSI effects that will be discussed below, if C_{1X} is neglected, as in Ref. [99], the $X(3872) \to D^0\bar{D}^0\pi^0$ width will be practically the same

independent from whether the $X(3872)$ is considered as an isoscalar molecule or a $D^0\bar{D}^{*0}$ state. In the latter case, the width would be proportional to $\tilde{g}^2$ [99],

$$\tilde{g}^2 = -\left(\frac{dG_0}{dE}\right)^{-1}\Bigg|_{E=M_{X(3872)}}, \tag{8.3.10}$$

$$G_0(E) = \int_\Lambda \frac{d^3\vec{q}}{(2\pi)^3}\frac{1}{E - M_{D^0} - M_{D^{*0}} - \vec{q}^{\,2}/2\mu_{D^0D^{*0}}}, \tag{8.3.11}$$

where $G_0(E)$ is the UV regularized $D^0\bar{D}^{*0}$ loop function[11]. However, if the $X(3872)$ were an isoscalar state,

$$|X(3872)\rangle = \frac{1}{\sqrt{2}}\left(|D^0\bar{D}^{*0}\rangle + |D^+D^{*-}\rangle\right), \tag{8.3.12}$$

one, naively, would expect to obtain a width around a factor two smaller, because now the coupling of the $X(3872)$ state to the $D^0\bar{D}^{*0}$ pair would be around a factor $\sqrt{2}$ smaller as well [99]

$$\left(g_0^X\right)^2 \simeq \left(g_c^X\right)^2 \simeq -\left(\frac{dG_0}{dE} + \frac{dG_c}{dE}\right)^{-1}\Bigg|_{E=M_X}, \tag{8.3.13}$$

where G_c is the loop function in the charged charm meson channel. The approximations would become equalities if the isovector interaction is neglected (it is much smaller than the isoscalar one as can be seen in Eq. (8.2.3)). Were $\frac{dG_0}{dE} \simeq \frac{dG_c}{dE}$, the above values would be equal to $\tilde{g}^2/2$ approximately. However, after considering the mass differences between the neutral and charged channels and, since $\frac{dG_i}{dE} \propto 1/\sqrt{B_i}$ [$B_i > 0$ is the binding energy of either the neutral (~ 0.2 MeV) or charged (~ 8 MeV) channels], at the mass of the $X(3872)$ one actually finds

$$\left(\frac{dG_0}{dE}\right)\Bigg|_{E=M_X} \gg \left(\frac{dG_c}{dE}\right)\Bigg|_{E=M_X} \tag{8.3.14}$$

so that $\left(g_0^X\right)^2 \simeq \tilde{g}^2$. Therefore, the prediction for the decay width would hardly change.

All these considerations are affected by the $D\bar{D}$ FSI effects which will be discussed next.

8.3.2 $D\bar{D}$ FSI Effects

To account for the FSI effects, we include in the analysis the $D\bar{D} \to D\bar{D}$ T-matrix, which is obtained by solving the LSE in coupled channels with the $V_{D\bar{D}}$ potential given in Eq. (8.2.6). We use the physical masses of the neutral ($D\bar{D}$) and charged (D^+D^-) channels. Thus, considering both the $D^0\bar{D}^{*0}$ and $D^{*0}\bar{D}^0$ meson pairs as intermediate states, the decay amplitude for the mechanism depicted in Fig. 8.2(b) reads

$$\begin{aligned}\mathcal{T}^{(0)}_{\rm loop} &= -16i\frac{gg_0^X}{f_\pi}\sqrt{M_X}M_{D^{*0}}M_{D^0}^3\,\vec{\epsilon}_X\cdot\vec{p_\pi} \\ &\quad T_{00\to00}(m_{23})\,I(M_{D^{*0}}, M_{D^0}, M_{D^0}, \vec{p}_\pi),\end{aligned} \tag{8.3.15}$$

[11] Notice that although the loop function is linearly divergent, its derivative with respect E is convergent, and thus it only shows a residual (smooth) dependence on γ/Λ if a Gaussian cutoff is used, with $\gamma^2 = 2\mu_{D^0D^{*0}}(M_{D^0} + M_{D^{*0}} - M_X)$. Were a sharp cutoff used, there would be no any dependence on the cutoff because of the derivative.

where $T_{00\to 00}$ is the T-matrix element for the $D^0\bar{D}^0 \to D^0\bar{D}^0$ process, and the three-point loop function is defined as

$$I\left(M_1, M_2, M_3, \vec{p}_\pi\right) = i\int \frac{d^4q}{(2\pi)^4} \frac{1}{q^2 - M_1^2 + i\varepsilon} \frac{1}{(P-q)^2 - M_2^2 + i\varepsilon} \frac{1}{(q-p_\pi)^2 - M_3^2 + i\varepsilon}, \tag{8.3.16}$$

with $P^\mu = (M_X, \vec{0})$ in the rest frame of the $X(3872)$. This loop integral is convergent. Since all the intermediate mesons in the present case are highly non-relativistic, the three-point loop can be treated non-relativistically. The analytic expression for this loop function at the leading order of the non-relativistic expansion can be found in Eq. (A2) of Ref. [197] (see also Ref. [44]). For the specific kinematics of this decay, the loop function in the neutral channel has an imaginary part, which turns out to be much larger than the real one, except in a narrow region involving the highest pion momenta.

Similarly, the amplitude for the mechanism with charged intermediate charm mesons is given by

$$\mathcal{T}^{(c)}_{\text{loop}} = 16i\frac{gg_c^X}{f_\pi}\sqrt{M_X} M_{D^{*0}} M_{D^0} M_{D^\pm}^2\, \vec{\epsilon}_X \cdot \vec{p_\pi} \; T_{+-\to 00}(m_{23})\, I(M_{D^{*\pm}}, M_{D^\pm}, M_{D^\pm}, \vec{p}_\pi), \tag{8.3.17}$$

where $T_{+-\to 00}$ is the T-matrix element for the $D^+D^- \to D^0\bar{D}^0$ process. The loop function is now purely real because the $D^+D^-\pi^0$ channel is closed, and its size is significantly smaller than in the case of the neutral channel. The sign difference between the amplitudes of Eqs. (8.3.15) and (8.3.17) is due to the sign difference between the $D^{*-} \to D^-\pi^0$ and $\bar{D}^{*0} \to \bar{D}^0\pi^0$ transition amplitudes.

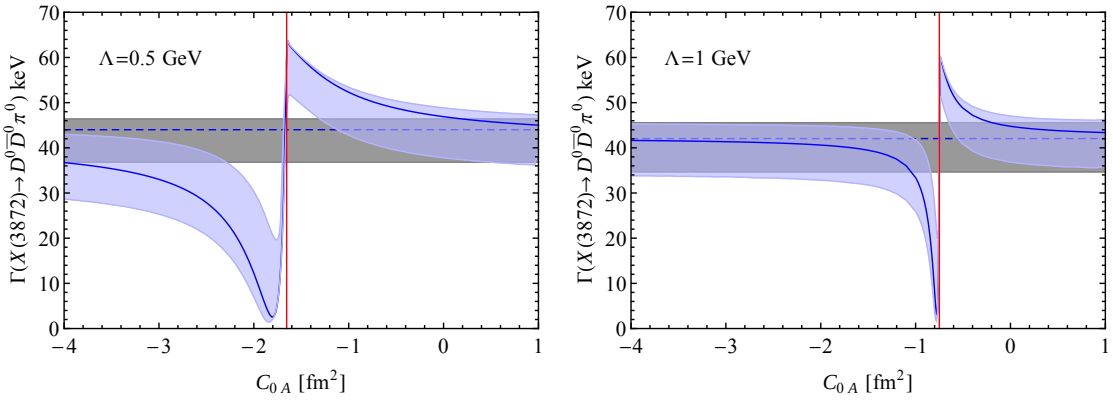

Figure 8.3: *Dependence of the $X(3872) \to D^0\bar{D}^0\pi^0$ partial decay width on the low-energy constant C_{0a}. The UV cutoff is set to $\Lambda = 0.5$ GeV (1 GeV) in the left (right) panel. The blue error bands contain $D\bar{D}$ FSI effects, while the grey bands stand for the tree level predictions of Eq. (8.3.7). The solid (full calculation) and dashed (tree level) lines stand for the results obtained with the central values of the parameters. The vertical lines denote the values of C_{0a} for which a $D\bar{D}$ bound state is generated at the $D^0\bar{D}^0$ threshold.*

For consistency, despite the three-point loop functions in Eqs. (8.3.15)–(8.3.17) being finite, they should however be evaluated using the same UV renormalization scheme as that employed

in the $D^{(*)}\bar{D}^{(*)}$ EFT. The applicability of the EFT relies on the fact that long range physics should not depend on the short range details. Hence, if the bulk of contributions of the loop integrals came mostly from large momenta (above 1 GeV for instance), the calculation would not be significant. Fortunately, this is not the case, and the momenta involved in the integrals are rather low. Indeed, the biggest FSI contribution comes from the imaginary part of the loop function in the neutral channel, which is hardly sensitive to the UV cutoff. Thus and for the sake of simplicity, FSI effects have been calculated using the analytical expressions for the three-point loop integral mentioned above, valid in the $\Lambda \to \infty$ limit. Nevertheless, we have numerically computed these loop functions with 0.5 and 1 GeV UV Gaussian cutoffs and found small differences[12] in the final results [$\Gamma(X(3872) \to D^0\bar{D}^0\pi^0)$ versus C_{0a}] discussed in Fig. 8.3. Indeed, the changes turn out to be almost inappreciable for $\Lambda = 1$ GeV, and they are, at most, of the order of few percent in the $\Lambda = 0.5$ GeV case. Moreover, even then, these differences are well accounted for the error bands shown in the figure.

To compute $T_{00\to 00}$ and $T_{+-\to 00}$ we need the $D\bar{D}$ potential given in Eq. (8.2.6). With the inputs (masses of the $X(3872)$ and $Z_b(10610)$ resonances and the ratio $R_{X(3872)}$) discussed in Section 8.2, three of the four couplings, that describe the heavy meson-antimeson s-wave interaction at LO in the heavy quark expansion, can be fixed. The value of the contact term parameter C_{0a} is undetermined, and thus we could not predict the $D\bar{D}$ FSI effects parameter-free in this $X(3872)$ decay. These effects might be quite large, because for a certain range of C_{0a} values, a near-threshold isoscalar pole could be dynamically generated in the $D\bar{D}$ system [25] (see also Chapter 3).

To investigate the impact of the FSI, in Fig. 8.3 we show the dependence of the partial decay width on C_{0a}. For comparison, the tree-level results are also shown in the same plots. The vertical lines denote the values of C_{0a} when there is a $D\bar{D}$ bound state at threshold. When C_{0a} takes smaller values, the binding energy becomes larger; when C_{0a} takes larger values, the pole moves to the second Riemann sheet and becomes a virtual state. Around the values denoted by the vertical lines, the pole is close to threshold no matter on which Riemann sheet it is. One can see an apparent deviation from the tree-level results in this region. The wavy behaviour is due to the interference between the FSI and the tree-level terms. The existence of a low lying $D\bar{D}$ bound state has, as a consequence, a decrease of the partial decay width to $D^0\bar{D}^0\pi^0$, the reason being that there's a substantial probability of a direct decay to the $D\bar{D}$ bound state and a neutral pion. On the other hand, if there is a virtual state near the threshold, the decay width will increase owing to rescattering effects[13].

When the partial decay width will be measured in future experiments, a significant deviation from the values in Eq. (8.3.7) will indicate a FSI effect, which could eventually be used to extract the value of C_{0a}. Outside the wavy region, the FSI contribution is small, and it will be unlikely to obtain any conclusive information on C_{0a} from the experimental $\Gamma(X(3872) \to D^0\bar{D}^0\pi^0)$ width. However, there exist theoretical hints pointing out the existence of a $D\bar{D}$ bound state close to threshold. In the scheme of Ref. [25] and Chapter 3, the $Z_b(10610)$ mass input was not used. There it was assumed that the $X(3915)$ and $Y(4140)$ were $D^*\bar{D}^*$and $D_s^*\bar{D}_s^*$ molecular states. These two inputs were used to fix completely the heavy meson-antimeson interaction, and a $D\bar{D}$ molecular isoscalar state was predicted at around 3710 MeV. A state in the vicinity of 3700 MeV was also predicted in Ref. [105], within the hidden gauge formalism, using an extension of the $SU(3)$ chiral Lagrangians to $SU(4)$ that implements a particular pattern of $SU(4)$ flavour

[12]The largest changes affect to the charged channel (Fig. 8.2(c)). This is because there, the three meson loop integral is purely real. However this FSI mechanism, as we will discuss below, provides a very small contribution to the total decay width.

[13]The mechanism is analogous, for instance, to the large capture cross-section of thermal neutrons by protons or the near threshold enhancement of deuteron photo-disintegration, both of which are triggered by the existence of a virtual state in the singlet neutron-proton channel.

symmetry breaking. Experimentally, there is support for that resonance around 3720 MeV from the analysis of the $e^+e^- \to J/\psi D\bar{D}$ Belle data [139] carried out in [138]. However, the broad bump observed above the $D\bar{D}$ threshold by the Belle Collaboration in the previous reaction could instead be produced by the $\chi_0(2P)$ state [58, 198].

In Ref. [199], the authors show that the charged component D^+D^{*-} in the $X(3872)$ is essential to obtain a width for the $X(3872) \to J/\psi\gamma$ compatible with the data. In the process studied in this work, at tree-level, the charged component does not directly contribute, though it could indirectly modify the $X(3872)D^0\bar{D}^{*0}$ coupling g_0^X. However, because the $X(3872)$ resonance is placed so close to the $D^0\bar{D}^{*0}$ threshold, we argued that this is not really the case and such a component hardly changes the prediction for the decay width. When the FSI is taken into account, one may ask whether the charged component is important or not, since it can now contribute as the intermediate state which radiates the pion. We find, however, that this contribution plays a small role here, leading to changes of about ten percent at most for the $\Lambda = 0.5$ GeV case, and much smaller when the UV cutoff is set to 1 GeV. These variations are significantly smaller than the uncertainty bands displayed in Fig. 8.3. Therefore, we conclude that the relative importance of the charge component in the $X(3872)$ depends on the process in question. When the observable is governed by the wave function of the $X(3872)$ at the origin, it can be important as the case studied in Ref. [199]. For our case, the decay is more sensitive to the long-distance structure of the $X(3872)$, then the charged component is not as important as the neutral one. At this point, we can also comment on the processes $X(3872) \to D^0\bar{D}^0\gamma$ and $X(3872) \to D^+D^-\gamma$, where the $D\bar{D}$ system has now a negative C parity in contrast to the pionic decay. The decay amplitudes, when neglecting possible contributions from the $\psi(3770)$, are similar to the one in Eq. (8.3.2). Near the $D\bar{D}$ threshold, the intermediate D^{*0} is almost on-shell, and the virtuality of the charged D^* is much larger. Thus, the partial decay width into the $D^+D^-\gamma$ should be much smaller than the one into the $D^0\bar{D}^0\gamma$, see Ref. [191].

Since we published these results in Ref. [5], new high precision measurements of the masses of the D^0 and D^{*0} mesons have become available [200], which have led to a more precise determination of the $X(3872)$ binding energy, $B = 13 \pm 192$ keV. This new determination of $B = 13 \pm 192$ keV makes much more probable the very low binding energies close to zero, or an unbound resonance. In this case, we would like to point out that the decay width should decrease, and eventually should vanish, as the binding energy approaches zero. Because of the quite limited phase space available in this $p-$wave decay, the decay width, however, increases very rapidly as the binding energy departs from zero. In any case, the lower errors displayed in Eq. (8.3.7) and Fig. 8.3 should be now considered with some caution. Moreover, the effect of the D^{*0} width, neglected in the present calculation, becomes sizable for binding energies below 10 keV. The improved experimental information on the $X(3872)$ will be used in the following chapter where we will study hadron and electromagnetic decays of the 2^{++} HQSS partner of the $X(3872)$.

8.4 Conclusions

In this chapter, we have explored the decay of the $X(3872)$ into the $D^0\bar{D}^0\pi^0$ using an effective field theory based on the hadronic molecule assumption for the $X(3872)$. This decay is unique in the sense that it is sensitive to the long-distance structure of the $X(3872)$ as well as the strength of the s-wave interaction between the D and $\bar{D}$. We show that if there is a near threshold pole in the $D\bar{D}$ system, the partial decay width can be very different from the result neglecting the FSI effects. Thus, this decay may be used to measure the so far unknown parameter C_{0a} in this situation. Such information is valuable to better understand the interaction between a heavy-light and a heavy-light antimeson. In view that some of the XYZ states which are

attracting intensive interests are good candidates for the heavy meson hadronic molecules, it is desirable to carry out a precise measurement of that width. It is also worth mentioning that since this decay is sensitive to the long-distance structure, the contribution of the $X(3872)$ charged component ($D^+D^{*-} - D^{*+}D^-$) is not important even when the $D\bar{D}$ FSI is taken into account. We have also discussed how a future measurement of the $d\Gamma/d|\vec{p}_{D^0}|$ distribution might provide valuable information on the $X(3872)$ wave function at the fixed momentum $\Psi(\vec{p}_{D^0})$ as well. This additional knowledge of the wave function of the $X(3872)$ resonance might be essential to disentangle the inner structure of the resonance.

Chapter 9

Decay widths of the spin-2 partners of the $X(3872)$

9.1 Introduction

Within the molecular description of the $X(3872)$, the existence of a X_2 [$J^{PC} = 2^{++}$] s-wave $D^*\bar{D}^*$ bound state was predicted in the EFT approach of Refs. [25] as it has been discussed at length in the previous chapters of this thesis. As a result of the HQSS, the binding energy of the X_2 resonance was found to be similar to that of the $X(3872)$, *i.e.*,

$$M_{X_2} - M_{X(3872)} \approx M_{D^*} - M_D \approx 140 \text{ MeV}. \tag{9.1.1}$$

The existence of such a state was also suggested in Refs. [46, 107, 189, 201, 202]. Both the $X(3872)$ and the X_2, to be denoted by $X_2(4013)$ in what follows, have partners in the bottom sector (see Chapter 5),[1] which we will call X_b and X_{b2}, respectively, with masses approximately related by

$$M_{X_{b2}} - M_{X_b} \approx M_{B^*} - M_B \approx 46 \text{ MeV}. \tag{9.1.2}$$

It is worthwhile to mention that states with 2^{++} quantum numbers exist as well as spin partners of the 1^{++} states in the spectra of the conventional heavy quarkonia and tetraquarks. However, the mass splittings would only accidentally be the same as the fine splitting between the vector and pseudoscalar charmed mesons, see Eq. (9.1.1).[2] For instance, the mass splitting between the first radially excited charmonia with 2^{++} and 1^{++} in the well-known Godfrey–Isgur quark model is 30 MeV [204], which is much smaller than the value in Eq. (9.1.1). In a quark model calculation with screened potential, the $2^{++} - 1^{++}$ mass splitting for the $2P$ charmonia is around 40 MeV [205]. As for the tetraquark states, the corresponding mass splitting predicted in Ref. [206] is 70 MeV, which is again much smaller than $M_{D^*} - M_D$. Notice that it is generally believed that the $\chi_{c2}(2P)$ has been discovered [31, 164], and its mass is much lower than $2M_{D^*}$. Therefore, we conclude that a possible discovery of a 2^{++} charmonium-like state with a mass

[1] In Chapter 5, the bottom and charm sectors are connected by assuming the bare couplings in the interaction Lagrangian to be independent of the heavy quark mass. This assumption will also be used throughout this work.

[2] Were these states due to threshold cusps, the splittings would be the same as those of the hadronic molecules. However, it was shown in Ref. [203] that narrow near threshold peaks in the elastic channel cannot be produced by threshold cusps.

around 4013 MeV as a consequence of HQSS [26] would provide a strong support for the interpretation that the $X(3872)$ is dominantly a $D\bar{D}^*$ hadronic molecule. It is thus very important to search for such a tensor resonance, as well as the bottom analogues, in various experiments and in lattice QCD (LQCD) simulations.

Some exotic hidden charm sectors on the lattice have been recently studied [207, 208, 209, 210, 211], and evidence for the $X(3872)$ from $D\bar{D}^*$ scattering on the lattice has been found [208], while the quark mass dependence of the $X(3872)$ binding energy was discussed in Refs. [212, 213]. The 2^{++} sector has not been exhaustively addressed yet in LQCD, though a state with these quantum numbers and a mass of $(m_{\eta_c} + 1041 \pm 12)$ MeV$= (4025 \pm 12)$ MeV, close to the value we are predicting in the thesis, was reported in Ref. [207]. The simulation used dynamical fermions, novel computational techniques and the variational method with a large basis of operators. The calculations were performed on two lattice volumes with pion mass $\simeq 400$ MeV. There exists also the feasibility study presented in Chapter 4 [2] of future LQCD simulations, where the EFT approach of Chapter 3 [1] was formulated in a finite box.

On the other hand, despite the theoretical predictions on their existence, none of these hypothetical particles has been observed so far. Nevertheless, they are being and will be searched for in current and future experiments such as BESIII, LHCb, CMS, Belle-II and PANDA. It is thus of paramount importance to provide theoretical estimates on their production rates in various experiments, as well as the dominant decay modes and widths.[3] The production of these states in hadron colliders and electron–positron collisions has been studied in Refs. [214, 215]. In this chapter, we will investigate the dominant decay modes of the spin-2 partners of the $X(3872)$, i.e. the $X_2(4013)$ and X_{b2}, and provide an estimate of their decay widths.

Besides, we will also discuss the radiative $X_2 \to D\bar{D}^*\gamma$ and $X_{b2} \to \bar{B}B^*\gamma$ transitions. These decay modes are more sensitive to the long-distance structure of the resonances and might provide valuable details on their wave-functions. The situation is similar to that of the $X(3872) \to D^0\bar{D}^0\pi^0$ decay studied in Chapter 8. Also here, the widths will be affected by the $D\bar{D}^*$ or $B\bar{B}^*$ final state interaction (FSI). FSI effects are expected to be large because they should be enhanced by the presence of the isovector $Z_c(3900)$ and $Z_b(10610)$ resonances located near the $D\bar{D}^*$ and $\bar{B}B^*$ thresholds, respectively. Besides, FSI corrections will be also sensitive to the negative C-parity isoscalar $D\bar{D}^*$ or $\bar{B}B^*$ interaction. Eventually, precise measurements of these radiative decay widths might provide valuable information on the interaction strength in this sector, which would be important in understanding the $P^{(*)}\bar{P}^{(*)}$ system and other exotic systems related to it through heavy quark symmetries.

The structure of the chapter is as follows. First in Sect. 9.2, we briefly discuss the relation of the charm and bottom 2^{++} states with the $X(3872)$ resonance, and in Sect. 9.3 we present our predictions for the $X_2 \to D\bar{D}, D\bar{D}^*$ hadron decays and the $X_{b2} \to B\bar{B}, B\bar{B}^*$ ones in the bottom sector. In Sect. 9.4, the X_2 and X_{b2} radiative decays are investigated, paying special attention to the loop mechanisms responsible for the FSI contributions. The conclusions of this work are outlined in Sect. 9.5 and in addition, there are three additional appendices collected in Sect. 9.6. In the first one (subsect. 9.6.1), we give specific details of the four-heavy-meson contact interaction needed to compute the $D\bar{D}^*$ FSI effects. In Subsect. 9.6.2 we discuss the validity of the perturbative treatment of the $D\bar{D}$ for the X_2. Finally, in Subsect. 9.6.3, we give some details on the evaluation of different three-point loop functions that appear in the computation of the hadronic and radiative decays.

[3] If a resonance is too broad, say $\Gamma \gtrsim 200$ MeV, it would be very difficult to be identified since it is highly nontrivial to distinguish the signal for a broad resonance from various backgrounds.

9.2 HQSFS, the X(3872) resonance and the charm and bottom X_2 states

In this section, we give a brief description of the more important features of our HQSFS scheme and use it to describe some characteristics of the $X(3872)$ and X_2 states.

9.2.1 $X(3872)$

As in the previous chapters, we start assuming the $X(3872)$ to be a positive C-parity $D\bar{D}^*$ bound state, with quantum numbers $J^{PC} = 1^{++}$. We know that for the $X(3872)$, isospin breaking is important [99] as this bound state is especially shallow. As a consequence, the neutral $(D^0\bar{D}^{*0})$ and charged (D^+D^{*-}) channels should be treated independently. The coupled-channel[4] LO contact potential, neglecting OPE effects, in the 1^{++} sector is given by (let us recall Eq.(3.2.29))

$$V_{X(3872)} = \frac{1}{2}\begin{pmatrix} C_{0X}+C_{1X} & C_{0X}-C_{1X} \\ C_{0X}-C_{1X} & C_{0X}+C_{1X} \end{pmatrix}, \tag{9.2.1}$$

with C_{0X} and C_{1X} LECs that need to be fixed from some input. This interaction is used as kernel of the LSE conveniently UV regularized by using a standard Gaussian regulator,

$$T(E;\vec{p}\,',\vec{p}) = V(\vec{p}\,',\vec{p}) + \int \frac{d^3\vec{q}}{(2\pi)^3} V(\vec{p}\,',\vec{q}) \frac{1}{E-\vec{q}^{\,2}/2\mu_{12}-M_1-M_2+i\varepsilon} T(E;\vec{q},\vec{p}) \,, \tag{9.2.2}$$

$$\langle \vec{p}|V|\vec{p}\,'\rangle = C_{IX}\; e^{-\vec{p}^{\,2}/\Lambda^2}\; e^{-\vec{p}\,'^2/\Lambda^2}, \tag{9.2.3}$$

with C_{IX} any of the LECs of Eq. (9.2.1) in the case of the $X(3872)$, or the relevant ones for any other J^{PC} sector and take cutoff values $\Lambda = 0.5 - 1$ GeV.

The LECs C_{0X} and C_{1X} are determined (see again Chapter 3 for the details) from $M_{X(3872)} = (3871.69 \pm 0.17)$ MeV (mass average quoted by the PDG [98]) and the isospin violating ratio of the decay amplitudes for the $X(3872) \to J/\psi\pi\pi$ and $X(3872) \to J/\psi\pi\pi\pi$ decay modes, $R_{X(3872)} = 0.26 \pm 0.07$ [101]. We use in this chapter $m_{D^0} = (1864.84 \pm 0.07)$ MeV, $m_{D^+} = (1869.61 \pm 0.10)$ MeV, $m_{D^{*0}} = (2006.96 \pm 0.10)$ MeV and $m_{D^{*+}} = (2010.26 \pm 0.07)$ MeV [98]. Note that $m_{D^0} + m_{D^{*0}} = (3871.80 \pm 0.12)$ MeV, and the uncertainty in the value of this lowest threshold affects the precision of the $X(3872)$ binding energy. We have taken into account this effect by adding in quadratures the PDG error of the $X(3872)$ mass and that of the neutral channel threshold and assign this new error to the mass of the resonance, that now reads $M_{X(3872)} = (3871.69 \pm 0.21)$ MeV. For the LECs, we obtain[5]:

$$C_{0X} = -1.70^{+0.03}_{-0.07}\; (-0.731^{+0.006}_{-0.015})\,\text{fm}^2, \qquad C_{1X} = -0.09^{+0.54}_{-0.41}\; (-0.38^{+0.12}_{-0.10})\,\text{fm}^2 \,, \tag{9.2.4}$$

for $\Lambda = 0.5(1.0)$ GeV. Errors, at the 68% confidence level (CL), have been obtained from a Monte Carlo (MC) simulation assuming uncorrelated Gaussian distributions for the two inputs $(M_{X(3872)}, R_{X(3872)})$. In the simulation, we have rejected MC samples for which the $X(3872)$ turned out to be unbound, since the scheme we are following only allows to determine the properties of the resonance when it is bound.

[4] Actually, positive C-parity combinations in both the neutral $D^0\bar{D}^{*0}$ and charged $D^+\bar{D}^{*-}$ channels are being considered.

[5] Note the LECs take different values than in the previous chapters because here we have used the most recent update for the D^0, D^{*0}, D^+ and D^{*+} masses in the PDG

9.2.2 $X_2(4013)$: $J^{PC} = 2^{++}$, charm sector

HQSS predicts that the s-wave $D^*\bar{D}^*$ interaction in the 2^{++} sector is, up to corrections suppressed by the charm quark mass, identical to that in the $X(3872)$ sector (1^{++}) and given by Eq. (9.2.1). Thus, in the 2^{++} sector, the potential in the $\left[(D^{*0}\bar{D}^{*0}), (D^{*+}D^{*-})\right]$ coupled channel space reads (see also Chapter 3)

$$V_{2^{++}} = \frac{1}{2}\begin{pmatrix} C_{0X}+C_{1X} & C_{0X}-C_{1X} \\ C_{0X}-C_{1X} & C_{0X}+C_{1X} \end{pmatrix} + \mathcal{O}(q/m_c), \tag{9.2.5}$$

with the same structure and involving the same LECs that in the $X(3872)$ channel. Besides, in the above equation $m_c \sim 1.5$ GeV is the charm quark mass and $q \sim \Lambda_{\rm QCD}$, a scale related to the light degrees of freedom. Taking $\Lambda_{\rm QCD} \sim 300$ MeV [98], corrections of the order of 20% to the interaction predicted by HQSS cannot be discarded. Nevertheless, it seems natural to expect a 2^{++} $D^*\bar{D}^*$ loosely bound state (X_2), the HQSS partner of the $X(3872)$, and located in the vicinity of the $D^{*0}\bar{D}^{*0}$ threshold (~ 4014 MeV), see [25] and Chapters 3 and 5. This is illustrated in the X_2 binding energy distributions depicted in Fig. 9.1. Neglecting the $\mathcal{O}(q/m_c)$ corrections to the LECs, and using those obtained from the $X(3872)$ resonance, we find a clear signal (blue histograms) of a weakly bound state. However, the case is less robust when the latter corrections are taken into account. Thus, because of the additional 20% HQSS uncertainty, the area below the red shaded $\Lambda = 0.5$ GeV ($\Lambda = 1$ GeV) histogram is only 0.77 (0.68). This means that approximately a 23% (32%) of $X(3872)$ events [$(M_{X(3872)}, R_{X(3872)})$ MC samples] do not produce a X_2 pole in the first RS, since the strength of the resulting interaction in the 2^{++} sector would not be attractive enough to bind the state, though a virtual state in the second RS will be generated instead. Given the existence of the $X(3872)$ as a $D\bar{D}^*$ molecule, if the X_2 resonance exists, we would expect its mass (binding energy) to lie most likely in the interval $[2m_{D^{*0}}, 4006$ MeV] ($[0, 8]$ MeV), as shown in Fig. 9.1. Note that the discussion in Chapter 5 was simpler, because there we worked in the isospin symmetric limit and used the averaged masses of the heavy mesons, which are larger than those of the physical D^0 and D^{*0} mesons.

For later use, we also need the couplings of the X_2 to its neutral ($D^{*0}\bar{D}^{*0}$) and charged ($D^{*+}D^{*-}$) components, $g_0^{X_2}$ and $g_c^{X_2}$, respectively. They are defined from the residues of the T-matrix at the pole in the different channels. This is to say,

$$\left(g_0^{X_2}\right) = \lim_{E\to X_2}\left[E - M_{X_2}\right] \times T_{11}(E) \tag{9.2.6}$$

$$\left(g_c^{X_2}\right) = \lim_{E\to X_2}\left[E - M_{X_2}\right] \times T_{22}(E) \tag{9.2.7}$$

The $g_0^{X_2}$ and $g_c^{X_2}$ couplings turn out to be slightly different because the X_2 resonance is an admixture of isospin 0 and 1, since its binding energy is much smaller than the energy difference between the two thresholds [99]. Considering the HQSS uncertainties, we find:

$$10^2 g_0^{X_2} = 1.4^{+1.1}_{-0.4} \ \ (1.5^{+1.1}_{-0.4}) \ \ \text{MeV}^{-1/2}\,, \tag{9.2.8}$$

$$10^2 g_c^{X_2} = 1.5^{+1.4}_{-0.2} \ \ (1.3^{+1.3}_{-0.3}) \ \ \text{MeV}^{-1/2}\,, \tag{9.2.9}$$

for $\Lambda = 0.5(1.0)$ GeV.

9.2.3 X_{b2}: $J^{PC} = 2^{++}$, bottom sector

Owing to the heavy flavour symmetry, the LO 2^{++} $B^*\bar{B}^*$ interaction is given by Eq. (9.2.5) as well, and thus we should also expect a 2^{++} $B^*\bar{B}^*$ bound state (X_{b2}), the HQSFS partner of the

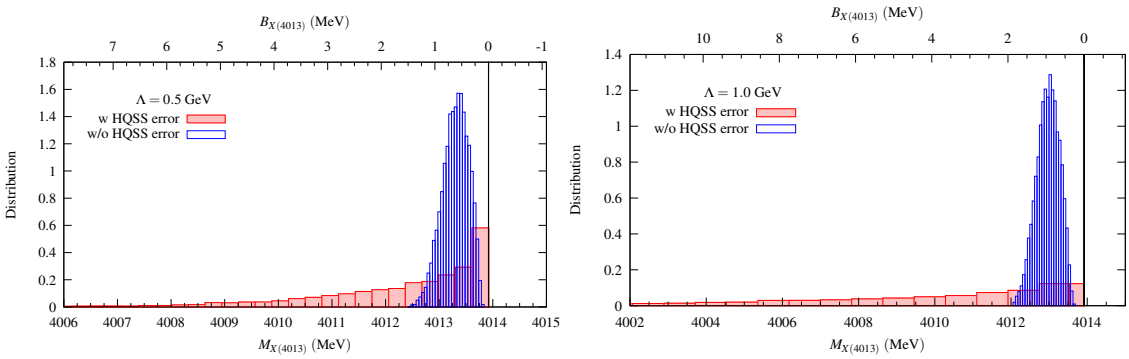

Figure 9.1: *X_2 binding energy histograms obtained from the interaction of Eq. (9.2.5) using LECs distributions determined from the $X(3872)$ resonance inputs (blue) or using LECs distributions additionally modified to account for the HQSS systematic error (red). Left and right plots correspond to UV cutoffs of 0.5 and 1 GeV, respectively. MC sample $(C_{0X}+C_{1X}, C_{0X}-C_{1X})$ pairs fitted to the input $(M_{X(3872)}, R_{X(3872)})$ distributions are first generated and are used to evaluate the X_2 mass. $X(3872)$ mass trials above threshold are rejected. To evaluate the red shaded histogram, and to account for the HQSS 20% uncertainty in the 2^{++} interaction, each of the members of any MC sample $(C_{0X}+C_{1X}, C_{0X}-C_{1X})$ pair is multiplied by independent $N(\mu=1,\sigma=0.2)$ Gaussian distributed random quantities $r_\pm$.*

$X(3872)$, located close to the $B^*\bar{B}^*$ threshold ($\sim$ 10650 MeV) (Chapter 5). The X_{b2} binding energy distributions are shown in Fig. 9.2 for the two UV cutoffs employed in this work. We have used the same masses for the neutral and charged mesons, $m_B = (m_{B^0}+m_{B^+})/2 = 5279.42$ MeV and $m_{B^*} = 5325.2$ MeV. Note that, according to the PDG [98], $|(m_{B^{*0}}-m_{B^0})-(m_{B^{*+}}-m_{B^+})| <$ 6 MeV CL=95.0%, and $m_{B^0} - m_{B^+} = (0.32 \pm 0.06)$ MeV, from where we might expect isospin breaking effects for the B^* mesons to be significantly smaller than in the charm sector. With the bottom mesons being much heavier than their charmed cousins, the expected X_{b2} binding energy is significantly larger than in the charm sector, around a few tens of MeV, and thus we do not expect any significant isospin breaking effects and the X_{b2} resonance would be a pure isoscalar ($I = 0$) state.

As can be seen in Fig. 9.2, in this case we have a robust prediction even when HQSS uncertainties (20%) are taken into account. We obtain the mass and the coupling from the residue at the pole for $\Lambda = 0.5$ (1.0) GeV:

$$E_{X_{b2}} = 10631^{+7}_{-8}\left(10594^{+22}_{-26}\right)\text{MeV}, \qquad 10^2 g^{X_{b2}} = 5.9^{+2.9}_{-1.9}\left(6.4^{+2.8}_{-2.0}\right)\text{MeV}^{-1/2}. \tag{9.2.10}$$

This bound state, being isoscalar, equally couples to the neutral and charged components and, therefore: $g_0^{X_{b2}} = g_c^{X_{b2}} = \frac{1}{\sqrt{2}} g^{X_{b2}}$. Our predictions in Eq. (9.2.10), both for the mass and the $B^*\bar{B}^*$ coupling of the resonance show some dependence on the UV cutoff, which is to some extent diminished when HQSS uncertainties are taken into account. Nevertheless, this Λ dependence might hint to non-negligible subleading corrections (among others, pion exchange and coupled channel effects [25], which can be larger here than in the charm sector due to the larger binding energy and larger meson masses). We will compute the decay widths for both UV regulators, and the spread of results will account for this source of uncertainty.

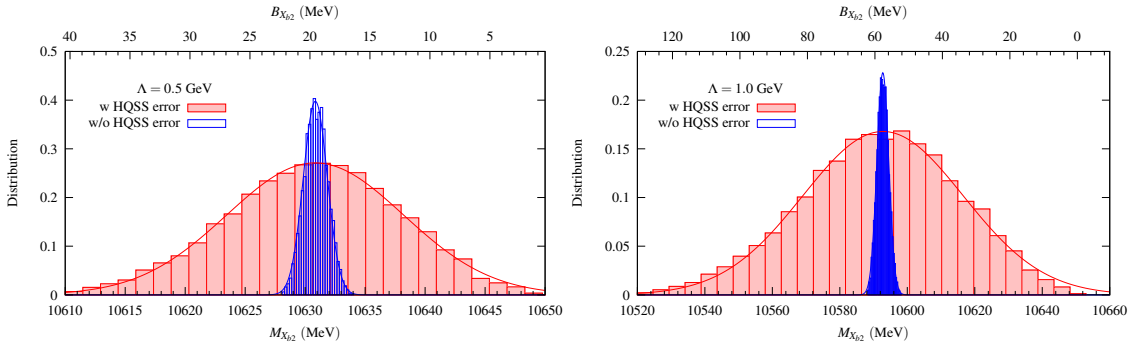

Figure 9.2: *Same as in Fig. 9.1 but in the bottom sector. To better appreciate the distribution details, the $\Lambda = 0.5$ (1) GeV red histogram, which includes the 20% HQSS error, has been multiplied by a factor of 5 (10).*

9.3 The hadronic X_2 and X_{b2} decays

The quantum numbers, $J^{PC} = 2^{++}$, of these resonances constrain their possible decay channels. In this chapter, for hadronic modes we only consider the decays into two heavy hadrons: $X_2 \to D\bar{D}$ and $X_2 \to D\bar{D}^*(D^*\bar{D})$, and the analogous processes $X_{b2} \to B\bar{B}$ and $X_{b2} \to B\bar{B}^*(B^*\bar{B})$. We expect that these d-wave decay modes should largely saturate the widths of these states. Because the $D\bar{D}$ couples in a d-wave to the 2^{++} system, its contribution to the mass renormalization of the X_2 is of higher order (see discussion in Subsect. 9.6.2 below). We thus did not include the $D\bar{D}$ as a coupled channel in the T-matrix, but treat it perturbatively. This means that the transitions are mediated by the exchange of a pion. The relevant $\pi P^{(*)} P^{(*)}$ vertices are taken from the LO Lagrangian of heavy meson chiral perturbation theory [89, 90, 92, 93] (see Subsect. 2.3.2). At LO, besides the pion decay constant, $f_\pi = 92.2$ MeV, there appears only one additional $D^* D\pi$ coupling (g). We take $g = 0.570 \pm 0.006$ as inferred from the new value of $\Gamma = (83.4 \pm 1.8)$ keV for the D^{*+} decay width quoted by the PDG [98]. This is mostly determined by the recent BABAR Collaboration measurement [216] of this width, which is approximately a factor 12 times more precise than the previous value, $\Gamma = (96 \pm 4 \pm 22)$ keV by the CLEO Collaboration [217]. Thus, we end up with an uncertainty of the order 1% for g. Though the hadronic X_2 and X_{b2} widths evaluated in this section will be proportional to g^4, this source of error ($\sim 4\%$) will be much smaller than others and it will be ignored in what follows.

9.3.1 Charm decays

$X_2(4013) \to D\bar{D}$

We will first consider the $X_2(4013) \to D^+ D^- (D^0 \bar{D}^0)$ decay, which proceeds through the Feynman diagrams depicted in Fig. 9.3. We treat charm mesons non-relativistically, and neglect $p_{D^*,\bar{D}^*}/m_{D^*}$ terms and the temporal components in the $D^*, \bar{D}^*$ propagators. We obtain for the $X_2(4013) \to D^+ D^-$ process, in the resonance rest frame and with q and k the 4-momenta of the

	without pion-exchange FF		with pion-exchange FF	
	$\Lambda = 0.5$ GeV	$\Lambda = 1$ GeV	$\Lambda = 0.5$ GeV	$\Lambda = 1$ GeV
$\Gamma(X_2 \to D^+D^-)$ [MeV]	$3.3^{+3.4}_{-1.4}$	$7.3^{+7.9}_{-2.1}$	$0.5^{+0.5}_{-0.2}$	$0.8^{+0.7}_{-0.2}$
$\Gamma(X_2 \to D^0\bar{D}^0)$ [MeV]	$2.7^{+3.1}_{-1.2}$	$5.7^{+7.8}_{-1.8}$	$0.4^{+0.5}_{-0.2}$	$0.6^{+0.7}_{-0.2}$
$\Gamma(X_2 \to D^+D^{*-})$ [MeV]	$2.4^{+2.1}_{-1.0}$	$4.4^{+3.1}_{-1.2}$	$0.7^{+0.6}_{-0.3}$	$1.0^{+0.5}_{-0.2}$
$\Gamma(X_2 \to D^0\bar{D}^{*0})$ [MeV]	$2.0^{+2.1}_{-0.9}$	$3.5^{+3.5}_{-1.0}$	$0.5^{+0.6}_{-0.2}$	$0.7^{+0.5}_{-0.2}$

Table 9.1: *$X_2(4013) \to D\bar{D}, D\bar{D}^*$ decay widths using different UV Gaussian regulators for the $D^*\bar{D}^*X_2$ form factor and with/without including a pion-exchange vertex form factor (FF) in each of the $D^*D\pi$ and $D^*D^*\pi$ vertices in the three-point loop function. The decay widths of the $X_2(4013) \to \bar{D}D^*$ modes are the same thanks to C-parity. Uncertainties are obtained from a Monte Carlo simulation using the X_2 binding energy histograms displayed in Fig. 9.1 (red shaded) and the $g_0^{X_2}$ and $g_c^{X_2}$ couplings given in Eqs. (9.2.8) and (9.2.9). Note that the procedure takes into account 20% HQSS uncertainties and the correlations between X_2 masses (binding energies) and $g_0^{X_2}$ and $g_c^{X_2}$ couplings. Errors on the widths provide 68% CL intervals.*

D and $\bar{D}$ final mesons ($\vec{q} = -\vec{k}$, $q^0 + k^0 = M_{X_2}$),

$$
\begin{aligned}
-i\,\mathcal{T}(\lambda)_{D^+D^-} \;&=\; -\frac{Ng^2}{f_\pi^2}\epsilon_{ij}(\lambda)\cdot \\
&\left\{ g_c^{X_2}\int \frac{d^4l}{(2\pi)^4}\,\frac{l^i\,l^j}{\left[(l+q)^2 - m_{D^{*+}}^2 + i\varepsilon\right]\left[(k-l)^2 - m_{D^{*-}}^2 + i\varepsilon\right]\left(l^2 - m_{\pi^0}^2 + i\varepsilon\right)}\right. \\
&\left. +2g_0^{X_2}\int \frac{d^4l}{(2\pi)^4}\,\frac{l^i\,l^j}{\left[(l+q)^2 - m_{D^{*0}}^2 + i\varepsilon\right]\left[(k-l)^2 - m_{\bar{D}^{*0}}^2 + i\varepsilon\right]\left(l^2 - m_{\pi^-}^2 + i\varepsilon\right)}\right\} \\
&= i\frac{Ng^2}{f_\pi^2}\epsilon_{ij}(\lambda)\left\{ g_c^{X_2} I^{ij}(m_{D^{*+}}, m_{\pi^0}; M_{X_2}, q^\mu) + 2g_0^{X_2} I^{ij}(m_{D^{*0}}, m_{\pi^-}; M_{X_2}, q^\mu)\right\},
\end{aligned}
\tag{9.3.1}
$$

where $\epsilon_{ij}(\lambda)$ is the symmetric spin-2 tensor with λ denoting the polarization of the X_2 state and $N = \sqrt{8M_{X_2}m_{D^*}^2}\left(\sqrt{m_D m_{D^*}}\right)^2$ accounts for the normalization of the heavy meson fields[6] and some additional factors needed when the couplings $g_{c,0}^{X_2}$, as determined from the residues at the pole of the EFT T-matrix, are used for the $X_2D^*\bar{D}^*$ vertex. For the neutral and charged pion masses, we have used the values quoted by the PDG [98] and heavy meson isospin averaged masses to compute N. Besides, I^{ij} is a three-point loop function, the detailed evaluation of which is relegated to the Appendix of Subsect. 9.6.3.[7] The loop is seemingly logarithmically divergent. However, since the X_2 polarization is traceless, the divergent part which comes with a Kronecker delta does not contribute. This is because the decay occurs in a d-wave, thus the loop momentum is converted to external momenta, and the remaining part of the integral is convergent. Nevertheless, we will include two different form factors in the computation of the three-point loop function. One is inherited from the UV regularization/renormalization

[6] As already mentioned in previous chapters we use a non-relativistic normalization for the heavy mesons, which differs from the traditional relativistic one by a factor $\sqrt{M_H}$.

[7] In the computation of I^{ij}, we are consistent with the former approximations, and we use non-relativistic charm meson propagators.

procedure sketched in Eq. (9.2.3) and employed to render the LSE T-matrix finite. In addition, we will include a second form factor to account for the large virtuality of the pion in the loop. We will discuss this at length below and in Subsect. 9.6.3.

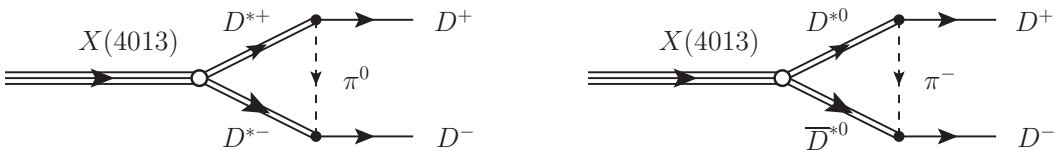

Figure 9.3: *Feynman diagrams for the $X_2(4013) \to D^+D^-$ decay. Diagrams for the $X_2(4013) \to D^0\bar{D}^0$ transition are similar, with the appropriate changes of the exchanged pion charges.*

Analogously, the $X_2(4013) \to D^0\bar{D}^0$ amplitude is,

$$-i\,\mathcal{T}(\lambda)_{D^0\bar{D}^0} = i\frac{Ng^2}{f_\pi^2}\epsilon_{ij}(\lambda)\cdot \Big\{2g_c^{X_2} I^{ij}(m_{D^{*+}}, m_{\pi^+}; M_{X_2}, q^\mu) + g_0^{X_2} I^{ij}(m_{D^{*0}}, m_{\pi^0}; M_{X_2}, q^\mu)\Big\}\,. \tag{9.3.2}$$

The two-body decay width in the X_2 rest-frame reads [98]:

$$\frac{d\Gamma_a}{d\Omega(\hat{q})} = \frac{1}{5}\sum_\lambda |\mathcal{T}(\lambda)_a|^2 \frac{|\vec{q}|}{32\pi^2 M_{X_2}^2}, \qquad a = D^+D^-,\ D^0\bar{D}^0\ . \tag{9.3.3}$$

The sum over the X_2 polarizations can be easily done in the c.m. frame,

$$\sum_\lambda \epsilon_{mn}(\lambda)\epsilon_{ij}^*(\lambda) = \frac{1}{2}\left[\delta_{mi}\delta_{nj} + \delta_{ni}\delta_{mj} - \frac{2}{3}\delta_{mn}\delta_{ij}\right], \quad m,n,i,j = 1,2,3\ . \tag{9.3.4}$$

As discussed in Appendix 9.6.3, the three-point loop function has a tensor structure of the type

$$I^{ij}(\vec{q}) = I_0(\vec{q}^2)\, q^i q^j + I_1(\vec{q}^2)\,\delta^{ij}\,|\vec{q}|^2\ . \tag{9.3.5}$$

The I_1 term carries the UV divergence, which however does not contribute to the width, because it vanishes after the contraction with the traceless spin-2 polarization tensor. Therefore, only the I_0 term is relevant, which is free of UV divergences. Moreover, the contraction of $I^{ij}(\vec{q})\, I^{mn}(\vec{q})$ with $\sum_\lambda \epsilon_{mn}(\lambda)\epsilon_{ij}^*(\lambda)$ [Eq. (9.3.4)] leads to a factor of $2\vec{q}^4/3$. Thus, the integration over the solid angle $d\Omega(\hat{q})$ trivially gives 4π, and the width scales like $|\vec{q}|^5$ as expected for a d-wave process.

Our predictions for the $X_2(4013) \to D^+D^-, D^0\bar{D}^0$ decays are compiled in the Table 9.1. If we look at the first two columns of results in the table, we find widths of the order of a few MeV, with asymmetric errors that favour larger values. This is mostly due to the similar asymmetry of the uncertainties quoted for the $g_0^{X_2}$ and $g_c^{X_2}$ couplings in Eqs. (9.2.8) and (9.2.9).

Our scheme is based on a low-energy EFT, in which the momenta should be smaller than a hard scale which serves as a momentum cutoff [see Eq. (9.2.3)]. The high-momentum modes are out of control in the low-energy EFT. Therefore in the computation of the width, we include a Gaussian regulator at the $D^*\bar{D}^*X_2$ vertex, as discussed in Eq. (9.6.17). The cutoff should be the same as the one used in generating the X_2 as it is related to the same unitary cut in the $D^*\bar{D}^*$ system. In Fig. 9.4, we display, as an example, the dependence of the $I_0(m_{D^{*0}}, m_{\pi^0}; M_{X_2}, q^\mu[m_{F_1} = m_{F_2} = m_{D^0}])$ integrand [see Eqs. (9.6.17)-(9.6.18)] on the pion

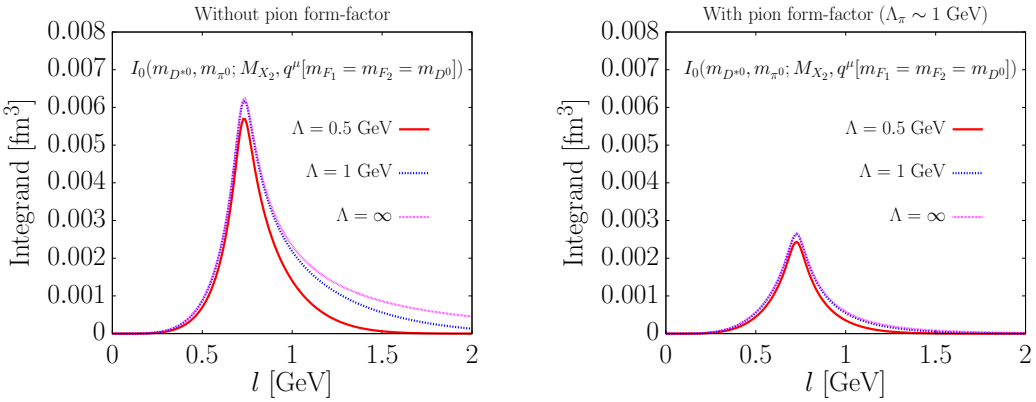

Figure 9.4: *Dependence of the* $I_0(m_{D^{*0}}, m_{\pi^0}; M_{X_2}, q^\mu[m_{F_1} = m_{F_2} = m_{D^0}])$ *integrand [see Eqs.* (9.6.17)-(9.6.18)*] on the pion loop momentum* $|\vec{l}|$*. For the* X_2 *mass we have used* 4013 *MeV. Results with and without the inclusion of the pion form factor [Eq.* (9.6.18)*] squared are presented in the right and left plots, respectively. In both cases, three different choices of the Gaussian regulator [Eq.* (9.6.17)*] in the* $D^*\bar{D}^*X_2$ *vertex have been considered.*

loop momentum. In the left plot we see that in spite of including the Gaussian X_2 form factor, large momenta above 1 GeV provide a sizable contribution to the integral ($\simeq 14\%$, 30% and 45% for $\Lambda = 0.5$ GeV, 1 GeV and ∞, respectively), which is an unwanted feature within the low-energy EFT scheme and signals a sizeable short-distance contribution. Indeed, the momentum of the exchanged pion, peaks at around 750 MeV, which is a somehow large value in the sense that the hard scale for the chiral expansion which controls the pionic coupling is $\Lambda_\chi \sim 1$ GeV. We see that below the peak, the curves for both cutoff values are very close to each other, and they are also close to the curve corresponding to the case without any regulator. This is the region where the low-energy expansion works and thus model-independent conclusions can be made. The curves start deviating from each other after the peak, that is, in the region with a pion momentum $\gtrsim \Lambda_\chi$. Because the loop integrals are not completely dominated by momentum modes well below Λ_χ, the widths of interest will bear an appreciable systematic uncertainty. This is reflected in the fact that the widths in the second column in Table 9.1 are larger than those in the first column by a factor around 2.[8]

On the other hand, the fact that the pion could be quite far off-shell should be reflected in the $D^*D\pi$ vertex, which should be corrected, similarly as it is done in the case of the $NN\pi$ one. Thus, to give an estimate of the hadronic decay widths, in the spirit of the Bonn potential [218], we have included a monopole pion-exchange vertex form factor, with a hadron scale of the order of 1 GeV, in each of the $D^*D\pi$ vertices [Eq. (9.6.18)]. Its effect on the internal pion momentum dependence of the $I_0(m_{D^{*0}}, m_{\pi^0}; M_{X_2}, q^\mu[m_{F_1} = m_{F_2} = m_{D^0}])$ integrand is shown in the right plot of Fig. 9.4. The large pion momenta contribution ($|\vec{l}| > 1$ GeV), which is not reliable in a low-energy EFT calculation, is reduced now to 6.5%, 13% and 16% for $\Lambda = 0.5$ GeV, 1 GeV and ∞, respectively. This makes also more appropriate the non-relativistic treatment of the charmed mesons adopted here. Besides, the dependence of the width on the UV Gaussian regulator is significantly softer, though the widths are further reduced by almost an order of magnitude.

We believe that the most realistic estimates are those obtained with the inclusion of the

[8]Note that the coupling constants obtained with both cutoffs are similar, see Eqs. (9.2.8) and (9.2.9), and thus the difference should come mainly from the loop integration.

pion-exchange form factor and the spread of results compiled in the Table 9.1 give a conservative estimate of the systematic uncertainties, beyond the mere existence of the $X_2(4013)$ state, as discussed in Sect. 9.2.2. We remind here that because of the additional 20% HQSS uncertainty, approximately a 23% (for $\Lambda = 0.5$ GeV, 32% for $\Lambda = 1$ GeV) of the $X(3872)$ events $[(M_{X(3872)}, R_{X(3872)})$ MC samples] do not produce the X_2 as a bound state pole, since the strength of the resulting interaction in the 2^{++} sector is not attractive enough to bind the $D^*\bar{D}^*$.

Nevertheless, assuming the existence of the X_2 state, and in view of the results given in Table 9.1, we estimate the $X_2 \to D\bar{D}$ partial width (including both the charged and neutral channels) to be

$$\Gamma(X_2 \to D\bar{D}) = \left(1.2 \pm \underbrace{0.3}_{\text{sys}\,(\Lambda)} {}^{+1.3}_{-0.4}\right) \text{ MeV}. \tag{9.3.6}$$

where the first error accounts for the dependence on the UV Gaussian regulator used in the $D^*\bar{D}^*X_2$ vertex, while the second one is obtained from the uncertainties given in Table 9.1. This latter error includes both some additional systematic (HQSS violations) and statistical ($X(3872)$ input used to fix the properties of the X_2 resonance) uncertainties. Notice that, as discussed above, the calculation is probably already beyond the valid range of the EFT due to the large contribution of high-momentum modes. We thus have adopted a more phenomenological strategy and used the pion-exchange form factor with a cutoff of 1 GeV to make an estimate of the decay widths. The values presented in Eq. (9.3.6) refer only to the last columns in Table 9.1 with a pion-exchange form factor.

$X_2(4013) \to D\bar{D}^*(D^*\bar{D})$

Here, we will study the D^+D^{*-}, and $D^0\bar{D}^{*0}$ channels, which proceeds through the Feynman diagrams depicted in Fig. 9.5. This is also a d-wave decay so that both angular momentum and parity are conserved. The decay widths are expected to be comparable to those found for the $X_2(4013) \to D\bar{D}$ decays, despite the phase space is considerably more reduced. This extra enhancement is caused by the extra multiplicity due to the spin of the final $D^*(\bar{D}^*)$ meson.

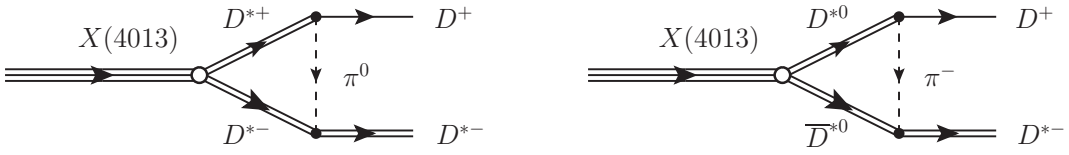

Figure 9.5: *Feynman diagrams for the $X_2(4013) \to D^+D^{*-}$ decay. Diagrams for the $X_2(4013) \to D^0\bar{D}^{*0}$ transition are similar, with the appropriate changes of the exchanged pion charges.*

As commented before, we treat charm mesons non-relativistically and obtain the decay amplitude for the $X_2(4013) \to D^+D^{*-}$ process as

$$\begin{aligned}\mathcal{T}(\lambda,\lambda_*)_{D^+D^{*-}} &= i\,\frac{N^* g^2}{f_\pi^2}\epsilon_{ij}(\lambda)\epsilon_{mnj}\epsilon^{*n}(\lambda_*)\Big\{g_c^{X_2} I^{im}(m_{D^{*+}}, m_{\pi^0}; M_{X_2}, q^\mu) \\ &\quad + 2g_0^{X_2} I^{im}(m_{D^{*0}}, m_{\pi^-}; M_{X_2}, q^\mu)\Big\}\,,\end{aligned} \tag{9.3.7}$$

in the resonance rest frame. Here, q is the 4-momenta of the D^+ meson, and $\epsilon^n(\lambda^*)$ is the polarization vector of the final D^{*-} meson with helicity λ_*, $N^* = \sqrt{8M_{X_2}m_{D^*}^2}\sqrt{m_D m_{D^*}^3}$ and ϵ_{imn}

is the 3-dimensional Levi-Civita antisymmetric tensor. Analogously, the $X_2(4013) \to D^0\bar{D}^{*0}$ amplitude is,

$$\begin{aligned}\mathcal{T}(\lambda,\lambda_*)_{D^0D^{*0}} &= i\,\frac{N^* g^2}{f_\pi^2}\epsilon_{ij}(\lambda)\epsilon_{mnj}\epsilon^{*n}(\lambda_*)\Big\{2g_c^{X_2} I^{im}(m_{D^{*+}}, m_{\pi^+}; M_{X_2}, q^\mu) \\ &\quad + g_0^{X_2} I^{im}(m_{D^{*0}}, m_{\pi^0}; M_{X_2}, q^\mu)\Big\}. \end{aligned} \tag{9.3.8}$$

The two-body decay width in the X_2 rest-frame in this case reads [98]:

$$\frac{d\Gamma_a}{d\Omega(\hat{q})} = \frac{1}{5}\sum_{\lambda,\lambda_*} |\mathcal{T}(\lambda,\lambda_*)_a|^2 \,\frac{|\vec{q}|}{32\pi^2 M_{X_2}^2}, \qquad a = D^+D^{*-}, D^0\bar{D}^{*0}\ . \tag{9.3.9}$$

The sum over the $\bar{D}^*$ and X_2 polarizations can be easily done, and we get

$$\begin{aligned}\sum_\lambda \epsilon_{ij}(\lambda)\epsilon^*_{rs}(\lambda)\sum_{\lambda_*}\epsilon^{*n}(\lambda_*)\epsilon^p(\lambda_*)\epsilon_{mnj}\epsilon_{lps} &= \frac{1}{6}\left[7\delta_{ml}\delta_{ir} + 2\delta_{il}\delta_{rm} - 3\delta_{lr}\delta_{mi}\right], \\ & \qquad i,l,m,r = 1,2,3\ . \end{aligned} \tag{9.3.10}$$

The above tensor structure should be contracted with $I^{im}(\vec{q})\, I^{rl}(\vec{q})$. We see that the sum over polarizations of Eq. (9.3.10) is orthogonal to δ_{im} and δ_{rl}, which guarantees also here that only the UV finite I_0 term of the three-point loop function is relevant. The contraction leads to a $\vec{q}^4$ factor,[9] and thus the width scales like $|\vec{q}|^5$, as expected for a d-wave decay.

Results for the $X_2 \to D\bar{D}^*$ decay widths are also compiled in Table 9.1. We only show predictions for the $X_2(4013) \to D^+D^{*-}(D^0\bar{D}^{*0})$ decays, because being the X_2 an even C-parity state, its decay modes into the charge conjugated final states have the same decay widths. In what respects to the effect of the form factors, the discussion runs in parallel to that in the Sect. 9.3.1, though the effect of the pion-exchange form factor is significantly smaller here (a factor 4 or 5 at most). As expected, the widths are comparable to those found for the $X_2 \to D\bar{D}$ decays. Finally, we estimate the partial $X_2 \to D\bar{D}^*\,(D^*\bar{D})$ width (including both the charged and neutral channels as well as the charge-conjugated modes) to be

$$\Gamma(X_2 \to D\bar{D}^*) + \Gamma(X_2 \to D^*\bar{D}) = \big(2.9 \pm \underbrace{0.5}_{\text{sys }(\Lambda)}\,{}^{+2.0}_{-1.0}\big)\ \text{MeV}. \tag{9.3.12}$$

where the errors have been estimated as in Eq. (9.3.6). The above result, together with that obtained previously for the $D\bar{D}$ channel, leads to a total X_2 width of the order of 2-8 MeV, assuming its existence.

Charm decays: further analysis of uncertainties

The uncertainties on the results compiled in Table 9.1 account both for reasonable estimates of HQSS corrections, as well as for the statistical errors on the inputs used to fix the LEC's that determine the properties (mass and $D^*\bar{D}^*$ couplings) of the X_2 resonance. Moreover we are

[9] In the $D\bar{D}$ mode, studied in Sect. 9.3.1 a factor of $2\vec{q}^4/3$ is obtained instead. Thus, neglecting the $D - D^*$ mass difference, because the loop integrals are the same, we would find

$$\left|\mathcal{T}_{D\bar{D}^*(D^*\bar{D})}\right|^2 \simeq \frac{3}{2}\,|\mathcal{T}_{D\bar{D}}|^2 \tag{9.3.11}$$

This extra factor 3/2 due to the spin-1 polarization vector produces an enhancement of the $D\bar{D}^*$ decay mode with respect to the $D\bar{D}$ one, which partially compensates the smaller available phase space.

	FFπ1	FFπ2	FFπ1	FFπ2	FFπ1	FFπ2	FFπ1	FFπ2
	FFX_2-G	FFX_2-G	FFX_2-L	FFX_2-L	FFX_2-G	FFX_2-G	FFX_2-L	FFX_2-L
Λ [GeV]	0.5	0.5	0.4	0.4	1	1	0.8	0.8
$\Gamma(X_2 \to D^+D^-)$	$0.5^{+0.5}_{-0.2}$	0.6	0.5	0.6	$0.8^{+0.7}_{-0.2}$	01.0	0.9	0.9
$\Gamma(X_2 \to D^0\bar{D}^0)$	$0.4^{+0.5}_{-0.2}$	0.5	0.4	0.4	$0.6^{+0.7}_{-0.2}$	0.7	0.6	0.6
$\Gamma(X_2 \to D^+D^{*-})$	$0.7^{+0.6}_{-0.3}$	0.9 (1.2)	0.7	0.8 (1.1)	$1.0^{+0.5}_{-0.2}$	1.2 (1.6)	1.0	1.1 (1.5)
$\Gamma(X_2 \to D^0\bar{D}^{*0})$	$0.5^{+0.6}_{-0.2}$	0.7 (0.9)	0.5	0.6 (0.8)	$0.7^{+0.5}_{-0.2}$	0.8 (1.2)	0.7	0.8 (1.1)

Table 9.2: $X_2(4013) \to D\bar{D}, D\bar{D}^*$ decay widths (in MeV units) using different UV regularization schemes for the $D^*\bar{D}^*X_2$ vertex and pion-exchange form factors. FFX_2-G and FFX_2-L stand for the results obtained with Gaussian (Eq. (9.2.3)) and Lorentzian (Eq. (9.3.14)) regularized local interactions, respectively. On the other hand, the widths in the columns FFπ1 and FFπ2 were obtained inserting the pion form factor of Eq. (9.6.18) and $F(\vec{l}^{\,2}, \Lambda_\pi) = e^{-\vec{l}^{\,2}/\Lambda_\pi^2}$ in each of the two $D^*D^{(*)}\pi$ vertices, respectively. In the latter case, we take $\Lambda_\pi = 1.2$ GeV, as determined in the QCDSR calculation of Ref. [219] for the $D^*D\pi$ coupling. In the $D\bar{D}^*$ decay mode, we also show results (in brackets) obtained when a larger cutoff, $\Lambda_\pi = 1.85$ GeV, is used in the $D^*D^*\pi$ vertex, as obtained in the QCDSR study carried out in Ref. [220] for this coupling. The results presented in Table 9.1 correspond to the [FFX_2-G & FFπ1] columns and for the rest of choices we only provide central values.

using an EFT to describe these decays, which means that there is an intrinsic uncertainty that can be determined systematically. We indicated the size of this error in Eqs. (9.3.6) and (9.3.12). For obtaining the EFT uncertainty we combined the predictions obtained for two different UV Gaussian cutoffs ($\Lambda = 0.5$ and 1 GeV) in the $D^*\bar{D}^*X_2$ vertex, and used the spread of values to quantify this error. The idea is that the residual dependence of the results on the cutoff should provide an insight into the size of subleading corrections.

Now, we try to further test the robustness of the systematic errors quoted in Eqs. (9.3.6) and (9.3.12). To that end, we have examined:

- The dependence of our results on the functional form of the UV regulators, both in the $D^*\bar{D}^*X_2$ and $D^*D^{(*)}\pi$ vertices.

  – We have a contact theory with a Gaussian regulator and a cutoff Λ between 0.5 and 1 GeV. This theory, though very simple, is the LO of an EFT expansion describing the low energy dynamics of heavy hadrons (see Ref. [11] for details). Within the EFT we can expand observable quantities as a power series of the type

$$A = \sum_\nu \hat{A}_\nu \left(\frac{p}{\Lambda_M}\right)^\nu , \tag{9.3.13}$$

  where p is the momenta of the hadrons and Λ_M the scale at which hadrons stop behaving as point-like particles (about the ρ mass). A LO calculation only keeps the first term in the series above. Hence it should have a relative error of order (p/Λ_M). We stress that this is expected to be so regardless of the exact regulator employed (Gaussian, Lorentzian, etc.), provided that the cutoff is at least of the order of Λ_M. The reason for that is that the calculations we show are renormalizable: once the counter-terms are fixed[10], they only contain negative powers of the cutoff Λ when we

[10] See for instance the discussion of Eqs. (23) and (24) of Ref. [99].

expand on the large cutoff limit. Hence, the uncertainty in the calculation is of order (p/Λ). By taking Λ of the order of Λ_M, observables are guaranteed to have a cutoff uncertainty of the order (p/Λ_M), equivalent to the EFT uncertainty.

There are several methods for making a more precise estimation of the EFT error: the one we use in Table 9.1 is to vary the cutoff around values of the order of Λ_M (hence the choice of the $0.5-1$ GeV cutoff window). EFT predictions for two different cutoffs differ by a factor of (p/Λ_M) and that is why we chose this particular way of assessing the errors.

Alternatively, one could use different regulators or form factors to assess the size of this error. This idea also gives a cross-check of the previous error estimates based on varying the cutoff. We have employed a different regulator to check that our former estimation of the EFT errors is correct and to show that the particular regulator employed is not important. We closely follow here the discussion of Sect. VII of Ref. [99] and consider a Lorentz form for the regulator

$$\langle \vec{p}\,|V|\vec{p}\,'\rangle = C_{IX}\left[\frac{\Lambda^2}{\Lambda^2+\vec{p}^{\,2}}\right]\left[\frac{\Lambda^2}{\Lambda^2+\vec{p}\,'^{\,2}}\right], \tag{9.3.14}$$

with two values of the cutoff, namely $\Lambda = 0.4$ and 0.8 GeV, which were obtained by multiplying the Gaussian cutoffs by a factor of $\sqrt{2/\pi}$ [99]. The resulting[11] widths are presented in Table 9.2 and turn out to be rather insensitive to the form of the regulator (this is to be understood within the limits of the expected EFT uncertainty).

– Next we have studied the dependence of the widths on the pion form factor that accounts for the off-shellness of the pion in the mechanisms depicted in Figs. 9.3 and 9.5. To that end we used the results from the QCD sum rule (QCDSR) calculations performed in Refs. [219, 220]. The first of these two works considers the $D^*D\pi$ vertex: it was found that the form factor is harder if the off-shell meson is heavy, implying that the size of the vertex depends on the exchanged meson. This means that a heavy meson will see the vertex as point-like, whereas the pion will see its extension. The authors of Ref. [219] find an on-shell value $g = 0.48\pm0.05$ (note the different definition used in this reference), around 1-2 sigmas below the value of 0.57 used in this work. In addition, they adjust their results for off-shell pions to a Gaussian form e^{l^2/Λ_π^2}, with l^μ the pion four momentum, and find $\Lambda_\pi = 1.2$ GeV. This form-factor[12], in the region of interest for this work, turns out to be in a good agreement with that used to obtain the results presented in Table 9.1. This can be seen in the new results showed in Table 9.2 and obtained with this new pion off-shell form-factor (FFπ2). Deviations from our previous estimates of the $X_2(4013) \to D\bar{D}, D\bar{D}^*$ decay widths are both much smaller than the (HQSS & exp) uncertainties quoted in Table 9.1, and well comprised within the systematic uncertainty generated when the $D^*\bar{D}^*X_2$ cutoff varies in the 0.5-1 GeV window.

[11] With the Lorentzian regularized local potential, we re-obtain the counter-terms C_{0X} and C_{1X} from the $X(3872)$ inputs, which are then used to find the mass of the X_2 resonance and its couplings to the $D^{*0}\bar{D}^{*0}$ and $D^{*-}D^{*+}$ meson pairs. These physical quantities hardly change, because the X_2 is a very loosely bound state and its dynamics is very little sensitive to the details of the $D^*\bar{D}^*$ interaction at short distances.

[12] To use the form factor of Ref. [219] in the computation of the widths, we have approximated the pion four momentum squared by $-\vec{l}^{\,2}$, which is sufficiently accurate because the dominant part of the integration comes from regions where the two virtual D^* and $\bar{D}^*$ mesons are almost on-shell. In this region, the energy of both heavy light vector mesons is approximately $M_{X_2}/2$ which coincides with that of the external heavy mesons, and hence l^0 is much smaller than $|\vec{l}|$.

In the $X_2 \to D\bar{D}^*$ decay, there also appears the $D^*D^*\pi$ coupling in one of the vertices, see Fig. 9.5. The off-shell behaviour of this vertex might differ from that of the $D^*D\pi$ one. This coupling was studied using QCDSR in [220] where, translating the definition used therein to the one used here, it was found an on-shell value $g = 0.56 \pm 0.07$ in good agreement with the HQSS expectations. The off-shell behaviour was described by a Gaussian, as in the case of the $D^*D\pi$ vertex, but with a significantly larger cutoff, Λ_π= 1.85 GeV. This significant difference is somehow surprising from the HQSS point of view, and we should note that the QCDSR actual calculations in [220] were carried out for significantly larger values of $l^2 > 4$ GeV^2 than in the case of the $D^*D\pi$ coupling analyzed in Ref. [219]. Nevertheless, we used this softer dependence for the $D^*D^*\pi$ vertex and re-computed the $D\bar{D}^*$ widths. Results are shown in brackets in Table 9.2. Changes are now larger, and in general are of the order of 50%, though they could be still accommodated within the HQSS and EFT uncertainties already considered in our original calculations. The large momenta of the external mesons, that can even exceed 0.5 GeV, make it possible that the short distance details of the decay mechanisms could be relevant. This is the weakest point in our scheme. The reason is that the EFT uncertainty is expected to be 0.5 GeV/$\Lambda_M \gtrsim 1/2$, as the variations of the $D\bar{D}^*$ widths in Table 9.2 seem to confirm, and the calculation is really on the limit of validity of this kind of description and should only be considered as a reasonable estimate.

- The contribution of decay mechanisms driven by the exchange of shorter range mesons (heavier than the pion).

  Since the momenta of the external charmed mesons can exceed 0.5 GeV, one might think that shorter range contributions such as the ρ and ω exchanges could be sizable, and even comparable to those of the diagrams depicted in Figs. 9.3 and 9.5 for the exchange of a pion. We will focus on the $X_2 \to D\bar{D}$ decay mode, where the momenta of the external mesons is the largest and we will begin by studying the effects of the exchange of a ρ meson. If we use the phenomenological $D^*D\rho$ Lagrangian given in Eq. (3) of Ref. [221], we find that the amplitudes of this new contribution can be obtained from those driven by pion exchange, and given in Eqs. (9.3.1) and (9.3.2), by replacing m_{π^0} and m_{π^+} by m_{ρ^0} and m_{ρ^+} in the loop integrals and

$$\frac{g^2}{f_\pi^2} \to -\frac{m_D}{m_{D^*}} g^2_{D^*D\rho} \tag{9.3.15}$$

  where we have neglected $|\vec{q}|^2/m^2_{D^{(*)}}$ terms, with $\vec{q}$ the c.m. three-momentum of the external D and $\bar{D}$ mesons. The coupling constant $g_{D^*D\rho}$ has been computed in various schemes [221, 222, 223, 224, 225] (ordinary and light cone QCDSR, vector dominance model, $SU(4)$, etc.) and it varies in the range $[2.8 \pm 0.1, 4.3 \pm 0.9]$ GeV^{-1} (see Table 5 of Ref. [225]). Taking $g_{D^*D\rho} \sim 5$ GeV^{-1}, in the highest part of the interval of calculated values, we would have $g^2_{D^*D\rho}/(g^2/f_\pi^2) \sim 2/3$, while a direct calculation of the loop integrals shows that those calculated using the ρ mass instead of the pion mass are around a factor of two smaller. All together indicates that the absolute values of the ρ-exchange amplitudes are about a factor of three smaller than those driven by the pion exchange. If one uses $g_{D^*D\rho} \sim 3$ GeV^{-1}, now in the lowest part of the interval of values, the ρ contribution will be, at the level of amplitudes, around eight times smaller than those considered in the present work. In any case, these effects are smaller than the HQSS and EFT uncertainties quoted in Table 9.1, and therefore it seems justified to neglect them. On the other hand, the

ω-exchange contributions are even smaller, around a factor of three, because this meson is neutral, and it cannot generate mechanisms where a light charged meson is exchanged.

In view of the results discussed in this subsection, we should acknowledge that as a result of the contribution from highly virtual pions, which is certainly in the limit of applicability of the low-energy EFT, the hadronic decay widths bear a large systematic uncertainty. Nevertheless, we have given arguments to be reasonably convinced that the results quoted in Eqs. (9.3.6) and (9.3.12) provide sensible estimates for the $X_2(4013) \to D\bar{D}, D\bar{D}^*$ widths.

In the next subsection, we will study these hadronic decays in the bottom sector. There, the considerations are parallel to those discussed here for the charm sector.

9.3.2 Bottom decays

Thanks to the heavy flavour symmetry, the results of the previous subsection can be trivially extended to the bottom sector. There, we have a robust prediction, even when HQSS uncertainties (20%) are taken into account, for the X_{b2} resonance (see Fig. 9.2). Moreover, all sort of non-relativistic approximations adopted in the current scheme are now more suited, since the range of variation of the internal pion momentum in the loops is similar to that shown in Fig. 9.4 for the charm sector.

On the other hand, as discussed in Sect. 9.2.3, we do not expect any significant isospin breaking effects and the X_{b2} resonance would be a pure $I = 0$ state, with equal coupling to its neutral and charged components. For simplicity, we will also neglect the tiny difference between B^0 and $B^\pm$ masses, and we will use a common mass $m_B = (m_{B^0} + m_{B^\pm})/2 = 5279.42$ MeV. Yet, for the pion mass that appears in the loop integral, we take the isospin averaged value $m_\pi = (2m_{\pi^\pm} + m_{\pi^0})/3$. Note that the relevant internal pion momentum is around 750 MeV. With all these approximations, we find

$$\begin{aligned}\Gamma(X_{b2} \to B\bar{B}) &= \frac{3g^4(g^{X_{b2}})^2}{5\pi f_\pi^4}\frac{m_B^2 m_{B^*}^4}{M_{X_{b2}}}\,|\vec{q}|^5\,\cdot \\ &\quad \Big(I_0(m_{B^*}, m_\pi; M_{X_{b2}}, q^\mu[m_{F_1} = m_{F_2} = m_B])\Big)^2,\end{aligned} \tag{9.3.16}$$

$$\begin{aligned}\Gamma(X_{b2} \to B\bar{B}^*) &= \frac{9g^4(g^{X_{b2}})^2}{10\pi f_\pi^4}\frac{m_B m_{B^*}^5}{M_{X_{b2}}}\,|\vec{q}|^5 \\ &\quad \Big(I_0(m_{B^*}, m_\pi; M_{X_{b2}}, q^\mu[m_{F_1} = m_B, m_{F_2} = m_{B^*}])\Big)^2,\end{aligned} \tag{9.3.17}$$

for any charge channel (B^+B^-, $B^0\bar{B}^0$, B^+B^{*-}, $B^0\bar{B}^{*0}$) or charge conjugation mode ($B^*\bar{B}$). Our results for these decay widths are presented in Table 9.3. We notice in passing that following heavy flavour symmetry we use the same value of $g = 0.570 \pm 0.006$ in the charm and bottom decays. It agrees very well with a recent lattice calculation with relativistic bottom quarks which gives $g_b = 0.569 \pm 0.076$ [226] (we have added the systematic and statistic errors in quadrature). Yet, lattice calculations with static heavy quarks tend to give smaller values, see Ref. [227] and references therein. For instance, the ALPHA Collaboration presented a precise computation with the result of $g_\infty = 0.492 \pm 0.029$ [227]. Thus we expect that the decay widths of Table 9.3 slightly overestimate the real ones.

For the $B\bar{B}$ mode we find a pronounced dependence on the Gaussian cutoff Λ employed in the dynamical generation of the resonance. This is inherited from the strong dependence of the X_{b2} mass on this UV cutoff, as discussed in Eq. (9.2.10), which affects the available phase space

	without pion-exchange FF		with pion-exchange FF	
	$\Lambda = 0.5$ GeV	$\Lambda = 1$ GeV	$\Lambda = 0.5$ GeV	$\Lambda = 1$ GeV
$\Gamma(X_{b2} \to B\bar{B})$ [MeV]	$26.0^{+1.0}_{-3.3}$	8^{+15}_{-7}	$4.4^{+0.1}_{-0.4}$	$0.7^{+1.4}_{-0.6}$
$\Gamma(X_{b2} \to B\bar{B}^*)$ [MeV]	$7.1^{+3.4}_{-3.7}$	–	$2.0^{+0.9}_{-1.0}$	–

Table 9.3: *$X_{b2} \to B\bar{B}, B\bar{B}^*$ decay widths (here $B\bar{B}^{(*)}$ refers to any of the neutral or charged modes, but it is not the sum of both). The results are given for different treatments of the three-point loop function. The errors have been obtained using the Monte Carlo analysis explained in Table 9.1, but now considering the X_{b2} mass histograms displayed in Fig. 9.2 and the coupling given in Eq. (9.2.10). The decay width of the $X_{b2} \to \bar{B}B^*$ mode is the same because of charge conjugation symmetry.*

for the decay. With all these shortcomings, we expect a partial width in the 1-10 MeV range, when both charge modes are considered.

In the $B\bar{B}^*$ decay mode, the impact of the Gaussian regulator is even larger, because it turns out that for $\Lambda = 1$ GeV, the central value of the resonance mass $M_{X_{b2}} = 10594^{+22}_{-26}$ MeV is located below the threshold $m_B + m_{B^*} \sim 10604$ MeV. Thus, in that case, the decay will be forbidden. For $\Lambda = 0.5$ GeV, we estimate a width also in the 4-12 MeV range, when the four possible decay modes (B^+B^{*-}, $B^0\bar{B}^{*0}$, B^-B^{*+}, $\bar{B}^0B^{*0}$) are considered.

9.4 The X_2 and X_{b2} radiative decays

In this section, we study the $X_2 \to D\bar{D}^*\gamma$ and $X_{b2} \to \bar{B}B^*\gamma$ decays. The interaction of the photon with the s-wave heavy mesons contains two contributions that correspond to the magnetic couplings to the light and heavy quarks [96] (see Subsect. 2.3.3). Both terms are needed to understand the observed electromagnetic branching fractions of the D^{*+} and D^{*0} because a cancellation between the two terms accounts for the very small width of the D^{*+} relative to the D^{*0} [98]. Actually, one finds [96, 97]:

$$\Gamma(D^{*0} \to D^0\gamma) = \frac{\alpha}{3}\frac{m_{D^0}}{m_{D^{*0}}}\left(\beta_1 + \frac{2}{3m_c}\right)^2 E_\gamma^3, \quad \beta_1 = \frac{2}{3}\beta - \frac{g^2 m_K}{8\pi f_K^2} - \frac{g^2 m_\pi}{8\pi f_\pi^2}, \tag{9.4.1}$$

$$\Gamma(D^{*+} \to D^+\gamma) = \frac{\alpha}{3}\frac{m_{D^+}}{m_{D^{*+}}}\left(\beta_2 + \frac{2}{3m_c}\right)^2 E_\gamma^3, \quad \beta_2 = -\frac{1}{3}\beta + \frac{g^2 m_\pi}{8\pi f_\pi^2}, \tag{9.4.2}$$

where E_γ is the photon energy, m_c the charm quark mass and $\alpha \sim 1/137.036$ the fine-structure constant. In the non-relativistic constituent quark model $\beta = 1/m_q \sim 1/330\ \text{MeV}^{-1}$, where m_q is the light constituent quark mass. Heavy meson chiral perturbation theory allows one to improve upon this approximation by including corrections from loops with light Goldstone bosons, which give $\mathcal{O}(\sqrt{m_q})$ corrections [96].

Using isospin symmetry to relate $\Gamma(D^{*0} \to D^0\pi^0)$ and $\Gamma(D^{*+} \to D^0\pi^+)$, correcting by the slightly different available p-wave phase space in each of the two decays, and taking into account the experimental D^{*0} and D^{*+} widths and radiative branching fractions quoted by the PDG [98], we find:

$$\Gamma(D^{*0} \to D^0\gamma) = (22.7 \pm 2.6)\ \text{keV}, \qquad \Gamma(D^{*+} \to D^+\gamma) = (1.33 \pm 0.33)\ \text{keV}. \tag{9.4.3}$$

These values differ from those used in Ref. [97] because of the recent accurate BABAR measurement of the D^{*+} decay width, mentioned in Sect. 9.3, which is around 10% smaller than the previous CLEO one used in Ref. [97]. Fixing the charm quark mass to $m_c = 1.5$ GeV, we fit the parameter β to the above experimental values and find $\beta^{-1} = (293 \pm 11)$ MeV.

In what follows, we will study decays of the type $X_2 \to P\bar{P}^*\gamma$, being P and P^* pseudoscalar and vector heavy-light mesons, respectively. Let us define p_1^μ, p_2^μ and p_3^μ as the four vectors of the final photon, pseudoscalar and vector mesons, respectively. Besides, let us define the invariant masses $m_{ij}^2 = p_{ij}^2 = (p_i + p_j)^2$, which satisfy

$$m_{12}^2 + m_{13}^2 + m_{23}^2 = M_{X_2}^2 + m_1^2 + m_2^2 + m_3^2 = M_{X_2}^2 + m_P^2 + m_{P^*}^2. \tag{9.4.4}$$

Since, as we will see, the Feynman amplitudes depend only on the invariant masses m_{12}^2 and m_{23}^2 of the final γP and $P\bar{P}^*$ pairs, respectively, we can use the standard form for the Dalitz plot [45, 98]

$$d\Gamma = \frac{1}{(2\pi)^3}\frac{1}{32M_{X_2}^3}\overline{|\mathcal{T}|}^2 dm_{23}^2 dm_{12}^2, \tag{9.4.5}$$

with $\overline{|\mathcal{T}|}^2$ the absolute value squared of the decay amplitude with the initial and final polarizations being averaged and summed, respectively. Thus, we readily obtain

$$\Gamma = \frac{1}{(2\pi)^3}\frac{1}{32M_{X_2}^3}\int_{(m_P+m_{P^*})^2}^{M_{X_2}^2} dm_{23}^2 \int_{(m_{12}^2)_{\min}}^{(m_{12}^2)_{\max}} dm_{12}^2 \overline{|\mathcal{T}|}^2, \tag{9.4.6}$$

where for a given value of m_{23}^2, the range of m_{12}^2 is determined by its values when $\vec{p}_P$ is parallel or anti-parallel to $\vec{p}_\gamma$ [98]:

$$\begin{aligned}(m_{12}^2)_{\max} &= (E_\gamma^* + E_P^*)^2 - (p_\gamma^* - p_P^*)^2,\\ (m_{12}^2)_{\min} &= (E_\gamma^* + E_P^*)^2 - (p_\gamma^* + p_P^*)^2,\end{aligned} \tag{9.4.7}$$

with $E_P^* = (m_{23}^2 + m_P^2 - m_{P^*}^2)/2m_{23}$ and $E_\gamma^* = (M_X^2 - m_{23}^2)/2m_{23}$ the energies of the P meson and photon in the m_{23} c.m. frame, respectively, and $p_{P,\gamma}^*$ the moduli of the corresponding 3-momenta.

Because of parity conservation, this is a p-wave decay and hence the photon momentum always appears in the amplitudes. In the X_2 rest frame, it is given by $|\vec{p}_\gamma| = E_\gamma = M_{X_2}^2 - m_{23}^2/(2M_{X_2})$.

9.4.1 $X_2(4013) \to D\bar{D}^*\gamma$

We will first consider the $X_2(4013) \to D^0\bar{D}^{*0}\gamma$ decay, which proceeds according to the Feynman diagrams depicted in Fig. 9.6. This decay can take place directly through the radiative transition of the constituent D^{*0} as shown in Fig. 9.6(a), which is the tree level approximation. However, there are other mechanisms driven by the $D\bar{D}^*$ FSI. After emitting the photon, the vector meson D^{*0} transits into the D^0, and it can interact with the other constituent in the X_2 as shown in Fig. 9.6(b). There is a third (c) mechanism in which the photon is emitted from the $\bar{D}^{*0}$ meson, and the virtual $D^{*0}\bar{D}^0$ rescatter into $D^0\bar{D}^{*0}$. Finally, Fig. 9.6(d) and (e) present another possibility, namely the decay can also occur through the charged $D^{*+}D^{*-}$ component of the X_2 resonance, and the virtual charged D^+D^{*-} and $D^{*+}D^-$ pairs then rescatter into $D^0\bar{D}^{*0}$. Because the X_2 has a well defined charge parity (+), the decay width into the charge conjugated mode $\bar{D}^0D^{*0}\gamma$ is the same. The Feynman diagrams contributing to the $D^+D^{*-}\gamma$ decay mode are similar with obvious replacements.

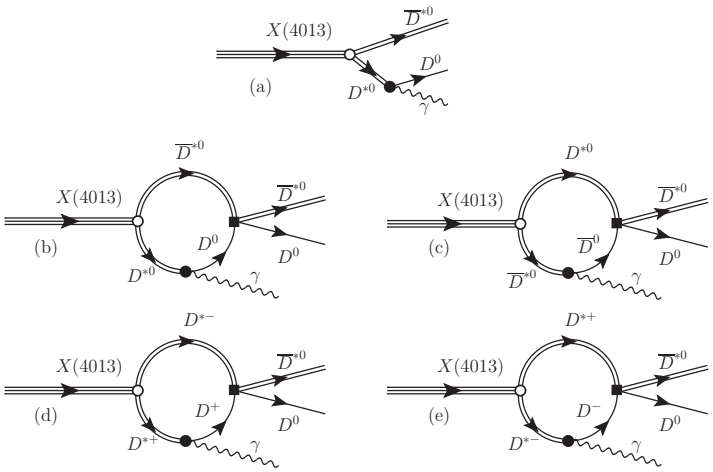

Figure 9.6: *Feynman diagrams for the $X_2(4013) \to D^0\bar{D}^{*0}\gamma$ decay. Diagrams for the $D^+D^{*-}\gamma$ transition are similar.*

Tree Level Approximation

The Feynman amplitude of the mechanism depicted in Fig. 9.6(a) reads (as in the previous sections, we treat the charm mesons non-relativistically)

$$-i\mathcal{T}(\lambda,\lambda_*,\lambda_\gamma)_{D^0\bar{D}^{*0}\gamma} = \\ = g_0^{X_2}(m_{12})\sqrt{4\pi\alpha}N_\gamma\left(\beta_1+\frac{2}{3m_c}\right)\frac{\epsilon_{ijm}\epsilon^{jn}(\lambda)\epsilon^{*n}(\lambda_*)\epsilon_\gamma^{*i}(\lambda_\gamma)p_\gamma^m}{2m_{D^{*0}}\left(m_{12}-m_{D^{*0}}+i\varepsilon\right)}, \tag{9.4.8}$$

with m_{12} the invariant mass of the final γD^0 pair. Besides, $\epsilon^i(\lambda_\gamma)$ is the polarization vector of the final photon with helicity λ_γ, $\vec{p}_\gamma$ is its three momentum and $N_\gamma = \sqrt{8M_{X_2}m_{D^*}^2}\sqrt{m_D m_{D^*}}$ accounts for the normalization of the heavy meson fields and the $X_2D^{*0}\bar{D}^{*0}$ coupling. Finally,

$$g_0^{X_2}(m_{12}) = g_0^{X_2}\times e^{-(\vec{p}_{12}^{\,2}-\gamma^2)/\Lambda^2} = g_0^{X_2}\times e^{-m_{D^{*0}}(m_{D^{*0}}-m_{12})/\Lambda^2} \tag{9.4.9}$$

with $\vec{p}_{12}^{\,2} \simeq m_{D^{*0}}(M_{X_2}-m_{D^{*0}}-m_{12})$ and $\gamma^2 = m_{D^{*0}}(M_{X_2}-2m_{D^{*0}}) < 0$. The Gaussian form factor is inherited from the $D^{(*)}\bar{D}^{(*)}$ EFT UV renormalization scheme.

We have neglected the D^{*0} width in the above propagator because, since it is quite small, its inclusion only leads to small numerical variations in the decay rate which are certainly smaller than uncertainties induced by the errors in the coupling $g_0^{X_2}$ and the mass of the $X_2(4013)$ resonance. Similarly, the use of the non-relativistic D^{*0} propagator instead of $\left(m_{12}^2-m_{D^{*0}}^2+i\varepsilon\right)^{-1}$ leads also to numerically negligible differences, as compared to the HQSS corrections. The sum over the $\bar{D}^{*0}$, γ and X_2 polarizations can be easily done, and we get

$$\overline{|\mathcal{T}|}^2_{D^0\bar{D}^{*0}} = \frac{16\pi\alpha M_{X_2}m_{D^*}m_D}{3}\left(g_0^{X_2}(m_{12})\right)^2\frac{\left(\beta_1+\frac{2}{3m_c}\right)^2}{\left(m_{12}-m_{D^{*0}}+i\varepsilon\right)^2}\vec{p}_\gamma^{\,2}. \tag{9.4.10}$$

The amplitude for $D^+\bar{D}^{*-}\gamma$ decay is readily obtained from Eq. (9.4.9) making the obvious replacements: $g_0^{X_2} \to g_c^{X_2}$, $\beta_1 \to \beta_2$ and $(m_{D^0}, m_{D^{*0}}) \to (m_{D^+}, m_{D^{*+}})$. Performing the phase

space integration, we find at tree level (assuming the existence of the X_2 state)

$$\Gamma(X_2(4013) \to D^0 \bar{D}^{*0}\gamma)_{\rm tree} = 18^{+2}_{-6}\left(16^{+2}_{-9}\right)\ \text{keV}, \tag{9.4.11}$$

$$\Gamma(X_2(4013) \to D^+ D^{*-}\gamma)_{\rm tree} = 0.10^{+0.10}_{-0.05}\left(0.09^{+0.06}_{-0.03}\right)\ \text{keV}, \tag{9.4.12}$$

where the values outside and inside the parentheses are obtained with $\Lambda = 0.5$ and 1 GeV, respectively. The errors account for the uncertainty, both in the mass of the X_2 state and in its couplings $g^{X_2}_{0,c}$, derived from the $X(3872)$ input ($M_{X(3872)}$ and the ratio $R_{X(3872)}$ of the decay amplitudes for the $X(3872) \to J/\psi\rho$ and $X(3872) \to J/\psi\omega$ decays) and the HQSS corrections, as explained in the the caption of Table 9.1. We have neglected additional uncertainties stemming from the error on β ($\simeq 3\%$), because it is totally uncorrelated to those discussed above, and it is much smaller than those affecting for instance the $g^{X_2}_{0,c}$ couplings. The neutral mode width is much larger than the charged one, thanks to the bigger magnetic $D^*D\gamma$ coupling and a larger available phase space.

In analogy with the discussion of Eqs. (8.3.8) and (8.3.9) in Chapter 8 for the $X(3872) \to D^0\bar{D}^0\pi^0$ decay, in the X_2 radiative processes the relative distance of the $D^*\bar{D}^*$ pair can be as large as allowed by the size of the $X_2(4013)$ resonance, since the final state is produced by the one body decay of the $\bar{D}^*$ meson instead of by a strong two body transition. Thus, the radiative $D\bar{D}^*\gamma$ decays might provide details on the long-distance part of the resonance wave function. For instance, the $d\Gamma/d|\vec{p}_{\bar{D}^{*0}}|$ [$d\Gamma/d|\vec{p}_{D^{*-}}|$] distribution is related to the $X_2(4013)$ wave-function $\Psi(\vec{p}_{\bar{D}^{*0}})$ [$\Psi(\vec{p}_{D^{*-}})$] [6]. This is in sharp contrast to the $D\bar{D}$ and $D\bar{D}^*$ decay modes studied in the previous sections, which turned out to be strongly sensitive to short distance dynamics of the resonance, as revealed by the notorious dependence on the UV form factors.

However, all these considerations are affected by the $D\bar{D}^*$ FSI effects to be discussed next.

$D\bar{D}^*$ FSI Effects

To account for the FSI effects, we include in the analysis the $D\bar{D}^* \to D\bar{D}^*$ and $D^*\bar{D} \to D\bar{D}^*$ T-matrices. The EFT provides these matrices (some specific details are given in Subsect. 9.6) and are obtained by solving the LSE [Eq. (9.6.3)] in coupled channels with the $V_{D^{(*)}\bar{D}^{(*)}}$ potential given in Eq. (9.6.2). Some isospin symmetry breaking effects are taken into account because the physical masses of the neutral ($D\bar{D}^*$) and charged (D^+D^{*-}) channels are used in Eq. (9.6.3). The $X_2 \to D^0\bar{D}^{*0}\gamma$ decay amplitude for the mechanisms depicted in Fig. 9.6(b) and (c) reads

$$\begin{aligned} -i\mathcal{T}(\lambda,\lambda_*,\lambda_\gamma)^{\rm FSI\,(b+c)}_{D^0\bar{D}^{*0}\gamma} &= -g_0^{X_2}\sqrt{4\pi\alpha}N_\gamma\left(\beta_1+\frac{2}{3m_c}\right) \\ &\quad \epsilon_{ijm}\epsilon^{jn}(\lambda)\epsilon^{*n}(\lambda_*)\epsilon^{*i}_\gamma(\lambda_\gamma)p^m_\gamma \\ &\quad \times\ 4m_D m_{D^*}\,\widehat{T}_{00\to 00}(m_{23})\,J(m_{D^{*0}},m_{D^{*0}},m_{D^0},\vec{p}_\gamma), \end{aligned} \tag{9.4.13}$$

where m_{23} is the invariant mass of the final $D^0\bar{D}^{*0}$ pair,

$$\widehat{T}_{00\to 00}(m_{23}) \equiv T_{D^0\bar{D}^{*0}\to D^0\bar{D}^{*0}}(m_{23}) + T_{D^{*0}\bar{D}^0\to D^0\bar{D}^{*0}}(m_{23}), \tag{9.4.14}$$

and the three-point loop integral function $J\,(M_1,M_2,M_3,\vec{p}_\gamma)$ is discussed in the Appendix 9.6.3. The integral is convergent, however, for consistency it is evaluated using the same UV regularization scheme as that employed in the $D^{(*)}\bar{D}^{(*)}$ EFT. In sharp contrast with the hadronic decays studied above, the momenta involved in these integrals are rather low.

On the other hand, we see that in the (b)+(c) contribution there appears the combination $T_{D^0\bar{D}^{*0}\to D^0\bar{D}^{*0}}(m_{23}) + T_{D^{*0}\bar{D}^0\to D^0\bar{D}^{*0}}(m_{23})$. In the isospin limit, when the mass differences

between the neutral ($D^0\bar{D}^{*0}$) and charged (D^+D^{*-}) channels are neglected, we will find $\widehat{T}_{00\to 00} = (T^{I=0}_{C=-1}+T^{I=1}_{C=-1})/2$. From Eqs. (9.6.2) and (9.6.3), we find the C-parity odd isospin amplitudes,[13]

$$\left[T^I_{C=-1}\right]^{-1}(m_{23}) = C^{-1}_{IZ} + G_{D\bar{D}^*}(m_{23}), \qquad I=0,1\ , \tag{9.4.15}$$

with $G_{D\bar{D}^*} \simeq G_{D^0\bar{D}^{*0}} \simeq G_{D^+\bar{D}^{*-}}$ a common loop function. Note that the kernel of this LSE is fixed by the isoscalar (C_{0Z}) and the isovector (C_{1Z}) C(charge conjugation) $=-1$ terms of $V_{D^{(*)}\bar{D}^{(*)}}$. This is a trivial consequence of the conservation of this symmetry, taking into account that the X_2 and the photon are even and odd C-parity states, respectively.

The (d) and (e) FSI contributions of Fig. 9.6 are similar, with obvious replacements. We find

$$\begin{aligned} -i\mathcal{T}(\lambda,\lambda_*,\lambda_\gamma)^{\rm FSI\,(d+e)}_{D^0\bar{D}^{*0}\gamma} = & -g_c^{X_2}\sqrt{4\pi\alpha}N_\gamma\left(\beta_2+\frac{2}{3m_c}\right) \\ & \epsilon_{ijm}\epsilon^{jn}(\lambda)\epsilon^{*n}(\lambda_*)\epsilon^{*i}_\gamma(\lambda_\gamma)p^m_\gamma \\ & \times\left\{4m_Dm_{D^*}\widehat{T}_{+-\to 00}(m_{23})\right\}J(m_{D^{*+}},m_{D^{*+}},m_{D^+},\vec{p}_\gamma), \end{aligned} \tag{9.4.16}$$

where

$$\widehat{T}_{+-\to 00}(m_{23}) \equiv T_{D^+D^{*-}\to D^0\bar{D}^{*0}}(m_{23}) + T_{D^{*+}D^-\to D^0\bar{D}^{*0}}(m_{23}), \tag{9.4.17}$$

and in the isospin limit, we would have $\widehat{T}_{+-\to 00} = (T^{I=0}_{C=-1} - T^{I=1}_{C=-1})/2$.

For the $X_2(4013)\to D^+D^{*-}\gamma$ decay, the FSI contribution is

$$\begin{aligned} -i\mathcal{T}(\lambda,\lambda_*,\lambda_\gamma)^{\rm FSI}_{D^+\bar{D}^{*-}\gamma} &= -\sqrt{4\pi\alpha}N_\gamma\epsilon_{ijm}\epsilon^{jn}(\lambda)\epsilon^{*n}(\lambda_*)\epsilon^{*i}_\gamma(\lambda_\gamma)p^m_\gamma\ 4m_Dm_{D^*} \\ & \left\{g_c^{X_2}\left(\beta_2+\frac{2}{3m_c}\right)\left[\widehat{T}_{+-\to+-}(m_{23})J(m_{D^{*+}},m_{D^{*+}},m_{D^+},\vec{p}_\gamma)\right]\right. \\ & \left. + g_0^{X_2}\left(\beta_1+\frac{2}{3m_c}\right)\left[\widehat{T}_{00\to+-}(m_{23})J(m_{D^{*0}},m_{D^{*0}},m_{D^0},\vec{p}_\gamma)\right]\right\}, \end{aligned} \tag{9.4.18}$$

with

$$\widehat{T}_{+-\to+-}(m_{23}) = T_{D^+D^{*-}\to D^+D^{*-}}(m_{23}) + T_{D^{*+}D^-\to D^+D^{*-}}(m_{23}), \tag{9.4.19}$$

$$\begin{aligned} \widehat{T}_{00\to+-}(m_{23}) &= T_{D^0\bar{D}^{*0}\to D^+D^{*-}}(m_{23}) + T_{D^{*0}\bar{D}^0\to D^+D^{*-}}(m_{23}) \\ &= \widehat{T}_{+-\to 00}(m_{23}). \end{aligned} \tag{9.4.20}$$

and $\widehat{T}_{+-\to+-}(m_{23}) = \widehat{T}_{00\to 00}(m_{23})$ in the isospin limit.

Taking into account isospin corrections, induced by the meson mass differences, all the needed T-matrices ($\widehat{T}_{00\to 00}, \widehat{T}_{+-\to 00}$ and $\widehat{T}_{+-\to+-}$) can be calculated by solving the coupled channel LSE, Eq. (9.6.3), with the $V_{D^{(*)}\bar{D}^{(*)}}$ potentials of Eq. (9.6.2), as mentioned above. Thanks to the conservation of C-parity, the FSI corrections will depend only on C_{0Z} and C_{1Z}. Indeed, one finds

$$\begin{aligned} \begin{pmatrix} \widehat{T}_{00\to 00} & \widehat{T}_{+-\to 00} \\ \widehat{T}_{00\to+-} & \widehat{T}_{+-\to+-} \end{pmatrix}^{-1} &= \widehat{\mathcal{F}}^{-1}_\Lambda(E)\cdot \\ \cdot\left\{\begin{pmatrix} \frac{C_{0Z}+C_{1Z}}{2} & \frac{C_{0Z}-C_{1Z}}{2} \\ \frac{C_{0Z}-C_{1Z}}{2} & \frac{C_{0Z}+C_{1Z}}{2} \end{pmatrix}^{-1} - \begin{pmatrix} G_{D^0\bar{D}^{*0}} & 0 \\ 0 & G_{D^+\bar{D}^{*-}} \end{pmatrix}\right\}&\cdot\widehat{\mathcal{F}}^{-1}_\Lambda(E)\ , \end{aligned} \tag{9.4.21}$$

[13] Here and for simplicity we do not write the on-shell UV Gaussian form factors [see Eqs.(9.6.3) and (9.6.6)].

with $\widehat{\mathcal{F}}_\Lambda(E) = \text{Diag}\left(f_\Lambda^{\text{neu}}(E), f_\Lambda^{\text{ch}}(E)\right)$, where the Gaussian form factors are defined after Eq. (9.6.6).

The $Z_b(10610)$ observed in Ref. [43] carries electric charge, and its neutral partner was also reported by the Belle Collaboration [158]. It lies within a few MeV of the $B\bar{B}^*$ threshold and it is tempting to speculate about it as a hadronic molecule. Belle also reported the discovery of a second exotic electrically charged bottomonium state [43], $Z_b(10650)$ in the vicinity of the $B^*\bar{B}^*$ threshold. For both the $Z_b(10610)$ and $Z_b(10650)$ states, $J^P = 1^+$ are favored from angular analyses.

Within our scheme, we assume that the $Z_b(10610)$ resonance is an isovector $\left(B\bar{B}^* + B^*\bar{B}\right)/\sqrt{2}$ s-wave bound state with $J^{PC} = 1^{+-}$ (see Chapter 5). Note, HQSS predicts the interaction of the $B^*\bar{B}^*$ system with $I = 1$, $J^{PC} = 1^+$ quantum numbers to be identical to that of the $B\bar{B}^*$ pair in the $Z_b(10610)$ sector. Thus, HQSS naturally explains [27] the approximate degeneracy of the $Z_b(10610)$ and $Z_b(10650)$. Taking for the $Z_b(10610)$ binding energy (2.0 ± 2.0) MeV [44], we could fix a third linear combination of the LECs that appear in the LO Lagrangian of Eq. (2.3.24) in Chapter 2.

$$C_{1Z} \equiv C_{1a} - C_{1b} \quad = \quad -0.75^{+0.10}_{-0.17}\ (-0.30^{+0.02}_{-0.04})\,\text{fm}^2 \tag{9.4.22}$$

for $\Lambda = 0.5(1.0)$ GeV. Errors have been obtained with a procedure similar to that described in the discussion of Eq. (9.2.4) and used in the case of the $X(3872)$. Assuming heavy quark flavour symmetry, the above value of C_{1Z} could be also used in the charm sector, subject to corrections of the order of $\mathcal{O}(\Lambda_{\text{QCD}}/m_c) \simeq 20\%$ that we take into account. Therefore, we predict the existence of the isovector charmonium partners of the $Z_b(10610)$ and the $Z_b(10650)$, though as virtual states in the second Riemann sheet (see Chapter 5), which probably correspond to the recently observed charged charmonium-like[14] $Z_c(3900)$ and $Z_c(4025)$ states [161, 162, 163, 165, 228]. These resonances lie close to the $D\bar{D}^*$ and $D^*\bar{D}^*$ thresholds, respectively, while $J^P = 1^+$ quantum numbers are favored from some angular analyses.

Due to the presence of the $Z_c(3900)$ close to threshold, one should expect the loop (FSI) mechanisms depicted in Fig. 9.6 to be important since $T^{I=1}_{C=-1}$ must have a pole. However, the value of $C_{0Z} = (C_{0a} - C_{0b})$ is still unknown. It is not determined by the inputs deduced from the $X(3872)$ and $Z_b(10610)$ states used in the present analysis. The situation here is analogous to the $D\bar{D}$ FSI effects in the $X(3872) \to D^0\bar{D}^0\pi^0$ decay, discussed in Chapter 8. Thus, depending on the value of C_{0Z}, there can be an isoscalar $J^{PC} = 1^{+-}$ $D\bar{D}^*$ s-wave bound state or not. For instance, considering the case for $\Lambda = 0.5$ GeV and taking the central value for $C_{0Z} \sim -2.5$ fm^2 one finds a bound state pole in the $D\bar{D}^*$ system bound by around 10 MeV; if $C_{0Z} \sim -1.5$ fm^2, there will be a $D\bar{D}^*$ bound state almost at threshold; if the value of C_{0Z} is larger, there will be no bound state pole any more. Therefore, the information of C_{0Z} will be crucial in understanding the $D\bar{D}^*$ system and other exotic systems related to it through heavy quark symmetries. Conversely, as we will see, the X_2 radiative decay width could be used to extract information on the fourth LEC, C_{0Z}, thanks to the FSI effects.

To investigate the impact of the FSI, in Fig. 9.7 we show the dependence of the partial $X_2(4013) \to D\bar{D}^*\gamma$ decay widths on C_{0Z}. For comparison, the tree-level results are also shown in the same plots. As expected, for the decay into the $D^0\bar{D}^{*0}\gamma$ channel, the FSI effects turn out to be important, and for some values of C_{0Z}, they dominate the decay width. The maximum effects

[14]The simple EFT scheme employed in this work does not allow for finite width resonances, only for virtual or bound states. The merit of that EFT is actually making a connection between the $Z_b(10610/10650)$ and $Z_c(3900/4025)$ resonances on the basis of heavy flavor symmetry, not so much predicting the exact location. In that simple theory, we treat the $Z_b(10610)$ as a stable bound state and that is the reason why Z_c's are predicted to be virtual states. Had we used a more complete EFT that takes into account the finite width of the $Z_b(10610)$ and includes next-to-leading corrections, then we would have predicted the Z_c's as resonances and located them more accurately in the complex plane.

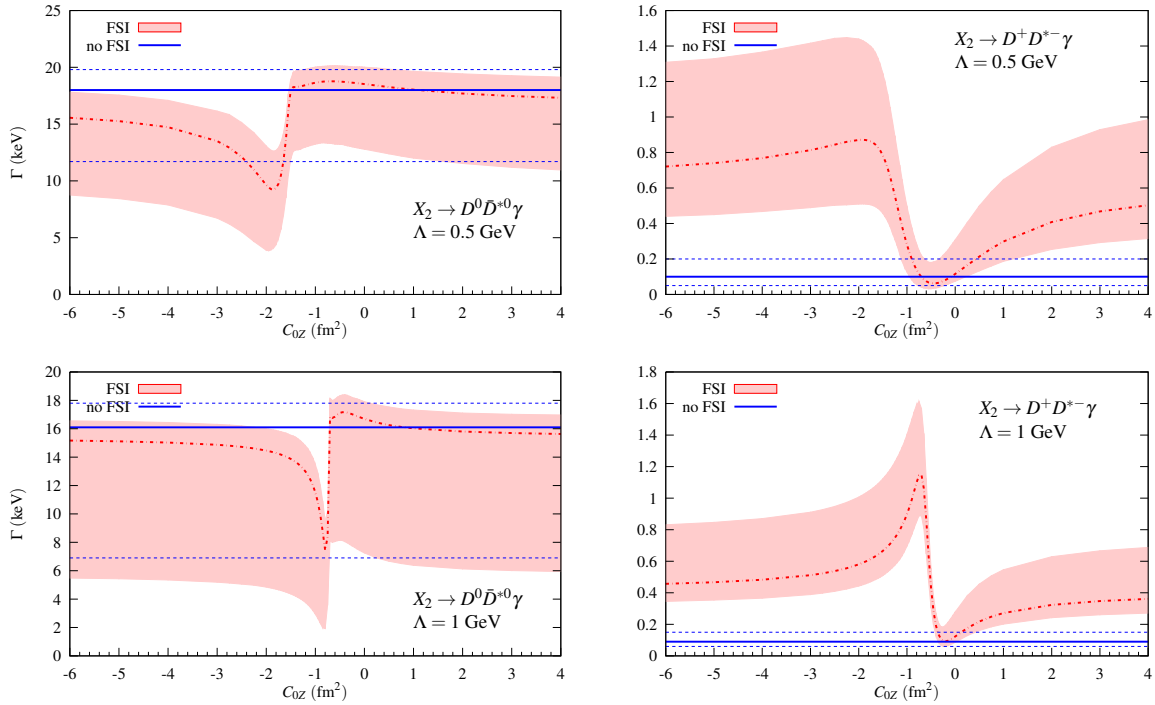

Figure 9.7: *Dependence of the $X_2(4013) \to D^0\bar{D}^{*0}\gamma$ and the $X_2(4013) \to D^+D^{*-}\gamma$ partial decay widths on the low-energy constant C_{0Z}. The UV cutoff is set to $\Lambda = 0.5$ GeV (1 GeV) in the top (bottom) panels. The red error bands contain the $D\bar{D}^*$ FSI effects, while the three horizontal blue lines stand for the tree level predictions of Eqs. (9.4.11) and (9.4.12). Besides the uncertainties on the mass and the couplings of the X_2 resonance, the errors on C_{1Z} quoted in Eq. (9.4.22), together with the expected 20% heavy quark flavour symmetry corrections when it is used in the charm sector, are also accounted in the 68% CL bands displayed in the panels. The red dash-dotted (full calculation) and solid blue (tree level) lines stand for the results obtained with the central values of the parameters.*

of the FSI mechanisms approximately occur for values of C_{0Z} which give rise to an isoscalar 1^{+-} $D\bar{D}^*$ bound or virtual state close to threshold. One can see an apparent deviation from the tree-level results in this region. When C_{0Z} takes smaller values, the binding energy of the bound state increases and moves apart from threshold; when C_{0Z} takes larger values, the pole moves deeper into a non-physical RS and becomes a virtual state further from the threshold. In both situations, the FSI corrections turn out to be less important. On the other hand, the FSI corrections are always important in the $D^+D^{*-}\gamma$ channel. This is because the tree level amplitude involves only the $D^{*\pm}D^{\pm}\gamma$ magnetic coupling, while FSI brings in the neutral magnetic coupling, which is much larger than the former one. This is also the reason, besides phase space, why the tree level width is much larger in the neutral mode than in the charged one, as commented above.

Notice that in the above calculations, we did not include the contribution from the coupled-channel FSI $D^*\bar{D}^* \to D\bar{D}^*$ which can come from replacing the $D^*D\gamma$ vertices in Fig. 9.6 by the $D^*D^*\gamma$ ones[15]. We have checked that this is a good approximation when the resummation of the charmed meson scattering is switched off. This is partly because the loop integral defined

[15]The electric part of the $D^*D^*\gamma$ vertex does not contribute to the FSI X_2 decay width amplitude when the quantum numbers of the final $D^*\bar{D}^*$ pair are 1^{+-}, with the two heavy mesons in relative $s-$wave. Thus, we are left with the contribution from the magnetic coupling, as in the $D^*D\gamma$ case.

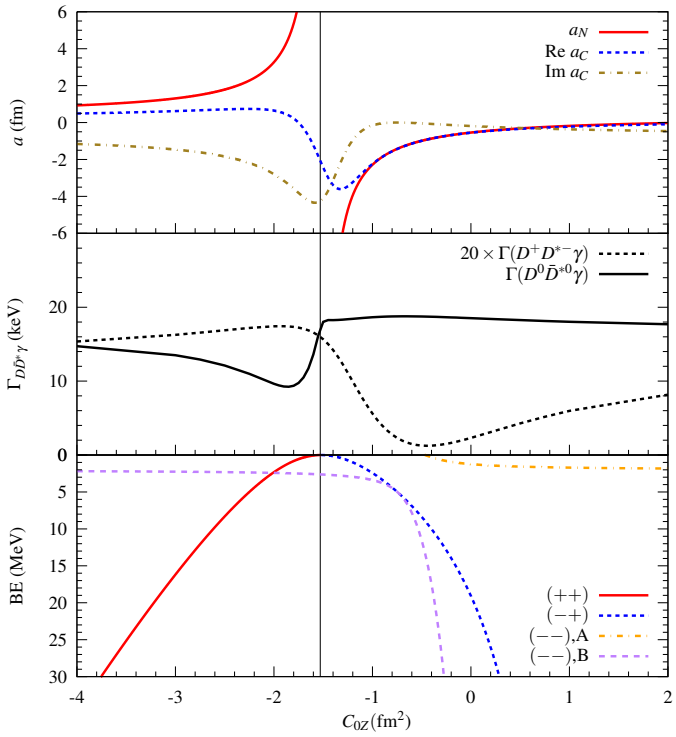

Figure 9.8: *Dependence on C_{0Z} of several physical quantities predicted in this work. In all cases an UV cutoff $\Lambda = 0.5$ GeV is employed in the Gaussian regulator. Top: $\widehat{T}_{00\to00}$ and $\widehat{T}_{+-\to+-}$ scattering lengths a_N (red solid curve) and a_C (blue dashed and green dash-dotted curves), respectively. They are defined as $a_i = \mu_i \widehat{T}_i(E = M_{1i} + M_{2i})/2\pi$, with μ_i the corresponding reduced mass and $(M_{1i}, M_{2i}) = (m_{D^0}, m_{D^{*0}})$ and $(m_{D^\pm}, m_{D^{*\pm}})$ for the neutral and charged channels, respectively. The scattering length a_C is complex because the neutral threshold is lower than the charged one, and therefore it is open. Middle: Central values of the $X_2(4013) \to D^0\bar{D}^{*0}\gamma$ (solid curve) and $X_2(4013) \to D^+D^{*-}\gamma$ (dashed curve) partial decay widths including FSI effects. Bottom: Position of the poles of the odd C-parity $D\bar{D}^* \to D\bar{D}^*$ T-matrix, with respect to the neutral $(m_{D^0} + m_{D^{*0}})$ threshold. Poles found in the various RS's are shown (see the text for details). The red solid curve shows the evolution of the bound state with C_{0Z}, while the dashed and the dash-dotted curves show that of the virtual ones. The vertical black line marks the value of C_{0Z} for which a $D\bar{D}^*$ bound state is generated at the $D^0\bar{D}^{*0}$ threshold.*

in Eq. (9.6.19) takes a larger absolute value for the considered diagrams than for those with the $D^*D^*\gamma$ vertices in most region of the phase space. The only exceptional region is where the photon has a very low energy so that the $D^*\bar{D}^*$ are almost on-shell. However, after integrating over the phase space, this region has little contribution to the partial decay width because of the p_γ^3 suppression since the photon is p-wave relative to the 1^{+-} $D\bar{D}^*$ system. The resummation would introduce a complication due to the presence of the $Z_c(4025)$ which couples dominantly to the $D^*\bar{D}^*$ in the 1^{+-} channel. It contributes mainly to the region close to the pole position of the $Z_c(4025)$. Again, this corresponds to the region with the very low-energy photon and thus suppressed due to phase space. Therefore, we expect that the neglected contribution discussed here has little impact; in particular, we have incorporated a sizable uncertainty in the results.

To better understand the dependence of the $X_2(4013) \to D\bar{D}^*\gamma$ decay widths on C_{0Z} in the bottom panel of Fig. 9.8 we show the pole positions of the odd C-parity $D\bar{D}^* \to D\bar{D}^*$ T-matrix

as functions of this LEC and for an UV cutoff of 0.5 GeV. There are two coupled channels, the neutral one which has the lowest threshold, and the charged channel. As a consequence, there are three relevant RS's (among four). The first of them [(++)] is the physical one, while the two non-physical RS's are reached by changing the sign of the imaginary part of the momentum inside of the loop functions G in Eq. (9.4.21) of the first channel [(−+)] or the momenta of both channels [(−−)]. Each of these non-physical RS's are continuously connected with the physical one on the real axis above the relevant thresholds. The solid red and dashed blue curves stand for poles in the (++) and (−+) RS's, respectively. For sufficiently large negative values of C_{0Z}, there is a bound state (a pole below threshold and located in the physical RS), which becomes less bound when $|C_{0Z}|$ decreases. For a value of this LEC around -1.5 fm^2, marked in Fig. 9.8 with a vertical black line, this state reaches the threshold. When C_{0Z} is further increased, the pole jumps into the (−+) RS, becoming thus a virtual state (a pole below threshold and located in a non-physical RS) and it moves away from the threshold. In the medium panel we show the central values of the $X_2(4013)$ radiative widths for both decay modes as a function of C_{0Z}, which were already presented in Fig. 9.7. As can be seen, it is around this critical value $C_{0Z} = -1.5$ fm^2, when the FSI effects are larger for both decays, due to the vicinity of the pole to the threshold. This happens regardless of whether it is a bound or a virtual state, since the presence of the pole in both situations greatly enhances the odd C-parity $D\bar{D}^* \to D\bar{D}^*$ T-matrix near threshold. This can be appreciated in the top panel of Fig. 9.8, where the dependence of the $\widehat{T}_{00\to 00}$ and $\widehat{T}_{+-\to +-}$ scattering lengths on C_{0Z} is shown.

Thus we have understood why in the region of values of C_{0Z} around -1.5 fm^2, FSI corrections strongly affect the $D^0\bar{D}^{*0}\gamma$ decay width: this channel has the lowest threshold and the bound or virtual state is located on or nearby it. For the charged decay mode, the width exhibits a maximum for values of C_{0Z} also in this region, followed by a clear minimum placed now in the vicinity of $C_{0Z} \sim C_{1Z}$. Notice that when $C_{0Z} = C_{1Z}$, $\widehat{T}_{00\to +-}$ vanishes (see Eq. (9.4.21)) and therefore the contribution due to the neutral mesons, driven by the largest magnetic coupling (β_1), in the FSI loops disappears. The exact position of the minimum is modulated by the further interference between the tree level and the FSI charged loops, which are comparable.

In the bottom panel, we also observe a virtual state pole, the position of which is rather insensitive[16] to C_{0Z}. It is originated by the interaction in the $I = 1$ sector, C_{1Z}, and it should be related to the $Z_c(3900)$ exotic charmonium-like state reported by the BESIII and Belle collaborations. Within our LO EFT scheme, we do not find a $D\bar{D}^*$ bound state, but instead a pole located near threshold in a non-physical RS (Chapter 5).

[16]The situation is more complicated, as can be seen in the plot. There is a narrow region of values of C_{0Z} around $[-0.4, -0.2]$ fm^2, where the virtual state moves quickly away from threshold, shortly reappearing again (orange dash-dotted line) in a position similar to the one that it had at the left of $C_{0Z} = -0.4$ fm^2. More in detail, in a narrow region included in the above interval of values of C_{0Z}, two poles (virtual) in the (−−) RS coexist. Among these two poles, the decay width should be influenced only by the one closest to threshold, since it overshadows the second one placed deeper in the real axis. On the other hand, for $C_{0Z} = -0.75$ fm^2 the (−−) RS virtual state (magenta, B) coincides with the one located in the (−+) RS (blue). This is easy to understand since at this point $C_{0Z} = C_{1Z} \equiv C_Z$ and then according to Eq. (9.4.21) the off-diagonal interaction term vanishes. In this situation, neutral and charged channels decouple, the scattering length a_C is real, and the determinant $(1 - C_Z G_{D^0\bar{D}^{*0}})(1 - C_Z G_{D^+\bar{D}^{*-}})$ would vanish when either of the two factors in brackets is zero. It turns out that the factor $(1 - C_Z G_{D^0\bar{D}^{*0}})$ vanishes at the same energy both in the (−+) and (−−) RS's, since by construction the $G_{D^0\bar{D}^{*0}}$ loop function is identical in both unphysical sheets. However, the charged factor $(1 - C_Z G_{D^+\bar{D}^{*-}})$ does not lead to any further pole for $C_{0Z} = C_{1Z} = -0.75$ fm^2 and $\Lambda = 0.5$ GeV. In the $\Lambda = 1$ GeV case, not shown in Fig. 9.8, it happens that for $C_{0Z} = C_{1Z} = -0.3$ fm^2, there exist identical poles in the (−+) and (−−), and (+−) and (−−) RS's, respectively, whose origin can be traced to the above discussion having in mind that now both terms in the decomposition of the determinant lead to poles.

9.4.2 $X_{b2} \to \bar{B}B^*\gamma$

The expressions found in the charm sector can be readily used here, having in mind the following correspondence: $D^0 \leftrightarrow B^-$, $D^+ \leftrightarrow \bar{B}^0$, $\bar{D}^0 \leftrightarrow \bar{B}^+$, and $D^- \leftrightarrow B^0$. Since the heavy quark flavour symmetry ensures that g and $\beta_{1,2}$ are the same in the b and c systems (up to corrections of the order $\Lambda_{\rm QCD}/m_c$), the expressions of Eqs. (9.4.1) and (9.4.2) can be used to predict the widths for the B^* radiative decays [96],

$$\Gamma(B^{*-} \to B^-\gamma) = \frac{\alpha}{3}\frac{m_B}{m_{B^*}}\left(\beta_1 - \frac{1}{3m_b}\right)^2 E_\gamma^3 = (0.49 \pm 0.05)\ \text{keV}, \tag{9.4.23}$$

$$\Gamma(\bar{B}^{*0} \to \bar{B}^0\gamma) = \frac{\alpha}{3}\frac{m_B}{m_{B^*}}\left(\beta_2 - \frac{1}{3m_b}\right)^2 E_\gamma^3 = (0.23 \pm 0.02)\ \text{keV}, \tag{9.4.24}$$

where we have taken the value $m_b = 4.8$ GeV for the bottom quark mass.

As in the study of its hadronic decays, we assume the X_{b2} to be a pure $I = 0$ state, with equal coupling to its neutral and charged components, $g_0^{X_{b2}} = g_c^{X_{b2}} = \frac{1}{\sqrt{2}} g^{X_{b2}}$. The isospin breaking effects for the B^* mesons are expected to be small and the tiny difference between the B^0 and $B^\pm$ masses can safely be neglected as well. In this limit we find at tree level

$$\begin{aligned} -i\mathcal{T}(\lambda, \lambda_*, \lambda_\gamma)_{\bar{B}B^*\gamma} &= \frac{g^{X_{b2}}(m_{12})}{\sqrt{2}}\sqrt{4\pi\alpha}N_\gamma^b\left(\beta_a - \frac{1}{3m_b}\right) \\ &\times \frac{\epsilon_{ijm}\epsilon^{jn}(\lambda)\epsilon^{*n}(\lambda_*)\epsilon_\gamma^{*i}(\lambda_\gamma)p_\gamma^m}{2m_{B^*}\,(m_{12} - m_{B^*} + i\varepsilon)}, \end{aligned} \tag{9.4.25}$$

where $\beta_a = \beta_1(\beta_2)$ for the $B^-B^{*+}\gamma(\bar{B}^0B^{*0}\gamma)$ mode, the normalization factor $N_\gamma^b = \sqrt{8M_{X_{b2}}m_{B^*}^2}$ $\sqrt{m_B m_{B^*}}$, and m_{12} is the invariant mass of the final $\gamma\bar{B}$ pair. These amplitudes lead to

$$\Gamma(X_{b2} \to B^-B^{*+}\gamma)_{\rm tree} = 13^{+23}_{-10}\ \text{eV}, \quad \Gamma(X_{b2} \to \bar{B}^0B^{*0}\gamma)_{\rm tree} = 6^{+10}_{-5}\ \text{eV}, \tag{9.4.26}$$

where the values have been obtained with $\Lambda = 0.5$ GeV. We remind that for $\Lambda = 1$ GeV, the central value of the resonance mass $M_{X_{b2}}$ is located below the threshold $m_B + m_{B^*} \sim 10604$ MeV and the decay is forbidden. The errors reflect the uncertainty in the inputs from the $X(3872)$ and the HQSS breaking corrections, as outlined in the caption of Table 9.3. The widths are of the order of a few eV, significantly smaller than those of the radiative decays of the B^{*0} and B^{*-} meson because of the quite reduced phase space available (~ 20 MeV) for this p-wave decay. They are also orders of magnitude smaller than $\Gamma(X_2 \to D^0\bar{D}^{*0}\gamma)$ as a result of $\Gamma(D^{*0} \to D^0\gamma) \gg \Gamma(B^* \to B\gamma)$.

The amplitude for the FSI mechanisms is readily evaluated and we find

$$\begin{aligned} -i\mathcal{T}(\lambda, \lambda_*, \lambda_\gamma)^{\rm FSI}_{\bar{B}B^*\gamma} &= -\sqrt{4\pi\alpha}N_\gamma^b\frac{g^{X_{b2}}}{\sqrt{2}}4m_B m_{B^*} \\ &\epsilon_{ijm}\epsilon^{jn}(\lambda)\epsilon^{*n}(\lambda_*)\epsilon_\gamma^{*i}(\lambda_\gamma)p_\gamma^m J(m_{B^*}, m_{B^*}, m_B, \vec{p}_\gamma) \\ &\times\left\{\left(\beta_1 - \frac{1}{3m_b}\right)\left[\frac{T^{I=0}_{C=-1}(m_{23}) \pm T^{I=1}_{C=-1}(m_{23})}{2}\right]_{\bar{B}B^*}\right. \\ &\left. + \left(\beta_2 - \frac{1}{3m_b}\right)\left[\frac{T^{I=0}_{C=-1}(m_{23}) \mp T^{I=1}_{C=-1}(m_{23})}{2}\right]_{\bar{B}B^*}\right\}, \end{aligned} \tag{9.4.27}$$

where the $+-$ $(-+)$ combination stands for the $B^-B^{*+}\gamma$ $(\bar{B}^0B^{*0}\gamma)$ decay mode and m_{23} is now the invariant mass of the $\bar{B}B^*$ pair. The C-parity odd isospin amplitudes are obtained by solving Eq. (9.4.15) using the bottom sector loop function $G_{\bar{B}B^*}$.

FSI corrections turn out to be important, as can be appreciated in Fig. 9.9. This is because we are generating in the $T^{I=1}_{C=-1}$ amplitude a bound state [the $Z_b(10610)$ resonance], almost at threshold (binding energy (2.0 ± 2.0) MeV [44]), that enhances the loop mechanisms, as we discussed in the charm sector. If we pay attention for instance to the charged $B^- B^{*+}\gamma$ mode, we could appreciate a distinctive feature: there appears a destructive interference pattern between the tree level and the FSI amplitudes. Thanks to our MC procedure where correlations are consistently propagated, we also observe a reduction of the size in the uncertainties. Besides the uncertainties on the mass and the couplings of the X_{b2} resonance, the errors on C_{1Z} quoted in Eq. (9.4.22) are also accounted for in the 68% CL bands displayed in the panels. Actually, these latter uncertainties should have also an important impact on the total CL bands. This is because variations of C_{1Z} allow for situations where the pole is located precisely at threshold (zero binding energy) or bound by about 4 MeV. In the first case the FSI contribution should be larger than that obtained with the central value of C_{1Z}, which correspond to a binding energy of 2 MeV. These big 68% CL bands makes hard to disentangle any further dependence on C_{0Z}, which in this case turns out to be quite mild.

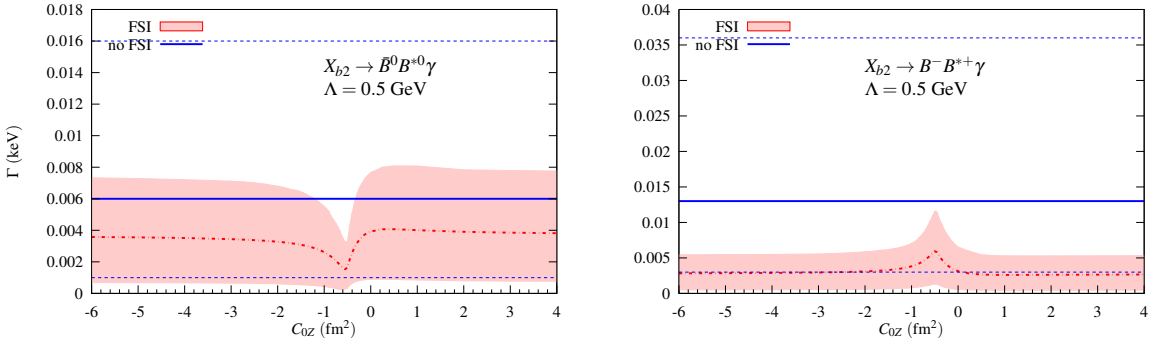

Figure 9.9: *Dependence of the $X_{b2} \to \bar{B}^0 B^{*0}\gamma$ and $X_{b2} \to B^- B^{*+}\gamma$ partial decay widths on the low-energy constant C_{0Z}. The red error bands contain the $\bar{B}B^*$ FSI effects, while the three horizontal blue lines stand for the tree level predictions of Eq. (9.4.26).*

9.5 Conclusions

In this chapter, we have studied the hadronic and radiative decays of a molecular $P^*\bar{P}^*$ state with quantum numbers $J^{PC} = 2^{++}$ in the charm (X_2) and bottom (X_{b2}) sectors using an EFT approach. We have considered the $X(3872)$ resonance as a $J^{PC} = 1^{++}$ $D\bar{D}^*$ hadronic molecule. The X_2 and the X_{b2} states will be HQSFS partners of the $X(3872)$ with masses and couplings to the $P^*\bar{P}^*$ heavy meson pair determined by the properties of the $X(3872)$ resonance.

The hadronic d-wave $X_2 \to D\bar{D}$ and $X_2 \to D\bar{D}^*$ two-body decays are driven via one pion exchange. We observed that as a result of the contribution from highly virtual pions, which is out of control in the low-energy EFT, these hadronic decay widths (hence the total width of the X_2 as well) bear a large systematic uncertainty. Even though the momenta involved in these decays probably lie outside the range of applicability of EFT the calculations are still valuable as a way to find reasonable estimates of these decay widths, which we expect to almost saturate the X_2 decay width. To this end and in analogy to the Bonn potential, we have included a monopole pion-exchange form factor, with a cutoff around 1 GeV, in each of the $D^*D\pi$ and $D^*D^*\pi$ vertices

to suppress the contribution of large momenta. We finally estimate the partial widths of both processes to be of the order of a few MeV. The analysis runs in parallel in the bottom sector with the assumption that the bare contact terms in the Lagrangian are independent of m_Q. In this sector, we also find widths of the order of a few MeV.

We discussed the radiative $X_2 \to D\bar{D}^*\gamma$ and $X_{b2} \to \bar{B}B^*\gamma$ decays as well. The widths are small, of the order of keV's (eV's) in the charm (bottom) sectors. Furthermore, they are affected by the $D\bar{D}^*$ or $B\bar{B}^*$ FSI mechanisms. FSI effects are large because they are enhanced by the presence of the isovector $Z_c(3900)$ and $Z_b(10610)$ resonances located near the $D^0\bar{D}^{*0}$ and $\bar{B}B^*$ thresholds, respectively. In the charm sector, FSI corrections turn out to be also sensitive to the negative C-parity isoscalar $D\bar{D}^*$ interaction (C_{0Z}). Thus, future precise measurements of these radiative decay widths might provide valuable information on this LEC, which cannot be in principle determined from the properties of the $X(3872)$, $Z_b(10610)$ and $Z_b(10650)$ resonances. Constraints on this latter LEC are important in order to understand the dynamics of the $P^{(*)}\bar{P}^{(*)}$ system.

9.6 Appendix

9.6.1 Local $D\bar{D}^* \to D\bar{D}^*$ Interactions

From the Lagrangian of Eq. (3.2.1) (Chapter 3), the interaction in the particle basis $\left\{D^0\bar{D}^{*0}, D^{*0}\bar{D}^0, D^+D^{*-}, D^{*+}D^-\right\}$ space reads:[17]

$$\begin{aligned} V_{D^{(*)}\bar{D}^{(*)}} &= A^T \times \mathrm{Diag}(C_{0Z}, C_{0X}, C_{1Z}, C_{1X}) \times A \qquad (9.6.1)\\ &= \frac{1}{2}\begin{pmatrix} C_{0a}+C_{1a} & -C_{0b}-C_{1b} & C_{0a}-C_{1a} & C_{1b}-C_{0b} \\ -C_{0b}-C_{1b} & C_{0a}+C_{1a} & C_{1b}-C_{0b} & C_{0a}-C_{1a} \\ C_{0a}-C_{1a} & C_{1b}-C_{0b} & C_{0a}+C_{1a} & -C_{0b}-C_{1b} \\ C_{1b}-C_{0b} & C_{0a}-C_{1a} & -C_{0b}-C_{1b} & C_{0a}+C_{1a} \end{pmatrix}, \end{aligned}$$

with $C_{0Z} = C_{0a} - C_{0b}$ and the orthogonal matrix A given by:

$$A = \frac{1}{2}\begin{pmatrix} 1 & 1 & 1 & 1 \\ 1 & -1 & 1 & -1 \\ 1 & 1 & -1 & -1 \\ 1 & -1 & -1 & 1 \end{pmatrix}. \qquad (9.6.2)$$

Equation (9.6.2) trivially follows from the fact that the $\mathcal{L}_{4H}$ interaction of Eq. (3.2.1) is diagonal in the isospin basis and the charge conjugation is well defined.[18] The interaction given in Eq. (9.6.2) can be used as the kernel of an UV finite LSE to obtain the T-matrix that we use to account for the FSI in the radiative decays studied in Section 9.4,

$$[T_{D^{(*)}\bar{D}^{(*)}}(E)]^{-1} = \mathcal{F}_\Lambda^{-1}(E) \cdot \left\{[V_{D^{(*)}\bar{D}^{(*)}}]^{-1} - \widehat{G}(E)\right\} \cdot \mathcal{F}_\Lambda^{-1}(E), \qquad (9.6.3)$$

with the two particle regularized matrix propagator defined as

$$\widehat{G}(E) = \mathrm{Diag}\left(G_{D^0\bar{D}^{*0}}, G_{D^{*0}\bar{D}^0}, G_{D^+D^{*-}}, G_{D^{*+}D^-}\right), \qquad (9.6.4)$$

$$G_{ij}(E) = \int \frac{d^3\vec{q}}{(2\pi)^3} \frac{e^{-2\vec{q}^{\,2}/\Lambda^2}}{E - \vec{q}^{\,2}/2\mu_{ij} - M_i - M_j + i\varepsilon}, \qquad (9.6.5)$$

[17] In the bottom sector, the corresponding basis is: $\left\{B^-B^{*+}, B^{*-}B^+, \bar{B}^0B^{*0}, \bar{B}^{*0}B^0\right\}$.

[18] For instance in the charm sector, the C-parity states are $[D\bar{D}^*]_{1,2} = \frac{D\bar{D}^* \pm D^*\bar{D}}{\sqrt{2}}$ ($1 \leftrightarrow +$, $2 \leftrightarrow -$). As we have mentioned, in our convention, the C-parity of these states is independent of the isospin and it is equal to ∓ 1.

where trivially $G_{D^0\bar{D}^{*0}} = G_{D^{*0}\bar{D}^0}$ and $G_{D^+D^{*-}} = G_{D^{*+}D^-}$. In addition, the on-shell UV Gaussian form factor matrix reads

$$\mathcal{F}_\Lambda(E) = \text{Diag}\left(f_\Lambda^{\text{neu}}(E), f_\Lambda^{\text{neu}}(E), f_\Lambda^{\text{ch}}(E), f_\Lambda^{\text{ch}}(E)\right) \tag{9.6.6}$$

with $f_\Lambda^{(a)}(E) = \exp(-\vec{k}_a^2/\Lambda^2)$ and $\vec{k}_a^2 = 2\mu_a(E - M_{1a} - M_{2a})$, with $a = (\text{neu}), (\text{ch})$.

9.6.2 Validity of the perturbative treatment of the $D\bar{D}$ for the X_2

In this appendix, we argue that the d-wave $D\bar{D}$ may be treated perturbatively in the 2^{++} system. Even though this was already discussed in Ref. [25], we have included here a new argument grounded on a different EFT to make a more compelling case on the smallness of this contribution to the X_2 mass. We compare the power counting of the self-energy diagrams of the X_2 from the d-wave $D\bar{D}$ and the s-wave $D^*\bar{D}^*$ two-point loops, see Fig. 9.10. If the $D\bar{D}$ loop is suppressed in comparison with the $D^*\bar{D}^*$ one, it will validate the perturbative treatment of the $D\bar{D}$. Because in our case the heavy mesons are non-relativistic, we can apply a velocity counting for the loops analogous to the power counting of the heavy meson loops in heavy quarkonium transitions [197, 229].

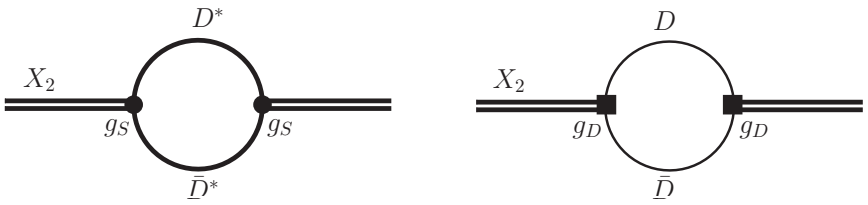

Figure 9.10: *The X_2 self-energy diagrams from the s-wave $D^*\bar{D}^*$ and d-wave $D\bar{D}$, respectively.*

For the $D^*\bar{D}^*$ loop, the velocity counting of the self-energy reads as

$$\Sigma_{D^*\bar{D}^*} \sim g_S^2 \frac{v^5}{(v^2)^2} = g_S^2\, v, \tag{9.6.7}$$

where g_S denotes the value of the s-wave coupling of the X_2 to the $D^*\bar{D}^*$, v denotes the velocity of the D^* meson, v^5 is for the loop integral measure since the non-relativistic energy is counted as $\mathcal{O}(v^2)$, and $1/(v^2)^2$ accounts for the two non-relativistic propagators.

Similarly, for the $D\bar{D}$ loop, denoting the velocity of the D meson by w, the velocity counting is given by

$$\Sigma_{D\bar{D}} \sim g_D^2 \frac{w^5 w^4}{(w^2)^2} = g_D^2\, w^5, \tag{9.6.8}$$

where g_D is the d-wave coupling constant normalized to have the same dimension as g_S, and the factor of w^4 in the denominator comes from the two d-wave vertices.

Therefore, we obtain the ratio

$$r_{D/S} \equiv \frac{\Sigma_{D\bar{D}}}{\Sigma_{D^*\bar{D}^*}} = \frac{g_D^2}{g_S^2}\frac{w^5}{v}. \tag{9.6.9}$$

The question is now how g_D compares with g_S. We can estimate g_D by considering the one-pion exchange diagram considered in this chapter as illustrated in Fig. 9.11. Because the X_2 is very

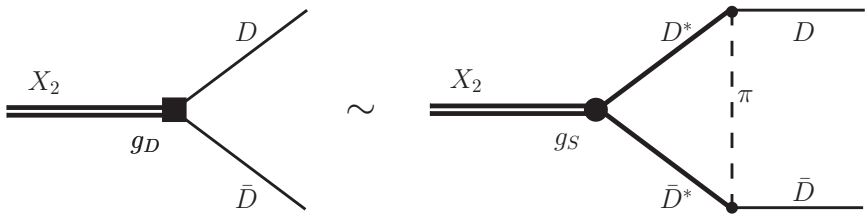

Figure 9.11: *The contact term of the d-wave coupling of the X_2 to the $D\bar{D}$ may be estimated by the one-pion exchange diagram.*

close to the $D^*\bar{D}^*$ threshold, we should count each of the $D^*(\bar{D}^*)$ propagators as $1/v^2$. This is equivalent to affirm that the cut due to the $D^*\bar{D}^*$ in the triangle diagram in Fig. 9.11 is the same as that in the $D^*\bar{D}^*$ bubble diagram of the X_2 self-energy. Thus, we can count the D^* in both diagrams in the same way. But the pion propagator should be counted differently. The reason is that because the X_2 couples to the $D\bar{D}$ in a d-wave, the momenta in the $D^*D\pi$ vertices of the one-pion exchange diagram should become the momenta of the D and $\bar{D}$, $q_D = m_D w$, and the pion momentum is of the same order as we discussed in Sect. 9.3.1. This is to say that the pion propagator should be counted as $1/w^2$ rather than $1/v^2$. Thus, expressing the content of Fig. 9.11 in terms of power counting gives

$$g_D w^2 \sim g_S \frac{v^5}{(v^2)^2 w^2} \left(\frac{g}{\Lambda_\chi}\right)^2 (m_D w)^2 = \left[g_S g^2 \frac{v}{w^2} \left(\frac{m_D}{\Lambda_\chi}\right)^2\right] w^2, \tag{9.6.10}$$

where g is the axial coupling constant in Heavy Meson Chiral Perturbation Theory (Eq. (2.3.34)), and $\Lambda_\chi = 4\pi f_\pi$ is the hard scale for the chiral expansion.

Numerically, for the case of the X_2, we have $w \simeq \sqrt{(M_{X_2} - 2M_D)/M_D} \simeq 0.38$, and $v \simeq \sqrt{(M_{X_2}) - 2M_D/M_D} \sim 0.06$ if we take 7 MeV as the binding energy (recall that we have the charged $D^*\bar{D}^*$ channel explicitly whose threshold is around 7 MeV above the neutral one). With these values, we use Eqs. (9.6.9) and (9.6.10), which leads to $g_D \sim 0.6\, g_S$, to obtain an estimate of the contribution of the d-wave $D\bar{D}$ to the X_2 self-energy relative to the s-wave $D^*\bar{D}^*$,

$$r_{D/S} \sim 0.05. \tag{9.6.11}$$

The above value suggests a high suppression of the d-wave $D\bar{D}$ in comparison with the s-wave $D^*\bar{D}^*$. We notice that the power counting of Ref. [25] indicates that the size of the $D\bar{D}$ loop is N^{4}LO (next-to-next-to-next-to-next-to-leading order), in line with the velocity power counting arguments.

9.6.3 Three-point loop functions

Hadron decays

In this section we address the tensor three-point loop function that appears in the hadron decay amplitudes studied in the Sect. 9.3. It is composed by a pion, and two heavy meson ($P^*\bar{P}^*$)

propagators. The integral reads ($\vec{q} = -\vec{k}$, $q^0 + k^0 = M_{X_2}$)

$$\begin{aligned} I^{ij}(M, m; M_{X_2}, q^\mu) &= \\ &= i \int \frac{d^4 l}{(2\pi)^4} \frac{l^i\, l^j}{[(l+q)^2 - M^2 + i\varepsilon]\,[(k-l)^2 - M^2 + i\varepsilon]\,(l^2 - m^2 + i\varepsilon)} \\ &\simeq \frac{i}{4M^2} \int \frac{d^4 l}{(2\pi)^4} \frac{l^i\, l^j}{(l^0 + q^0 - \omega_h + i\varepsilon)\,(k^0 - l^0 - \omega_h + i\varepsilon)\,(l^2 - m^2 + i\varepsilon)}, \end{aligned} \tag{9.6.12}$$

where M is the mass of the heavy particles in the loop, m is the mass for the light intermediate particle, M_{X_2} is the total c.m. energy, and q and k are the external 4-momenta of the two particles in the final state of masses m_{F_1} and m_{F_2}, respectively. In addition,

$$q^0 = \frac{M_{X_2}^2 + m_{F_1}^2 - m_{F_2}^2}{2M_{X_2}}, \quad k^0 = \frac{M_{X_2}^2 + m_{F_2}^2 - m_{F_1}^2}{2M_{X_2}}, \tag{9.6.13}$$

and $\omega_h = M + (\vec{q} + \vec{l})^{\,2}/2M$ is the non-relativistic energy of the virtual heavy mesons. Using Cauchy's theorem to integrate over the virtual pion energy l^0, we obtain:[19]

$$\begin{aligned} I^{ij}(M, m; M_{X_2}, q^\mu) &\simeq \\ &\simeq \frac{1}{4M^2} \int \frac{d^3 l}{(2\pi)^3} l^i l^j \frac{M_{X_2} - 2\omega_h - 2\omega}{2\omega(k^0 - \omega - \omega_h)(q^0 - \omega - \omega_h)(M_{X_2} - 2\omega_h)}\,, \end{aligned} \tag{9.6.14}$$

for $|m_{F_1}^2 - m_{F_2}^2| < 2mM_{X_2} < 4Mm$ to guarantee that the integral in Eq. (9.6.13) is real, and $\omega(\vec{l}) = \sqrt{m^2 + \vec{l}^{\,2}}$. The loop integral I^{ij} presents a logarithmic UV divergence. Indeed, I^{ij} admits a tensor decomposition

$$I^{ij}(\vec{q}) = I_0(\vec{q}^{\,2})\, q^i q^j + I_1(\vec{q}^{\,2})\, \delta^{ij}\, |\vec{q}|^2\,. \tag{9.6.15}$$

The I_1 term presents an UV divergence, but it does not contribute to the amplitude because it annihilates the traceless spin-2 polarization tensor. This means that only the I_0 term is relevant. It can be computed as:

$$\begin{aligned} I_0(M, m; M_{X_2}, \vec{q}^{\,2}) &\simeq \frac{1}{32M^2\pi^2\vec{q}^{\,2}} \int_0^{+\infty} \frac{dl\, l^4}{\omega} \\ &\times \int_{-1}^{+1} dx P_2(x) \frac{M_{X_2} - 2\omega_h(l,x) - 2\omega}{(k^0 - \omega - \omega_h(l,x))(q^0 - \omega - \omega_h(l,x))(M_{X_2} - 2\omega_h(l,x))}, \end{aligned} \tag{9.6.16}$$

with $\omega_h(l,x) = M + (\vec{l}^{\,2} + \vec{q}^{\,2} + 2|\vec{l}||\vec{q}|x)/2M$, and P_2 the Legendre's polynomial of order 2. This term is not UV divergent because in the limit $l \to +\infty$ all dependence on x, besides $P_2(x)$, disappears and the integration over x gives zero. The convergence of the integral is greatly enhanced because $P_2(x)$ is orthogonal to x as well. Moreover, the same type of arguments guarantees that $I_0(M, m; M_{X_2}, \vec{q}^{\,2}) \sim$ const. in the $\vec{q}^{\,2} \to 0$ limit. Numerically, we use non-relativistic kinematics to compute $|\vec{q}|$ in the evaluation of $I_0(M, m; M_{X_2}, \vec{q}^{\,2})$ in Eq. (9.6.17), *i.e.*, $\vec{q}^{\,2} \simeq 2\mu_{F_1F_2}(M_{X_2} - m_{F_1} - m_{F_2})$. However, to guarantee the appropriate d-wave phase space,

[19] If $m_{F_1} = m_{F_2}$, $k^0 = q^0 = M_{X_2}/2$ and the loop function now reads,

$$I^{ij}(M, m; M_{X_2}, \vec{q}) \simeq \frac{1}{8M^2} \int \frac{d^3 l}{(2\pi)^3} \frac{l^i l^j}{\omega(M_{X_2}/2 - \omega - \omega_h)(M_{X_2}/2 - \omega_h)}, \quad M_{X_2} < 2M\,.$$

we use relativistic kinematics to evaluate $q^i q^j$ in Eq. (9.6.15) and the $|\vec{q}|$ phase-space factor that appears in Eqs. (9.3.3) and (9.3.9).

For consistency with the scheme adopted in Eq. (9.2.3), we include a Gaussian regulator in the $P^*\bar{P}^*X_2$ vertex by multiplying the integrand in Eq. (9.6.17) by the exponential factor,

$$\frac{e^{-\left(\vec{q}+\vec{l}\right)^2/\Lambda^2}}{e^{-\gamma^2/\Lambda^2}} = \frac{e^{-\left(\vec{l}^2+\vec{q}^2+2|\vec{l}||\vec{q}|x\right)/\Lambda^2}}{e^{-\gamma^2/\Lambda^2}} \tag{9.6.17}$$

with $0 > \gamma^2 = M(M_{X_2} - 2M)$. We divide by the factor $e^{-\gamma^2/\Lambda^2}$, because it was incorporated in the $P^*\bar{P}^*X_2$ coupling.

In addition, the exchanged pion is highly virtual, and one might include a vertex form factor of the form

$$F(\vec{l}^{\,2}, \Lambda_\pi) = \frac{\Lambda_\pi^2}{\vec{l}^{\,2} + \Lambda_\pi^2}, \qquad \Lambda_\pi \sim 1 \text{ GeV}, \tag{9.6.18}$$

in each of the two $\pi P^{(*)} P^{(*)}$ vertices.

Radiative decays

In the computation of the FSI effects on the radiative decays of the X_2 and X_{b2} resonances in the Sect. 9.4, the following three-point loop function appeared

$$\begin{aligned} J\left(M_1, M_2, M_3, \vec{p}_\gamma\right) \;&=\; \\ &= i \int \frac{d^4q}{(2\pi)^4} \frac{1}{q^2 - M_1^2 + i\varepsilon} \frac{1}{(P-q)^2 - M_2^2 + i\varepsilon} \frac{1}{(q-p_\gamma)^2 - M_3^2 + i\varepsilon} \\ &\simeq \frac{i}{8M_1M_2M_3} \int \frac{d^4q}{(2\pi)^4} \frac{1}{q^0 - M_1 - \vec{q}^{\,2}/2M_1 + i\varepsilon} \\ &\quad \times \frac{1}{M_{X_2} - q^0 - M_2 - \vec{q}^{\,2}/2M_2 + i\varepsilon} \frac{1}{q^0 - E_\gamma - M_3 - (\vec{q} - \vec{p}_\gamma)^2/2M_3 + i\varepsilon} \\ &= \frac{\mu_{12}\mu_{23}}{2M_1M_2M_3} \int \frac{d^3q}{(2\pi)^3} \frac{1}{(\vec{q}^{\,2} + c - i\varepsilon)} \frac{1}{(\vec{q}^{\,2} - 2\mu_{23}\, \vec{q}\cdot\vec{p}_\gamma/M_3 + c' - i\varepsilon)}, \end{aligned} \tag{9.6.19}$$

with $P^\mu = (M_{X_2}, \vec{0})$ in the rest frame of the X_2 and $\mu_{ij}^{-1} = (M_i^{-1} + M_j^{-1})$. In addition, $b_{12} = M_1 + M_2 - M_{X_2}$, $b_{23} = M_2 + M_3 + E_\gamma - M_{X_2}$, $c = 2\mu_{12}b_{12}$ and $c' = 2\mu_{23}b_{23} + \mu_{23}\vec{p}_\gamma^{\,2}/M_3$. Since all the intermediate mesons in the present case are non-relativistic, the three-point loop has been treated non-relativistically. This loop integral is convergent and its analytic expression can be found in Eq. (A2) of Ref. [197]. However, for consistency, despite the three-point loop function in Eq. (9.6.19) being finite, it should be evaluated using the same UV renormalization scheme as that employed in the $D^{(*)}\bar{D}^{(*)}$ EFT. This is accomplished by including in the integrand of Eq. (9.6.19) a Gaussian form factor, $F_\Lambda(\vec{q})$ defined as

$$F_\Lambda(\vec{q}) = e^{-\left(\vec{q}^{\,2} - \gamma^2\right)/\Lambda^2} e^{-\left(\vec{q}^{\,2}_{\rm cm} - \vec{q}^{\,2}_{\rm on\,shell}\right)/\Lambda^2}. \tag{9.6.20}$$

Here $\gamma^2 = 2\mu_{12}(M_{X_2} - M_1 - M_2)$, $\vec{q}^{\,2}_{\rm on\,shell} = 2\mu_{23}(m_{23} - M_2 - M_3)$, with $m_{23}^2 = (P - p_\gamma)^2 = M_{X_2}^2 - 2M_{X_2}E_\gamma$, and

$$\vec{q}^{\,2}_{\rm cm} = \frac{M_2(\vec{q} - \vec{p}_\gamma)^2 + M_3\vec{q}^{\,2}}{M_2 + M_3}. \tag{9.6.21}$$

Note that the first exponential factor accounts for the off-shellness in the $X_2 D^{*0}\bar{D}^{*0}$ coupling, as in Eq. (9.4.9), while the second one accounts for the virtuality of the incoming mesons in the

$D\bar{D}^* \to D\bar{D}^*$ and $D^*\bar{D} \to D\bar{D}^*$ T-matrices. Note that, after the inclusion of this factors, an analytical expression for the integral cannot be easily obtained, and it needs to be computed numerically.

Conclusions and Outlook

In this section we briefly summarize the work contained in this thesis, highlighting the most important results and, finally, mentioning possible perspectives to extend this research in the future.

We have proposed the existence, and studied the dynamics, of several exotic meson-antimeson molecules in the quarkonium spectrum. We have been interested in molecular states with hidden-charm or bottom degrees of freedom, and have studied these systems from an EFT point of view. Thus, we have proposed an EFT based on the underlying QCD symmetries that arise in the infinite quark mass limit. In this limit, the dynamics of an infinitely heavy quark is independent from its spin and flavour. At LO and assuming light $SU(3)$-flavour symmetry, the most general $P^{(*)}\bar{P}^{(*)}$ interaction compatible with HQSS only depends on four undetermined LECs. Indeed, at LO the EFT entails a remarkable simplification and it only involves contact range interactions among the heavy-light meson and antimeson fields. HQSS and $SU(3)$-light flavour symmetry provide relationships among the $P^{(*)}\bar{P}^{(*)}$ interactions in different sectors. As a consequence, these four parameters are enough to describe twenty-four (that is the multiplicity of the $P^{(*)}\bar{P}^{(*)}$ space without considering spin-isospin third components or states that are connected by a C-parity transformation) different channels.

The undetermined LECs are fitted to reproduce the position of some experimental resonances, whose nature is unknown, but assumed to be molecular. The resonance $X(3872)$ and the isovector $Z_b(10610)/Z_b'(10650)$ located very close to the $D\bar{D}^*$, $B\bar{B}^*$ and $B^*\bar{B}^*$ thresholds, respectively, are of special interest at this respect. Besides, we have also shown that the isospin violating decays of the $X(3872)$ can be used to constrain the interaction between the D and the $\bar{D}^*$ mesons in the isovector channel. Once the LO LECs are fixed, predictions for different exotic states have been formulated. We have found that if the identification of those resonances as molecular states is accurate, there is no reason to believe that other molecular states might not appear in the hadronic spectrum. This set of predicted states compose a family (related through HQSFS) of exotic states. Particularly interesting are the predictions for a isoscalar 1^{++} $B\bar{B}^*$ bound state with a mass about 10580 MeV which may be searched for in the $\Upsilon(1s,2s)$ $\pi^+\pi^-\pi^0$ mass distribution; and the isovector charmonium partners of the $Z_b(10610)/Z_b'(10650)$, which probably correspond to the very recently observed $Z_c(3900)$ and $Z_c(4025)$ resonances by the BESIII Collaboration. The $J^{PC}=2^{++}$ partners of the $X(3872)$ resonance, both in the charm and bottom sectors, are also of special interest since their existence would strongly support the molecular interpretation of the $X(3872)$ resonance.

Moreover, we have shown that the existence of heavy-light meson-antimeson molecules implies the possibility of partners composed of a heavy-light meson and a doubly heavy baryon. In this regard, the $D\bar{D}^*$ molecular nature of the $X(3872)$ hints at the existence of several baryonic partners with isospin $I=0$ and $J^P=\frac{5}{2}^-$ or $\frac{3}{2}^-$. We have also discussed that if the $Z_b(10650)$ turns out to be a $B^*\bar{B}^*$ bound state, we can be confident of the existence of $\Xi_{bb}^*\bar{B}^*$ hadronic molecules

with quantum numbers $I(J^P) = 1\left(\frac{1}{2}^-\right)$ and $I(J^P) = 1\left(\frac{3}{2}^-\right)$. These states will be difficult to accommodate in conventional constituent quark models because they can be considered to be triply heavy pentaquarks.

We have also addressed the interaction of pairs of charmed mesons with hidden charm in a finite box. The energy levels in the box are computed within this model, and from them some synthetic data have been generated. These data have been then employed to study the inverse problem of getting the energies of the bound states and phase shifts for $D\bar{D}$ or $D^*\bar{D}^*$ systems. Different strategies were investigated using the lowest two levels for different values of the box size, and the errors produced were studied. Starting from the upper level, fits to the synthetic data were carried out to determine the scattering length and effective range plus the binding energy of the ground state. A similar strategy using the effective range formula was considered with a simultaneous fit to the two levels; one above and the other one below the threshold. This method turned out to be more efficient than the previous one. Finally, a method based on the fit to the data by means of a potential and a conveniently regularized loop function, was shown to be very efficient and it allowed us to produce accurate results in the infinite volume starting from levels of the box with errors far larger than the uncertainties obtained in the final results.

On the other hand, we have also shown that the regularization method based on Gaussian wave functions is rather efficient in the analysis and as a byproduct a practical and fast method to calculate the Lüscher function with high precision has been presented.

We have also studied the HQSS partners of the $X(3872)$ resonance using a correlation function approach in the heavy quark limit. We have discussed even and odd C-parity currents that can be used to study the $X(3872)$ and its HQSS partners in QCDSR or LQCD calculations. The isospin structure was also discussed within this framework.

In the final two chapters of the thesis, we first studied the $X(3872) \to D^0\bar{D}^0\pi^0$ decay. This decay mode is more sensitive to the long-distance structure of the $X(3872)$ resonance than its $J/\psi\ \pi\pi$ and $J/\psi\ \pi\pi\pi$ decays, which are mainly controlled by the details of the $X(3872)$ wave function at short distances. We also showed that the $D^0\bar{D}^0$ final state interaction can be important, and that a precise measurement of this partial decay width can provide valuable information on the interaction strength between the $D^{(*)}\bar{D}^{(*)}$ charm mesons.

Next we paid attention to the 2^{++} molecular state, X_2, partner of the $X(3872)$, which would be a loosely bound $D^*\bar{D}^*$ state. The X_2 is expected to decay dominantly into d-wave $D\bar{D}$, $D\bar{D}^*$ and $\bar{D}D^*$ pairs. We have computed the decay widths of the X_2 resonance into the above channels, as well as those of its bottom partner, X_{b2}, whose mass is determined thanks to heavy flavour symmetry. We have found partial widths of the X_2 and X_{b2} of the order of a few MeV. Finally, we have also studied the radiative $X_2 \to D\bar{D}^*\gamma$ and $X_{b2} \to B\bar{B}^*\gamma$ decays. As in the case of the $X(3872) \to D^0\bar{D}^0\pi^0$ decay, these decay modes are more sensitive to the long-distance structure of the resonances and to the $D\bar{D}^*$ or $B\bar{B}^*$ final state interactions.

As a final remark, we would like to stress that through this work, an special attention has been paid to estimate both systematic (HQSFS breaking corrections for instance) and statistical (induced by those of the experimental inputs) uncertainties affecting our theoretical predictions. To that end, Monte Carlo techniques have revealed as powerful and trustworthy tools.

To finish, we outline possible ideas for future projects, that will naturally extend the work presented in this thesis.

1. The simplest way of improving the work is having access to some more experimental inputs that could better constrain the LECs that appear at LO in the EFT expansion. Thus, new experimental information on new exotic states that could be interpreted as loosely bound

dimeson molecules would be highly welcome. In parallel, similar improvement can be achieved if we were able to determine the LECs from a well founded model. Examples of such theoretical schemes could be hidden-gauge or $SU(8)$ spin-symmetry-based models, etc.

2. The inclusion of NLO effects in the contact Lagrangian, and the consideration of coupled-channel effects and the pion exchange interaction, would give rise to more accurate predictions. In addition, the dependence in the Gaussian regulator should, in principle, be diminished as well. However, the number of undetermined LECs would increase in this type of analysis.

3. Heavy Flavour Symmetry (used to relate dynamics in the charm and the bottom sector) imposes some $\frac{1}{m_Q}$ scaling laws for the LECs of the effective theory. In principle, one can foresee two different scaling laws,

$$C_b \sim C_c, \qquad \text{or} \qquad C_b \sim C_c \frac{m_c}{m_b}.$$

It is not completely clear which one of them is correct. In this thesis we have always assumed that the leading contribution to the counter-terms was independent of the heavy quark flavour (first scaling law). That is to say, the LECs are the same in the charm and bottom sectors (up to corrections of the order $\mathcal{O}\left(\frac{\Lambda_{QCD}}{m_Q}\right)$). The fact that OPE interactions provide heavy flavour independent interactions seems to support this scaling law. Results obtained within constituent quark models and the hidden gauge approach are also compatible with this first scaling law. Nevertheless, the study of the consequences derived from the second possibility seems also adequate, as suggested in Ref. [22], since it will lead naturally to a heavy quark mass independent renormalization scheme. That would require revisiting the analysis performed with the first scaling law and compare the new and old results. Of course, the comparison of the different predictions with future measurements of the charm and bottom spectra would be decisive to test the goodness of each assumption.

4. The Green function analysis carried out for hidden heavy flavour meson molecules could be used to obtain additional degeneracy relationships in other hadron systems involving heavy quarks. Specifically, meson-baryon states with hidden charm or bottom quantum numbers can be studied with an analogous formalism.

5. One can take advantage of a recent study on the quark mass dependence of the $X(3872)$ binding energy and extend our previous study of Chapter 4 in a finite box to address the dynamics of hidden charm molecules, both for finite volumes and non-physical pion masses. In this way, we could make more efficiently contact with results from LQCD simulations, since we would provide useful information to guide both the chiral and the continuum extrapolations.

6. Connected to the second point, a more detailed analysis on the Z_c's resonances looks timely. At LO, these resonances only appear as bound or virtual states. Any of these two interpretations seems insufficient according to the current experimental data. The inclusion of additional elements in the scheme, such as OPE and coupled-channel effects might effectively account for this discrepancy.

7. Some of the molecular resonances studied in this work, in particular the isoscalar ones, should have some mixings with genuine constituent quark model components. Such components might affect some of their properties, in special, those of the very loosely bound

ones. It is of capital importance to construct a model where genuine quark and hadron molecular degrees of freedom could be simultaneously considered.

Bibliography

[1] C. Hidalgo-Duque, J. Nieves, and M. P. Valderrama, "Light flavor and heavy quark spin symmetry in heavy meson molecules," *Phys.Rev.*, vol. D87, no. 7, p. 076006, 2013.

[2] M. Albaladejo, C. Hidalgo-Duque, J. Nieves, and E. Oset, "Hidden charm molecules in finite volume," *Phys.Rev.*, vol. D88, no. 1, p. 014510, 2013.

[3] F.-K. Guo, C. Hidalgo-Duque, J. Nieves, and M. P. Valderrama, "Consequences of Heavy Quark Symmetries for Hadronic Molecules," *Phys.Rev.*, vol. D88, p. 054007, 2013.

[4] F.-K. Guo, C. Hidalgo-Duque, J. Nieves, and M. P. Valderrama, "Heavy-antiquarkdiquark symmetry and heavy hadron molecules: Are there triply heavy pentaquarks?," *Phys.Rev.*, vol. D88, no. 5, p. 054014, 2013.

[5] C. Hidalgo-Duque, J. Nieves, A. Ozpineci, and V. Zamiralov, "X(3872) and its Partners in the Heavy Quark Limit of QCD," *Phys.Lett.*, vol. B727, p. 432, 2013.

[6] F.-K. Guo, C. Hidalgo-Duque, J. Nieves, A. Ozpineci, and M. P. Valderrama, "Detecting the long-distance structure of the $X(3872)$," *Eur.Phys.J.*, vol. C74, p. 2885, 2014.

[7] C. Garcia-Recio, C. Hidalgo-Duque, J. Nieves, L. Salcedo, and L. Tolos, "Compositeness of the strange, charm and beauty odd parity Λ states," arxiv.1506.04235.

[8] M. Voloshin and L. Okun, "Hadron Molecules and Charmonium Atom," *JETP Lett.*, vol. 23, p. 333, 1976.

[9] A. De Rujula, H. Georgi, and S. Glashow, "Molecular Charmonium: A New Spectroscopy?," *Phys.Rev.Lett.*, vol. 38, p. 317, 1977.

[10] S. Fleming, M. Kusunoki, T. Mehen, and U. van Kolck, "Pion interactions in the $X(3872)$," *Phys.Rev.*, vol. D76, p. 034006, 2007.

[11] M. P. Valderrama, "Power Counting and Perturbative One Pion Exchange in Heavy Meson Molecules," *Phys.Rev.*, vol. D85, p. 114037, 2012.

[12] E. Braaten and M. Kusunoki, "Low-energy universality and the new charmonium resonance at 3870-MeV," *Phys.Rev.*, vol. D69, p. 074005, 2004.

[13] T. Mehen and J. W. Powell, "Heavy Quark Symmetry Predictions for Weakly Bound B-Meson Molecules," *Phys.Rev.*, vol. D84, p. 114013, 2011.

[14] G. Ecker, J. Gasser, A. Pich, and E. de Rafael, "The Role of Resonances in Chiral Perturbation Theory," *Nucl.Phys.*, vol. B321, p. 311, 1989.

[15] E. Epelbaum, U. G. Meissner, W. Gloeckle, and C. Elster, "Resonance saturation for four nucleon operators," *Phys.Rev.*, vol. C65, p. 044001, 2002.

[16] E. Epelbaum, H.-W. Hammer, and U.-G. Meissner, "Modern Theory of Nuclear Forces," *Rev.Mod.Phys.*, vol. 81, p. 1773, 2009.

[17] R. Machleidt and D. Entem, "Chiral effective field theory and nuclear forces," *Phys.Rept.*, vol. 503, p. 1, 2011.

[18] N. Isgur and M. B. Wise, "Weak Decays of Heavy Mesons in the Static Quark Approximation," *Phys.Lett.*, vol. B232, p. 113, 1989.

[19] N. Isgur and M. B. Wise, "Weak Transition Form-Factors between Heavy Mesons," *Phys.Lett.*, vol. B237, p. 527, 1990.

[20] M. Neubert, "Heavy quark symmetry," *Phys.Rept.*, vol. 245, p. 259, 1994.

[21] A. V. Manohar and M. B. Wise, "Heavy quark physics," *Camb.Monogr.Part.Phys.Nucl.Phys.Cosmol.*, vol. 10, p. 1, 2000.

[22] M. T. AlFiky, F. Gabbiani, and A. A. Petrov, "X(3872): Hadronic molecules in effective field theory," *Phys.Lett.*, vol. B640, p. 238, 2006.

[23] M. Voloshin, "Radiative transitions from $\Upsilon(5S)$ to molecular bottomonium," *Phys.Rev.*, vol. D84, p. 031502, 2011.

[24] J. Nieves and M. P. Valderrama, "Deriving the existence of $B\bar{B}^*$ bound states from the X(3872) and Heavy Quark Symmetry," *Phys.Rev.*, vol. D84, p. 056015, 2011.

[25] J. Nieves and M. P. Valderrama, "The Heavy Quark Spin Symmetry Partners of the X(3872)," *Phys.Rev.*, vol. D86, p. 056004, 2012.

[26] F.-K. Guo, C. Hanhart, and U.-G. Meissner, "Implications of heavy quark spin symmetry on heavy meson hadronic molecules," *Phys.Rev.Lett.*, vol. 102, p. 242004, 2009.

[27] A. Bondar, A. Garmash, A. Milstein, R. Mizuk, and M. Voloshin, "Heavy quark spin structure in Z_b resonances," *Phys.Rev.*, vol. D84, p. 054010, 2011.

[28] M. J. Savage and M. B. Wise, "Spectrum of baryons with two heavy quarks," *Phys.Lett.*, vol. B248, p. 177, 1990.

[29] N. Brambilla, S. Eidelman, B. Heltsley, R. Vogt, G. Bodwin, *et al.*, "Heavy quarkonium: progress, puzzles, and opportunities," *Eur.Phys.J.*, vol. C71, p. 1534, 2011.

[30] S. Choi *et al.*, "Observation of a narrow charmonium - like state in exclusive $B^{\pm} \to K^{\pm}\pi^{+}\pi^{-}J/\psi$ decays," *Phys.Rev.Lett.*, vol. 91, p. 262001, 2003.

[31] S. Uehara *et al.*, "Observation of a $\chi'(c2)$ candidate in $\gamma\gamma \to D\bar{D}$ production at BELLE," *Phys.Rev.Lett.*, vol. 96, p. 082003, 2006.

[32] X. Liu and S.-L. Zhu, "Y(4143) is probably a molecular partner of Y(3930)," *Phys.Rev.*, vol. D80, p. 017502, 2009.

[33] T. Branz, T. Gutsche, and V. E. Lyubovitskij, "Hadronic molecule structure of the Y(3940) and Y(4140)," *Phys.Rev.*, vol. D80, p. 054019, 2009.

[34] G.-J. Ding, "Possible Molecular States of $D_s^* \bar{D}_s^*$ System and Y(4140)," *Eur.Phys.J.*, vol. C64, p. 297, 2009.

[35] S. Uehara *et al.*, "Observation of a charmonium-like enhancement in the $\gamma\gamma \to \omega J/\psi$ process," *Phys.Rev.Lett.*, vol. 104, p. 092001, 2010.

[36] T. Aaltonen *et al.*, "Evidence for a Narrow Near-Threshold Structure in the $J/\psi\phi$ Mass Spectrum in $B^+ \to J/\psi\phi K^+$ Decays," *Phys.Rev.Lett.*, vol. 102, p. 242002, 2009.

[37] B. Aubert *et al.*, "Observation of a broad structure in the $\pi^+\pi^- J/\psi$ mass spectrum around 4.26-GeV/c^2," *Phys.Rev.Lett.*, vol. 95, p. 142001, 2005.

[38] A. Martinez Torres, K. Khemchandani, D. Gamermann, and E. Oset, "The Y(4260) as a $J/\psi K\bar{K}$ system," *Phys.Rev.*, vol. D80, p. 094012, 2009.

[39] X. Wang *et al.*, "Observation of Two Resonant Structures in $e^+e^- \to \pi^+\pi^-\psi(2S)$ via Initial State Radiation at Belle," *Phys.Rev.Lett.*, vol. 99, p. 142002, 2007.

[40] G. Pakhlova *et al.*, "Observation of a near-threshold enhancement in the $e^+e^- \to \Lambda^+(c)\Lambda^-(c)$ cross section using initial-state radiation," *Phys.Rev.Lett.*, vol. 101, p. 172001, 2008.

[41] F.-K. Guo, C. Hanhart, and U.-G. Meissner, "Evidence that the Y(4660) is a f(0)(980)ψ' bound state," *Phys.Lett.*, vol. B665, p. 26, 2008.

[42] F.-K. Guo, J. Haidenbauer, C. Hanhart, and U.-G. Meissner, "Reconciling the X(4630) with the Y(4660)," *Phys.Rev.*, vol. D82, p. 094008, 2010.

[43] A. Bondar *et al.*, "Observation of two charged bottomonium-like resonances in $\Upsilon(5S)$ decays," *Phys.Rev.Lett.*, vol. 108, p. 122001, 2012.

[44] M. Cleven, F.-K. Guo, C. Hanhart, and U.-G. Meissner, "Bound state nature of the exotic Z_b states," *Eur.Phys.J.*, vol. A47, p. 120, 2011.

[45] J. Beringer *et al.*, "Review of Particle Physics (RPP)," *Phys.Rev.*, vol. D86, p. 010001, 2012.

[46] N. A. Tornqvist, "From the deuteron to deusons, an analysis of deuteron - like meson meson bound states," *Z.Phys.*, vol. C61, p. 525, 1994.

[47] A. De Rujula, H. Georgi, and S. Glashow, "Molecular Charmonium: A New Spectroscopy?," *Phys.Rev.Lett.*, vol. 38, p. 317, 1977.

[48] J. D. Weinstein and N. Isgur, "Do Multi-Quark Hadrons Exist?," *Phys.Rev.Lett.*, vol. 48, p. 659, 1982.

[49] D. Acosta *et al.*, "Observation of the narrow state $X(3872) \to J/\psi\pi^+\pi^-$ in $\bar{p}p$ collisions at $\sqrt{s} = 1.96$ TeV," *Phys.Rev.Lett.*, vol. 93, p. 072001, 2004.

[50] V. Abazov *et al.*, "Observation and properties of the $X(3872)$ decaying to $J/\psi\pi^+\pi^-$ in $p\bar{p}$ collisions at $\sqrt{s} = 1.96$ TeV," *Phys.Rev.Lett.*, vol. 93, p. 162002, 2004.

[51] B. Aubert *et al.*, "Study of the $B \to J/\psi K^-\pi^+\pi^-$ decay and measurement of the $B \to X(3872)K^-$ branching fraction," *Phys.Rev.*, vol. D71, p. 071103, 2005.

[52] S. Chatrchyan *et al.*, "Measurement of the X(3872) production cross section via decays to $J/\psi\pi\pi$ in $p\bar{p}$ collisions at $\sqrt{s} = 7$ TeV," *JHEP*, vol. 1304, p. 154, 2013.

[53] R. Aaij *et al.*, "Determination of the X(3872) meson quantum numbers," *Phys.Rev.Lett.*, vol. 110, no. 22, p. 222001, 2013.

[54] T. Aaltonen *et al.*, "Precision Measurement of the X(3872) Mass in $J/\psi\pi^+\pi^-$ Decays," *Phys.Rev.Lett.*, vol. 103, p. 152001, 2009.

[55] K. Abe *et al.*, "Observation of a near-threshold omega J/ψ mass enhancement in exclusive $B \to K\omega J/\psi$ decays," *Phys.Rev.Lett.*, vol. 94, p. 182002, 2005.

[56] J. Lees *et al.*, "Study of $X(3915) \to J/\psi\omega$ in two-photon collisions," *Phys.Rev.*, vol. D86, p. 072002, 2012.

[57] S. L. Olsen, "Is the X(3915) the $\chi_{c0}(2P)$?," *Phys.Rev.*, vol. D91, no. 5, p. 057501, 2015.

[58] F.-K. Guo and U.-G. Meissner, "Where is the $\chi_{c0}(2P)$?," *Phys.Rev.*, vol. D86, p. 091501, 2012.

[59] X. Li and M. Voloshin, "$X(3915)$ as a $D_s\bar{D}_s$ bound state," *Phys.Rev.*, vol. D91, no. 11, p. 114014, 2015.

[60] C. Shen *et al.*, "Evidence for a new resonance and search for the Y(4140) in the $\gamma\gamma \to \phi J/\psi$ process," *Phys.Rev.Lett.*, vol. 104, p. 112004, 2010.

[61] R. Aaij *et al.*, "Search for the $X(4140)$ state in $B^+ \to J/\psi\phi K^+$ decays," *Phys.Rev.*, vol. D85, p. 091103, 2012.

[62] W. Greiner and J. Reinhardt, *Quantum electrodynamics.* Theoretical physics, Berlin: Springer, 1992.

[63] I. J. R. Aitchison and A. J. G. Hey, *Gauge theories in particle physics: a practical introduction; 4th ed.* Boca Raton, FL: CRC Press, 2013.

[64] W. Greiner, S. Schramm, and E. Stein, *Quantum chromodynamics; 3rd ed.* Berlin: Springer, 2007.

[65] T. Muta, *Foundations of quantum chromodynamics: an introduction to perturbative methods in gauge theories; 3rd ed.* World Scientific Lecture Notes in Physics, Singapore: World Scientific, 2010.

[66] H. Georgi, "An Effective Field Theory for Heavy Quarks at Low-energies," *Phys.Lett.*, vol. B240, p. 447, 1990.

[67] H. Miyazawa, "Spinor Currents and Symmetries of Baryons and Mesons," *Phys.Rev.*, vol. 170, p. 1586, 1968.

[68] H. Georgi and M. B. Wise, "Superflavor Symmetry for Heavy Particles," *Phys.Lett.*, vol. B243, p. 279, 1990.

[69] D. Lichtenberg, "Symmetry and Supersymmetry in Hadrons Containing Both Heavy and Light Quarks," *J.Phys.*, vol. G16, p. 1599, 1990.

[70] M. J. White and M. J. Savage, "Semileptonic decay of baryons with two heavy quarks," *Phys.Lett.*, vol. B271, p. 410, 1991.

[71] H. Thacker, E. Eichten, and J. Sexton, "The Three-Body Potential for Heavy Quark Baryons in Lattice QCD," *Nucl.Phys.Proc.Suppl.*, vol. 4, p. 234, 1988.

[72] S. Gottlieb, "Portrait of a proton," Tech. Rep. UCSD-10-P-10-248, Calif. Univ. San Diego, San Diego, CA, Jul 1985.

[73] S. Weinberg, "Dynamical approach to current algebra," *Phys.Rev.Lett.*, vol. 18, p. 188, 1967.

[74] R. F. Dashen, "Chiral SU(3) x SU(3) as a symmetry of the strong interactions," *Phys.Rev.*, vol. 183, p. 1245, 1969.

[75] S. Scherer and M. R. Schindler, *A Primer for Chiral Perturbation Theory.* Lecture Notes in Physics, Berlin: Springer, 2012.

[76] A. Pich, "Chiral perturbation theory," *Rept.Prog.Phys.*, vol. 58, p. 563, 1995.

[77] A. D. Martin and T. D. Spearman, *Elementary-particle theory.* Amsterdam: North-Holland, 1970.

[78] S. Mandelstam, "Analytic properties of transition amplitudes in perturbation theory," *Phys.Rev.*, vol. 115, p. 1741, 1959.

[79] J. R. Taylor, *Scattering theory: the quantum theory on nonrelativistic collisions.* New York, NY: Wiley, 1972.

[80] J. J. Sakurai and J. Napolitano, *Modern quantum mechanics; 2nd ed.* San Francisco, CA: Addison-Wesley, 2011.

[81] R. Casalbuoni, A. Deandrea, N. Di Bartolomeo, R. Gatto, F. Feruglio, *et al.*, "Phenomenology of heavy meson chiral Lagrangians," *Phys.Rept.*, vol. 281, p. 145, 1997.

[82] A. F. Falk, H. Georgi, B. Grinstein, and M. B. Wise, "Heavy Meson Form-factors From QCD," *Nucl.Phys.*, vol. B343, p. 1, 1990.

[83] D. B. Kaplan, M. J. Savage, and M. B. Wise, "A New expansion for nucleon-nucleon interactions," *Phys.Lett.*, vol. B424, p. 390, 1998.

[84] D. B. Kaplan, M. J. Savage, and M. B. Wise, "Two nucleon systems from effective field theory," *Nucl.Phys.*, vol. B534, p. 329, 1998.

[85] J. Gegelia, "EFT and N N scattering," *Phys.Lett.*, vol. B429, p. 227, 1998.

[86] M. C. Birse, J. A. McGovern, and K. G. Richardson, "A Renormalization group treatment of two-body scattering," *Phys.Lett.*, vol. B464, p. 169, 1999.

[87] U. van Kolck, "Effective field theory of short range forces," *Nucl.Phys.*, vol. A645, p. 273, 1999.

[88] V. Baru, A. Filin, C. Hanhart, Y. Kalashnikova, A. Kudryavtsev, *et al.*, "Three-body $D\bar{D}\pi$ dynamics for the X(3872)," *Phys.Rev.*, vol. D84, p. 074029, 2011.

[89] B. Grinstein, E. E. Jenkins, A. V. Manohar, M. J. Savage, and M. B. Wise, "Chiral perturbation theory for f D(s) / f D and B B(s) / B B," *Nucl.Phys.*, vol. B380, p. 369, 1992.

[90] M. B. Wise, "Chiral perturbation theory for hadrons containing a heavy quark," *Phys.Rev.*, vol. D45, p. 2188, 1992.

[91] C. G. Boyd and B. Grinstein, "Chiral and heavy quark symmetry violation in B decays," *Nucl.Phys.*, vol. B442, p. 205, 1995.

[92] G. Burdman and J. F. Donoghue, "Union of chiral and heavy quark symmetries," *Phys.Lett.*, vol. B280, p. 287, 1992.

[93] T.-M. Yan, H.-Y. Cheng, C.-Y. Cheung, G.-L. Lin, Y. Lin, *et al.*, "Heavy quark symmetry and chiral dynamics," *Phys.Rev.*, vol. D46, p. 1148, 1992.

[94] A. Khodjamirian and R. Ruckl, "QCD sum rules for exclusive decays of heavy mesons," *Adv.Ser.Direct.High Energy Phys.*, vol. 15, p. 345, 1998.

[95] V. Belyaev, V. M. Braun, A. Khodjamirian, and R. Ruckl, "$D^*D\pi$ and $B^*B\pi$ couplings in QCD," *Phys.Rev.*, vol. D51, p. 6177, 1995.

[96] J. F. Amundson, C. G. Boyd, E. E. Jenkins, M. E. Luke, A. V. Manohar, *et al.*, "Radiative D^* decay using heavy quark and chiral symmetry," *Phys.Lett.*, vol. B296, p. 415, 1992.

[97] J. Hu and T. Mehen, "Chiral Lagrangian with heavy quark-diquark symmetry," *Phys.Rev.*, vol. D73, p. 054003, 2006.

[98] K. Olive *et al.*, "Review of Particle Physics," *Chin.Phys.*, vol. C38, p. 090001, 2014.

[99] D. Gamermann, J. Nieves, E. Oset, and E. Ruiz Arriola, "Couplings in coupled channels versus wave functions: application to the X(3872) resonance," *Phys.Rev.*, vol. D81, p. 014029, 2010.

[100] S.-K. Choi, S. Olsen, K. Trabelsi, I. Adachi, H. Aihara, *et al.*, "Bounds on the width, mass difference and other properties of $X(3872) \to \pi^+\pi^- J/\psi$ decays," *Phys.Rev.*, vol. D84, p. 052004, 2011.

[101] C. Hanhart, Y. Kalashnikova, A. Kudryavtsev, and A. Nefediev, "Remarks on the quantum numbers of X(3872) from the invariant mass distributions of the $\rho J/\psi$ and $\omega J/\psi$ final states," *Phys.Rev.*, vol. D85, p. 011501, 2012.

[102] C. Garcia-Recio and L. Salcedo, "SU(6)$\supset$SU(3)xSU(2) and SU(8)$\supset$SU(4)xSU(2) Clebsch-Gordan coefficients," *J.Math.Phys.*, vol. 52, p. 043503, 2011.

[103] D. Gamermann and E. Oset, "Isospin breaking effects in the X(3872) resonance," *Phys.Rev.*, vol. D80, p. 014003, 2009.

[104] J. Yamagata-Sekihara, J. Nieves, and E. Oset, "Couplings in coupled channels versus wave functions in the case of resonances: application to the two $\Lambda(1405)$ states," *Phys.Rev.*, vol. D83, p. 014003, 2011.

[105] D. Gamermann, E. Oset, D. Strottman, and M. Vicente Vacas, "Dynamically generated open and hidden charm meson systems," *Phys.Rev.*, vol. D76, p. 074016, 2007.

[106] D. Gamermann and E. Oset, "Axial resonances in the open and hidden charm sectors," *Eur.Phys.J.*, vol. A33, p. 119, 2007.

[107] R. Molina and E. Oset, "The Y(3940), Z(3930) and the X(4160) as dynamically generated resonances from the vector-vector interaction," *Phys.Rev.*, vol. D80, p. 114013, 2009.

[108] K. G. Wilson, "Confinement of Quarks," *Phys.Rev.*, vol. D10, p. 2445, 1974.

[109] R. Gupta, "Introduction to Lattice QCD," Tech. Rep. hep-lat/9807028. LA-UR-98-3271, Los Alamos Nat. Lab., Los Alamos, NM, Jul 1998.

[110] Z. Fodor and C. Hoelbling, "Light Hadron Masses from Lattice QCD," *Rev.Mod.Phys.*, vol. 84, p. 449, 2012.

[111] M. Luscher, "Volume Dependence of the Energy Spectrum in Massive Quantum Field Theories. 2. Scattering States," *Commun.Math.Phys.*, vol. 105, p. 153, 1986.

[112] M. Luscher, "Two particle states on a torus and their relation to the scattering matrix," *Nucl.Phys.*, vol. B354, p. 531, 1991.

[113] M. Luscher, "Volume Dependence of the Energy Spectrum in Massive Quantum Field Theories. 1. Stable Particle States," *Commun.Math.Phys.*, vol. 104, p. 177, 1986.

[114] S. Beane, P. Bedaque, A. Parreno, and M. Savage, "Two nucleons on a lattice," *Phys.Lett.*, vol. B585, p. 106, 2004.

[115] S. Beane *et al.*, "The Deuteron and Exotic Two-Body Bound States from Lattice QCD," *Phys.Rev.*, vol. D85, p. 054511, 2012.

[116] X. Feng, K. Jansen, and D. B. Renner, "A new moving frame to extract scattering phases in lattice QCD," *PoS*, vol. LATTICE2010, p. 104, 2010.

[117] S. Aoki *et al.*, "Lattice QCD Calculation of the ρ Meson Decay Width," *Phys.Rev.*, vol. D76, p. 094506, 2007.

[118] M. Gockeler *et al.*, "Extracting the ρ resonance from lattice QCD simulations at small quark masses," *PoS*, vol. LATTICE2008, p. 136, 2008.

[119] S. Aoki *et al.*, "Calculation of ρ meson decay width from the PACS-CS configurations," *PoS*, vol. LATTICE2010, p. 108, 2010.

[120] X. Feng, K. Jansen, and D. B. Renner, "Resonance Parameters of the ρ-Meson from Lattice QCD," *Phys.Rev.*, vol. D83, p. 094505, 2011.

[121] J. Frison *et al.*, "ρ decay width from the lattice," *PoS*, vol. LATTICE2010, p. 139, 2010.

[122] C. Lang, D. Mohler, S. Prelovsek, and M. Vidmar, "Coupled channel analysis of the ρ meson decay in lattice QCD," *Phys.Rev.*, vol. D84, p. 054503, 2011.

[123] S. Prelovsek, C. Lang, D. Mohler, and M. Vidmar, "Decay of ρ and a_1 mesons on the lattice using distillation," *PoS*, vol. LATTICE2011, p. 137, 2011.

[124] J. J. Dudek, R. G. Edwards, and C. E. Thomas, "Energy dependence of the ρ resonance in $\pi\pi$ elastic scattering from lattice QCD," *Phys.Rev.*, vol. D87, no. 3, p. 034505, 2013.

[125] L. Roca and E. Oset, "Scattering of unstable particles in a finite volume: the case of $\pi\rho$ scattering and the $a_1(1260)$ resonance," *Phys.Rev.*, vol. D85, p. 054507, 2012.

[126] S. Prelovsek, T. Draper, C. B. Lang, M. Limmer, K.-F. Liu, *et al.*, "Lattice study of light scalar tetraquarks with I=0,2,1/2,3/2: Are σ and κ tetraquarks?," *Phys.Rev.*, vol. D82, p. 094507, 2010.

[127] C. Alexandrou, J. O. Daldrop, M. Dalla Brida, M. Gravina, L. Scorzato, *et al.*, "Lattice investigation of the scalar mesons $a_0(980)$ and κ using four-quark operators," *JHEP*, vol. 1304, p. 137, 2013.

[128] Z. Fu, "Preliminary lattice study of σ meson decay width," *JHEP*, vol. 1207, p. 142, 2012.

[129] Z. Fu, "Lattice QCD study of the s-wave $\pi\pi$ scattering lengths in the I=0 and 2 channels," *Phys.Rev.*, vol. D87, p. 074501, 2013.

[130] D. Mohler and R. Woloshyn, "D and D_s meson spectroscopy," *Phys.Rev.*, vol. D84, p. 054505, 2011.

[131] M. Kalinowski and M. Wagner, "Strange and charm meson masses from twisted mass lattice QCD," *PoS*, vol. ConfinementX, p. 303, 2012.

[132] D. Mohler, S. Prelovsek, and R. Woloshyn, "$D\pi$ scattering and D meson resonances from lattice QCD," *Phys.Rev.*, vol. D87, no. 3, p. 034501, 2013.

[133] S. Ozaki and S. Sasaki, "Lattice study of $J/\psi - \phi$ scattering at low energies to search for narrow resonance," *PoS*, vol. LATTICE2012, p. 160, 2012.

[134] T. Kawanai and S. Sasaki, "Charmonium-nucleon interaction from lattice QCD with a relativistic heavy quark action," *PoS*, vol. LATTICE2010, p. 156, 2010.

[135] Y.-B. Yang, Y. Chen, L.-C. Gui, C. Liu, Y.-B. Liu, *et al.*, "Lattice study on η_{c2} and X(3872)," *Phys.Rev.*, vol. D87, p. 014501, 2013.

[136] L. Liu, K. Orginos, F.-K. Guo, C. Hanhart, and U.-G. Meissner, "Interactions of Charmed Mesons with Light Pseudoscalar Mesons from Lattice QCD and Implications on the Nature of the $D_{s0}^*(2317)$," *Phys.Rev.*, vol. D87, p. 014508, 2013.

[137] A. Martinez Torres, L. Dai, C. Koren, D. Jido, and E. Oset, "The KD, ηD_s interaction in finite volume and the nature of the $D_{s0}^*(2317)$ resonance," *Phys.Rev.*, vol. D85, p. 014027, 2012.

[138] D. Gamermann and E. Oset, "Hidden charm dynamically generated resonances and the $e^+e^- \to J/\psi D\bar{D}, J/\psi D\bar{D}^*$ reactions," *Eur.Phys.J.*, vol. A36, p. 189, 2008.

[139] P. Pakhlov *et al.*, "Production of New Charmoniumlike States in $e^+e^- \to J/\psi D^{(*)}\bar{D}^{(*)}$ at $s^{1/2} \sim 10$ GeV," *Phys.Rev.Lett.*, vol. 100, p. 202001, 2008.

[140] M. Doring, U.-G. Meissner, E. Oset, and A. Rusetsky, "Unitarized Chiral Perturbation Theory in a finite volume: Scalar meson sector," *Eur.Phys.J.*, vol. A47, p. 139, 2011.

[141] J. Oller, E. Oset, and A. Ramos, "Chiral unitary approach to meson meson and meson - baryon interactions and nuclear applications," *Prog.Part.Nucl.Phys.*, vol. 45, p. 157, 2000.

[142] M. Doring, J. Haidenbauer, U.-G. Meissner, and A. Rusetsky, "Dynamical coupled-channel approaches on a momentum lattice," *Eur.Phys.J.*, vol. A47, p. 163, 2011.

[143] M. Doring and U. G. Meissner, "Finite volume effects in pion-kaon scattering and reconstruction of the $\kappa(800)$ resonance," *JHEP*, vol. 1201, p. 009, 2012.

[144] M. Albaladejo, J. Oller, E. Oset, G. Rios, and L. Roca, "Finite volume treatment of $\pi\pi$ scattering and limits to phase shifts extraction from lattice QCD," *JHEP*, vol. 1208, p. 071, 2012.

[145] N. A. Tornqvist, "Isospin breaking of the narrow charmonium state of Belle at 3872-MeV as a deuson," *Phys.Lett.*, vol. B590, p. 209, 2004.

[146] F. E. Close and P. R. Page, "The $D^{*0}\bar{D}^0$ threshold resonance," *Phys.Lett.*, vol. B578, pp. 119–123, 2004.

[147] P. F. Bedaque, I. Sato, and A. Walker-Loud, "Finite volume corrections to pi-pi scattering," *Phys.Rev.*, vol. D73, p. 074501, 2006.

[148] E. T. Whittaker and G. N. Watson, *A Course of Modern Analysis.* Cambridge University Press, fourth ed., 1927. Reprinted 1990.

[149] H. M. Edwards, *Riemann's zeta function.* Academic Press [A subsidiary of Harcourt Brace Jovanovich, Publishers], New York-London, 1974. Pure and Applied Mathematics, Vol. 58.

[150] A. Tomaradze, S. Dobbs, T. Xiao, K. K. Seth, and G. Bonvicini, "Is the Exotic Hadron $X(3872)$ a $D^0\bar{D}^{*0}$ Molecule: Precision Determination of the Binding Energy of $X(3872)$," no. arXiv:1212.4191, 2012.

[151] E. Oset, "On ambiguities of sign determination of the S-matrix from energy levels in a finite box," *Eur.Phys.J.*, vol. A49, p. 32, 2013.

[152] Z. Davoudi and M. J. Savage, "Improving the Volume Dependence of Two-Body Binding Energies Calculated with Lattice QCD," *Phys.Rev.*, vol. D84, p. 114502, 2011.

[153] H. Toki, C. Garcia-Recio, and J. Nieves, "Photon induced Lambda(1520) production and the role of the K* exchange," *Phys.Rev.*, vol. D77, p. 034001, 2008.

[154] M. Albaladejo and J. Oller, "On the size of the sigma meson and its nature," *Phys.Rev.*, vol. D86, p. 034003, 2012.

[155] S. Weinberg, "Evidence That the Deuteron Is Not an Elementary Particle," *Phys.Rev. B*, vol. 137, p. 672, 1965.

[156] L. Landau, "Small binding energies in quantum field theory," *Zh. Eksp. Teor. Fiz*, vol. 39, p. 1856, 1960.

[157] D. Kreinick, "Recent Results in Bottomonium / Ties to Charmonium," *eConf*, vol. C070805, p. 18, 2007.

[158] I. Adachi *et al.*, "Evidence for a $Z_b^0(10610)$ in Dalitz analysis of $\Upsilon(5S) \to \Upsilon(nS)\pi^0\pi^0$," no. arXiv:1207.4345, 2012.

[159] E. Epelbaum and J. Gegelia, "Regularization, renormalization and 'peratization' in effective field theory for two nucleons," *Eur.Phys.J.*, vol. A41, p. 341, 2009.

[160] I. Adachi *et al.*, "Study of Three-Body $\Upsilon(10860)$ Decays," no. arXiv:1209.6450, 2012.

[161] M. Ablikim *et al.*, "Observation of a Charged Charmoniumlike Structure in $e^+e^- \to \pi^+\pi^- J/\psi$ at $\sqrt{s}$ =4.26GeV," *Phys.Rev.Lett.*, vol. 110, p. 252001, 2013.

[162] Z. Liu *et al.*, "Study of $e^+e^- \to \pi^+\pi^- J/\psi$ and Observation of a Charged Charmoniumlike State at Belle," *Phys.Rev.Lett.*, vol. 110, p. 252002, 2013.

[163] M. Ablikim *et al.*, "Observation of a charged charmoniumlike structure in $e^+e^- \to (D^*\bar{D}^*)^\pm\pi^\mp$ at $\sqrt{s} = 4.26$GeV," *Phys.Rev.Lett.*, vol. 112, p. 132001, 2014.

[164] B. Aubert *et al.*, "Observation of the $\chi_{c2}(2P)$ meson in the reaction $\gamma\gamma \to D\bar{D}$ at BABAR," *Phys.Rev.*, vol. D81, p. 092003, 2010.

[165] T. Xiao, S. Dobbs, A. Tomaradze, and K. K. Seth, "Observation of the Charged Hadron $Z_c^\pm(3900)$ and Evidence for the Neutral $Z_c^0(3900)$ in $e^+e^- \to \pi\pi J/\psi$ at $\sqrt{s} =$ 4170 MeV," *Phys.Lett.*, vol. B727, p. 366, 2013.

[166] M. C. Birse, "Power counting with one-pion exchange," *Phys.Rev.*, vol. C74, p. 014003, 2006.

[167] Z.-F. Sun, J. He, X. Liu, Z.-G. Luo, and S.-L. Zhu, "$Z_b(10610)^\pm$ and $Z_b(10650)^\pm$ as the $B^*\bar{B}$ and $B^*\bar{B}^*$ molecular states," *Phys.Rev.*, vol. D84, p. 054002, 2011.

[168] T. D. Cohen and P. M. Hohler, "Doubly heavy hadrons and the domain of validity of doubly heavy diquark-anti-quark symmetry," *Phys.Rev.*, vol. D74, p. 094003, 2006.

[169] M. Mattson *et al.*, "First observation of the doubly charmed baryon $\Xi^+(cc)$," *Phys.Rev.Lett.*, vol. 89, p. 112001, 2002.

[170] M. Moinester *et al.*, "First observation of doubly charmed baryons," *Czech.J.Phys B.*, vol. 53, p. 201, 2003.

[171] A. Ocherashvili *et al.*, "Confirmation of the double charm baryon $\Xi^+(cc)(3520)$ via its decay to pD^+K^-," *Phys.Lett.*, vol. B628, p. 18, 2005.

[172] S. J. Brodsky, F.-K. Guo, C. Hanhart, and U.-G. Meissner, "Isospin splittings of doubly heavy baryons," *Phys.Lett.*, vol. B698, p. 251, 2011.

[173] Y. Namekawa *et al.*, "Charmed baryons at the physical point in 2+1 flavor lattice QCD," *Phys.Rev.*, vol. D87, no. 9, p. 094512, 2013.

[174] R. Lewis and R. Woloshyn, "Bottom baryons from a dynamical lattice QCD simulation," *Phys.Rev.*, vol. D79, p. 014502, 2009.

[175] C. Albertus, E. Hernandez, and J. Nieves, "Hyperfine mixing in $b \to c$ semileptonic decay of doubly heavy baryons," *Phys.Lett.*, vol. B683, p. 21, 2010.

[176] J. Flynn, E. Hernandez, and J. Nieves, "Triply Heavy Baryons and Heavy Quark Spin Symmetry," *Phys.Rev.*, vol. D85, p. 014012, 2012.

[177] M. Genovese, J. Richard, F. Stancu, and S. Pepin, "Heavy flavor pentaquarks in a chiral constituent quark model," *Phys.Lett.*, vol. B425, p. 171, 1998.

[178] I. W. Stewart, M. E. Wessling, and M. B. Wise, "Stable heavy pentaquark states," *Phys.Lett.*, vol. B590, p. 185, 2004.

[179] T. D. Cohen, P. M. Hohler, and R. F. Lebed, "On the existence of heavy pentaquarks: The Large N(c) and heavy quark limits and beyond," *Phys.Rev.*, vol. D72, p. 074010, 2005.

[180] M. A. Shifman, A. Vainshtein, and V. I. Zakharov, "QCD and Resonance Physics. Sum Rules," *Nucl.Phys.*, vol. B147, p. 385, 1979.

[181] P. Colangelo, F. De Fazio, and S. Nicotri, "$X(3872) \to D\bar{D}\gamma$ decays and the structure of X_{3872}," *Phys.Lett.*, vol. B650, p. 166, 2007.

[182] T. Aliev, A. Ozpineci, and V. Zamiralov, "Mixing Angle of Hadrons in QCD: A New View," *Phys.Rev.*, vol. D83, p. 016008, 2011.

[183] P. Ortega, J. Segovia, D. Entem, and F. Fernandez, "Coupled channel approach to the structure of the X(3872)," *Phys.Rev.*, vol. D81, p. 054023, 2010.

[184] Y.-R. Liu, X. Liu, W.-Z. Deng, and S.-L. Zhu, "Is $X(3872)$ Really a Molecular State?," *Eur.Phys.J.*, vol. C56, p. 63, 2008.

[185] R. M. Albuquerque, X. Liu, and M. Nielsen, "Exotic B_c-like molecules in QCD Sum Rules," *Phys.Lett.*, vol. B718, p. 492, 2012.

[186] C. Hanhart, Y. Kalashnikova, A. E. Kudryavtsev, and A. Nefediev, "Two-photon decays of hadronic molecules," *Phys.Rev.*, vol. D75, p. 074015, 2007.

[187] E. S. Swanson, "Short range structure in the X(3872)," *Phys.Lett.*, vol. B588, p. 189, 2004.

[188] M. Voloshin, "Interference and binding effects in decays of possible molecular component of X(3872)," *Phys.Lett.*, vol. B579, p. 316, 2004.

[189] W. H. Liang, R. Molina, and E. Oset, "Radiative open charm decay of the Y(3940), Z(3930), X(4160) resonances," *Eur.Phys.J.*, vol. A44, p. 479, 2010.

[190] E. Braaten and J. Stapleton, "Analysis of $J/\psi\pi^+\pi^-$ and $D^0\bar{D}^0\pi^0$ Decays of the X(3872)," *Phys.Rev.*, vol. D81, p. 014019, 2010.

[191] M. Voloshin, "X(3872) diagnostics with decays to $D\bar{D}\gamma$," *Int.J.Mod.Phys.*, vol. A21, p. 1239, 2006.

[192] G. Gokhroo *et al.*, "Observation of a Near-threshold $D^0\bar{D}^0\pi^0$ Enhancement in $B \to D^0\bar{D}^0\pi^0 K$ Decay," *Phys.Rev.Lett.*, vol. 97, p. 162002, 2006.

[193] T. Aushev *et al.*, "Study of the $B \to X(3872)(D^0\bar{D}^{*0})K$ decay," *Phys.Rev.*, vol. D81, p. 031103, 2010.

[194] C. Hanhart, Y. Kalashnikova, A. E. Kudryavtsev, and A. Nefediev, "Reconciling the X(3872) with the near-threshold enhancement in the $D^0\bar{D}^{*0}$ final state," *Phys.Rev.*, vol. D76, p. 034007, 2007.

[195] K. Abe *et al.*, "Evidence for $X(3872) \to \gamma J/\psi$ and the sub-threshold decay $X(3872) \to \omega J/\psi$," no. arXiv:0505037, 2005.

[196] P. del Amo Sanchez *et al.*, "Evidence for the decay $X(3872) \to J/\psi\ \omega$," *Phys.Rev.*, vol. D82, p. 011101, 2010.

[197] F.-K. Guo, C. Hanhart, G. Li, U.-G. Meissner, and Q. Zhao, "Effect of charmed meson loops on charmonium transitions," *Phys.Rev.*, vol. D83, p. 034013, 2011.

[198] K.-T. Chao, "Interpretations for the X(4160) observed in the double charm production at B factories," *Phys.Lett.*, vol. B661, p. 348, 2008.

[199] F. Aceti, R. Molina, and E. Oset, "The $X(3872) \to J/\psi\gamma$ decay in the $D\bar{D}^*$ molecular picture," *Phys.Rev.*, vol. D86, p. 113007, 2012.

[200] A. Tomaradze, S. Dobbs, T. Xiao, K. K. Seth, and G. Bonvicini, "High precision measurement of the masses of the D^0 and K_S mesons," *Phys.Rev.*, vol. D89, no. 3, p. 031501, 2014.

[201] E. Swanson, "$D\bar{D}^*$ and $D^*\bar{D}^*$ molecules," *J.Phys.Conf.Ser.*, vol. 9, p. 79, 2005.

[202] Z.-F. Sun, Z.-G. Luo, J. He, X. Liu, and S.-L. Zhu, "A note on the $B^*\bar{B}, B^*\bar{B}*, D^*\bar{D}, D^*\bar{D}*$, molecular states," *Chin.Phys.*, vol. C36, p. 194, 2012.

[203] F.-K. Guo, C. Hanhart, Q. Wang, and Q. Zhao, "Could the near-threshold XYZ states be simply kinematic effects?," *Phys.Rev.*, vol. D91, no. 5, p. 051504, 2015.

[204] S. Godfrey and N. Isgur, "Mesons in a Relativized Quark Model with Chromodynamics," *Phys.Rev.*, vol. D32, p. 189, 1985.

[205] B.-Q. Li, C. Meng, and K.-T. Chao, "Coupled-Channel and Screening Effects in Charmonium Spectrum," *Phys.Rev.*, vol. D80, p. 014012, 2009.

[206] L. Maiani, F. Piccinini, A. Polosa, and V. Riquer, "Diquark-antidiquarks with hidden or open charm and the nature of X(3872)," *Phys.Rev.*, vol. D71, p. 014028, 2005.

[207] L. Liu *et al.*, "Excited and exotic charmonium spectroscopy from lattice QCD," *JHEP*, vol. 1207, p. 126, 2012.

[208] S. Prelovsek and L. Leskovec, "Evidence for X(3872) from DD* scattering on the lattice," *Phys.Rev.Lett.*, vol. 111, p. 192001, 2013.

[209] S. Prelovsek and L. Leskovec, "Search for $Z_c^+(3900)$ in the 1^{+-} Channel on the Lattice," *Phys.Lett.*, vol. B727, p. 172, 2013.

[210] S. Prelovsek, C. Lang, L. Leskovec, and D. Mohler, "Study of the Z_c^+ channel using lattice QCD," *Phys.Rev.*, vol. D91, no. 1, p. 014504, 2015.

[211] M. Padmanath, C. Lang, and S. Prelovsek, "X(3872) and Y(4140) using diquark-antidiquark operators with lattice QCD," no. arXiv:1503.03257, 2015.

[212] V. Baru, E. Epelbaum, A. Filin, C. Hanhart, U.-G. Meissner, *et al.*, "Quark mass dependence of the X(3872) binding energy," *Phys.Lett.*, vol. B726, p. 537, 2013.

[213] M. Jansen, H. W. Hammer, and Y. Jia, "Light quark mass dependence of the X(3872) in XEFT," *Phys.Rev.*, vol. D89, p. 014033, 2014.

[214] F.-K. Guo, U.-G. Meiner, W. Wang, and Z. Yang, "Production of the bottom analogs and the spin partner of the $X(3872)$ at hadron colliders," *Eur.Phys.J.*, vol. C74, no. 9, p. 3063, 2014.

[215] F.-K. Guo, U.-G. Meiner, and Z. Yang, "Production of the spin partner of the X(3872) in e^+e^- collisions," *Phys.Lett.*, vol. B740, p. 42, 2015.

[216] J. Lees *et al.*, "Measurement of the $D*(2010)^+$ meson width and the $D^{*+}(2010) - D^0$ mass difference," *Phys.Rev.Lett.*, vol. 111, no. 11, p. 111801, 2013.

[217] A. Anastassov *et al.*, "First measurement of $\Gamma(D^{*+})$ and precision measurement of $m(D^{*+}) - m(D^0)$," *Phys.Rev.*, vol. D65, p. 032003, 2002.

[218] R. Machleidt, K. Holinde, and C. Elster, "The Bonn Meson Exchange Model for the Nucleon Nucleon Interaction," *Phys.Rept.*, vol. 149, p. 1, 1987.

[219] F. Navarra, M. Nielsen, and M. Bracco, "$D^*D\pi$ form-factor revisited," *Phys.Rev.*, vol. D65, p. 037502, 2002.

[220] F. Carvalho, F. Duraes, F. Navarra, and M. Nielsen, "Hadronic form-factors and the J/ψ secondary production cross section: An Update," *Phys.Rev.*, vol. C72, p. 024902, 2005.

[221] Y.-s. Oh, T. Song, and S. H. Lee, "J/ψ absorption by π and ρ mesons in meson exchange model with anomalous parity interactions," *Phys.Rev.*, vol. C63, p. 034901, 2001.

[222] Z.-H. Li, T. Huang, J.-Z. Sun, and Z.-H. Dai, "Strong couplings of heavy mesons to a light vector meson in QCD," *Phys.Rev.*, vol. D65, p. 076005, 2002.

[223] Z.-G. Wang, "Analysis of the vertices DDV and D^*DV with light-cone QCD sum rules," *Eur.Phys.J.*, vol. C52, p. 553, 2007.

[224] M. Bracco, M. Chiapparini, F. Navarra, and M. Nielsen, "ρD^*D^* vertex from QCD sum rules," *Phys.Lett.*, vol. B659, p. 559, 2008.

[225] B. Osorio Rodrigues, M. Bracco, M. Nielsen, and F. Navarra, "$D^*D\rho$ vertex from QCD sum rules," *Nucl.Phys.*, vol. A852, p. 127, 2011.

[226] J. Flynn, P. Fritzsch, T. Kawanai, C. Lehner, C. Sachrajda, *et al.*, "The $B^*B\pi$ coupling with relativistic heavy quarks," *PoS*, vol. LATTICE2013, p. 408, 2014.

[227] F. Bernardoni, J. Bulava, M. Donnellan, and R. Sommer, "Precision lattice QCD computation of the $B^*B\pi$ coupling," *Phys.Lett.*, vol. B740, p. 278, 2015.

[228] M. Ablikim *et al.*, "Observation of a Charged Charmoniumlike Structure $Z_c(4020)$ and Search for the $Z_c(3900)$ in $e^+e^- \to \pi^+\pi^- h_c$," *Phys.Rev.Lett.*, vol. 111, no. 24, p. 242001, 2013.

[229] F.-K. Guo, C. Hanhart, and U.-G. Meissner, "On the extraction of the light quark mass ratio from the decays $\psi' \to J/\psi\ \pi^0(\eta)$," *Phys.Rev.Lett.*, vol. 103, p. 082003, 2009.